ADVANCED APPROACHES FOR MODELING TRACE METAL SORPTION IN AQUEOUS SYSTEMS

by

James Arthur Dyer

A dissertation submitted to the Faculty of the University of Delaware in partial fulfillment of the requirements for the degree of Doctor of Philosophy in Plant and Soil Sciences

Fall 2002

ProQuest Information and Learning Company
300 North Zeeb Road
P.O. Box 1346
Ann Arbor, MI 48106-1346

ADVANCED APPROACHES FOR MODELING TRACE METAL SORPTION IN AQUEOUS SYSTEMS

by

James Arthur Dyer

Approved: _____
Donald L. Sparks, Ph.D.
Chair of the Department of Plant and Soil Sciences

Approved: _____
Robin W. Morgan, Ph.D.
Dean of the College of Agriculture and Natural Resources

Approved: _____
Conrado M. Gempesaw II, Ph.D.
Vice Provost for Academic and International Programs

I certify that I have read this dissertation and that in my opinion it meets the academic and professional standard required by the University as a dissertation for the degree of Doctor of Philosophy.

Signed: 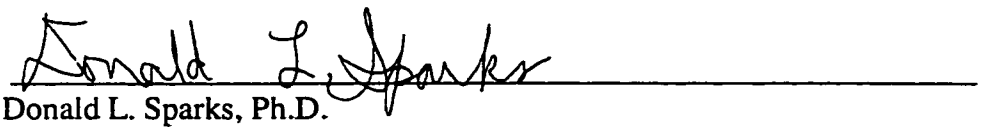

Donald L. Sparks, Ph.D.
Professor in charge of dissertation

I certify that I have read this dissertation and that in my opinion it meets the academic and professional standard required by the University as a dissertation for the degree of Doctor of Philosophy.

Signed: 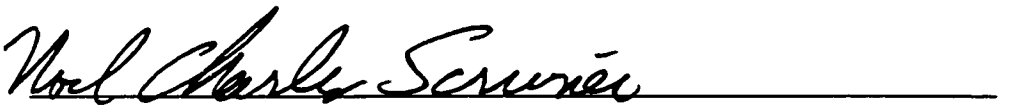

Noel C. Scrivner, Ph.D.
Industrial sponsor and member of dissertation committee

I certify that I have read this dissertation and that in my opinion it meets the academic and professional standard required by the University as a dissertation for the degree of Doctor of Philosophy.

Signed: 

Yan Jin, Ph.D.
Member of dissertation committee

I certify that I have read this dissertation and that in my opinion it meets the academic and professional standard required by the University as a dissertation for the degree of Doctor of Philosophy.

Signed: 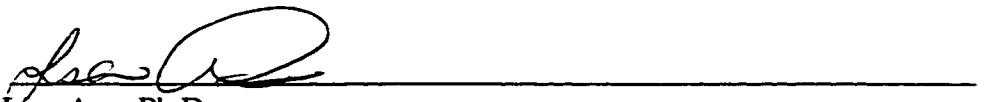

Lisa Axe, Ph.D.
Member of dissertation committee

ACKNOWLEDGMENTS

Donald L. Sparks, Ph.D., for offering me the challenge and opportunity to pursue a Doctor of Philosophy degree, while working full time for DuPont and remaining committed to my family and my spiritual life. Don's guidance, influence, good nature, and constant cooperation have opened new doors for me in my career at DuPont.

Noel C. Scrivner, Ph.D., P.E., for his vision, mentoring, leadership, unyielding support, and friendship over the past ten years. I could never have accomplished this without him. He is the best in the business.

Lisa Axe, Ph.D., and Yan Jin, Ph.D., not only for their advice and support throughout my doctoral research, but also for taking the time to be important members of my dissertation committee.

Paras Trivedi, Ph.D., for living up to his end of the deal. Without his professionalism and dedication to the experimental research program, I could never have accomplished this work.

Jehangir E. Vevai, Ph.D., Hugh J. Campbell, Ph.D., and the DuPont Company for their financial support and encouragement.

Marshall Rafal, Ph.D., and Stephen J. Sanders at OLI Systems, Inc. for delivering the computer modeling tools necessary to conduct this research.

My friends and colleagues at DuPont who have helped and encouraged me throughout my graduate education.

The St. Mary's Men's Faith Sharing Group who helped give me the spiritual strength to remain dedicated to this challenge in my life.

I sincerely thank all who have played a role, however small, in helping me to succeed in this endeavor.

DEDICATION

To my wife, Yvette, for her love, patience, support, and sacrifices over the past ten years. I could never have accomplished this without you. Thank you for always being there for me.

To my three beautiful girls, Mary Elizabeth, Catherine Anne, and Emily Grace, for making me laugh and for helping me to realize what is really important in life.

To my parents, Arthur and Elizabeth Dyer, for making all the sacrifices that parents must make for their children throughout their lives. I love you very much.

To God the Father, God the Son, God the Holy Spirit, and the Blessed Virgin Mary for blessing me with so many special gifts and for always watching over my family and me.

TABLE OF CONTENTS

Appendix

LIST OF TABLES

LIST OF FIGURES

NOMENCLATURE

a_i	activity of species *i*
A_s	specific surface area of sorbent, m^2/g
C_A	mineral acid added during potentiometric titration of sorbent, equiv./L
C_B	mineral base added during potentiometric titration of sorbent, equiv./L
C_1	inner-layer capacitance term for triple-layer model, F/m^2
C_2	outer-layer capacitance term for triple-layer model, F/m^2
COV_i	coefficient of variation, σ_{Yi}/Y_i
F	Faraday's constant, 96,485 coul/mole
$[H^+]$	hydrogen ion molal concentration, moles/kg H_2O
K_i	conditional equilibrium constant
K_i^{int}	intrinsic or thermodynamic equilibrium constant
K_{a1}^{int}	intrinsic acidity constant for the surface deprotonation reaction: $\equiv FeOH_2^+ = \equiv FeOH + H^+$
K_{a2}^{int}	intrinsic acidity constant for the surface deprotonation reaction: $\equiv FeOH = \equiv FeO^- + H^+$
N	number of resamples
n	sample size
N_s	surface site density, moles sites/mole sorbent
$N_{s,\,total}$	proton-active site density used in Zn models, moles sites/mole sorbent
$N_{s,\,Zn}$	Zn-active site density used in Zn models, moles sites/mole sorbent
$[OH^-]$	hydroxyl ion molal concentration, moles/kg H_2O

Pb_{aq}	total lead in bulk aqueous solution, mg/L or moles/kg H_2O
Pb_{sorb}	total lead sorbed on surface of ferrihydrite, moles Pb/mole Fe
q	excess acid added during potentiometric titration, equiv./L
R	gas constant, 8.314 coul-V/mole-K
R_{avg}	arithmetic average of nonlinear regression fit parameters obtained from the OLI Software (R for each data point is the ratio of the model-calculated value to the experimental value (or vice versa), such that R is ≥ 1.0)
T	absolute temperature, K
Zn_{aq}	total zinc in bulk aqueous solution, mg/L or moles/kg H_2O
Zn_{sorb}	total zinc sorbed on surface of ferrihydrite, moles Zn/mole Fe
ΔpK_a	equals ($K_{a2}^{int} - K_{a1}^{int}$) when the protonation/deprotonation reactions are written as dissociation reactions
γ_i	activity coefficient for the M^{z+} ion in the bulk aqueous solution
γ_s	lumped surface activity coefficient used in OLI model to account for nonidealities of the surface complex species
Γ	surface loading, moles metal/mole Fe
Ψ_o	electric potential at o-plane in TLM or at surface in GTLM
Ψ_β	electric potential at β-plane in TLM
σ_i	standard deviation of variable *i*

ABSTRACT

As new and revised regulations drive trace-metal effluent limits to part-per-billion and lower levels, the ability to predict the speciation and mobility of trace metals in aqueous systems becomes vitally important. Only a handful of studies have combined molecular- and macroscopic-scale investigations with surface complexation model (SCM) development to predict trace-metal speciation and partitioning in aqueous systems over a wide range of conditions. Even fewer studies have addressed error propagation through SCMs to assess uncertainty or have demonstrated the practical application of these models in helping to solve industrial trace-metal emissions problems.

In this research, an extensive collection of new macroscopic and spectroscopic data was used to assess the ability of the modified triple-layer model (TLM) to predict single-solute lead (Pb) and zinc (Zn) sorption onto 2-line ferrihydrite in $NaNO_3$ solutions as a function of pH, ionic strength, and concentration. Multistage ferrihydrite sorption systems were also evaluated for their effectiveness in reducing single-solute Pb and Zn concentrations in contaminated water streams to very low levels. Finally, a methodology was demonstrated not only for quantifying the impact of model input-parameter uncertainties on output-parameter uncertainty, but also for identifying the input parameters which have the most impact on output uncertainty.

Regression of constant-pH isotherm data, together with potentiometric titration and pH edge data, was found to be a much more rigorous test of a SCM than fitting pH edge data alone. When combined with spectroscopic data, the choices of

feasible surface species/site types were limited to a few. In agreement with spectroscopic data, very good fits of the Pb isotherm data were obtained with a two-species, one-site model using the bidentate/monodentate species pairs $(\equiv FeO)_2Pb/\equiv FeOHPb^{2+}$ and $(\equiv FeO)_2Pb/\equiv FeOPb^{+}-NO_3^{-}$. For Zn, a one-species, one-Zn-sorption-site model using the bidentate surface complex, $(\equiv FeO)_2Zn$, provided excellent fits of the data. There was no evidence for surface precipitation at high loadings over the pH range 4.5 to 7.5 in either case. Regressing edge data in the absence of isotherm and spectroscopic data resulted in a fair number of surface-species/site-type combinations that provided acceptable fits of the edge data, but unacceptable fits of the isotherm data. Surprisingly, best-fit equilibrium "constants" for the Pb and Zn surface complexes required adjustment with pH in order to fit the isotherm data. For Zn, the density of Zn sorption sites also had to be varied with pH to fit the data. A surface activity coefficient term was also introduced in the TLM for both metals to reduce the ionic-strength dependence of sorption.

Experimental data and modeling results showed that a multistage sorption system can significantly reduce Pb and Zn effluent concentrations for the same total amount of sorbent or, alternatively, dramatically lower total sorbent consumption for the same effluent concentration. Model predictions were made using a steady-state, multistage, equilibrium adsorber model that was developed for and integrated into the OLI Software's Environmental Simulation Program (OLI Systems, Inc., Morris Plains, NJ). The modified TLM was used to simulate Pb or Zn surface-liquid equilibria within the adsorber model. Engineering screening evaluations indicated that a 2- to 3-stage sorption process can provide significant economic savings when compared to a 1-stage process operating with the same target effluent metal concentration.

Additional equilibrium stages beyond 2 or 3 provide diminishing economic returns. The major economic driver for multiple contacting stages was found to be reduced capital investment and operating costs for sludge handling. dewatering, and disposal.

Finally, using a novel uncertainty analysis module in the OLI Software, error propagation through the modified TLM was studied using the isotherm, pH edge, and multistage treatment data for both metals. When coupled with the nonlinear equation solver's gain matrix, the linearized local extrapolation and error propagation models in the OLI ElectroChem code provided a satisfactory alternative to a more rigorous, time-consuming Monte Carlo simulation.

In summary, this research has shown that existing SCMs appear unable to predict single-solute metal sorption onto 2-line ferrihydrite over a wide range of conditions using a single set of best-fit thermodynamic equilibrium constants. Still, the SCMs are valuable tools, for example, in predicting trace metal speciation and removal in multistage ferrihydrite treatment systems. While many advances have been made over the past decade, much work still needs to be done in fine-tuning the thermodynamic framework and databases for the SCMs.

Chapter 1

INTRODUCTION

1.1 Rationale and Scope of Research

Over the past decade, the fate, transport, bioavailability, and toxicity of trace metals in the environment have received increasing attention in the research, regulatory, and industrial communities. As a result, trace-metal discharges from industrial manufacturing processes are being increasingly scrutinized and regulated. In the past, many metals were not regulated in industrial wastewater discharges, and even when they were regulated, the effluent limits were relatively high, i.e., on the order of parts per million (ppm) by weight. For example, Clean Water Act industry guidelines for the Organic Chemicals, Plastics, and Synthetic Fibers (OCPSF) industry limit the effluent concentrations of five metals (zinc, copper, nickel, lead, and total chromium) in direct-discharge point sources using end-of-pipe biological treatment to a maximum daily limit of 2.61 ppm , 3.38 ppm, 3.98 ppm, 0.69 ppm, and 2.77 ppm by weight, respectively (U.S. EPA, 1996). However, new or revised regulations are now pushing metal effluent limits to part-per-billion (ppb) and, in some cases, part-per-trillion (ppt) levels. Examples include the revised maximum contaminant level (MCL) for arsenic in drinking water (lowered from 50 ppb to 10 ppb) and proposed Total Maximum Daily Load (TMDL) regulations that will establish point and nonpoint source load restrictions to meet very stringent federal water quality standards.

In addition, proposed RCRA and Sediment Management regulations are seeking to significantly reduce ongoing and future contamination of groundwater and surface water as the result of trace-metal leaching from solid waste and sediments. Examples include more severe restrictions on land-based wastewater treatment and nonhazardous waste disposal (including biosolids), increased regulation of mineral processing waste, and the development of a contaminated sediment management strategy that will guide the regulation of contaminated sediment cleanup and establish permit limits to prevent future contamination of rivers, lakes, and other waterbodies. In short, these new and proposed regulations create a significant compliance challenge for industry.

In the chemical industry, trace metals often originate as catalysts, raw material impurities, and corrosion products within the manufacturing process. In developing biochemical manufacturing processes, trace amounts of metals are added as essential nutrients for bacterial growth; these nutrients usually end up in the waste biomass that is generated by the process. Typical metals and metalloids of concern include copper, nickel, zinc, lead, chromium, cadmium, cobalt, mercury, and arsenic. In addition, metals have been and, in some cases, still are integral to the products themselves. Examples include titanium dioxide, colored pigments, inorganic pesticides, and metal-coated parts. A key purge point for metals in an industrial process is the wastewater treatment plant. The metals are discharged in the treated wastewater effluent and the biological solids. This greatly influences a manufacturing plant's ability to beneficially reuse biosolids (e.g., through land application) and to comply with part-per-billion Water Quality Criteria limits for metals in receiving waters.

In recent years, contaminated sediment management has surfaced as one of the top environmental issues for the chemical industry. The actions proposed by the U.S. EPA in their Contaminated Sediment Strategy will potentially lower the manufacturing industry's NPDES (National Pollutant Discharge Elimination System) permit limits for metals and increase the likelihood of investigations and remediation of sediments. A conservative estimate of the potential impact of proposed U.S. EPA Water Sediment Quality Criteria on a large chemical company is hundreds of millions of dollars in remediation costs and new investment to comply with more stringent wastewater discharge permits.

The chemical industry, therefore, has a substantial business incentive to better understand and predict the speciation, fate, and transport of trace metals in aqueous systems. For example, corporations need to help lead regulators in developing technically sound water- and sediment-quality regulations. In addition, chemical industry customers are showing increased concern about trace metals in the products they purchase. Demands for zero-mercury sulfuric acid and low-arsenic titanium dioxide are becoming commonplace. Finally, where end-of-pipe control or remediation is required, scientific tools and engineering models will be needed to conceptualize and design cost-effective treatment strategies, including natural recovery where appropriate.

Because metals are often present in wastewater effluents, groundwater, and surface water at concentrations well below their respective solubility limits, large fractions of the discharged metals are often complexed with dissolved organic matter (such as humic and fulvic acids) and/or sorbed onto biological and inorganic suspended solids, including hydrous iron, aluminum, and manganese oxides.

Moreover, in soils and sediments, clay minerals and mineral oxides, such as goethite and ferrihydrite, play a major role in controlling the fate and mobility of trace metals in the environment.

One of the keys in understanding and predicting the mobility and bioavailability of trace metals in the environment, and in identifying a cost-effective control strategy, is the aqueous geochemistry of the system under consideration. A number of commercial (Environmental Simulation Program, OLI Systems, Inc., Morris Plains, New Jersey; The Geochemist's Workbench®, Rockware, Inc., Golden, Colorado) and public-domain (MINTEQA2, U.S. EPA, Athens, Georgia; MINEQL+, Environmental Research Software, Hallowell, Maine; PHREEQC, USGS, Denver, Colorado) geochemical speciation codes exist for simulating the behavior of metals in aqueous systems. However, the existing sorption (i.e., surface complexation) models in these codes are often inadequate for modeling sorption reactions in complex industrial systems involving multiple (i.e., competing) metals. In fact, in a recent publication, Sarkar et al. (1999) noted that "if the objective of modeling is to develop an approach for predicting multi-element adsorption from basic data, such as that describing the adsorption of a single element, then another approach must be developed." In addition, many of the thermodynamic equilibrium constants for surface complexes published in the peer-reviewed literature are based on fitting a limited set of pH sorption edges covering a narrow range of environmental conditions (e.g., metal concentration, ionic strength, background electrolyte, temperature, and so on) without the aid of state-of-the-art spectroscopic techniques to confirm surface speciation. This includes the frequently used generalized two-layer model (GTLM) database for hydrous ferric oxide (Dzombak and Morel, 1990). Finally, many existing surface

complexation modeling codes are limited to simulating reactions in a single, batch-equilibrium stage. The capability to simulate steady- and unsteady-state metal sorption in a multistage, flow system is absent in most commercial and public-domain chemical equilibrium software packages. This severely limits an engineer's ability to predict the speciation, fate, and transport of trace metals in complex aqueous systems containing sorptive surfaces.

The DuPont Company has been actively funding laboratory research at the University of Delaware aimed at better understanding single- and multi-solute metal sorption onto iron oxides. The objectives of this funded research are four-fold:

1. To generate a consistent database of macroscopic pH sorption edge and constant-pH isotherm data.
2. To model this data using advanced surface complexation modeling approaches.
3. To validate the modeled-predicted surface speciation using state-of-the-art x-ray spectroscopic techniques.
4. To demonstrate the practical application of this scientific information in solving real industrial problems.

Research activities have focused on lead, zinc, and nickel sorption onto 2-line ferrihydrite (48-hour-aged hydrous ferric oxide). This sorbent represents one of the more important and ubiquitous sorbents for metals in the environment. Ferric iron oxyhydroxides are prevalent as coatings on mineral surfaces and as suspended, colloidal material in oxic groundwater systems as the result of the oxidation and precipitation of soluble ferrous iron. In addition, the DuPont Company's titanium dioxide business has a substantial stake in supporting customers in using coproduct $FeCl_3$ in wastewater treatment applications. The precipitated amorphous ferric hydroxide in this application is an important sink for trace metals.

The ultimate goal is to be better able to predict the speciation and mobility of trace metals in heterogeneous solid-water systems, such as soils and sediments. The research summarized in this dissertation seeks to develop and demonstrate an improved methodology for predicting metal sorption onto hydrous ferric oxides over a wide range of conditions as well as to show the practical application of this information in single-stage and multistage aqueous sorption systems.

1.2 Literature Review

1.2.1 Single-Metal Sorption Onto Hydrous Ferric Oxide (HFO)

Extensive studies of metal cation and anion sorption onto HFO have been conducted over the years. Dzombak and Morel (1990) critically reviewed most of the single-solute HFO sorption data generated prior to 1990; this data has been regressed to obtain best-fit intrinsic equilibrium constants, which have been nicely compiled in the generalized two-layer model (GTLM). Interestingly, a review of Dzombak and Morel (1990) shows that out of 184 cation and anion data sets included in their evaluation, 83% were pH sorption edges and only 17% were equilibrium isotherms. For metal cations alone, 84% were pH edges and 16% were isotherms. This suggests that the equilibrium constants for each metal will have limited applicability over a wide range of metal concentration if the pH sorption edges used to generate the K-values did not cover a wide enough range of metal/HFO concentration ratios. Equilibrium isotherms usually cover 5 to 8 orders of magnitude in metal concentration. If done at multiple pH values and ionic strengths (if necessary), regression of equilibrium isotherm data will be a much more rigorous test of any surface complexation model. The focus of this research project was on lead (Pb) and zinc

(Zn) sorption onto ferrihydrite; therefore, the single-solute literature review below will focus on these metals only.

Sources of single-solute Pb sorption data found in the literature include Gadde and Laitinen (1973), Gadde and Laitinen (1974), Kinniburgh et al. (1976), Swallow (1978), Benjamin (1979), Leckie et al. (1980), Swallow et al. (1980), and Scheinost et al. (2001). Duplicate sources were not included in this list (e.g., Benjamin and Leckie, 1981). All sources contain pH sorption edge data, except for Scheinost et al. (2001), which contains kinetic data for Pb sorption onto 2-line ferrihydrite at pH 5 (sorption vs. time), and Benjamin (1979), which presents the only published Pb sorption isotherm for HFO (pH 4.5). Despite the fact that Pb is a fairly common constituent found in contaminated soils, sediments, and some groundwater streams, the number of sorption studies on HFO is somewhat limited. In fact, Dzombak and Morel (1990) used only the 0.1 and 1 ppm pH sorption edge data of Benjamin (1979) and Leckie et al. (1980) in their regression analysis. The isotherm data of Benjamin (1979) was not used to obtain their best-fit equilibrium constant for Type 1 sites (high-affinity sites). In addition, the Pb sorption equilibrium constant for Type 2 sites in the GTLM is estimated based on linear free-energy relationships.

A much more extensive set of data exists for zinc sorption onto HFO. Gadde and Laitinen (1974), Kinniburgh et al. (1976), Leckie et al. (1980), Benjamin and Bloom (1981), Benjamin (1983), Schultz et al. (1987), Crawford et al. (1993), and Misak et al. (1996) present Zn sorption edge data only. Meanwhile, Kinniburgh et al. (1977), Benjamin (1979), Dempsey and Singer (1980), Kinniburgh and Jackson (1982), Harvey and Linton (1984), Kanungo (1994), and Trivedi and Axe (2000) present both pH sorption edge and equilibrium isotherm data. Trivedi and Axe (2000)

report isotherms for pH 6, 7, and 8 over 3 to 4 orders of magnitude in Zn concentration. Harvey and Linton (1984) present isotherms for pH 6.25, 6.5, 6.75, 7.0, and 7.25 covering 3 to 3.5 orders of magnitude in Zn concentration. Kinniburgh and Jackson (1982) cover 4 orders of magnitude in Zn concentration at pH 5.5 and 6.5, while Benjamin (1979) provides a pH-6.4 isotherm spanning 3 log units in Zn concentration. The other isotherm data sets are limited to 1 to 2 orders of magnitude in Zn concentration. Dzombak and Morel (1990) used a blend of Zn edges and isotherms to determine the best-fit equilibrium constants for both Type 1 and Type 2 sites. Their preferred data sets included Kinniburgh et al. (1977), Benjamin (1979), Dempsey and Singer (1980), Leckie et al. (1980), and Kinniburgh and Jackson (1982).

A review of published single-solute sorption data for Pb and Zn on HFO shows that it is dominated by pH sorption edges, especially for Pb. In fact, there is only one isotherm for Pb (pH 4.5) that covers at least 3 orders of magnitude in metal concentration. For Zn, on the other hand, a blend of isotherms and edges exists. In particular, there are at least four sources of isotherm data for Zn that cover multiple pH values and more than 3 orders of magnitude in metal concentration. This suggests that GTLM predictions for Pb onto HFO may be questionable, even for single-solute applications that fall outside the range of conditions covered by the regressed data sets. Model predictions for Zn, on the other hand, offer greater potential for broader application.

1.2.2 Evolution of Surface Complexation Models for Predicting Metal-Cation Sorption

The sorption of metal cations onto mineral oxide surfaces has been shown over many years to depend not only on solutions conditions, but also on the chemical

and physical properties of both the sorbent(s) and sorbates (Dzombak and Morel, 1990; Stumm, 1992; Hayes and Katz, 1996; Koretsky, 2000). Solution conditions impacting metal cation sorption include pH, ionic strength, temperature, metal and sorbent concentrations, the presence/absence of competing metals, and the nature and concentration of the background electrolyte(s), such as nitrate, perchlorate, carbonate, and chloride. In general, metal cation sorption is a strong function of pH. Plots of percent metal sorbed vs. pH, referred to as pH sorption edges, are the most common means of conveying the pH dependence of sorption in the peer-reviewed literature. Sorbent properties of importance include sorbent type, surface area, and crystallographic formation history, which all determine the number of available binding sites (i.e., the site density). Sorbate properties that impact sorption include metal ion type, oxidation state of the metal, ion charge, and hydrolysis characteristics.

Sorption behavior for a specific metal-solute/sorbent system over a range of conditions is frequently represented using a constant-pH isotherm (Hayes and Katz, 1996), which relates the amount of metal sorbed to the solid (e.g., moles metal/gram sorbent) to its equilibrium concentration in solution (e.g., moles metal/L). The shape of the isotherm varies, and depends on the range of metal concentration studied (i.e., surface coverage), pH, and a host of other system conditions as outlined above. In general, however, the extent of sorption increases with increasing solute concentration. This relationship often becomes highly nonlinear at relatively high metal concentrations due to site saturation and/or changes in the sorption mechanism (e.g., surface precipitation). Several empirical and semi-empirical equilibrium isotherm models have been used over the years to describe this relationship (Koretsky, 2000). They include the linear partition-coefficient model, the Langmuir isotherm model, and

the Freundlich isotherm model. The most simple is the linear partition-coefficient model

$$\Gamma_{Me} = K_d[Me] \qquad [1.1]$$

where Γ_{Me} is the sorbed metal concentration in moles/g and [Me] is the equilibrium metal concentration in solution in moles/L. This model typically applies over a narrow concentration range only in dilute systems with low surface coverage and constant pH. However, because of its simplicity, the linear partition-coefficient model is frequently incorporated into advection-dispersion equations in fate and transport models to describe metal sorption over a wide range of conditions (Koretsky, 2000).

The Langmuir isotherm model is given by

$$\Gamma_{Me} = \frac{S_T K_L[Me]}{1 + K_L[Me]} \qquad [1.2]$$

where S_T is the total site density (moles per unit mass or unit area), and K_L is the Langmuir constant (L/mole) for the equilibrium reaction

$$\equiv S + Me = \equiv SMe \qquad [1.3]$$

In the Langmuir model, all surface sites are assumed to be identical and have equal adsorption energies, and adsorption is assumed to occur until a monolayer of sorbate forms at the mineral surface (Langmuir, 1918). For this reason, the Langmuir model limits sorption to a finite number of surface sites as given by S_T. A two-site Langmuir model is also available to represent data where sorption is thought to occur on two distinct sites with different adsorption energies.

The Freundlich isotherm equation, given by

$$\Gamma_{Me} = K_F[Me]^{1/n} \qquad [1.4]$$

is used to model sorption onto solids with multiple types of surface sites or onto heterogeneous solids, such as soils (Sposito, 1984). The model simulates the sequential filling of surface sites with progressively decreasing adsorption energies. The adsorption constants in all three of these isotherm models, however, are system dependent. For example, they do not specifically account for the strong pH dependency of metal ion sorption. Almost always, the constants are limited to constant-pH conditions (Hayes and Katz, 1996). In addition, they do not account explicitly for the development of electrical charge on the sorbent surface with the addition or removal of surface species (Koretsky, 2000). Additional reaction processes that can occur during sorption at higher metal concentrations include bulk precipitation of the sorbing metal as well as the formation of surface polymers and precipitates. These mechanisms are not specifically taken into account in the isotherm model; therefore, adherence of experimental sorption data to any of these isotherms does not imply that the reaction mechanism is adsorption alone (Sposito, 1984).

Surface complexation models (SCMs), on the other hand, attempt to explicitly account for the reaction processes actually occurring at the solid-water interface. These models assume that metal ions form complexes with surface functional groups in a manner similar to metal-ligand complexation reactions in solution (Katz and Hayes, 1995a). SCMs are thermodynamic models that differ in their physical description of the solid-water interfacial region (i.e., the location of sorbed species with respect to the surface as well as the description of surface charge-potential relationships across the interfacial region) and in their assumptions regarding number of site types and the structure and composition of the sorbed species. SCMs, therefore, represent an attempt to move toward mechanistically based sorption models.

In theory, the thermodynamic or intrinsic equilibrium constants (K^{int}) derived from SCMs should be much less system-dependent than the equilibrium constants derived from the empirical/semi-empirical isotherm models described above (Koretsky, 2000). The K^{int} values, therefore, should be independent of pH and ionic strength, and depend only on the sorbent type and sorbing metal. This does not always hold true, however, in real systems. The major SCMs in use today include the nonelectrostatic model (NEM), the constant-capacitance model (CCM), the diffuse-layer model (DLM) or generalized two-layer model (GTLM), the modified triple-layer model (TLM), and the CD MUSIC model. As emphasized by Dzombak and Morel (1990), SCMs share four common characteristics. First, the mineral surfaces are assumed to be flat planes of surface hydroxyl sites and equations are written that describe the reactions at these specific sites. Second, mass-law equations describe the equilibrium reactions at the mineral surfaces. Third, variable charge at the mineral surface is the direct result of chemical reactions at the surface. Fourth, the effect of surface charge on the measured equilibrium constants (K^{app}) can be calculated using an electrostatic or Coulombic correction factor, enabling the K^{int} values to be extracted from experimental data sets. The discussion below will not focus on describing the different surface complexation models, but instead will highlight the evolution of surface complexation models in terms of their ability to model metal-cation sorption over a wide range of aqueous solution conditions.

1.2.2.1 Early Evolution of SCMs

Much of the early work with SCMs was focused on the development of the models themselves and the application of the models to fit limited sets of potentiometric titration and metal sorption data. In particular, the metal sorption data

were often limited to pH sorption edges covering a limited range of conditions. Fits of constant-pH sorption isotherms were limited. Schindler and Kamber (1968) and Hohl and Stumm (1976) discuss the formulation of the CCM; Stumm et al. (1970), Huang and Stumm (1973) and Dzombak and Morel (1990) outline the formulation behind the DLM and GTLM; and Yates et al. (1974), Davis et al. (1978), and Davis and Leckie (1978) present the framework for the original TLM. Hayes and Leckie (1986, 1987) later modified the original TLM to allow inner-sphere metal complexes to form on the innermost o-plane. In a highly referenced piece of work, Westall and Hohl (1980) evaluated the ability of five different SCMs—CCM, DLM, original TLM, Basic Stern (AgI) and Basic Stern (Hg)—to fit acid-base titration data for γ-Al_2O_3 in 0.1 M $NaClO_4$ and for TiO_2 (rutile) in 0.1, 0.01, and 0.001 M KNO_3. The authors found that all five models could fit the titration data equally well. This led them to conclude that the models were of the correct mathematical form to represent the data, but they were not necessarily mechanistically correct.

Before the advent of in situ spectroscopic and microscopic techniques in the late 1980s, researchers were very limited in their ability to probe the surface of mineral oxides to determine the surface speciation. As a result, assumptions about surface speciation in the early applications of SCMs were largely based on macroscopic observations, such as the shift (or lack thereof) in pH sorption edges with ionic strength. Examples of early applications of SCMs to fit metal sorption edge data without the aid of microscopic/spectroscopic techniques, include the single-solute sorption of Pb, Cd, Cu, Zn, and Ag onto γ-Al_2O_3, HFO, α-SiO_2, α-FeOOH, and TiO_2 (Davis and Leckie, 1978); Cu, Pb, Zn, and Cd sorption onto goethite in major ion seawater and 0.1 M $NaNO_3$ (Balistrieri and Murray, 1982); uranyl sorption onto HFO,

goethite, and hematite in 0.1 M $NaNO_3$ solutions containing up to 0.01 M $NaHCO_3$ (Hsi and Langmuir, 1985); Pb, Cu, and Zn sorption onto δ-MnO_2 in the presence/absence of Ca (Catts and Langmuir, 1986); single-solute Pb, Cd, and Ba sorption onto goethite in $NaNO_3$ solutions of varying ionic strength (Hayes, 1987); thorium sorption onto goethite in major ion seawater and 0.4 M NaCl solutions (Hunter et al., 1988); and Cd sorption onto HFO in the presence of alkaline earth metals (Cowan et al., 1991). Table 1.1 summarizes these studies and describes the SCM and types of surface complexes used to obtain best fits of the pH sorption edge data.

The work of Dzombak and Morel (1990) represented one of the first attempts to use a single SCM to regress a wide cross-section of metal cation and anion sorption data for a single sorbent—hydrous ferric oxide. After critically reviewing most of the single-solute sorption data for HFO generated before 1990, they regressed the "acceptable" surface titration and metal sorption data to determine best-fit intrinsic equilibrium constants for each metal. In most (but not all) cases, the data was regressed using two site types—0.005 moles high-energy Type-1 sites/mole Fe and 0.2 moles low-energy Type-2 sites/mole Fe. These best-fit equilibrium constants are included as part of the GTLM. As mentioned above, out of 184 cation and anion data sets included in their evaluation, 83% were pH sorption edges and only 17% were constant-pH equilibrium isotherms. In most cases, good fits to the metal cation sorption data were obtained using the $\equiv FeOMe^+$ surface complex for both site types. Exceptions are Cr(III), where $\equiv FeOCrOH^+$ was used, and Sr(II), where $\equiv FeOSrOH$ was used in addition to $\equiv FeOSr^+$ for Type 2 sites. Smith and Jenne (1988) made an early attempt to compile, evaluate, and predict "recommended" parameters for the

Table 1.1 Summary of surface complexation modeling studies using pH sorption edges alone.

Reference	Sorbents	Metals	Study Type	SCM	Electrolytes	Surface Complexes Used
Davis & Leckie (1978)	γ-Al_2O_3, HFO, α-SiO_2, α-FeOOH, TiO_2	Pb, Cd, Cu, Zn, Ag	Single-solute	Original TLM	Various	$\equiv SO^-–Me^{2+}$ and/or $\equiv SO^-–MeOH^+$
Balistrieri & Murray (1982)	α-FeOOH	Cu, Pb, Zn, Cd	Single-solute w/ competition from seawater ions	Original TLM	Major ion seawater or 0.1 M $NaNO_3$	$\equiv FeO^-–Me^{2+}$ and/or $\equiv FeO^-–MeOH^+$
Hsi & Langmuir (1985)	HFO, α-FeOOH, Hematite	U(VI)	Single-solute	Original TLM	0.1 M $NaNO_3$ with up to 0.01 M $NaHCO_3$	$\equiv FeO^-–UO_2OH^+$, $\equiv FeO^-–(UO_2)_3(OH)_5^+$, $\equiv FeOH_2^+–UO_2(CO_3)_2^{2-}$, $\equiv FeOH_2^+–UO_2(CO_3)_3^{4-}$
Catts & Langmuir (1986)	δ-MnO_2	Pb, Cu, Zn, Ca	Single-solute and bisolute with Ca	Original TLM	0.01 M $NaNO_3$, $10^{-3.6}$ M $CaSO_4$	$\equiv MnO^-–Me^{2+}$, $\equiv MnO^-–MeOH^+$, $\equiv MnO^-–Me(OH)_2$, and $\equiv MnO^-–MeNO_3^+$ for Cu and Zn; $\equiv MnO^-–Pb^{2+}$ and $\equiv MnO^-–PbOH^+$ for Pb.
Hayes (1987)	α-FeOOH	Pb, Cd, Ba	Single-solute	Modified TLM	Various molalities of $NaNO_3$	$\equiv FeOMe^+$ for Pb and Cd; $\equiv FeO^-–Ba^{2+}$ and $\equiv FeO^-–BaOH^+$ for Ba
Hunter et al. (1988)	α-FeOOH	Th	Single-solute w/ competition from electrolyte ions	Original TLM	Major ion seawater or 0.4 M NaCl	$\equiv FeO^-–Th^{4+}$, $\equiv FeO^-–ThOH^{3+}$, $\equiv FeO^-–Th(OH)_2^{2+}$, $\equiv FeO^-–Th(OH)_3^+$, $\equiv FeO^-–Th(OH)_4$, $\equiv FeO^-–ThSO_4^{2+}$,

Table 1.1 Continued.

Reference	Sorbents	Metals	Study Type	SCM	Electrolytes	Surface Complexes Used
Cowan et al. (1991)	HFO	Cd, Ca	Bisolute	NEM and Modified TLM	0.1 M $NaNO_3$	$\equiv FeOMe^+$ for NEM; $\equiv FeOCd^+$, $\equiv FeOCa^+$, and $\equiv(FeO)_2^{2-}-Ca^{2+}$ for TLM
Kanungo (1994)	HFO	Mn, Co, Zn, Ni	Single-solute with competition from electrolyte ions	Modified TLM	Major ion seawater, 0.1-0.5 M NaCl & 0.1 M KNO_3.	$\equiv FeOZn^+$, $\equiv FeO^--Co^{2+}$, $\equiv FeO^--Ni^{2+}$, $\equiv FeOMnOH$, and $(FeO)_2MnOH^-$
Gunner-iusson (1994)	α-FeOOH	Cd	Single-solute	CCM	0.1 M NaCl, 0.1 M $NaNO_3$, & 1:1 mixture	$\equiv FeOHCd^{2+}$, $\equiv FeOCd^+$, $\equiv FeOCdOH$, $\equiv FeOHCdCl^+$, $\equiv FeOCdCl$
Gunner-iusson et al. (1994)	α-FeOOH	Pb	Single-solute	CCM	0.1 M NaCl, 0.1 M $NaNO_3$, & 1:1 mixture	$\equiv FeOHPb^{2+}$, $\equiv FeOPb^+$, $\equiv FeOPbOH$, $\equiv FeOHPbCl^+$, $\equiv FeOPbCl$, $\equiv FeOPbOHCl^-$
Kooner et al. (1995)	α-FeOOH	Cu, Pb, Zn	Single-solute	Modified TLM	0.1 M $NaNO_3$	$\equiv FeOMe^+$
Marmier et al. (1999)	Magnetite	Yb(III) and Ni	Single-solute	NEM, DLM, CCM	0.1 M $NaNO_3$	$\equiv FeOYb^{2+}$, $\equiv FeOYbOH^+$, and $\equiv FeONi(OH)_2^-$
Palmqvist et al. (1999)	α-FeOOH	Pb, Cu, Zn	Single- and bisolute	CCM	0.1 M $NaNO_3$	$\equiv FeOHMe^{2+}$, $\equiv FeOMe^+$, $\equiv FeOMeOH$ for Cu and Pb; $\equiv FeOZn^+$, $\equiv(FeOH)_2Zn^{2+}$, $\equiv FeOZn(OH)_2^-$ for Zn
Christl & Kretz-schmar (1999)	Hematite	Pb and Cu	Single- and bisolute	2-pK basic Stern & Modified TLM	0.1 M $NaNO_3$	$\equiv SOPb^+$, $\equiv SO^--Pb^{2+}$, $\equiv SOCu^+$, $\equiv SO^--Cu^{2+}$, $\equiv SO^--CuOH^+$,

original TLM for both cation and anion sorption onto hydrous oxides of iron (goethite and HFO) and manganese (δ-MnO_2). Almost all of the data sets used in the compilation were pH sorption edges. For divalent metal cation sorption onto hydrous iron oxides, Smith and Jenne (1988) provide recommended equilibrium constants for the surface complexes $\equiv SO^-–Me^{2+}$ and $\equiv SO^-–MeOH^+$ for each metal.

Even in recent years, pH sorption edge data alone are still being used to obtain best-fit model parameters for SCMs. For example, Kanungo (1994) investigated Mn, Co, Zn, and Ni sorption onto HFO in major ion seawater, 0.1-0.5 M NaCl, and 0.1 M KNO_3. Gunneriusson (1994) and Gunneriusson et al. (1994) studied Cd and Pb sorption, respectively, onto goethite in the presence and absence of chloride ion at 3-4 different metal/Fe ratios. Kooner et al. (1995) evaluated the sorption behavior of Cu, Pb, and Zn with goethite in 0.1 M $NaNO_3$ solutions as a function of pH, metal concentration, sorbent concentration, and ionic strength. Marmier et al. (1999) investigated Yb(III) and Ni(II) sorption onto magnetite in 0.1 M $NaNO_3$ solutions, while Palmqvist et al. (1999) evaluated single-solute, bisolute, and trisolute Pb, Cu, and Zn sorption onto goethite in 0.1 M $NaNO_3$ solutions. Finally, Christl and Kretzschmar (1999) studied single-solute and bisolute Pb and Cu sorption onto hematite in 0.1 M $NaNO_3$ solutions. Table 1.1 summarizes these more recent studies, and describes the SCM and types of surface complexes that were used to obtain the best fits of the pH sorption edge data. Notice the wide array of surface complexes that were employed to simply fit pH sorption edges over a limited range of conditions.

1.2.2.2 Using SCMs to Simulate Systems Over a Wide Range of Conditions

In the ideal world, the best-fit equilibrium constants and associated SCM parameters for a particular metal/sorbent system would be based on both single-solute

and multisolute sorption data (edges and isotherms) covering a wide range of conditions (i.e., ionic strength, background electrolytes, surface coverage, and so on). In addition, these data would be generated in the same lab, preferably using the same experimentalist. However, this ideal type of study is nonexistent (and unrealistic) for numerous reasons, such as the cost to complete such a study and the typical three- to four-year duration for Ph.D. studies. Despite this, since around 1995, some research scientists have attempted to evaluate the suitability of SCMs over a wider range of conditions.

Katz and Hayes (1995a, 1995b) evaluated the use of the modified TLM for predicting Co(II) sorption onto α-Al_2O_3 over a wide range of conditions. Using pH sorption edges, TLM parameters were calibrated using a moderate-coverage (0.1%) data set; these values were then used to predict Co sorption over a wide range of surface coverage (0.05% to 10%), pH (5 to 9), and ionic strength (0.001 to 0.1 M $NaNO_3$). A single-site model with one surface complex ($\equiv AlOCo^+$) was used. The analysis showed that a range of TLM parameter values could fit the calibration data set equally well; however, when Co sorption data covering a range of conditions were considered, an optimal set of TLM parameter values were identified ($C_1 = 1.1$, $N_s = 2$-3 sites/nm^2, $\Delta pK_a = 4$). For high surface-coverage data (> 10%), the model was shown to underpredict sorption due to the hypothesized formation of multinuclear species. To extend the model predictions, polymer and/or surface precipitation reactions were added. Three different approaches for multinuclear surface complex formation were considered—a surface solid solution model (Farley et al., 1985), a surface polymer model, and a surface continuum model. The solid solution model of Farley et al. (1985) invokes a coprecipitation surface reaction at higher coverage, whereby the

composition of the solid solution varies continuously between that of the original solid [e.g., $Fe(OH)_{3\,(s)}$] and a pure precipitate of the sorbing cation [e.g., $Co(OH)_{2\,(s)}$]. The activity of the surface precipitate is a function of the total mass of solid material in the system [e.g., $Fe(OH)_{3\,(s)} + Co(OH)_{2\,(s)}$]. In the surface polymer approach, two additional multinuclear inner-sphere complexes [$\equiv AlO(Co)_2(OH)_2^+$ and $\equiv AlO(Co)_4(OH)_5^{2+}$] were included in the model. In the continuum model, the two polymer reactions above plus one precipitation reaction were included. In contrast to Farley et al. (1985), the activity of the surface precipitate depended on the total concentration of mononuclear and multinuclear surface complex species, rather than the total mass of solids in the system. Modeling results showed that all 3 approaches worked reasonably well up to 100% surface coverage. However, the continuum model was chosen as the preferred approach, because it was consistent with spectroscopic data available at the time.

Tiffreau et al. (1995) used a modified, one-site GTLM to describe mercury (II) [Hg(II)] sorption onto both HFO and ∝-SiO_2. Using previously published constant-pH isotherm (pH 6–11) and pH sorption edge data in $NaClO_4$, NaCl, and $NaNO_3$ solutions of various concentrations, the authors were able to reproduce the data well from low to high surface coverage. For both oxides, best fits to the data were obtained when the surface complexes $\equiv SOHg^+$, ≡SOHgOH, and ≡SOHgCl were included in the model. In addition, for HFO, a nonideal $Hg(OH)_2$-$Fe(OH)_3$ solid solution model was needed at high surface coverage to fit the isotherm data.

Robertson and Leckie (1998) conducted experimental and modeling studies that evaluated the ability of three SCMs (DLM, modified TLM, and Robertson-modified TLM) to predict Cu sorption onto goethite for three pH values (4.07, 5.07,

6.07), two ionic strengths (0.01 and 0.1 M $NaClO_4$), three orders of magnitude in Cu surface coverage (0.00001-0.03 moles Cu/mole Fe), and six orders of magnitude in Cu solution concentration (10^{-10}-10^{-4} M). The Robertson-modified TLM is identical to the modified TLM (Hayes, 1987), except in the handling of the background electrolyte interactions with the surface. In the former case, the background electrolyte ions accumulate in the β-plane to screen surface charge, but they do not form outer-sphere complexes with the surface OH-groups. The results showed that fits of the Cu isotherms improved significantly with 2 to 3 types of Cu binding sites versus just one type. Copper affinity for these sites differed substantially (Δ of 2-3 log units for each K_{iCu}). All three models provided good fits to the Cu sorption isotherms; however, the two modified TLMs provided the best fits to the potentiometric titration data. For the DLM, three site types and the surface complexes $\equiv FeOCu^+$ and $\equiv FeOCuOH$ provided the best fits to the three constant-pH Cu isotherms. For the modified TLM, several combinations of surface complexes provided good fits— $\equiv FeOCuOH$ alone, $\equiv FeOCu^+$ plus $\equiv FeOCuOH$, and $\equiv FeOCu^+$ plus $\equiv FeOCu^+$–ClO_4^-. For the Robertson-modified TLM, the best fit was obtained with $\equiv FeOCu^+$ plus $\equiv FeOCuOH$.

Using a modified GTLM, Karthikeyan and Elliott (1999) simulated the adsorption and coprecipitation of Cu by HFO and HAO over a range of pH (5-9.5) and surface coverage (up to about 0.5 moles Cu/mole Fe). The GTLM parameters (N_s for both site types, pK_{a1}, pK_{a2}, pK_{sMe}, pK_{wMe}, pK_{spCu}, etc.) for Cu were adjusted to provide best fits for the two different sorbents and sorption mechanisms. As surface coverage increased, the model had to incorporate different surface complexes (e.g., $\equiv FeOCuOH$ for adsorption onto HFO; $\equiv(AlO)_2Cu$ for adsorption onto HAO) than traditionally used in Dzombak and Morel's version of the GTLM, in addition to surface precipitation.

The surface precipitation model was based on the Farley et al. (1985) approach outlined in Dzombak and Morel (1990). Comparable, but different, modeling parameters (site densities and mass-law constants) were obtained for the 4 different cases (HFO and HAO, and adsorption vs. coprecipitation). According to the model results, the solubility of the Cu surface precipitate decreased in the order HFO-Ads. > HFO-Coppt. > HAO-Ads. > HAO-Coppt. This was verified by independent spectroscopic studies.

Sarkar et al. (1999) used the modified TLM to simulate Hg(II) sorption onto quartz and gibbsite as a function of pH, ionic strength, anionic ligands (NO_3^-, Cl^-, SO_4^{2-}, and PO_4^{3-}), and competing metals (Ni and Pb). All pH sorption edge experiments were conducted at the same Hg (0.6 μM) and sorbent concentrations (3.3 g/L). In $NaNO_3$ electrolyte solutions, the surface complexes $\equiv SO^-–HgOH^+$ and $\equiv SOHg(OH)_2^-$ provided good fits to the edge data. When Cl^- was added to the system, the edges shifted to higher pH, and the surface complex $\equiv SOHgOHCl^-$ had to be added to the model. Sulfate decreased Hg sorption on both sorbents due to the formation of the $Hg(OH)_2SO_4^{2-}$ solution complex. Model parameters for $\equiv SO^-–HgOH^+$ and $\equiv SOHg(OH)_2^-$ had to be adjusted for gibbsite only. Phosphate decreased Hg sorption on quartz due to the formation of Hg-PO_4 solution complexes; however, it increased sorption on gibbsite, which was accounted for by the addition of the $\equiv AlOPO_3Hg(OH)_2^{2-}$ surface complex to the model. In the presence of Pb or Ni at 23:1 and 80:1 Me:Hg molar ratios, respectively, Hg sorption decreased by more than two fold. The modified TLM overpredicted Hg sorption in the bisolute systems using equilibrium constants obtained from fits of the single-solute Hg, Pb, and Ni edges. Improved fits were obtained when the equilibrium constants for $\equiv SO^-–HgOH^+$ and

$\equiv SOHg(OH)_2^-$ were lowered in value. The authors concluded that the Hg sorption constants derived from single-solute systems could not be employed to simulate sorption in multisolute, competitive systems.

1.2.2.3 Moving Toward a Predictive Surface Complexation Model

The use of any surface complexation model requires definition of a large number of parameters, including site densities and surface areas for the solid sorbents, equilibrium constants for protonation, deprotonation, metal sorption, and background-electrolyte sorption reactions, and, for the CCM and TLM, capacitance values. This is in addition to making assumptions about the number of site types and the types of surface species that can form (Koretsky, 2000). Over the past six years, Sverjensky and colleagues at the Johns Hopkins University have developed techniques for estimating the values of a number of SCM parameters based on the physical and chemical properties of the solutes and sorbents themselves. The focus of this development work has been primarily on a one-site "extended" TLM, despite some early work with the CCM and the DLM. Koretsky et al. (1998) showed how site densities could be estimated based on crystal chemical considerations when measured values are not available. Sverjensky (2001) has developed a correlation between the inner-layer TLM capacitance value ($1/C_1$) and the crystallographic or hydrated radius of the monovalent electrolyte cation, which enables prediction of C_1 for a variety of aqueous electrolytes and oxides. High-dielectric-constant solids, such as rutile, anatase, and magnetite, correlate with the crystallographic radius of the electrolyte cation, while low-dielectric-constant solids, such as hematite, quartz, goethite, alumina, and amorphous silica, correlate with the hydrated radius of the electrolyte cation. Sverjensky and Sahai (1996) developed algorithms based on the inverse of the

dielectric constant of the solid sorbent and the average Pauling bond strength in the solid to predict surface protonation and deprotonation equilibrium constants for use with the CCM, DLM, and extended TLM. Following this, Sahai and Sverjensky (1997) developed an approach for predicting the electrolyte adsorption equilibrium constants for the extended TLM. The predictions are based on the dielectric constant of the solid, the charge of the electrolyte ion, the effective radius of the adsorbed electrolyte, and the electrostatic radius of the electrolyte ion in aqueous solution. At this time, the predictive methods and correlations are limited to single metals sorbing on crystalline mineral oxides. Amorphous sorbents, such as HFO, do not fit in the predictive thermodynamic framework.

Criscenti and Sverjensky (1999) further extended these predictive approaches for TLM parameter estimation by investigating the role of electrolyte anions (ClO_4^-, NO_3^-, and Cl^-) in divalent metal sorption onto crystalline metal oxide and hydroxide surfaces. A review of experimental pH sorption edge data for Cd, Pb, Co, UO_2, Zn, Cu, Ba, Sr, and Ca sorption onto quartz, silica, goethite, corundum, γ-alumina, anatase, birnessite, and magnetite, from nitrate, perchlorate, and chloride electrolyte solutions over a wide range of ionic strengths (0.0001 to 1.0 M), showed that metal sorption is a function of the background electrolyte. In $NaNO_3$ solutions, metal sorption was minimally impacted by ionic strength. In NaCl solutions, on the other hand, metal sorption decreased substantially with an increase in ionic strength. In $NaClO_4$ solutions, metal sorption increased with increasing ionic strength in most cases; however, no effect or a decrease in sorption with increasing ionic strength also occurred. Analysis of the sorption edge data using the extended TLM revealed that divalent metal sorption onto solids with high dielectric constants (e.g., goethite, γ-

alumina, corundum, and anatase) was best described in nitrate solutions by surface complexes of the form $\equiv SOHM^{2+}–NO_3^-$, in $NaClO_4$ solutions by $\equiv SOHMClO_4^+$, and in NaCl solutions by $\equiv SOHMCl^+$. Metal sorption onto low-dielectric-constant solids, such as quartz and silica, may be accompanied by the ClO_4^- ion in $NaClO_4$ solutions; however, in $NaNO_3$ and NaCl solutions, metal sorption is dominated by the surface complexes $\equiv SOM^+$ and $\equiv SOMOH$.

A much different approach for developing a more predictive SCM has been taken by Van Riemsdijk, Hiemstra, and coworkers over the past decade (Hiemstra et al., 1989a, 1989b; Hiemstra and Van Riemsdijk, 1996; Venema et al., 1996). The CD-MUSIC model (charge distribution, multisite, complexation model) is based on the assumptions that

1. Various types of surface groups exist at the solid-water interface, each of which possesses its own proton affinity constant.

2. The charge of an adsorbing ion that forms an inner-sphere surface complex is distributed over its ligands, which are present in two different electrostatic planes.

The premise is that, in single-site models, the differences in surface hydroxyl site reactivities are averaged into the equilibrium constants. In the CD MUSIC model, these differences in site reactivity are more completely captured in six different site types—singly, doubly, and triply coordinated surface oxygen atoms that bond to either one or two surface protons (Koretsky, 2000). The CD approach treats the charge from surface complexes as being spatially distributed across the interfacial region (i.e., Pauling concept of charge distribution), rather than treating surface complexes as point charges as is done in the TLM, DLM, GTLM, and CCM. While this model may be more mechanistically correct, it also requires more in-depth knowledge of the crystal

structure of the solid sorbent. The model also introduces its own adjustable parameters (e.g., *f*, the fraction of the charge of the sorbing ion that is attributed to the surface plane) that must be optimized to fit the sorption data.

1.2.2.4 Integration of Surface Complexation Models with X-Ray Spectroscopic Techniques

One of the first studies to use X-ray absorption fine structure spectroscopy (XAFS) to validate the surface speciation assumptions in a surface complexation model was Hayes (1987). The newly developed modified TLM was used to simulate selenate and selenite sorption onto goethite in $NaNO_3$ solutions of varying ionic strength. The best fits to the edge data were obtained using inner-sphere surface complexes for selenite (little ionic-strength dependence) and outer-sphere surface complexes for selenate (marked ionic-strength dependence). Extended XAFS (EXAFS) results confirmed that selenite formed a bidentate, inner-sphere complex with two surface Fe atoms, while selenate adsorbed as an outer-sphere complex, retaining its waters of hydration (spectra identical to that of aqueous-phase selenate ions).

Waite et al. (1994) used the results of EXAFS studies to optimize GTLM fits for U(VI) sorption onto ferrihydrite over a wide range of U(VI) concentrations and pH, and at two partial pressures of CO_2. EXAFS results indicated that uranium speciation in two ferrihydrite samples at 10% and 18% surface coverage was dominated by an inner-sphere, mononuclear, bidentate complex of the type $(\equiv FeO_2)UO_2$. There was no evidence of polynuclear surface complex species at circumneutral pH. Modeling results using this one species and two site types (strong and weak) reproduced the pH sorption edge data well. In the presence of carbonate, an

additional surface species was added to the model for both site types—$(\equiv FeO_2)UO_2CO_3^{2-}$. Manipulation of the strong and weak site densities was required to fit all the data. Compared to values recommended by Dzombak and Morel (1990), decreasing the strong site density from 0.005 to 0.0018 moles sites/mole Fe and increasing the weak site density from 0.2 to 0.8732 moles sites/mole Fe greatly improved the model fits. When compared to the modeling results of Hsi and Langmuir (1985) in Table 3, which were not validated by EXAFS, these findings suggest a much simpler surface speciation involving only mononuclear surface complexes.

Brown et al. (1998) used XAFS results to formulate a surface complexation model for Co(II) sorption onto γ-Al_2O_3 as a function of pH and surface coverage. The authors were able to validate the work of Katz and Hayes (1995a, 1995b), who found that Co sorption from low to high surface coverage could be modeled using the sorption sequence: mononuclear complexes, polynuclear complexes, precipitation. Using a single-site, modified TLM supported by XAFS data, good fits to pH sorption edge data were obtained using the inner-sphere, bidentate, mononuclear complexes, $\equiv(AlOH)_2CoOH^+$ and $\equiv(AlOH)_2Co(OH)_2$, the inner-sphere dimer, $\equiv(AlOH)_2AlOCo_2OH^{2+}$, the inner-sphere nonamer, $\equiv(AlOH)_4(AlO)_4\ Co_9(OH)_{14}$, and the surface precipitate, $Co(OH)_2$. Values of N_{Co} (average number of Co atoms among near neighbors of each sorbed Co) obtained from XAFS showed an increasing trend from 0 to 4.5 as Co surface coverage increased from 0.1 to 12 μmoles/m^2. N_{Co} is equal to 6 for pure $Co(OH)_2$, suggesting that the surface precipitate coexisted with mono- and/or low-N_{Co} multinuclear species.

Katz and Boyle-Wight (2001) used macroscopic data for the sorption of Cd(II), Co(II), and Sr(II) onto α-Al_2O_3 in combination with XAFS data to develop a triple-layer surface complexation model for predicting single-solute sorption over a range of pH, surface coverage, and ionic strength. XAFS results indicated that Co and Cd sorbed as inner-sphere complexes, while Sr sorbed as an outer-sphere complex. For Co, surface precipitation was also observed at higher coverage. The XAFS results were used to define the appropriate modified TLM surface complexation reactions. Modeling results for Co predicted that sorption is dominated by the mononuclear, inner-sphere complex $\equiv SOCo^+$ at low coverage, and by Co/Al surface precipitates at high surface coverage. A solid solution model (Farley et al., 1985) was included in the modified TLM to predict the formation of a mixed-metal-hydroxide surface precipitate. Only a one-site model was needed. The Cd data, on the other hand, were modeled with a two-site modified TLM using the surface complexes $\equiv SOCd^+$ and $\equiv SOHCdNO_3^+$ for the high-energy sites and $\equiv SOCd^+$ alone for the low-energy sites. A solid-solution model was not needed for Cd at high coverage. Finally, the ionic-strength-dependence of Sr sorption was predicted using the surface complexes $\equiv SO^- - Sr^{2+}$ and $\equiv SO^- - SrOH^+$.

1.2.2.5 XAFS Investigations of Pb and Zn Sorption Onto HFO and Goethite

Table 1.2 summarizes published XAFS investigations of Pb and Zn sorption onto HFO and goethite. For Pb, there appears to be strong support for the formation of mononuclear, inner-sphere, bidentate surface complexes on both HFO and goethite at all pH values and surface coverages studied. Only some early work by Roe et al. (1991) suggested the possibility of Pb surface-polymer formation at higher loadings. Bargar et al. (1997), however, attributed this to the presence of basic

Table 1.2 XAFS studies of Pb and Zn sorption onto HFO and goethite.

Reference	Solid	Metals	Study Type	Surface Speciation	Conditions
Manceau et al. (1992)	HFO	Pb	Single-solute adsorption	Mononuclear, inner-sphere, bidentate at edge sites	pH 6.5, 7% surface coverage
Ford et al. (1999)	Aged ferrihydrite coprecipitate	Pb	Single-solute coprecip-itation	Mononuclear, inner-sphere, bidentate	pH 6: 0.05 mol Pb/mol Fe; aged up to 380 hr at 70°C. pH 11: 0.1 mol Pb/mol Fe; aged 26 hr at 70°C.
Scheinost et al. (2001)	2-line ferrihydrite	Pb, Cu	Single-solute & bisolute adsorption	Cu & Pb: Edge-sharing, bidentate, inner-sphere for all time, solid morphology, and competing metals	pH 5, 0.018-0.036 mol metal/mol Fe, 2-45 days equilibration time with metal.
Waychunas et al. (1995)	HFO	Zn	Single-solute adsorption	Corner-sharing, inner-sphere, bidentate	N/A
O'Day et al. (1998)	Fe oxyhy-droxide in natural sulfide-bearing sediments	Zn	Multi-solute (Zn, Pb, Cd, Cu)	Bidentate, inner-sphere @ low Zn/Fe; Disordered Zn clusters @ increasing Zn/Fe	1-2 wt% Zn, 50-300 ppm Cd, 500-2000 ppm Pb, pH 5.7-8.0
Trivedi (2001)	HFO	Zn	Single-solute adsorption	Outer-sphere for all pH, temp., & loading	pH 6-8, 0.09-0.9 mol Zn/mol Fe
Roe et al. (1991)	Goethite	Pb	Single-solute adsorption	Inner-sphere @ low loading; surface polymers @ higher loadings (no evidence of surface precip.)	pH 4-8; 0.006-0.089 mol Pb/mol Fe
Bargar et al. (1997)	Goethite	Pb	Single-solute adsorption	Mononuclear, bidentate, inner-sphere at edges for all pH & surface coverage	pH 6-8, 0.008-0.04 mol Pb/mol Fe

Table 1.2 Continued.

Reference	Solid	Metals	Study Type	Surface Speciation	Conditions
Schlegel et al. (1997)	Goethite	Zn	Single-solute adsorption	Edge- and corner-sharing inner-sphere complex in 6-fold coordination	pH 7, 0.0012 moles Zn/mole Fe (~10% proton site coverage)
Manceau et al. (2000)	Natural & aged, synthetic goethite coprecipitates	Zn, Ni	Single-solute coprecipi-tation for synthetic; multisolute in natural (Cr, Mn, Co, Ni, Cu, Zn)	Ni: Possible clustering in synthetic sample; in natural sample, 75% Ni substituted for Fe & 25% as $Ni(OH)_2$-MnO_2 mixed-layer phase. Zn: Zn substituted for Fe in both samples.	Natural: 0.73 wt% Cr, 0.88% Mn, 0.166% Co, 0.898% Ni, 0.263% Cu, 0.026% Zn Synthetic: 0.03 mol Me/mol (Fe+Me), aged @ 70°C for 93 days
Trivedi (2001)	Goethite	Zn	Single-solute adsorption	Inner-sphere for all pH	pH 6-7, 0.001-0.0018 mol Zn/mol Fe (~ site saturation)

Pb(II)-nitrate precipitates in the XAFS samples, rather than to the formation of multinuclear Pb(II) surface complexes. The XAFS findings for Zn, on the other hand, show somewhat more diversity. For HFO, two studies concluded that inner-sphere, bidentate surface complexes predominate, while Trivedi (2001) saw evidence for the formation of outer-sphere surface complexes. O'Day et al. (1998) also suggested the possibility of disordered Zn clusters forming at higher Zn/Fe ratios in a natural sediment sample. In the case of goethite, inner-sphere complexes appear to dominate Zn surface speciation. Based on the limited number of XAFS studies for these two metals, there is a clear need for additional multidisciplinary research investigations that couple XAFS studies with both macroscopic sorption experiments and surface complexation model development. In particular, multidisciplinary studies of this sort that address sorption in multisolute systems are even more sorely needed.

1.2.3 Uncertainty in Surface Complexation Model Predictions

Recently, Crumbling et al. (2001) discussed the challenge of managing uncertainty in environmental decisions involving contaminated site cleanup. They argued that most environmental decision makers assume that the quality of data pertaining to a contaminated site is mainly determined by the analytical methods used, and they ignore the importance of uncertainties in the techniques used to collect the samples in the first place. As a result, efforts to improve data quality center on increasing analytical laboratory oversight, rather than on developing better approaches to manage the largest sources of uncertainty, which are the issues related to sampling in the field. The key is to manage the total environmental decision uncertainty (i.e., the contribution of both analytical and sampling uncertainties), which means being able to identify the largest component(s) of that overall uncertainty. In this case, the

largest source of uncertainty turns out to be sampling representativeness. In SCMs, uncertainty in the predicted partitioning of trace metals between the solid and aqueous phases depends on both analytical uncertainty (e.g., uncertainty in pH measurements, temperature, reagent weights/volumes, impurity levels, etc.) and model parameter uncertainty (e.g., assumptions about site density, capacitance values, equilibrium constants, and so on). By the same token, it is important for a practitioner of surface complexation modeling to appreciate which parameters are the largest contributors to the overall uncertainty in a particular system.

The number of papers that deal directly with uncertainty in SCMs is very limited. In reality, the handful of SCM papers summarized below deal more with sensitivity analyses (some qualitative, some quantitative) than with true uncertainty analyses. As noted by Criscenti et al. (1996), standard geochemical codes are not currently designed for rigorous error propagation. In fact, sensitivity analyses are typically performed by varying the input variables one at a time and performing a separate equilibrium speciation calculation for each case. This can be cumbersome for more than a few input variables.

Goldberg (1991) discusses the sensitivity of the CCM and modified TLM to the site density parameter, N_s. The ability of both SCMs to describe anion sorption onto goethite using both inner- and outer-sphere complexes was found to be highly sensitive to the value of N_s. The use of a goodness of fit criterion led to the choice of an inner-sphere sorption mechanism for small site densities and an outer-sphere sorption mechanism for large values of N_s. Experimentally determined values of surface site density were found to vary by an order of magnitude depending upon the

method used. The author concluded that the uncertainty in N_s invalidated the use of SCMs as a means to predict the anion sorption mechanism.

The ability of the DLM, CCM, and modified TLM to fit sets of potentiometric titration data as a function of changes in model parameters was evaluated by Hayes et al. (1991) using FITEQL and acid-base titration data for goethite, ∝-alumina, and titanium dioxide. For all three SCMs, increasing N_s led to a decrease in the best-fit log K values for the surface acidity constants (K_{a1} and K_{a2}). For the CCM, the best-fit surface acidity constants were relatively insensitive to changes in the capacitance term, C_1, especially when C_1 was greater than 1.2 F/m^2. For the modified TLM, the best-fit surface acidity constants were less sensitive to changes in the value of C_1 when C_1 was greater than 1.2 F/m^2. For a given C_1 value, the best-fit TLM values for the background electrolyte binding constants (K_{C+} and K_{A-}) were sensitive to changes in ΔpK_a up to ΔpK_a values of 3. For ΔpK_a values greater than 3, no changes in the best-fit electrolyte binding constants were observed. The authors also found that, in general, the number or density of titration data points had little effect on the values of the best-fit model parameters. Similarly, fitting only the acid or base leg of the titration curve had only a small impact on the values of the best-fit equilibrium constants. The effects of absolute and relative error in total acid added and measured pH were also evaluated. For changes in the relative and absolute error in total acid added of 0.0 to 0.5 and 2.0E-06 to 0.0 M, respectively, the impact on the best-fit log K values was < 0.2 log units. Similarly, for an absolute error in measured pH of 0.25 units, the best-fit log K values changed by < 0.1 log units.

Lumsdon and Evans (1994) suggest that artifacts can be introduced into calculated SCM parameters if the experimental methodology for conducting

potentiometric titrations is not consistent with the rigorous removal of CO_2 from the system. The authors found that goethite suspensions that have been purged with CO_2-free N_2 for two months had measured points of zero (pzc) charge that ranged from 9.0-9.3 as compared to published data sets for goethite in which the pzc was reported as 7.35-8.65. Despite this, least-squares fitting programs such as FITEQL were able to find an optimized set of SCM parameters to describe the titration data. Using the DLM, CCM, and modified TLM, optimum values for pK_{a1} and pK_{a2} were calculated to be larger than previously reported values. In addition, values for C_1 in the CCM and modified TLM had to be reduced to 0.4-0.8 F/m^2 to explain the titration data for ionic strengths in the range 0.001 to 0.1 M. In short, the authors were able to show how sensitive the SCM parameters can be to the presence/absence of CO_2 in the system.

Robertson and Leckie (1997) conducted an extensive analysis of the effects of pH, ionic strength, cation loading, model type, model fit, and surface complex type on model-predicted cation partitioning and proton release. Three SCMs were evaluated: the DLM, the modified TLM, and the Robertson-modified TLM. The analysis showed that:

1. For the same SCM, significant response differences can exist between different surface complexes.

2. For the same SCM, several surface complexes or combinations of surface complexes can fit the available data equally well.

3. Between SCMs, the responses of comparable surface complexes can differ substantially.

4. For the TLMs (in direct contrast to the DLM), some quite different surface complexes ($\equiv SOMe^+$, $\equiv SOMeOH$, $\equiv(SO)_2Me$, and $\equiv SOHMe^{2+}$) respond, over a certain range, almost identically to changes in system conditions.

5. Several SCMs may be able to provide good fits, although the optimum surface complexes may differ between the models.

In general, DLM sorption edges for a given surface complex show a much greater ionic strength dependence than the corresponding TLM edges. For a given ionic strength, *d*pMe/*d*pH for a given DLM surface complex can be strongly dependent on pH, whereas *d*pMe/*d*pH for comparable inner-sphere TLM surface complexes show little pH dependence (*d*pMe/*d*pH is a measure of how much the metal ion activity in solution must change, when pH is changed, to maintain the sorbed metal concentration constant). Outer-sphere TLM surface complexes show much greater ionic strength and pH dependencies than comparable inner-sphere TLM complexes. Within a model, the effect of total metal concentration differs significantly between complexes, while between models, the effect on comparable complexes showed significant differences. In general, *d*pMe/*d*pH showed greater sensitivity to changes in total metal concentration with the DLM than the TLM. Proton release for the DLM is highly dependent on pH and complex type; proton release for the TLM showed almost none of this dependence. The authors also showed that site heterogeneity is best assessed through constant-pH isotherm experiments if the data cover a sufficiently wide concentration range. A slope less than 1.0 at low surface coverage is an indication of surface heterogeneity. The authors concluded that the ability to choose between fits of possible surface complexes or combinations of complexes within and between SCMs will be very difficult without sorption data covering several orders of magnitude in ionic strength and metal:solid ratio. Still, spectroscopic, proton release, and site density data will also be needed in many cases to further constrain acceptable model/complex options.

Although it does not address surface complexation modeling specifically, Criscenti et al. (1996) present a methodology for propagating uncertainty through geochemical equilibrium speciation code calculations using Monte Carlo simulation and Generalized Sensitivity Analysis (GSA). Overall uncertainty was determined by first propagating analytical and thermodynamic uncertainties generated by Monte Carlo simulation through the geochemical code, thereby generating probability distributions for the calculated output parameters. In the second step, GSA was employed to separate the model responses into two groups (behavior and nonbehavior) based on specified performance criteria. Those responses that met the performance criterion were classified as behaviors, while those that did not were classified as nonbehaviors. The relative contribution of the uncertainty associated with each input variable to the output uncertainty was determined by comparing the cumulative distribution functions (CDFs) of the parameters in the two groups. If the difference in the behavior and nonbehavior CDFs for each parameter was statistically significant, then the uncertainty in the input parameter of interest contributed to the output uncertainty. The methodology was applied to two case studies—the pH of a sodium bicarbonate buffer solution and calcite saturation indices for the $Ca\text{-}CO_3\text{-}Na\text{-}Cl\text{-}H_2O$ system. The use of Monte Carlo simulation in combination with GSA helped to focus attention on the key parameters and uncertainties in the system. In addition, the combination of tools helped to distinguish between parameters that required more precise measurement and those that were known well enough for the specific problem of interest. This approach eliminated the need to vary one parameter at a time to determine the output sensitivity to each input parameter. Moreover, it allowed for the examination of the combined influence of several input parameters on the output.

The importance of uncertainty analysis in estimating environmental impacts and treatment technology performance is also highlighted by Goovaerts et al. (2001). Using Monte Carlo analysis, the authors propagated uncertainty in model parameters and the error component through the Michaelis-Menten equation, yielding a probability distribution for halogenated hydrocarbon degradation rates and cleanup times. They noted that models of microbial activity are typically fit to few data, which can lead to large errors in parameter estimates and uncertain prediction of reaction rates and degradation times. The same is true for SCMs, which are often fit to few data using input parameters with large uncertainties. The output parameters from SCMs, such as metal partition coefficients, are then used downstream as input parameters for fate and transport models to predict metal mobility. For this reason, it is important to be able to quantify the impact of input parameter uncertainty on SCM output parameters as well as to identify which input parameter(s) contribute most to the output uncertainty.

Other papers that have addressed error propagation through geochemical codes include Schecher and Driscoll (1987, 1988) and Nordstrom and Ball (1989). Schecher and Driscoll (1987, 1988) used Monte Carlo methods to evaluate the effect of uncertainties in thermodynamic equilibrium constants (i.e., K values for aqueous complexes and solids) and measured input parameters (i.e., pH, total F, SO_4^{2-}, Cl^-, Na^+, Al, etc.) on calculations of Al speciation in acidic drainage waters. For the thermodynamic parameters, experimental error associated with a given set of equilibrium constants resulted in only modest uncertainty in the thermodynamic predictions, with errors due to the determination of the $Al(OH)_3$ solubility product having the most significant impact. On the other hand, literature error (i.e., the casual

selection of equilibrium constants from the literature) resulted in as much as 100% variation in the concentration of Al complexes. For the measured input parameters, uncertainty in Al speciation was small (< 7%) and mainly due to imprecision in the measurement of total F and pH for fixed pH calculations and the measurement of SO_4^{2-} for variable pH calculations. Sampling error (vs. instrumental error) was the most significant component of the overall uncertainty in the measured input parameters. Nordstrom and Ball (1989) looked at the sensitivity of mineral saturation indices for calcite, fluorite, barite, gibbsite, and ferrihydrite computed with the WATEQ4F geochemical speciation code to changes in analytical and thermodynamic input parameters. By manually varying the input parameters to assess sensitivity, the authors were able to deduce that supersaturation does commonly occur and cannot be accounted for strictly by analytical and thermodynamic uncertainties. For example, kinetic effects seemed to be operative for fluorite, barite, and calcite, despite uncertainties in K_{sp} values and the absence/presence of key ion-pairs in the database. On the other hand, gibbsite supersaturation could be fully accounted for by degree-of-crystallinity effects on solubility, and/or organic complexes, and/or normal database uncertainties. Apparent supersaturation for ferric hydroxide was likely caused by < 0.1 μm colloidal particles in the water samples passing through the standard 0.45 μm field filter, although several other plausible explanations were also cited.

1.2.4 Treatment of Metal-Contaminated Wastewaters Using Amorphous Ferric Hydroxide

There is limited discussion in the literature of using a high-surface-area sorbent, such as HFO, in multistage crossflow or countercurrent stirred-tank reactors to reduce metals in contaminated wastewater to very low levels (e.g., 1 ppb). Trace

metals removal via an alkaline precipitation process typically results in metal effluent concentrations that are 1 ppm or higher due to the inherent solubility of the amorphous metal (hydr)oxide phases of interest and the inefficiency of commercial solid-liquid separation devices. Much lower effluent levels (ppb and less) are possible if one takes advantage of metal sorption onto high-surface-area solids, such as HFO. Treating a contaminated wastewater stream with HFO (or any other sorbent) in two or more equilibrium stages will

- reduce metal effluent concentrations to much lower levels than can be realized in one stage using an equivalent amount of sorbent, or
- reduce total sorbent consumption for the same target effluent concentration.

Experience in the chemical engineering field has shown that two to three contacting stages provide significant improvement over one stage, while additional stages beyond three often lead to diminishing returns. A decision on the number of stages often becomes a trade-off between capital investment for additional equipment, and operating costs for raw materials, energy, and waste disposal.

Merrill et al. (1985) examined the technical and economic feasibility of removing inorganic trace elements, such as arsenic (As), lead, chromium, selenium (Se), copper, zinc, cadmium, silver, and vanadium, from coal-fired power plant wastewater streams via coprecipitation with HFO. Focus was placed on As and Se removal. They found that metal removal efficiency was influenced by the element's oxidation state and concentration, iron dose, pH, and overall solution composition. Reaction kinetics were fast, and 1-hour contact times were sufficient. Results were reproducible, and could be simulated using sorption models. Only one equilibrium

contacting stage was considered. Ferric nitrate and lime were used as reagents in feasibility tests. Total arsenic and selenium levels in the five ash-pond effluent samples tested ranged from 5 to 120 ppb and 24 to 136 ppb, respectively. High removal efficiencies (95-99%) for As(III) and As(V) were achieved with a ferric-iron dose of 14 mg/L and a pH of 7.5 to 8.5. Se(IV) removal was 80-95% at the same iron dose and pH; however, Se(VI) removal was much lower at 5-15%. A review of the testing results showed that optimum removal of metals occurred at pH < 9 for As(V), pH 8-9 for As(III), pH < 7 for Se(IV), and pH < 4 for Se(VI). In this case, a two-stage process controlled at two different pH values (e.g., 4.5 and 8.5) might allow for satisfactory removal of all four contaminants. Staging might also prove more valuable when metal inlet concentrations are much higher than 100 ppb.

The adsorption and coprecipitation of Cu with HFO and HAO were evaluated by Karthikeyan et al. (1997). Using a single equilibrium stage, residual soluble Cu levels were compared following adsorption (contact with preformed oxide flocs) and coprecipitation (Cu added prior to HFO or HAO precipitation) over the pH range 6-9. Experimental conditions were 4.3 ppm initial Cu concentration, 1-hour equilibration time, 100 mg/L ferric chloride or alum, and vessels open to the atmosphere. For adsorption onto HAO, soluble Cu levels were markedly undersaturated with respect to $Cu(OH)_2$. Levels as low as 6 ppb were achieved at pH 8.75. Coprecipitation with HAO gave nearly identical results. In contrast, effluent Cu levels for adsorption onto HFO were comparable to adsorption onto HAO at pH < 6.5; however, by pH 7.5, they mirrored the solubility curve for $Cu(OH)_2$. On the other hand, Cu coprecipitation with HFO was even better than removal by HAO, achieving 6 ppb soluble Cu by pH 8. Adsorption isotherms suggested that a Cu surface

precipitate formed on HAO with a solubility product smaller than its HFO analogue. Maximum *adsorption* densities from the isotherms were 0.25 moles Cu/mole Fe for HFO and 0.07 moles Cu/mole Al for HAO. The dramatic improvement in Cu removal by coprecipitation suggested Cu substitution into the HFO lattice. The benefits of multiple equilibrium stages were not investigated.

Schultz et al. (1987) examined the feasibility of recycling ferrihydrite in a one-stage metal sorption process. The process consisted of metal ion sorption onto ferrihydrite from dilute solutions (0.01 mM each metal), followed by desorption into a more concentrated regenerant solution at acidic pH. The objective was to design a closed-loop process that reuses the ferrihydrite sorbent in subsequent sorption steps and recovers the metals from the concentrated regenerant solution by a process such as alkaline precipitation. The research showed that Cu, Pb, Cr(III), Zn, Ni, and Cd could be efficiently removed from solution at pH 9, and then be substantially recovered in a desorption step at pH 4.5. Reaction times of 1-3 hr were used in each step. However, except for Cd, a measurable fraction of the bound metals were not easily desorbed. This slowly reversible fraction increased with increasing pH and duration of the high-pH sorption stage, and increased more or less continuously in sequential cycles. The authors found that the mechanism leading to slow reversibility depended on contact between the metals and the ferrihydrite solid. Aging the sorbent in the absence of sorbed metals did not have nearly the same impact. Interestingly, the metals retained in the ferrihydrite lattice did not affect metals removal in five subsequent cycles for the concentration range studied. Even retention of Cr(III) at levels as high as 0.7 moles/mole Fe did not impact sorption of the other metals.

Edwards and Benjamin (1989) extended the work of Schultz et al. (1987) by considering the performance of the regenerated ferrihydrite sorbent over 50 cycles, rather than just six. Removal efficiency remained high (> 98%) and steady when treating both synthetic and real plating wastes containing between 1 and 3 ppm each of Cu, Ni, Zn, Cd, Pb, and Cr(III). In addition, the adsorption cycle time was reduced from 1-3 hours to 10 minutes, while the desorption time was 10-30 minutes instead of 1-3 hours. As a result, Cd, Zn, and Ni were nearly completely recovered in the regenerant solution at pH 3.5 and 4.5. Nearly all of the Cu was recovered at pH 3.5; however, a small portion (20% over 50 cycles) was retained by the ferrihydrite at pH 4.5. In contrast, over 70% of the sorbed Cr(III) remained bound to the solids at both pH 3.5 and 4.5, despite the shorter adsorption cycle time. After 50 cycles, the regenerant solution reached a total metals concentration of about 110 ppm. The study also considered the settleability of the ferrihydrite floc. Preformed ferrihydrite solids (0.45 g/L) were found to aid removal of 90% of the suspended iron oxyhydroxide solids within 3 minutes. Only 4% remained suspended after 50 minutes. In the absence of a coagulant, over 45% of the solids remained suspended after 50 minutes. Once again, only one equilibrium contacting stage was considered.

Employing a multistage, countercurrent, soil solvent-washing system, Khodadoust et al. (1999) showed that pentachlorophenol (PCP) and hydrocarbon levels in a contaminated soil could be significantly reduced via extraction with a 95% ethanol solution. Two- and three-stage countercurrent solvent washing was piloted using batches of 7.5 kg soil and 30 L of solvent. The solvent-washed soil was then rinsed with clean water in a final stage. The authors used an experimental procedure that approximates a continuous, countercurrent, multistage solvent-washing process

with a series of countercurrent, batch, equilibrium contacting stages. The results of the pilot-scale testing highlight the benefits of multistage contacting, whether the process is soil solvent washing or trace metal sorption onto HFO. PCP removal efficiency was 89% in a single stage, 95% in 2 stages, and 99% in 3 stages. Hydrocarbon removal efficiency was 77%, 86%, and 93%, respectively.

An alternative to batch or continuous stirred-tank reactor configurations for the ex situ treatment of metal-contaminated waters is a fixed-bed column containing a granular sorbent that can be regenerated over many cycles. Advocates of this alternative approach argue that dynamic flow in fixed beds is preferred over a continuous stirred-tank configuration, because it eliminates the need for potentially expensive solid-liquid separation facilities. A number of papers dealing with metals removal in fixed-bed columns have been published (Theis et al., 1992; Gao et al., 1995; Fan and Anderson, 1996; Smith, 1998; Smith and Amini, 2000). For example, Smith and Amini (2000) studied Pb removal in fixed-bed columns containing a recycled, granular, iron-bearing material recovered from surface finishing operations in cast-iron manufacture. Tests demonstrated that a water stream containing 10 ppm Pb at pH 5.5 could be effectively treated using an empty-bed contact time of ≥ 2.5 minutes; solid phase loading capacity was ~40,000 mg/kg at exhaustion. Efforts to regenerate the sorbent using aqueous EDTA and DTPA chloride salt solutions, however, resulted in relatively low Pb recovery (40-50%) and subsequent adsorption efficiency. In this work, as well as in Smith (1998), the modified TLM was used to describe equilibria for metal sorption onto the recycled iron-bearing sorbent; the iron sorbent was treated as a hydrous ferric oxide in aqueous solution. Model constants were derived from surface titration experiments, literature recommendations, and

regression of pH-sorption-edge data for each metal. More novel was the integration of the modified TLM into a dual-resistance mass-transport model to simulate the performance of the fixed-bed columns. In this case, fundamental macroscopic sorption data was coupled with an equilibrium and transport model to design and engineer a treatment process for reducing metal effluent concentrations to very low levels.

In summary, a strong argument can be made for conducting fundamental microscopic and macroscopic metal sorption studies when this information will be integrated into state-of-the-art metal surface complexation models to predict trace metal removal in industrially important processes. While there are some published studies in this area, the integration of SCMs into steady-state and dynamic flowsheet simulation codes is still in its infancy.

1.3 Research Justification

To remain profitable, the manufacturing industry must address trace-metal contamination problems via pollution prevention as well as cost-effective treatment and in-situ remediation strategies, including natural recovery. Success will hinge, among other things, on the ability to predict the speciation and mobility of trace metals in the aqueous systems of interest. Two leading environmental modeling firms have acknowledged that realistic models and tools for predicting metal speciation and complexation in sediment/water systems are key missing components in their sediment fate and transport models. More specifically, industrial practitioners are limited in their ability to reasonably account for important metal sorption and complexation reactions in their commercial aqueous simulation codes. Examples of trace-metal issues of real concern in the chemical industry are:

- Speciation, mobility, and bioavailability of trace metals in natural systems, including protected wetlands. Metals and metalloids of concern include Pb, As, Hg, Ni, Cu, Zn, Cd, and boron.

- Better understanding trace-metal removal via alkaline coprecipitation processes in the presence of competing anions and organic ligands.

- Competitive sorption and desorption of trace metals, such as Cu, Pb, Ni, Cd, Co, and Zn, onto/from iron oxides and hydroxides.

- Arsenic speciation, mobility, and transport in groundwater in contact with soils and sediments that are Ca-, Ba-, and Fe-rich.

The reality is that the dynamics of trace-metal movement in groundwater, soils, and sediments are not well understood. In many natural waters, and even in a good number of industrial wastewaters, the geochemical fate of most reactive substances (trace metals, organic compounds) is controlled by the reaction of solutes with solid surfaces, such as metal oxides or hydroxides, clay minerals, and biological solids (Stumm, 1992). While these sorption reactions can dominate metal speciation and mobility in the environment, the ability to accurately simulate these reactions in chemical equilibrium and fate and transport models is still lacking, particularly in cases where several trace metals compete for surface sites on multiple sorbents in the presence of complexing inorganic and organic ligands.

The term "sorption" is used when the reaction mechanism(s) for partitioning to a solid surface is not known (Sparks, 1995). Sorption includes a continuum of processes from adsorption of a metal ion onto a mineral surface, to coprecipitation of a metal ion with another metal oxide/hydroxide, to precipitation of the metal ion as a new hydroxide phase on the surface of a clay mineral or metal oxide

(i.e., surface precipitation). In the absence of a true understanding of the reaction mechanisms, sorption has traditionally been described using empirical equilibrium isotherm models that relate the sorbed metal concentration to its equilibrium concentration in the aqueous phase. However, because these models are empirical, rather than mechanistic, they tend to be unreliable when extrapolated beyond the range of conditions for which the empirical constants were derived. In fact, in many fate and transport models, a simple partitioning coefficient (K_d) that is based on empirical observations of laboratory or field data is used to describe the split between the sorbed and the dissolved phases (Sauve et al., 2000). In almost all cases, this partition coefficient does not adequately account for the effects of pH, ionic strength, temperature, metal-to-sorbent ratio, competing solutes, changes in the sorption mechanism, and mass-transfer limitations.

Over the past two decades, substantial research effort has been dedicated to developing chemical equilibrium models that are based on fundamental thermodynamic principles and that more accurately depict the reactions of the sorbates at the solid/water interface over a range of operating conditions (Hayes and Katz, 1996). These surface complexation models include the constant-capacitance model, generalized two-layer model, modified triple-layer model, CD-MUSIC model, and so on. However, the development and application of the majority of these SCMs through the early 1990s were done without the aid of molecular-scale microscopic and spectroscopic techniques for probing the mineral surface. In addition, Westall and Hohl (1980) astutely recognized that, for the same set of data, different surface complexation models could predict metal sorption onto mineral surfaces equally well, even though they were based on different molecular descriptions of the interfacial

reactions and used different numbers and types of fitting parameters. Finally, despite the plethora of macroscopic sorption and modeling studies published in the peer-reviewed literature over the past two decades, very few have addressed the ability of SCMs to predict the competitive sorption of metal cations and anions on solid surfaces as well as to account for the changes in reaction mechanisms with changes in pH, metal loading, and ionic strength. Without advances in the ability of SCMs to predict metal sorption in complex aqueous systems, the ability of engineers to bridge the gap between the fundamental science and real problems will rarely occur. The use of molecular-scale technologies, when coupled with macroscopic sorption studies and computer modeling, offers the potential to bridge this gap.

Equilibrium constants for the SCMs have historically been derived by fitting macroscopic equilibrium sorption data using a hypothesized set of surface complex reactions. In competitive sorption modeling studies, the single-solute sorption data is almost always used to obtain the intrinsic equilibrium constants (Ks) for the surface reactions. These intrinsic Ks are then used to predict sorption when competing metal ions are present. Invariably, the model overpredicts or underpredicts the competition depending on the sorbent site density and the degree of saturation of the surface. While the goal is to obtain intrinsic (thermodynamic) equilibrium constants that apply over a wide range of conditions, they are often "conditional" in the sense that they represent sorption equilibria over only a fairly narrow range of conditions.

Successful application of SCMs for predicting metal sorption, therefore, requires: (1) a self-consistent databank that is coupled with a robust, predictive thermodynamic framework for the aqueous solution chemistry; (2) quantitative

descriptions of the surface chemistry and properties of the various sorbents, including site types, site densities, acid-base chemistry, surface area, and so on; and (3) realistic depictions of the surface speciation and equilibrium reactions under a wide range of conditions. In field applications, predictive models will need to account for the dynamics or time dependency of metal ion movement through a soil or sediment column as well. The integration of equilibrium SCMs into reactive solute transport models has been rare, because of the computational challenges involved. Smith (1998) integrated the modified TLM into a dual-resistance mass-transport model to successfully simulate single-solute Pb, Zn, and Cd sorption equilibria in a fixed bed of recycled iron sorbent. However, no reference has been found in the literature on the use of SCMs to simulate competitive metal sorption in dynamic systems.

A number of commercial (Environmental Simulation Program, OLI Systems, Inc., Morris Plains, New Jersey; The Geochemist's Workbench®, Rockware Inc., Golden, Colorado) and public-domain (MINTEQA2, MINEQL+, FITEQL, PHREEQC 2.0) chemical equilibrium codes exist for simulating the behavior of metals in aqueous systems. However, existing surface complexation models in these codes are inadequate for modeling sorption reactions in complex industrial systems involving multiple (i.e., competing) metals. In addition, most all existing surface complexation modeling codes are limited to simulating reactions in a single batch-equilibrium stage. The capability to simulate competitive metal sorption in a multistage, flow system has been absent from both commercial and public-domain chemical equilibrium software.

The in-depth research review in this proposal highlights the scarcity of studies where molecular-scale and macroscopic-sorption data have been coupled with

surface complexation model development to predict metal-cation sorption over a wide range of conditions. There clearly is a need for the integration of these three legs of the metal-speciation stool—macroscopic data collected over a wide range of conditions, including the presence of competing metals, microscopic and spectroscopic data to validate the surface speciation, and application of a mechanistically based SCM to allow estimation of metal speciation and mobility in industrial and natural systems.

In addition, despite years of data collecting data on metal cation sorption, the bulk of the published equilibrium constants for surface complexes are based on fits of a limited number of pH sorption edges for single-solute systems. A much more rigorous test of these models would be to calibrate and validate the SCM against three or more constant-pH isotherms covering 5 to 7 orders of magnitude in metal concentration, in addition to a handful of pH sorption edges at several ionic strengths. This would help to constrain the model to a much smaller subset of sorption complexes and SCM parameters that can represent the data. The use of uncertainty analysis techniques to assess the impact of error propagation through SCMs is also needed.

Finally, demonstrating the practicality of this state-of-the-art scientific information in solving real industrial problems is still surprisingly limited. There is a real need to bridge the gap between the fundamental scientific insights and the engineering applications. To this end, integrating existing surface complexation models into steady-state and unsteady-state flowsheet simulators would be a huge step forward. For example, this would enable one to simulate the removal of trace metals from a contaminated wastewater stream in a multistage adsorption/coprecipitation process.

1.4 Research Objectives

To make progress toward meeting the long-term research needs outlined above, this research project focused on the following specific objectives:

1. Demonstrate how the integration of spectroscopic data on surface speciation with macroscopic sorption data covering a wide range of conditions leads to the determination of an optimum set(s) of surface complexation modeling parameters for single-solute Pb sorption onto 2-line ferrihydrite. The macroscopic data set for Pb included 3 constant-pH isotherms covering 5 to 6 orders of magnitude in Pb concentration and 6 pH sorption edges at different ionic strengths and Pb:sorbent ratios.

2. Repeat Objective 1 for single-solute Zn sorption onto 2-line ferrihydrite to demonstrate the feasibility and limitations of this methodology for calibrating surface complexation models.

3. Demonstrate an industrial application for these calibrated surface complexation models by developing and validating a steady-state, multistage, ferrihydrite adsorber model for treating a Pb-contaminated water stream to part-per-billion levels.

4. Using state-of-the-art uncertainty analysis techniques, demonstrate a methodology for quantifying the impact of analytical, thermodynamic, and SCM input-parameter uncertainties on the predicted output parameters (e.g., % metal sorbed, surface charge, soluble metal concentration, etc.) as well as for identifying which input parameters have the most impact on the output uncertainty.

1.5 References

Balistrieri L. S. and Murray J. W. (1982) The adsorption of Cu, Pb, Zn, and Cd on goethite from major ion seawater. *Geochim. Cosmochim. Acta* **46,** 1253-1265.

Bargar J. R., Brown G. E. Jr., and Parks G. A. (1997) Surface complexation of Pb(II) at oxide-water interfaces: II. XAFS and bond-valence determination of mononuclear Pb(II) sorption products and surface functional groups on iron oxides. *Geochim. Cosmochim. Acta* **61,** 2639-2652.

Benjamin M. M. (1979) Effects of competing metals and complexing ligands on trace metal adsorption at the oxide/solution interface. Ph.D. dissertation. Stanford University.

Benjamin M. M. (1983) Adsorption and surface precipitation of metals on amorphous iron oxyhydroxide. *Environ. Sci. Technol.* **17,** 686-692.

Benjamin M. M. and Bloom N. S. (1981) Effects of strong binding of anionic adsorbates on adsorption of trace metals on amorphous iron oxyhydroxide. In *Adsorption From Aqueous Solutions* (ed. P.H. Tewari), pp. 41-60. Plenum Press.

Benjamin M. M. and Leckie J. O. (1981) Competitive adsorption of Cd, Cu, Zn, and Pb on amorphous iron oxyhydroxide. *J. Colloid Interface Sci.* **83,** 410-419.

Brown G. E. Jr., Parks G. A., Bargar J. R., and Towle S. N. (1998) Use of x-ray absorption spectroscopy to study reaction mechanisms at metal oxide-water interfaces. In *Mineral-Water Interfacial Reactions: Kinetics and Mechanisms* (eds. D.L. Sparks and T.J. Grundl), ACS Symposium Series 715, pp. 14-36. American Chemical Society.

Catts J. G. and Langmuir D. (1986) Adsorption of Cu, Pb, and Zn by δMnO_2: Applicability of the site binding-surface complexation model. *Appl. Geochem.* **1,** 255-264.

Christl I. and Kretzschmar R. (1999) Competitive sorption of copper and lead at the oxide-water interface: Implications for surface site density. *Geochim. Cosmochim. Acta* **63,** 2929-2938.

Cowan C. E., Zachara J. M., and Resch C. T. (1991) Cadmium adsorption on iron oxides in the presence of alkaline-earth elements. *Environ. Sci. Technol.* **25,** 437-446.

Crawford R. J., Harding I. H., and Mainwaring D. E. (1993) Adsorption and coprecipitation of single heavy metal ions onto the hydrated oxides of iron and chromium. *Langmuir* **9,** 3050-3056.

Criscenti L. J. and Sverjensky D. A. (1999) The role of electrolyte anions (ClO_4^-, NO_3^-, and Cl^-) in divalent metal (M^{2+}) adsorption on oxide and hydroxide surfaces in salt solutions. *Am. J. Sci.* **299,** 828-899.

Criscenti L. J., Laniak G. F., and Erikson R. L. (1996) Propagation of uncertainty through geochemical calculations. *Geochim. Cosmochim. Acta* **60,** 3551-3568.

Crumbling D. M., Groenjes C., Lesnik B., Lynch K., Shockley J., van EE J., Howe R., Keith L., and McKenna J. (2001) Managing uncertainty in environmental decisions. *Environ. Sci. Technol.* **35,** 404A-409A.

Davis J. A. and Leckie J. O. (1978) Surface ionization and complexation at the oxide/water interface. II. Surface properties of amorphous iron oxyhydroxide and adsorption of metal ions. *J. Colloid Interface Sci.* **67,** 90-107.

Davis J. A., James R. O., and Leckie J. O. (1978) Surface ionization and complexation at the oxide/water interface. I. Computation of electrical double layer properties in simple electrolytes. *J. Colloid Interface Sci.* **63,** 480-499.

Dempsey B. A. and Singer P. C. (1980) The effects of calcium on the adsorption of zinc by MnO_x (s) and $Fe(OH)_3$ (am). In *Contaminants and Sediments, Volume 2, Analysis, Chemistry, and Biology* (ed. R.A. Baker), Chapter 18, pp. 333-352. Ann Arbor Science.

Dzombak D. A. and Morel F. M. M. (1990) *Surface Complexation Modeling: Hydrous Ferric Oxide.* John Wiley & Sons.

Edwards M. and Benjamin M. M. (1989) Regeneration and reuse of iron hydroxide adsorbents in treatment of metal-bearing wastes. *J. Water Pollut. Control Fed.* **61,** 481-490.

Fan H. and Anderson P. R. (1996) Development and evaluation of Mn oxide-coated composite adsorbent for the removal and recovery of heavy metals from metal contaminated wastewater. *Proceedings of the 50th Industrial Waste Conference*, pp. 217-226. Ann Arbor Press.

Farley K. J., Dzombak D. A., and Morel F. M. M. (1985) A surface precipitation model for the sorption of cations on metal oxides. *J. Colloid Interface Sci.* **106,** 226-242.

Ford R. G., Kemner K. M., and Bertsch P. M. (1999) Influence of sorbate-sorbent interactions on the crystallization kinetics of nickel- and lead-ferrihydrite coprecipitates. *Geochim. Cosmochim. Acta* **63,** 39-48.

Gadde R. R. and Laitinen H. A. (1973) Study of the sorption of lead by hydrous ferric oxide. *Environ. Letters* **5,** 223-235.

Gadde R. R. and Laitinen H. A. (1974) Studies of heavy metal adsorption by hydrous iron and manganese oxides. *Anal. Chem.* **46,** 2022-2026.

Gao Y., Sengupta A. K., and Simpson D. (1995) A new hybrid inorganic sorbent for heavy metals removal. *Water Res.* **29,** 2195-2205.

Goldberg S. (1991) Sensitivity of surface complexation modeling to the surface site density parameter. *J. Colloid Interface Sci.* **145,** 1-9.

Goovaerts P., Semrau J., and Lontoh S. (2001) Monte carlo analysis of uncertainty attached to microbial pollutant degradation rates. *Environ. Sci. Technol.* **35,** 3924-3930.

Gunneriusson L. (1994) Composition and stability of Cd(II)-chloro and –hydroxo complexes at the goethite (∝-FeOOH)/water interface. *J. Colloid Interface Sci.* **163,** 484-492.

Gunneriusson L., Lovgren L., and Sjoberg S. (1994) Complexation of Pb(II) at the goethite (∝-FeOOH)/water interface: The influence of chloride. *Geochim. Cosmochim. Acta* **58,** 4973-4983.

Harvey D. T. and Linton R. W. (1984) X-ray photoelectron spectroscopy (XPS) of adsorbed zinc on amorphous hydrous ferric oxide. *Colloids Surf.* **11,** 81-96.

Hayes K. F. (1987) Equilibrium, spectroscopic, and kinetic studies of ion adsorption at the oxide/aqueous interface. Ph.D. dissertation. Stanford University.

Hayes K. F. and Katz L. E. (1996) Application of x-ray absorption spectroscopy for surface complexation modeling of metal ion sorption. In *Physics and Chemistry of Mineral Surfaces* (ed. P.V. Brady), pp. 147-223. CRC Press.

Hayes K. F. and Leckie J. O. (1986) Mechanism of lead ion adsorption at the goethite-water interface. In *Geochemical Processes at Mineral Surfaces* (eds. J.A. Davis and K.F. Hayes), ACS Symposium Series 323, pp. 114-141. American Chemical Society.

Hayes K. F. and Leckie J. O. (1987) Modeling ionic strength effects on cation adsorption at the hydrous oxide/solution interfaces. *J. Colloid Interface Sci.* **115,** 564-572.

Hayes K. F., Redden G., Ela W., and Leckie J. O. (1991) Surface complexation models: An evaluation of model parameter estimation using FITEQL and oxide mineral titration data. *J. Colloid Interface Sci.* **142,** 448-469.

Hiemstra T. and Van Riemsdijk W. H. (1996) A surface structural approach to ion adsorption: The charge distribution (CD) model. *J. Colloid Interface Sci.* **179,** 488-508.

Hiemstra T., Van Riemsdijk W. H., and Bolt G. H. (1989a) Multisite proton adsorption modeling at the solid/solution interface of (hydr)oxides: A new approach. I. Model description and evaluation of intrinsic reaction constants. *J. Colloid Interface Sci.* **133,** 91-104.

Hiemstra T., De Wit J. C. M., and Van Riemsdijk W. H. (1989b) Multisite proton adsorption modeling at the solid/solution interface of (hydr)oxides: A new approach. II. Application to various important (hydr)oxides. *J. Colloid Interface Sci.* **133,** 105-117.

Hohl H. and Stumm W. (1976) Interaction of Pb^{2+} with hydrous γ-Al_2O_3. *J. Colloid Interface Sci.* **55,** 281-288.

Hsi C-K. D. and Langmuir D. (1985) Adsorption of uranyl onto ferric oxyhydroxides: Application of the surface complexation site-binding model. *Geochim. Cosmochim. Acta* **49,** 1931-1941.

Huang C. P. and Stumm W. (1973) Specific adsorption of cations on hydrous γ-Al_2O_3. *J. Colloid Interface Sci.* **43,** 409-420.

Hunter K. A., Hawke D. J., and Choo L. K. (1988) Equilibrium adsorption of thorium by metal oxides in marine electrolytes. *Geochim. Cosmochim. Acta* **52,** 627-636.

Kanungo S. B. (1994) Adsorption of cations on hydrous oxides of iron. II. Adsorption of Mn, Co, Ni, and Zn onto amorphous FeOOH from simple electrolyte solutions as well as from a complex electrolyte solution resembling seawater in major ion content. *J. Colloid Interface Sci.* **162,** 93-102.

Karthikeyan K. G., Elliott H. A., and Cannon F. S. (1997) Adsorption and coprecipitation of copper with the hydrous oxides of iron and aluminum. *Environ. Sci. Technol.* **31,** 2721-2725.

Karthikeyan K. G. and Elliott H. A. (1999) Surface complexation modeling of copper sorption by hydrous oxides of iron and aluminum. *J. Colloid Interface Sci.* **220,** 88-95.

Katz L. E. and Boyle-Wight E. J. (2001) Application of spectroscopic methods to sorption model parameter estimation. In *Physical and Chemical Processes of Water and Solute Transport/Retention in Soil*, (eds. H.M. Selim and D.L. Sparks), SSSA Special Publication No. 56, pp. 213-255. Soil Science Society of America.

Katz L. E. and Hayes K. F. (1995a) Surface complexation modeling. I. Strategy for modeling monomer complex formation at moderate surface coverage. *J. Colloid Interface Sci.* **170,** 477-490.

Katz L. E. and Hayes K. F. (1995b) Surface complexation modeling. II. Strategy for modeling polymer and precipitation reactions at high surface coverage. *J. Colloid Interface Sci.* **170,** 491-501.

Khodadoust A. P., Sorial G. A., Wilson G. J., Suidan M. T., Griffiths R. A., and Brenner R. C. (1999) Integrated system for remediation of contaminated soils. *J. Environ. Eng.* **125,** 1033-1041.

Kinniburgh D. G. and Jackson M. L. (1982) Concentration and pH dependence of calcium and zinc adsorption by iron hydrous oxide gel. *Soil Sci. Soc. Am. J.* **46,** 56-61.

Kinniburgh D. G., Jackson M. L., and Syers J. K. (1976) Adsorption of alkaline earth, transition, and heavy metal cations by hydrous oxide gels of iron and aluminum. *Soil Sci. Soc. Am. J.* **40,** 796-799.

Kinniburgh D. G., Sridhar K., and Jackson M. L. (1977) Specific adsorption of zinc and cadmium by iron and aluminum hydrous oxides. Proceedings of the 15th Hanford Life Sciences Symposium on Biological Implications of Metals in the Environment, Hanford, Washington, pp. 231-239.

Kooner Z. S., Cox C. D., and Smoot J. L. (1995) Prediction of adsorption of divalent heavy metals at the goethite/water interface by surface complexation modeling. *Environ. Toxicol. Chem.* **14,** 2077-2083.

Koretsky C. (2000) The significance of surface complexation reactions in hydrologic systems: A geochemist's perspective. *J. Hydrol.* **230,** 127-171.

Koretsky C. M., Sverjensky D. A., and Sahai N. (1998) A model of surface site types on oxide and silicate minerals based on crystal chemistry: Implications for site types and densities, multi-site adsorption, surface infrared spectroscopy, and dissolution kinetics. *Am. J. Sci.* **298,** 349-438.

Langmuir I. (1918) The adsorption of gases on plane surfaces of glass, mica, and platinum. *J. Am. Chem. Soc.* **40,** 1361-1403.

Leckie J. O., Benjamin M. M., Hayes K. F., Kaufman G., and Altmann S. (1980) *Adsorption/Coprecipitation of Trace Elements from Water with Iron Oxyhydroxide.* CS-1513, Electric Power Research Institute, Palo Alto, California.

Lumsdon D. G. and Evans L. J. (1994) Surface complexation model parameters for goethite (α-FeOOH). *J. Colloid Interface Sci.* **164,** 119-125.

Manceau A., Charlet L., Boisset M. C., Didier B., and Spandini L. (1992) Sorption and speciation of heavy metals on hydrous iron and manganese oxides. From microscopic to macroscopic. *Appl. Clay Sci.* **7,** 201-223.

Manceau A., Schlegel M. L., Musso M., Sole V. A., Gauthier C., Petit P. E., and Trolard F. (2000) Crystal chemistry of trace elements in natural and synthetic goethite. *Geochim. Cosmochim. Acta* **64,** 3643-3661.

Marmier N., Delisee A., and Fromage F. (1999) Surface complexation modeling of Yb(III), Ni(II), and Cs(I) sorption onto magnetite. *J. Colloid Interface Sci.* **211,** 54-60.

Merrill D. T., Maroney P. M., and Parker D. S. (1985) *Trace Element Removal by Coprecipitation with Amorphous Iron Oxyhydroxide: Engineering Evaluation.* CS-4087, Electric Power Research Institute, Palo Alto, California.

Misak N. Z., Ghoneimy H. F., and Morcos T. N. (1996) Adsorption of Co^{2+} and Zn^{2+} ions on hydrous Fe(III), Sn(IV), and Fe(III)/Sn(IV) oxides. II. Thermal behavior of loaded oxides, isotopic exchange equilibria, and percentage adsorption-pH curves. *J. Colloid Interface Sci.* **184,** 31-43.

Nordstrom D. K. and Ball J. W. (1989) Mineral saturation states in natural waters and their sensitivity to thermodynamic and analytic errors. *Sci. Geol. Bull.* **42,** 269-280.

O'Day P. A., Carroll S. A., and Waychunas G. A. (1998) Rock-water interactions controlling zinc, cadmium, and lead concentrations in surface waters and sediments, U.S. tri-state mining district. 1. Molecular identification using x-ray absorption spectroscopy. *Environ. Sci. Technol.* **32,** 943-955.

Palmqvist U., Ahlberg E., Lovgren L., and Sjoberg S. (1999) Competitive metal ion adsorption in goethite systems using *in situ* voltammetric methods and potentiometry. *J. Colloid Interface Sci.* **218,** 388-396.

Robertson A. P. and Leckie J. O. (1997) Cation binding predictions of surface complexation models: Effects of pH, ionic strength, cation loading, surface complex, and model fit. *J. Colloid Interface Sci.* **188,** 444-472.

Robertson A. P. and Leckie J. O. (1998) Acid/base, copper binding, and Cu^{2+}/H^{+} exchange properties of goethite, an experimental and modeling study. *Environ. Sci. Technol.* **32,** 2519-2530.

Roe A. L., Hayes K. F., Chisholm-Brause C., Brown G. E. Jr., Parks G. A., Hodgson K. O., and Leckie J. O. (1991) In situ x-ray absorption study of lead ion surface complexes at the goethite-water interface. *Langmuir* **7,** 367-373.

Sahai N. and Sverjensky D. A. (1997) Solvation and electrostatic model for specific electrolyte adsorption. *Geochim. Cosmochim. Acta* **61,** 2827-2848.

Sarkar D., Essington M. E., and Misra K. C. (1999) Adsorption of mercury(II) by variable charge surfaces of quartz and gibbsite. *Soil Sci. Soc. Am. J.* **63,** 1626-1636.

Sauve S., Hendershot W., and Allen H. E. (2000) Solid-solution partitioning of metals in contaminated soils: Dependence on pH, total metal burden, and organic matter. *Environ. Sci. Technol.* **34,** 1125-1131.

Schecher W. D. and Driscoll C. T. (1987) An evaluation of uncertainty associated with aluminum equilibrium calculations. *Water Resour. Res.* **23,** 525-534.

Schecher W. D. and Driscoll C. T. (1988) An evaluation of the equilibrium calculations within acidification models: The effect of uncertainty in measured chemical components. *Water Resour. Res.* **24,** 533-540.

Scheinost A. C., Abend S., Pandya K. I., and Sparks D. L. (2001) Kinetic controls on Cu and Pb sorption by ferrihydrite. *Environ. Sci. Technol.* **35,** 1090-1096.

Schindler P. and Kamber H. R. (1968) Die Aciditat von Silanolgruppen. *Helv. Chim. Acta* **51,** 1781-1786.

Schlegel M. L., Manceau A., and Charlet L. (1997) EXAFS study of Zn and ZnEDTA sorption at the goethite (∝-FeOOH)/water interface. *J. Phy. IV Fr.* **7,** 823-824.

Schultz M. F., Benjamin M. M., and Ferguson J. F. (1987) Adsorption and desorption of metals on ferrihydrite: Reversibility of the reaction and sorption properties of the regenerated solid. *Environ. Sci. Technol.* **21,** 863-869.

Smith E. H. (1998) Surface complexation modeling of metal removal by recycled iron sorbent. *J. Environ. Eng.* **124,** 913-920.

Smith E. H. and Amini A. (2000) Lead removal in fixed beds by recycled iron sorbent. *J. Environ. Eng.* **126,** 58-65.

Smith R. W. and Jenne E. A. (1988) *Compilation, Evaluation, and Prediction of Triple-Layer Model Constants for Ions on Fe(III) and Mn(IV) Hydrous Oxides.* PNL-6754, Pacific Northwest Laboratory, Battelle Memorial Institute.

Sparks D. L. (1995) *Environmental Soil Chemistry.* Academic Press.

Sposito G. (1984) *The Surface Chemistry of Soils.* Oxford University Press.

Stumm W. (1992) *Chemistry of the Solid-Water Interface.* John Wiley & Sons.

Stumm W., Huang C. P., and Jenkins S. R. (1970) Specific chemical intercation affecting the stability of dispersed systems. *Croat. Chem. Acta* **42,** 223-245.

Sverjensky D. A. (2001) Interpretation and prediction of triple-layer model capacitances and the structure of the oxide-electrolyte-water interface. *Geochim. Cosmochim. Acta* **65,** 3643-3655.

Sverjensky D. A. and Sahai N. (1996) Theoretical prediction of single-site surface-protonation equilibrium constants for oxides and silicates in water. *Geochim. Cosmochim. Acta* **60,** 3773-3797.

Swallow K. C. (1978) Adsorption of trace metals by hydrous ferric oxide. Ph.D. dissertation. Massachusetts Institute of Technology.

Swallow K. C., Hume D. N., and Morel F. M. M. (1980) Sorption of copper and lead by hydrous ferric oxide. *Environ. Sci. Technol.* **14,** 1326-1331.

Theis T. L., Iyer R., and Ellis S. K. (1992) Evaluating a new granular iron oxide for removing lead from drinking water. *J. Am. Water Works Assoc.* **84,** 101-105.

Tiffreau C., Lutzenkirchen J., and Behra P. (1995) Modeling the adsorption of mercury(II) on (hydr)oxides. I. Amorphous iron oxide and α-quartz. *J. Colloid Interface Sci.* **172,** 82-93.

Trivedi P. (2001) Predicting thermodynamic and transport parameters for metal contaminant sorption to hydrated metal oxides in aquatic systems. Ph.D. dissertation. New Jersey Institute of Technology.

Trivedi P. and Axe L. (2000) Modeling Cd and Zn sorption to hydrous metal oxides. *Environ. Sci. Technol.* **34,** 2215-2223.

U.S. EPA Office of Water Regulations and Standards (1996) *Code of Federal Regulations, Protection of the Environment.* 40 CFR 414.91, Office of the Federal Register, Washington, DC.

Venema P., Hiemstra T., and Van Riemsdijk W. H. (1996) Multisite adsorption of cadmium on goethite. *J. Colloid Interface Sci.* **183,** 515-527.

Waite T. D., Davis J. A., Payne T. E., Waychunas G. A., and Xu N. (1994) Uranium(VI) adsorption to ferrihydrite: Application of a surface complexation model. *Geochim. Cosmochim. Acta* **58,** 5465-5478.

Waychunas G. A., Fuller C. C., and Davis J. A. (1995) *Stanford Synchrotron Radiation Laboratory Activity Report.* pp. 78-80.

Westall J. and Hohl H. (1980) A comparison of electrostatic models for the oxide/solution interface. *Adv. in Colloid Interface Sci.*, **12,** 265-294.

Yates D. E., Levine S., and Healy T. W. (1974) Site-binding model of the electrical double layer at the oxide/water interface. *J. Chem. Farady Trans. I* **70,** 1807-1818.

Chapter 2

THERMODYNAMIC FRAMEWORK AND GEOCHEMICAL MODELING APPROACH

As part of this Ph.D. project, a unique, state-of-the-art surface complexation modeling toolbox was implemented in the OLI Software (OLI Systems, Inc., Morris Plains, New Jersey). The OLI Software is the DuPont Company's preferred aqueous electrolyte simulation code. In this research project, the OLI Software served as the experimental laboratory for these investigations. The macroscopic and spectroscopic data used as a basis for the modeling studies was generated by Paras Trivedi, a Post Doctoral Associate working with Dr. Donald L. Sparks at the University of Delaware. This was a joint research program funded by the DuPont Company through the Delaware Research Partnership.

2.1 Thermodynamic Framework for the Surface Complexation Models

The generalized two-layer model (GTLM) and the modified triple-layer model (TLM) were the two surface complexation models (SCMs) evaluated and used over the course of this research project. The nonelectrostatic model (NEM) was briefly considered during analysis of the potentiometric titration data for 2-line ferrihydrite. Structures of the interfacial region for the GTLM and modified TLM are shown in Figure 2.1. In this figure, M^{m+} is a metal ion with charge $m+$, L^{l-} is a ligand with charge $l-$, C^+ is a background electrolyte cation, and A^- is a background electrolyte anion. The remaining SCM parameters are defined below.

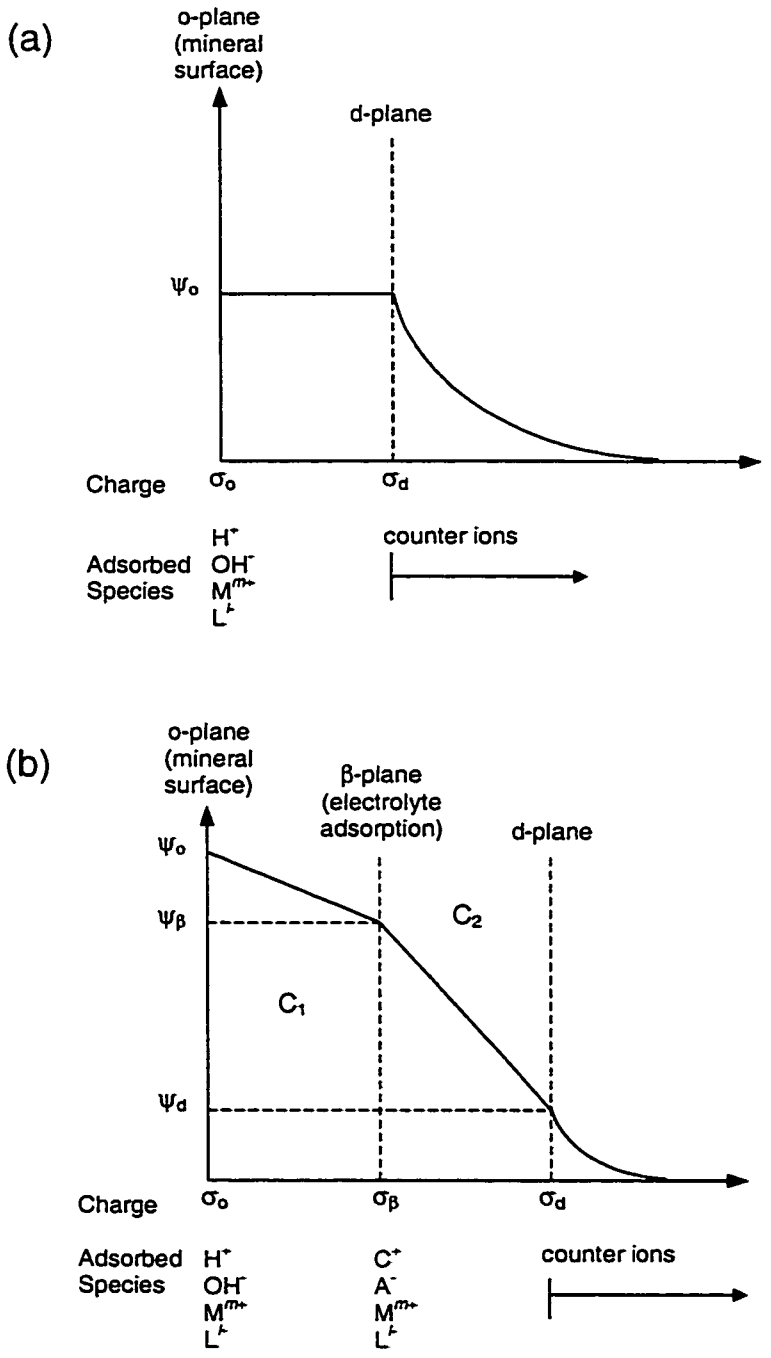

Figure 2.1 **Structure of the oxide-water interface for the (a) generalized two-layer model and (b) modified triple-layer model (after Goldberg, 1995).**

The Diffuse-Layer Model (DLM) was proposed by Stumm and students (Stumm et al., 1970; Huang & Stumm, 1973) and later developed as the GTLM by Dzombak and Morel (1990). The GTLM is an expansion of the basic DLM in that two site types, rather than one, are used for cation binding and surface precipitation is allowed at high cation and anion concentrations. The DLM/GTLM assumptions include (Goldberg, 1995):

1. All surface complexes are inner-sphere complexes.
2. The background electrolyte ions do not form surface complexes.
3. The surface is composed of two planes of charge.
4. The surface charge-potential relationships are given by the following equations:

$$\Psi_o = \Psi_d \qquad [2.1]$$

$$\sigma_d = -\left(8\,\varepsilon_o\,\varepsilon_w\,R\,T\,I\,\rho\,10^3\right)^{1/2}\sinh\left[\frac{ZF\Psi_d}{2RT}\right] \qquad [2.2]$$

$$\sigma_d = -\mathrm{sgn}(\Psi_d)\left\{2\,\varepsilon_o\,\varepsilon_w\,R\,T\rho\,10^3\sum_{i=1}^{n} m_i\left[\exp\left(\frac{-z_i F\Psi_d}{RT}\right)-1\right]\right\}^{1/2} \qquad [2.3]$$

where:

Ψ_o = potential at surface o-plane, V

Ψ_d = potential at the diffuse layer or d-plane, V

σ_d = surface charge density at the d-plane, Coul/m^2

$\mathrm{sgn}(\Psi_d)$ = +1 if $\Psi_d > 0$

= −1 if $\Psi_d < 0$

ε_o = permittivity of free space, 8.854E-12 Coul^2/J-m

ε_w = dielectric constant of water at T, dimensionless

R = gas constant, 8.314 J/mole-K = 8.314 coul-V/mole-K

T = absolute temperature, K

I = ionic strength, mol/kg H_2O

ρ = solution density, kg/L

Z = valence of background electrolyte, dimensionless

F = Faraday constant, 96,485 Coul/mole

m_i = molality of electrolyte *i*, mole/kg H_2O

z_i = valence of electrolyte *i*, dimensionless

Eq. [2.2] applies for symmetrical electrolytes, and Eq. [2.3] is the general form that applies for both symmetrical and asymmetrical electrolytes.

A representative sample of equilibrium reactions for protonation-deprotonation and metal and ligand surface complexation is shown below. The list of possible metal and ligand surface reactions is much more extensive.

$$\equiv XOH + H^+ \Leftrightarrow \equiv XOH_2^+ \quad [2.4]$$

$$\equiv XOH \Leftrightarrow \equiv XO^- + H^+ \quad [2.5]$$

$$\equiv XOH + M^{m+} \Leftrightarrow \equiv XOM^{(m-1)+} + H^+ \quad [2.6]$$

$$\equiv XOH + M^{m+} + H_2O \Leftrightarrow \equiv XOMOH^{(m-2)+} + 2H^+ \quad [2.7]$$

$$2(\equiv XOH) + M^{m+} \Leftrightarrow (\equiv XO)_2M^{(m-2)+} + 2H^+ \quad [2.8]$$

$$\equiv XOH + M^{m+} \Leftrightarrow \equiv XOHM^{m+} \quad [2.9]$$

$$\equiv XOH + L^{l-} \Leftrightarrow \equiv XL^{(l-1)-} + OH^- \quad [2.10]$$

$$\equiv XOH + L^{l-} + 2H^+ \Leftrightarrow \equiv XHL^{(l-2)-} + H_2O \quad [2.11]$$

The intrinsic equilibrium constants for Eqs. [2.4] through [2.11] are given by the following mass law expressions:

$$K_{a1}^{int} = \frac{a_{\equiv XOH_2^+}}{a_{\equiv XOH}\, a_{H^+}} \exp\left(\frac{F\Psi_o}{RT}\right) \qquad [2.12]$$

$$K_{a2}^{int} = \frac{a_{\equiv XO^-}\, a_{H^+}}{a_{\equiv XOH}} \exp\left(\frac{-F\Psi_o}{RT}\right) \qquad [2.13]$$

$$K_{XOM^{(m-1)+}}^{int} = \frac{a_{\equiv XOM^{(m-1)+}}\, a_{H^+}}{a_{\equiv XOH}\, a_{M^{m+}}} \exp\left(\frac{(m-1)F\Psi_o}{RT}\right) \qquad [2.14]$$

$$K_{XOMOH^{(m-2)+}}^{int} = \frac{a_{\equiv XOMOH^{(m-2)+}} \left(a_{H^+}\right)^2}{a_{\equiv XOH}\, a_{M^{m+}}\, a_{H2O}} \exp\left(\frac{(m-2)F\Psi_o}{RT}\right) \qquad [2.15]$$

$$K_{(XO)_2M^{(m-2)+}}^{int} = \frac{a_{(\equiv XO)_2M^{(m-2)+}} \left(a_{H^+}\right)^2}{\left(a_{\equiv XOH}\right)^2 a_{M^{m+}}} \exp\left(\frac{(m-2)F\Psi_o}{RT}\right) \qquad [2.16]$$

$$K_{XOHM^{m+}}^{int} = \frac{a_{\equiv XOHM^{m+}}}{a_{\equiv XOH}\, a_{M^{m+}}} \exp\left(\frac{mF\Psi_o}{RT}\right) \qquad [2.17]$$

$$K_{XL^{(l-1)-}}^{int} = \frac{a_{\equiv XL^{(l-1)-}}\, a_{OH^-}}{a_{\equiv XOH}\, a_{L^{l-}}} \exp\left(\frac{-(l-1)F\Psi_o}{RT}\right) \qquad [2.18]$$

$$K_{XHL^{(l-2)-}}^{int} = \frac{a_{\equiv XHL^{(l-2)-}}\, a_{H_2O}}{a_{\equiv XOH}\, a_{L^{l-}} \left(a_{H^+}\right)^2} \exp\left(\frac{-(l-2)F\Psi_o}{RT}\right) \qquad [2.19]$$

While written as activities in the mass law expressions, molalities are actually used for the surface complex species in equilibrium computations. The commonly accepted assumption is that the ratio of the activity coefficients for the surface species is equal to 1.0.

The charge balance equation is given by:

$$\sigma_o = \left[\frac{F\rho}{AC_s}\right]\{[\equiv XOH_2^+] - [\equiv XO^-] + (m\text{-}1)[\equiv XOM^{(m-1)+}] +$$

$$(m\text{-}2)[\equiv XOMOH^{(m-2)+}] + (m\text{-}2)[(\equiv XO)_2M^{(m-2)+}] + (m)[\equiv XOHM^{m+}] + \ldots$$

$$-(l\text{-}1)[\equiv XL^{(l-1)-}] - (l\text{-}2)[\equiv XHL^{(l-2)-}] - \ldots\} \qquad [2.20]$$

where σ_o is the surface charge density at the o-plane (Coul/m^2), A is the specific surface area (m^2/g), C_S is the sorbent concentration (g/L), and [...] is the concentration of each charged surface complex (mole/kg H_2O). The mass balance expression is given by:

$$[\equiv XOH]_T = [\equiv XOH] + [\equiv XOH_2^+] + [\equiv XO^-] + [\equiv XOM^{(m-1)+}] +$$

$$[\equiv XOMOH^{(m-2)+}] + [(\equiv XO)_2M^{(m-2)+}] + [\equiv XOHM^{m+}] + \ldots +$$

$$[\equiv XL^{(l-1)-}] + [\equiv XHL^{(l-2)-}] + \ldots \qquad [2.21]$$

$[\equiv XOH]_T$ is the total concentration of sites in mole/kg H_2O, and is related to the surface site density, N_s (sites/nm^2), by

$$[\equiv XOH]_T = N_s\, A\, C_S\, 10^{18}/(N_A\, \rho) \qquad [2.22]$$

where N_A is Avogadro's number (6.02252 x 10^{23} sites/mole).

Davis et al. (1978) and Davis and Leckie (1978) developed the original triple-layer model as an extension of the site binding model of Yates et al. (1974). The original TLM was later modified by Hayes and Leckie (1986, 1987) to include inner-sphere surface complexation, and is often referred to as the modified TLM. The modified TLM assumptions are (Goldberg, 1995):

1. Protons and hydroxyl ions form inner-sphere complexes.

2. The sorbing metal cations and ligands form either inner- or outer-sphere surface complexes.

3. The background electrolyte ions form outer-sphere surface complexes.

4. The surface is composed of three planes of charge.

5. The surface charge-potential relationships are given by Eq. [2.2] or [2.3] as well as by:

$$\sigma_o = C_1(\Psi_o - \Psi_\beta) \qquad [2.23]$$

$$\sigma_d = C_2(\Psi_d - \Psi_\beta) \qquad [2.24]$$

where C_1 is the inner-layer capacitance (Farad/m^2), C_2 is the outer-layer capacitance (Farad/m^2), and Ψ_β is the potential at the β-plane (Volts).

The equilibrium reactions and the associated mass law expressions given by Eqs. [2.4] through [2.19] apply for the modified TLM as well. In addition, examples of some outer-sphere surface complexation reactions are given by the following equilibrium and mass-law expressions:

$$\equiv XOH + C^+ \Leftrightarrow \equiv XO^- - C^+ + H^+ \qquad [2.25]$$

$$\equiv XOH + A^- + H^+ \Leftrightarrow \equiv XOH_2^+ - A^- \qquad [2.26]$$

$$\equiv XOH + M^{m+} \Leftrightarrow \equiv XO^- - M^{m+} + H^+ \qquad [2.27]$$

$$\equiv XOH + L^{l-} + H^+ \Leftrightarrow \equiv XOH_2^+ - L^{l-} \qquad [2.28]$$

$$\equiv XOH + M^{m+} + H_2O \Leftrightarrow \equiv XO^- - MOH^{(m-1)+} + 2H^+ \qquad [2.29]$$

$$\equiv XOH + L^{l-} + 2H^+ \Leftrightarrow \equiv XOH_2^+ - LH^{(l-1)-} \qquad [2.30]$$

$$K^{int}_{XO^- - C^+} = \frac{a_{\equiv XO^- - C^+}\, a_{H^+}}{a_{\equiv XOH}\, a_{C^+}} \exp\left(\frac{F(\Psi_\beta - \Psi_o)}{RT}\right) \qquad [2.31]$$

$$K^{int}_{XOH_2^+ - A^-} = \frac{a_{\equiv XOH_2^+ - A^-}}{a_{\equiv XOH}\, a_{A^-}\, a_{H^+}} \exp\left(\frac{F(\Psi_o - \Psi_\beta)}{RT}\right) \qquad [2.32]$$

$$K^{int}_{XO^- - M^{m+}} = \frac{a_{\equiv XO^- - M^{m+}}\, a_{H^+}}{a_{\equiv XOH}\, a_{M^{m+}}} \exp\left(\frac{F(m\Psi_\beta - \Psi_O)}{RT}\right) \quad [2.33]$$

$$K^{int}_{XOH_2^+ - L^{l-}} = \frac{a_{\equiv XOH_2^+ - L^{l-}}}{a_{\equiv XOH}\, a_{L^{l-}}\, a_{H^+}} \exp\left(\frac{F(\Psi_O - l\Psi_\beta)}{RT}\right) \quad [2.34]$$

$$K^{int}_{XO^- - MOH^{(m-1)+}} = \frac{a_{\equiv XO^- - MOH^{(m-1)+}} (a_{H^+})^2}{a_{\equiv XOH}\, a_{M^{m+}}\, a_{H2O}} \exp\left(\frac{F[(m-1)\Psi_\beta - \Psi_O]}{RT}\right) \quad [2.35]$$

$$K^{int}_{XOH_2^+ - LH^{(l-1)-}} = \frac{a_{\equiv XOH_2^+ - LH^{(l-1)-}}}{a_{\equiv XOH}\, a_{L^{l-}} (a_{H^+})^2} \exp\left(\frac{F[\Psi_O - (l-1)\Psi_\beta]}{RT}\right) \quad [2.36]$$

As before, not all possible metal and ligand surface complexation reactions are shown.

The charge balance expressions are:

$$\sigma_o + \sigma_\beta + \sigma_d = 0 \quad [2.37]$$

$$\sigma_o = \left[\frac{F\rho}{AC_s}\right]\{[\equiv XOH_2^+] - [\equiv XO^-] + (m\text{-}1)[\equiv XOM^{(m-1)+}] +$$

$$(m\text{-}2)[\equiv XOMOH^{(m-2)+}] + (m\text{-}2)[(\equiv XO)_2M^{(m-2)+}] +$$

$$(m)[\equiv XOHM^{m+}] + \ldots - (l\text{-}1)[\equiv XL^{(l-1)-}] - (l\text{-}2)[\equiv XHL^{(l-2)-}] -$$

$$[\equiv XO^- - C^+] + [\equiv XOH_2^+ - A^-] - [\equiv XO^- - M^{m+}] + [\equiv XOH_2^+ - L^{l-}] -$$

$$[\equiv XO^- - MOH^{(m-1)+}] + [\equiv XOH_2^+ - LH^{(l-1)-}] - \ldots\} \quad [2.38]$$

$$\sigma_\beta = \left[\frac{F\rho}{AC_s}\right]\{[\equiv XO^- - C^+] - [\equiv XOH_2^+ - A^-] + (m)[\equiv XO^- - M^{m+}] -$$

$$(l)[\equiv XOH_2^+ - L^{l-}] + (m\text{-}1)[\equiv XO^- - MOH^{(m-1)+}] + \ldots -$$

$$(l\text{-}1)[\equiv XOH_2^+ - LH^{(l-1)-}] - \ldots\} \quad [2.39]$$

where σ_β is the surface charge density at the β-plane (Coul/m^2), and *m* and *l* are the charges on the portions of the surface complexes located in that particular surface plane. The mass balance expression is given by:

$$[\equiv XOH]_T = [\equiv XOH] + [\equiv XOH_2^+] + [\equiv XO^-] + [\equiv XOM^{(m-1)+}] + [\equiv XOHM^{m+}] + [\equiv XOMOH^{(m-2)+}] + [(\equiv XO)_2M^{(m-2)+}] + [\equiv XL^{(l-1)-}] + [\equiv XHL^{(l-2)-}] + [\equiv XO^- - C^+] + [\equiv XOH_2^+ - A^-] + [\equiv XO^- - M^{m+}] + [\equiv XOH_2^+ - L^{l-}] + [\equiv XO^- - MOH^{(m-1)+}] + [\equiv XOH_2^+ - LH^{(l-1)-}] + \ldots \quad [2.40]$$

In the NEM, all surface complexes form at the surface or o-plane; therefore, Eqs. [2.4] through [2.11], [2.21], and [2.22] are valid. The primary difference between the GTLM and the NEM is that the electrostatic contribution to Gibbs Free Energy ($\Delta G_{Coulombic}$) is ignored in the NEM. As a result, the mass law expressions (Eqs. [2.12] through [2.19]) are written in the NEM formulation without the exponential term. Equations [2.1] through [2.3], [2.20], and [2.23] through [2.40] are not applicable to the NEM.

2.2 Geochemical Modeling Code

The OLI Software (OLI Systems, Inc., Morris Plains, New Jersey) is the geochemical modeling code that was used throughout this research project. The OLI Software is a commercial aqueous-electrolyte simulation code that models chemical speciation and redox reactions, equilibria between aqueous, vapor, organic liquid, and multiple solid phases, biochemical and inorganic reaction kinetics, and other advanced phenomena, such as ion exchange, membrane separation, carbon adsorption, and metal surface complexation. This software was chosen for this project because it is the preferred aqueous simulation code within the DuPont Company, is supported by a

thermodynamic database that is continuously maintained and updated, and is based on a thermodynamic framework that can predict thermodynamic properties over a wide range of temperature, pressure, and ionic strength.

The software is built around the OLI Engine, which is the foundation for the Environmental Simulation Program (ESP), Corrosion Simulation Program (CSP), and ElectroChem. Both ESP and ElectroChem were used in this project. ESP is capable of simulating, designing, and optimizing a wide variety of chemical and environmental processes, including complete process flowsheets. Over fifteen unit operation blocks are supported by the software, including absorbers, bioreactors, clarifiers, precipitators, mixers, strippers, crystallizers, neutralizers, controllers, and sensitivity blocks. ElectroChem is the original chemistry solver, and is a powerful and flexible tool for performing equilibrium point calculations at steady state (Sanders et al., 1988).

At the heart of the OLI Engine are the databank, the thermodynamic framework, and the equation solvers (Rafal et al., 1994b). The OLI databank contains thermodynamic and physical properties for over 8,300 inorganic and organic species. This includes virtually all chemical substances of environmental concern, such as nearly all DIPPR Project 801 components,[1] the majority of the EPA's List of Lists, most European Red, Gray, and Black Lists, and the inorganic chemistry for 92 elements from the Periodic Table. In addition, 12 major chelating/complexing ligands

[1] DIPPR (Design Institute for Physical Property Data) Project 801 was sponsored through the American Institute of Chemical Engineers by numerous chemical and petroleum companies. The product of the project was an extensive compilation of physical, thermodynamic, and transport properties for over 1600 compounds.

are included. The thermodynamic variables (Gibbs free energy, enthalpy, entropy, and heat capacity) in the databank are from six main sources (Scrivner et al., 1996):

- Glushko et al. (1965-1981) and Wagman et al. (1982) are utilized as data sources for many of the aqueous species at 298.15 K.
- Gurvich et al. (1989) and Chase et al. (1985) provide data for inorganic gases and solids as a function of temperature.
- Daubert and Danner (1989) is the source of the DIPPR organic nonaqueous data.
- Oelkers et al. (1995) supplies values for many of the aqueous complexes.

Each of these sources is a large and extensive compilation of thermodynamic data. They have been carefully evaluated and are highly referenced.

The thermodynamic framework is a state-of-the-art predictive framework that serves as the basis for calculating the complex, aqueous-based chemistry in equilibrium with the optional vapor, nonaqueous liquid, and solid phases. The framework uses generalized correlations based upon regressed experimental data in the databank to predict the required thermodynamic and physical properties for the chemical system at hand (i.e., infinite-dilution, standard-state values for Gibbs free energy, enthalpy, entropy, heat capacity, and volume, liquid-phase activity coefficient corrections for systems at finite concentrations, etc.). This is in contrast to an interpolative framework, such as Pitzer and NRTL-based methods, which are not supported by generalized correlations (OLI Systems, Inc., 1995).

The mathematical models which describe the aqueous system include the appropriate equilibrium equations (i.e., one equation for each physical phase and aqueous intraphase equilibrium reaction), an electroneutrality equation (i.e., a charge

balance), and a sufficient number of material balances to complete the model (Rafal et al., 1994a). Mathematical models of this type are generally highly nonlinear and require the use of robust equation solvers to effect rapid, reliable numerical solutions. Often, as many as 25 to 500 nonlinear algebraic equations need to be solved simultaneously. The robust numerical solver code that is part of the OLI Engine accomplishes this task. More details on the numerical solution algorithm are available in Rafal et al. (1994b).

The theoretical thermodynamic framework for predicting the equilibrium properties of the aqueous electrolyte systems is explained in detail by Zemaitis et al. (1986). In a more recent publication, Rafal et al. (1994a) discuss recent advances in temperature and pressure extrapolation as well as an approach for developing the mathematical model(s) and formulating the problem. More importantly, Shock and Helgeson (1988) present a semi-theoretical method for temperature and pressure extrapolation of standard state properties, along with procedures for estimating missing parameters.

The thermodynamic framework used in the OLI Software is based upon the references cited above. More specifically, the framework uses (Rafal et al., 1994b):

- The revised Helgeson Equation-of-State for predicting the standard state partial molal Gibbs free energy, enthalpy, entropy, heat capacity, and volume of all species, including organics, in water.

- A proprietary extension to the work of Bromley and Meissner (i.e., the Bromley-Zemaitis framework) for predicting excess thermodynamic properties.

- The Pitzer and Setschenow formulation for predicting excess thermodynamic properties of molecular species in water.

- The Enhanced SRK Equation-of-State for predicting vapor and nonaqueous liquid-phase thermodynamic properties. The equation applies to sparingly water-soluble organics which form an ideal, second liquid phase.

The real significance of this framework is that it is supported by correlation and extrapolation formulations which allow for the prediction of thermodynamic properties of just about any species over a wide range of conditions (Rafal et al., 1994b).

Building upon this impressive capability, DuPont and OLI Systems, Inc. jointly funded a development project in 2000 and 2001, led by this author, to upgrade the surface complexation modeling capability in the OLI Software. The following upgrades were made to the code:

- The addition of four surface complexation models—NEM, constant capacitance model (CCM), GTLM, and modified TLM.
- The integration of the SCMs into three OLI simulation platforms—ElectroChem (point equilibrium calculations), ESP (steady-state flowsheet simulator), and DynaChem (unsteady-state, multistage simulator).
- The ability to perform nonlinear regression of raw data to obtain equilibrium constants for the surface reactions.
- An allowance for multiple sorbents (inorganic, organic, and bacterial) and site types.
- The addition of the Dzombak & Morel (1990) database as a private databank.
- Revisions to the advanced uncertainty analysis module in ElectroChem to allow access to the SCM parameters.

These improvements to the OLI Software directly benefited this research project.

2.3 Modeling Protocol

Hayes and Katz (1996) emphasize that the major elements of surface complexation modeling involve

- selecting an SCM (e.g., GTLM or modified TLM),
- determining the metal (hydr)oxide surface parameters for the selected SCM from potentiometric titration and sorbent characterization data, and
- determining the intrinsic equilibrium constants for metal sorption using constant-pH isotherm, pH sorption edge, and spectroscopic data.

For the GTLM, the oxide surface parameters include the sorbent's specific surface area (A_s), the surface site density (N_s), and the two surface protolysis constants (K_{a1}^{int} and K_{a2}^{int}) given by Eqs. [2.12] and [2.13]. For the modified TLM, four additional parameters are needed to model the surface charging behavior: two interfacial capacitances (C_1 and C_2) and two background-electrolyte sorption equilibrium constants (K_{C+}^{int} and K_{A-}^{int}) given by Eqs. [2.31] and [2.32]. Simulating trace-metal sorption involves selecting the minimum numbers of SCM reactions and site types that are needed to describe the isotherm and edge data over a wide range of conditions. The choice of reactions is constrained by a knowledge of the proton stoichiometry and the type of surface species formed (inner- vs. outer-sphere). These major elements of surface complexation modeling are to some extent iterative. For example, if the site density and/or number of site types must be adjusted to fit a set of metal sorption isotherms and edges, then the surface protolysis and electrolyte sorption constants must be redetermined by re-regression of the potentiometric titration data. It will often be found, too, that several sets of SCM parameters will fit the titration and metal

sorption data equally well. In this case, the hope is that spectroscopic data will help to constrain the choices for metal surface species.

A more detailed modeling protocol is given below that generally applies to any SCM. This protocol was used to guide the modeling investigations conducted during this project.

1. Using potentiometric titration data at three different ionic strengths for 2-line ferrihydrite and the nonlinear regression routine in the OLI Software, determine a valid set(s) of SCM metal (hydr)oxide surface parameters for the SCM of interest. For the GTLM, this should be done for a range of site density (N_s) values at a fixed specific surface area, giving K_{a1}^{int} and K_{a2}^{int} as a function of N_s. For the modified TLM, this should be completed for a range of values for site density, ΔpK_a,[2] and C_1 at fixed specific surface area and C_2. This will produce a range of valid parameter sets for the modified TLM that will be later optimized with the metal cation sorption data. The criteria for judging a "best fit" to the titration data will be the value of R_{avg} obtained from the OLI Software's nonlinear regression program, in addition to visual inspection of a plot of the model titration curves with the actual data. For each regressed data point, the OLI nonlinear regression program calculates the ratio of the experimental value to the model-calculated value (or vice versa), such that R is always ≥ 1.0. A perfect fit is when $R = 1.0$. R_{avg}, therefore, will be the arithmetic average of the R values for all data points comprising a set of regressed titration data.

2. Evaluate the spectroscopic results and the impact of ionic strength on metal sorption to guide the selection of divalent metal cation surface reactions at low to moderate surface coverage. Hayes and Katz (1996) note that past XAFS studies have suggested that mononuclear species predominate at low to moderate surface coverage (0.1 to 10%) for strongly sorbing metals and at all coverages for weakly sorbing metals. Ionic-

[2] $\Delta pK_a = (pK_{a1}^{int} + pK_{a2}^{int})$ when the protonation/deprotonation reactions are written as in Eqs. [2.4] and [2.5].

strength dependence has often been used to differentiate between inner- and outer-sphere surface complexes (applies to TLM only). In this project, pH sorption edges generated at 2 or more ionic strengths will be used to assess the ionic-strength dependence of metal sorption.

3. Evaluate the spectroscopic results and the shape of the constant-pH isotherms to determine the need for multinuclear surface complexation reactions at higher surface coverage (i.e., surface polymers and surface precipitates).

4. Consider the behavior of the constant-pH sorption isotherms for the metals of interest to determine a reasonable starting point for site density and the possibility of site heterogeneity (i.e., the need for more than one type of site). Robertson and Leckie (1997) contend that if the slope of the isotherm curve(s) is less than 1.0 at low surface coverage, then site heterogeneity is probable.

5. Select an initial set of oxide surface parameters (from Step 1) and metal surface species for the SCM-of-interest based on the insights gained from Steps 2 through 4. These surface parameters and species will be used to regress the constant-pH isotherm data for the metal-of-interest to obtain a set of best-fit intrinsic equilibrium constants for single-solute sorption. These best-fit constants will then be used to assess how the model simulates the pH sorption edge data at multiple ionic strengths. Different combinations of viable metal surface complexes will be considered. The minimum numbers of site types and species that provide a good fit of the isotherm and edge data will be considered optimum. Once again, R_{avg} values for the x and y data from the nonlinear regression routine, plus visual inspection of graphical output, will be used to assess the best fit. This is also an iterative process, whereby the oxide surface parameters will need to be adjusted if surface site density must be changed. If there is evidence for site heterogeneity and/or multinuclear surface species, it may be necessary to regress the isotherm data in steps (low to high coverage), building complexity in terms of the number of site types and types of surface reactions with each step.

Typical values of GTLM and TLM oxide surface parameters for HFO based on previous modeling studies are summarized in Table 2.1.

2.4 References

Chase M. W. Jr., Davies C. A., Downey J. R. Jr., Frurip D. J., McDonald R. A., and Syverud A. N. (1985) JANAF thermochemical tables. 3rd ed., Suppl. No. 1. *J. Phys. Chem. Ref. Data* **14,** 1-1856.

Cowan C. E., Zachara J. M., and Resch C. T. (1991) Cadmium adsorption on iron oxides in the presence of alkaline-earth elements. *Environ. Sci. Technol.* **25,** 437-446.

Daubert T. E. and Danner R. P. (1989) *Physical and Thermodynamic Properties of Pure Chemicals: DIPPR Data Compilation.* Hemisphere Publishing Corp.

Davis J. A. and Leckie J. O. (1978) Surface ionization and complexation at the oxide/water interface. II. Surface properties of amorphous iron oxyhydroxide and adsorption of metal ions. *J. Colloid Interface Sci.* **67,** 90-107.

Davis J. A., James R. O., and Leckie J. O. (1978) Surface ionization and complexation at the oxide/water interface. I. Computation of electrical double layer properties in simple electrolytes. *J. Colloid Interface Sci.* **63,** 480-499.

Dzombak D. A. and Morel F. M. M. (1990) *Surface Complexation Modeling: Hydrous Ferric Oxide.* John Wiley & Sons.

Glushko V. P., Medvedev V. A., Bergman G. A., Vasil'ev B. P., Kolesov W. P., Gurvich L. V., Yungmand V. S., Khodakovskii I. L., Resnitskii L. A., Smirnova N. L., Gal'chenko G. L., Alekseev V. I., Vorob'ev A. F., Baibuz V. F., Kostryukov B. N., and Biryokov B. P. (1965-1981) *Thermo Constants of Compounds.* Academy of Sciences, Moscow, USSR, vols. 1-10.

Goldberg S. (1995) Adsorption models incorporated into chemical equilibrium models. In *Chemical Equilibrium and Reaction Models* (eds. R.H. Loeppert, A.P. Schwab, and S. Goldberg), pp. 75-112. SSSA Special Publication No. 42, Soil Science Society of America, Inc.

Table 2.1 Typical values of GTLM and TLM oxide surface parameters for hydrous ferric oxide based on previous studies.

SCM	Parameter	Value(s)	Reference
GTLM	N_s (Type 1) N_s (Type 2)	0.005 mol sites/mol Fe 0.200 mol sites/mol Fe	Dzombak and Morel (1990)
	N_s (Type 1) N_s (Type 2)	0.0018 mol sites/mol Fe 0.8732 mol sites/mol Fe	Waite et al. (1994)
	N_s (Type 1)	0.205 mol sites/mol Fe	Tiffreau et al. (1995)
	N_s (Type 1) N_s (Type 2)	0.027-0.066 mol sites/mol Fe 0.25-0.425 mol sites/mol Fe	Karthikeyan and Elliott (1999)
	Specific Surface Area	600 m^2/g 600 m^2/g 600 m^2/g 600 m^2/g	Dzombak and Morel (1990) Waite et al. (1994) Tiffreau et al. (1995) Karthikeyan and Elliott (1999)
	log K_{a1}, log K_{a2} (Eqs. [2.12] & [2.13])	7.29, -8.93 6.51, -9.13 7.29, -8.93 7.29, -8.93	Dzombak and Morel (1990) Waite et al. (1994) Tiffreau et al. (1995) Karthikeyan and Elliott (1999)
TLM	N_s	0.875 mol sites/mol Fe 0.933 mol sites/mol Fe 0.974 mol sites/mol Fe	Davis and Leckie (1978) Hsi and Langmuir (1985) Cowan et al. (1991)
	Specific Surface Area	600 m^2/g 700 m^2/g 600 m^2/g	Davis and Leckie (1978) Hsi and Langmuir (1985) Cowan et al. (1991)
	log K_{a1}, log K_{a2} (Eqs. [2.12] & [2.13])	5.1, -10.7 4.8, -11.1 5.4, -10.4	Davis and Leckie (1978) Hsi and Langmuir (1985) Cowan et al. (1991)
	C_1, C_2	1.4, 0.2 F/m^2 1.3, 0.2 F/m^2 1.25, 0.2 F/m^2	Davis and Leckie (1978) Hsi and Langmuir (1985) Cowan et al. (1991)
	log K_{C+}, log K_{A-} (Eqs. [2.31] & [2.32])	-9.0, 6.9 ($NaNO_3$) -9.3, 7.0 ($NaNO_3$) -8.3, 7.5 ($NaNO_3$)	Davis and Leckie (1978) Hsi and Langmuir (1985) Cowan et al. (1991)

Gurvich L.V., Veyts I. V., Medvedev V. A., Khachkuruzov G. A., Yungman V. S., Bergman G. A., Iorish V. S., Yurkov G. N., Gorbov S. I., Kuratova L. F., Trishcheva N. P., Przheval'skiy I. N., Leonidov V. Ya., Ezhov Yu. S., Tomberg S. E., Nazarenko I. I., Rogatskiy A. L., Dorofeyeva O. V., and Demidova M. S. (1989) *Thermodynamic Properties of Individual Substances.* 4th ed., USSR Academy of Sciences, Institute for High Temperatures and State Institute of Applied Chemistry, Hemisphere Publishing Corporation, vols. 1-5.

Hayes K. F. and Katz L. E. (1996) Application of x-ray absorption spectroscopy for surface complexation modeling of metal ion sorption. In *Physics and Chemistry of Mineral Surfaces* (ed. P.V. Brady), pp. 147-223. CRC Press.

Hayes K. F. and Leckie J. O. (1986) Mechanism of lead ion adsorption at the goethite-water interface. In *Geochemical Processes at Mineral Surfaces* (eds. J.A. Davis and K.F. Hayes), ACS Symposium Series 323, pp. 114-141. American Chemical Society.

Hayes K. F. and Leckie J. O. (1987) Modeling ionic strength effects on cation adsorption at the hydrous oxide/solution interfaces. *J. Colloid Interface Sci.* **115,** 564-572.

Hsi C-K. D. and Langmuir D. (1985) Adsorption of uranyl onto ferric oxyhydroxides: Application of the surface complexation site-binding model. *Geochim. Cosmochim. Acta* **49,** 1931-1941.

Huang C. P. and Stumm W. (1973) Specific adsorption of cations on hydrous γ-Al_2O_3. *J. Colloid Interface Sci.* **43,** 409-420.

Karthikeyan K. G. and Elliott H. A. (1999) Surface complexation modeling of copper sorption by hydrous oxides of iron and aluminum. *J. Colloid Interface Sci.* **220,** 88-95.

Oelkers E. H., Helgeson H. C., Shock E. L., Sverjensky D. A., Johnson J. W., and Pokrovskii V. A. (1995) Summary of the apparent standard partial molal gibbs free energies of aqueous species, minerals, and gases at pressures 1 to 5000 bars and temperatures 25 to 1000 °C. *J. Phys. Chem. Ref. Data* **24,** 1401-1560.

OLI Systems, Inc. (1995) ESP Databank. OLI Systems, Inc., Morris Plains, NJ.

Rafal M., Berthold J. W., Scrivner N. C., and Grise S. L. (1994a) Models for electrolyte solutions. In *Models for Thermodynamic and Phase Equilibria Calculations* (ed. S. I. Sandler), pp. 601-670. Marcel Dekker, Inc.

Rafal M., Black P., Sanders S. J., Tolmach P. I., and Young R. D. (1994b) Development of a comprehensive environmental simulation program. Presented at the AIChE 1994 Spring National Meeting, April 17-21, Atlanta, Ga.

Robertson A. P. and Leckie J. O. (1997) Cation binding predictions of surface complexation models: Effects of pH, ionic strength, cation loading, surface complex, and model fit. *J. Colloid Interface Sci.* **188,** 444-472.

Sanders S. J., Rafal M., Clark D. M., Young R. D., Scrivner N. C., Pease R. A., Grise S. L., and Diemer R. B. (1988) Modeling the separation of amino acids by ion-exchange chromatography. *Chem. Eng. Prog.* **92,** 47-54.

Scrivner N. C., Butler P. B., and Karmazyn J. (1996) Modeling: An excellent solution for remediation. Presented at the 69th Annual Conference and Exposition of the Water Environment Federation, October 5-9, Session No. 5, Dallas, TX.

Shock E. L. and Helgeson H. C. (1988) Calculation of the thermodynamics and transport properties of aqueous species at high pressures and temperatures: Correlation algorithms for ionic species and equation of state predictions to 5 kbar and 1000 °C. *Geochim. Cosmochim. Acta* **52,** 2009-2036.

Stumm W., Huang C. P., and Jenkins S. R. (1970) Specific chemical intercation affecting the stability of dispersed systems. *Croat. Chem. Acta* **42,** 223-245.

Tiffreau C., Lutzenkirchen J., and Behra P. (1995) Modeling the adsorption of mercury(II) on (hydr)oxides. I. Amorphous iron oxide and α-quartz. *J. Colloid Interface Sci.* **172,** 82-93.

Wagman D. D., Evans W. H., Parker V. B., Schumm R. H., Halow I., Bailey S. M., Churney K. L., and Nuttall R. L. (1982) The NBS tables of chemical thermodynamic properties. Selected values for inorganics and C1 and C2 organic substances in SI units. Suppl. No. 2. *J. Phys. Chem. Ref. Data* **11,** 1-392.

Waite T. D., Davis J. A., Payne T. E., Waychunas G. A., and Xu N. (1994) Uranium(VI) adsorption to ferrihydrite: Application of a surface complexation model. *Geochim. Cosmochim. Acta* **58,** 5465-5478.

Yates D. E., Levine S., and Healy T. W. (1974) Site-binding model of the electrical double layer at the oxide/water interface. *J. Chem. Farady Trans. I* **70,** 1807-1818.

Zemaitis J. F. Jr., Clark D. M., Rafal M., and Scrivner N. C. (1986) *Handbook of Aqueous Electrolyte Thermodynamics: Theory and Application. Design Institute for Physical Property Data.* American Institute of Chemical Engineers, Inc.

Chapter 3

LEAD SORPTION ONTO FERRIHYDRITE: NEW MODELING INSIGHTS

3.1 Abstract

Few studies have combined molecular- and macroscopic-scale investigations with surface complexation model (SCM) development to predict trace-metal speciation and partitioning in aqueous systems over a broad range of conditions. In this work, an extensive collection of new macroscopic and spectroscopic data was used to assess the ability of the modified triple-layer model (TLM) to predict single-solute lead(II) [Pb(II)] sorption onto 2-line ferrihydrite in $NaNO_3$ solutions as a function of pH, ionic strength, and concentration. Regression of constant-pH isotherm data, together with potentiometric titration and pH-edge data, was a much more rigorous test of the TLM than fitting pH-edge data alone. When combined with spectroscopic data, the choices of feasible surface species/site types were limited to a few. In agreement with the spectroscopic data, very good fits of the isotherm data were obtained with a two-species, one-site model using the bidentate-mononuclear/monodentate-mononuclear species pairs, $(\equiv FeO)_2Pb/\equiv FeOHPb^{2+}$ and $(\equiv FeO)_2Pb/\equiv FeOPb^{+}$–$NO_3^{-}$. Regressing edge data in the absence of isotherm and spectroscopic data resulted in a fair number of surface-species/site-type combinations that provided acceptable fits of the edge data, but unacceptable fits of the isotherm data. Surprisingly, best-fit equilibrium "constants" for the Pb(II) surface complexes required adjustment outside the pH range 4.5 to 5.5 in order to fit the isotherm data. In

addition, a surface activity term was needed to reduce the ionic-strength dependence of sorption for the species pair, $(\equiv FeO)_2Pb/\equiv FeOHPb^{2+}$. In light of this, the ability of existing SCMs to predict Pb(II) sorption onto 2-line ferrihydrite over a wide range of conditions seems questionable. While many advances have been made over the past decade, much work still needs to be done in fine-tuning the thermodynamic framework and databases for the SCMs.

3.2 Introduction

Numerous commercial and public-domain geochemical codes exist for predicting trace-metal speciation in aqueous systems; however, the existing surface complexation models (SCMs) in these codes often prove inadequate for simulating multisolute sorption reactions in complex industrial systems. One contributing factor is that published thermodynamic parameters for the surface complexes are often based on regressions of a handful of pH-sorption edges covering a narrow range of conditions, done without the aid of state-of-the-art spectroscopic techniques to confirm surface speciation.

Extensive studies of metal cation and anion sorption onto amorphous iron (hydr)oxides have been conducted over the years. Dzombak and Morel (1990) critically reviewed pre-1990 single-solute sorption data for hydrous ferric oxide (HFO); this data was regressed to obtain best-fit intrinsic equilibrium constants (K^{int}) for the Generalized Two-Layer Model (GTLM). Interestingly, only 17% of 184 cation/anion data sets were equilibrium isotherms. This suggests that these equilibrium constants will have limited applicability if the pH edges used to determine them did not cover a broad enough range of conditions. Constant-pH equilibrium isotherms, on the other hand, often cover 5 to 8 orders of magnitude in metal

concentration. If generated at multiple pH values, regression of constant-pH isotherm data, along with pH-sorption-edge data, is a much more rigorous test of the SCM.

Despite the fact that lead(II) [Pb(II)] is a common constituent found in contaminated soils, sediments, and some groundwater streams, previous studies of single-solute Pb(II) sorption onto HFO/ferrihydrite are somewhat limited (Dzombak and Morel, 1990; Scheinost et al., 2001). All studies report pH-edge data, except for Scheinost et al. (2001), which contains kinetic data for Pb(II) sorption onto 2-line ferrihydrite at pH 5, and Benjamin (1979), which provides the only published Pb(II) sorption isotherm for HFO (pH 4.5) prior to this work. Interestingly, Dzombak and Morel (1990) regressed only low-concentration edge data to obtain a best-fit K^{int} for Pb(II) sorption onto Type-1, high-affinity sites; K^{int} for Type-2, low-affinity sites in the GTLM was estimated based on linear-free-energy relationships.

Before the advent of in-situ spectroscopic and microscopic techniques, researchers were limited in their ability to probe the surface of mineral oxides to determine surface speciation. As a result, assumptions about surface speciation in early applications of SCMs were largely based on macroscopic observations, such as the shift (or lack thereof) in pH-sorption edges with ionic strength (Davis and Leckie, 1978; Balistrieri and Murray, 1982; Catts and Langmuir, 1986; Hunter et al., 1988; Cowan et al., 1991). Dzombak and Morel (1990) represented one of the first attempts to use a single SCM to regress a wide cross section of metal sorption data for a single sorbent. Even in recent years, however, pH-edge data alone are still being used to obtain best-fit model parameters for SCMs (Gunneriusson et al., 1994; Kanungo, 1994; Kooner et al., 1995; Christl and Kretzschmar, 1999). Since 1995, some studies have evaluated the applicability of SCMs over a wider range of concentration, pH, and

ionic strength conditions (Katz and Hayes, 1995a, b; Robertson and Leckie, 1998). For example, Katz and Hayes (1995a, b) proposed a surface continuum model for simulating cobalt(II) sorption onto α-Al_2O_3 from 0.05-100% surface coverage. Robertson and Leckie (1998) evaluated the ability of three different SCMs to predict copper (Cu) sorption onto goethite over 3 and 6 orders of magnitude in Cu surface coverage and solution concentration, respectively, at 3 different pH values. None of these studies, however, benefited from parallel spectroscopic investigations. A handful of studies have combined spectroscopic and macroscopic analyses with surface complexation modeling to simulate trace-metal sorption data (Hayes, 1987; Brown et al., 1998; Katz and Boyle-Wight, 2001); however, none were found for Pb(II) sorption onto HFO/ferrihydrite.

Application of a Law-of-Mass-Action (LMA)-based SCM requires the definition of many parameters, including site densities and surface areas for the sorbents, equilibrium constants for protonation, deprotonation, metal sorption, and background-electrolyte sorption reactions, and, in some cases, capacitance values. This is in addition to making assumptions about the number and types of sorption sites and surface species (Koretsky, 2000). In recent years, Sverjensky and coworkers have developed techniques for estimating the values of a number of LMA-based SCM parameters based on the physical and chemical properties of the solutes and sorbents themselves (Sverjensky and Sahai, 1996; Sahai and Sverjensky, 1997; Koretsky et al., 1998; Sverjensky, 2001); however, these predictive techniques are currently limited to crystalline sorbents. For an amorphous sorbent like ferrihydrite, regression of macroscopic data is still necessary. In an attempt to address potential limitations inherent in LMA-based SCMs (most notably, the mass balance constraints on surface

sites), Kulik (2000, 2002) has developed a multisite Gibbs energy minimization (GEM) approach for surface complexation modeling. Two important aspects of this work are the rigorous definition of standard and reference states for surface species and sites, and the use of a surface activity term to suppress the concentration of a surface complex as it nears a defined maximum site density.

An in-depth literature review highlighted the scarcity of studies where molecular- and macroscopic-scale data have been coupled with surface complexation modeling to predict metal-cation sorption over a broad range of conditions. Trivedi et al. (2002a) present comprehensive single-solute macroscopic and spectroscopic data for Pb(II) sorption onto 2-line ferrihydrite. This chapter will highlight the insights that come from integrating spectroscopic data on surface speciation with macroscopic isotherm and pH-sorption-edge data covering a wide range of conditions. In addition, it will point to potential limitations in using existing SCMs to determine an optimal set of surface complexation modeling parameters for single-solute Pb(II) sorption onto 2-line ferrihydrite.

3.3 Methods

3.3.1 Potentiometric Titration and Pb Sorption Data

Modeling studies were based on macroscopic and spectroscopic data for single-solute Pb(II) sorption onto 2-line ferrihydrite (N_2 atmosphere, room temperature, and 4-hour equilibration time) that are reported and discussed in Trivedi et al. (2002a). This includes the ferrihydrite preparation method as well as potentiometric titration data for ferrihydrite in 0.001, 0.01, and 0.1 M $NaNO_3$ solutions

(N_2 atmosphere and room temperature). Acid/base titration, constant-pH isotherm, and pH-sorption-edge data are also documented in Appendix A.

Titration data at each ionic strength were tabulated as excess acid (q, equiv./L) vs. pH, where

$$q \text{ (equiv./L)} = C_A - C_B - [H^+] + [OH^-] \qquad [3.1]$$

C_A and C_B are the total quantity of mineral acid and base, respectively, added at each titration point in equiv./L. The measured pH values at each ionic strength were used to determine molal concentrations for $[H^+]$ and $[OH^-]$ by taking into account activity coefficients for H^+ and OH^- and H_2O activity. The titration curves were then shifted slightly downward along the y-axis so that the common intersection point was at q = 0.0. All constant-pH isotherm and pH-edge data points were individually equilibrated in their own sample vials.

3.3.2 Geochemical Modeling Software

The OLI Software (OLI Systems, Inc., Morris Plains, NJ) is a commercial simulation package that models aqueous electrolyte equilibria, including chemical speciation and redox reactions, equilibria between aqueous, vapor, organic liquid, and multiple solid phases, biochemical and inorganic reaction kinetics, and ion exchange, adsorption, and coprecipitation phenomena. The system is built around the OLI Engine, which is the foundation for the Environmental Simulation Program (ESP), Corrosion Simulation Program (CSP), and ProChem. ProChem was used in this study, because it models single-stage equilibria at both steady and unsteady states (Sanders et al., 1988).

At the heart of the OLI Engine are the databank, the thermodynamic framework, and the equation solvers (Rafal et al., 1994b). The OLI databank contains

the thermodynamic and physical properties of over 8,300 inorganic and organic species. The thermodynamic variables (Gibbs free energy, enthalpy, entropy, and heat capacity) in the databank are from six main sources—Glushko et al. (1965-1981), Wagman et al. (1982), Chase et al. (1985), Daubert and Danner (1989), Gurvich et al. (1989), and Oelkers et al. (1995). Each of these sources is an extensive, carefully evaluated, and well-referenced compilation of thermodynamic data. The state-of-the-art thermodynamic framework uses generalized correlations based upon regressed experimental data in the databank to predict the required thermodynamic and physical properties for the chemical system of interest (i.e., infinite-dilution, standard-state values for Gibbs free energy, enthalpy, entropy, heat capacity, and volume, liquid-phase activity coefficients for systems at finite concentrations, and so on). The theoretical basis for the thermodynamic framework is explained elsewhere (Zemaitis et al., 1986; Rafal et al., 1994a). Shock and Helgeson (1988) describe the semi-theoretical basis for temperature and pressure extrapolation of standard state properties, along with procedures for estimating missing parameters. The aqueous activity coefficient model is an extension of the work of Bromley and Meissner (i.e., the Bromley-Zemaitis framework). It is a combination of the Debye-Huckel term for long-range electrostatic interactions and a semi-empirical expression for short-range interactions between cations and anions. In a multicomponent system, the activity coefficient of an ion *i* is given by (Zemaitis et al., 1986; Anderko et al., 1997):

$$\log \gamma_i = \frac{-Az_i^2 I^{1/2}}{1+I^{1/2}} +$$

$$\sum_{j}^{NO}\left[\frac{|z_i|+|z_j|}{2}\right]^2\left[\frac{(0.06+0.6B_{ij})|z_iz_j|}{\left(1+\frac{1.5}{|z_iz_j|}I\right)^2}+B_{ij}+C_{ij}I+D_{ij}I^2\right]m_j \qquad [3.2]$$

Details on the equation solvers used to solve the nonlinear equilibrium, electroneutrality, and mass balance equations can be found in Rafal et al. (1994b). Permissible operating ranges for the software can be found in Scrivner et al. (1996). The OLI equilibrium reactions and associated equilibrium constants used in this work are given in Table 3.1.

3.3.3 Surface Complexation Models

Four different surface complexation models are available in the OLI Software—the nonelectrostatic model (NEM), the constant capacitance model (CCM), the GTLM, and the modified triple-layer model (TLM). In this research, the NEM, GTLM, and TLM were all considered, although the TLM ultimately proved to be the preferred SCM as discussed below. The thermodynamic frameworks for the NEM, GTLM, and modified TLM are described in Hayes and Katz (1996), Dzombak and Morel (1990), and Sahai and Sverjensky (1998), respectively.

3.3.4 Modeling Protocol

Hayes and Katz (1996) served as a basis for the modeling protocol used in this study. First, the OLI Software's nonlinear regression routine was used to determine a valid set(s) of metal hydroxide surface parameters for the SCM of interest using potentiometric titration data for 2-line ferrihydrite at three different ionic strengths as reported in Trivedi et al. (2002a) and Appendix A. For the GTLM, this

Table 3.1 Equilibrium reactions and associated equilibrium constants used in the OLI triple-layer model simulations.

Equilibrium Reaction	K value at 25°C
$H_2O = H^+ + OH^-$	1.0144E-14
$HNO_3\ (aq) = H^+ + NO_3^-$	2.0128E+01
$NaNO_3\ (aq) = Na^+ + NO_3^-$	5.4253E+01
$PbO\ (aq) + H_2O = Pb^{2+} + 2OH^-$	1.0081E-11
$PbOH^+ = Pb^{2+} + OH^-$	3.9469E-07
$HPbO_2^- = PbO\ (aq) + OH^-$	9.0663E-04
$Pb(NO_3)^+ = Pb^{2+} + NO_3^-$	5.0233E-02
$Pb(NO_3)_2\ (aq) = Pb^{2+} + 2\ NO_3^-$	5.1579E-02
$Pb(NO_3)_3^- = Pb^{2+} + 3\ NO_3^-$	3.0272E-01
$PbO\ (s) + 2H^+ = Pb^{2+} + H_2O$	4.3298E+12
$\equiv FeOH_2^+ = \equiv FeOH + H^+$	Table 3.2 and Figure 3.8
$\equiv FeOH = \equiv FeO^- + H^+$	Table 3.2 and Figure 3.8
$\equiv FeOH_2^+ - NO_3^- = \equiv FeOH + H^+ + NO_3^-$	Table 3.2 and Figure 3.8
$\equiv FeO^- - Na^+ + H^+ = \equiv FeOH + Na^+$	Table 3.2 and Figure 3.8
$(\equiv FeO)_2Pb + 2H^+ = 2\equiv FeOH + Pb^{2+}$	Table 3.3
$\equiv FeOHPb^{2+} = \equiv FeOH + Pb^{2+}$	Table 3.3
$\equiv FeOPb^+ - NO_3^- + H^+ = \equiv FeOH + Pb^{2+} + NO_3^-$	Table 3.3
$\equiv FeOPbOH + 2H^+ = \equiv FeOH + Pb^{2+} + H_2O$	Figure 3.8
$\equiv FeOPb^+ + H^+ = \equiv FeOH + Pb^{2+}$	Figure 3.8

was done for a range of site density (N_s) values at a fixed specific surface area (A_s), giving K_{a1}^{int} and K_{a2}^{int} (the surface acidity constants) as a function of N_s. For the modified TLM, Hayes and Katz (1996) showed that various combinations of N_s, C_1, and ΔpK_a will provide adequate fits of potentiometric titration data for mineral oxides. For this reason, a 3-factor, face-centered-cube (FCC), response-surface experimental design was used to determine the values of N_s, C_1, and ΔpK_a that provide the best fit of the titration data (A_s and C_2 were held constant in the model). The experimental design was generated and analyzed using the MINITAB™ Statistical Software (Minitab Inc., State College, PA). Ranges of values considered for N_s, C_1, and ΔpK_a in the experimental design were 0.2-0.9 mole sites/mole Fe, 0.6-1.4 F/m^2, and 3.0-6.0, respectively. The criteria for judging the quality of fit were the value of R_{avg}, obtained from the OLI code's nonlinear regression program, and visual inspection of a plot of the model titration curves with the experimental data. A Marquardt nonlinear optimization algorithm was used throughout this work; the objective function minimized was the ratio (R_i) of the calculated to experimental values (or vice versa, such that R_i is always ≥ 1.0). R_i values were equally weighted, with a perfect fit being defined as $R_i = 1.0$. OLI has found that this objective function is more robust than least-squares minimization when regressing data values that range over many orders of magnitude, such as in constant-pH isotherms where Pb(II) solution concentrations will vary over 5 to 7 orders of magnitude. R_{avg} represents the arithmetic average of all R_i values for the regressed experimental data set.

Next, spectroscopic results and the impact of ionic strength on Pb(II) sorption were used to guide the selection of the Pb(II) surface complexation reactions at low to moderate surface coverage. Hayes and Katz (1996) note that past x-ray

absorption fine structure spectroscopy (XAFS) studies have suggested that mononuclear species predominate at low to moderate surface coverage (0.1 to 10%) for strongly sorbing metals and at all coverages for weakly sorbing metals. Ionic-strength dependence has also been used historically to infer the presence of inner- versus outer-sphere surface complexes (Sparks, 1995). In this study, pH edges generated at 3 different ionic strengths were used to assess the ionic-strength dependence of Pb(II) sorption. Spectroscopic results are summarized in Trivedi et al. (2002a).

Spectroscopic results and the shape of the constant-pH equilibrium isotherms were used to determine the need for multinuclear surface complexation reactions at higher surface coverage (i.e., surface polymers and/or surface precipitates). The constant-pH isotherms were also used to determine a reasonable starting point for N_s and to assess the possibility of site heterogeneity (i.e., the need for more than one site type). Robertson and Leckie (1997) found that site heterogeneity is likely if the slope of a constant-pH isotherm curve is less than 1.0 at low surface coverage.

Based on the above analyses of the macroscopic and spectroscopic data, an appropriate set of oxide surface-parameters (N_s, C_1, C_2, ΔpK_a, and A_s) and Pb(II) surface complex species were assumed for the SCM of interest. These surface parameters/species were used to regress the constant-pH isotherm data to obtain a set of best-fit equilibrium constants for single-solute Pb(II) sorption. The best-fit Ks were then used to assess how the model predicted the pH-edge data at multiple ionic strengths and initial Pb(II) concentrations. Various combinations of viable Pb(II) surface complexes were considered to evaluate the sensitivity of the model fits to the speciation assumptions. The minimum numbers of site types and species that

provided the best fit of the isotherm and pH-edge data were considered the optimum. Again, R_{avg} values for both the *x* [total Pb (aq)] and *y* [moles Pb/mole Fe] data from the nonlinear regression program, together with visual inspection of graphical output, were used to judge the quality of the fits. This step was an iterative process, whereby the oxide surface parameters were adjusted if N_s was altered.

3.4 Results and Discussion

3.4.1 Potentiometric Titration Data

The point of zero net proton charge (PZNPC) for 2-line ferrihydrite was determined to be 7.91, which falls within the range of point of zero charge values reported by others (Dzombak and Morel, 1990). Figures 3.1a, 3.1b, and 3.1c provide best fits of the potentiometric titration data for the NEM, GTLM, and TLM, respectively. Model parameters corresponding to each of these fits are given in Table 3.2. In all cases, A_s was fixed at 600 m^2/g. The NEM fit provides no functionality with ionic strength, and it significantly overpredicts surface charge as pH moves away from the PZNPC. The GTLM was better than the NEM and TLM at capturing the sharp curvature in the titration data at the pH extremes; however, it was inferior to the TLM in predicting the more linear surface-charging behavior over the pH range 5 to 9. Regardless of the number of site types and N_s, the general shape of the GTLM-predicted titration curves did not change substantially.

The modified TLM produced titration curves (Figure 3.1c) that were more linear over a wider pH range, especially as ionic strength increased. Unlike the NEM and GTLM, outer-sphere surface complexes involving the background electrolyte ions are included in the TLM; these complexes dominate surface charge, producing less

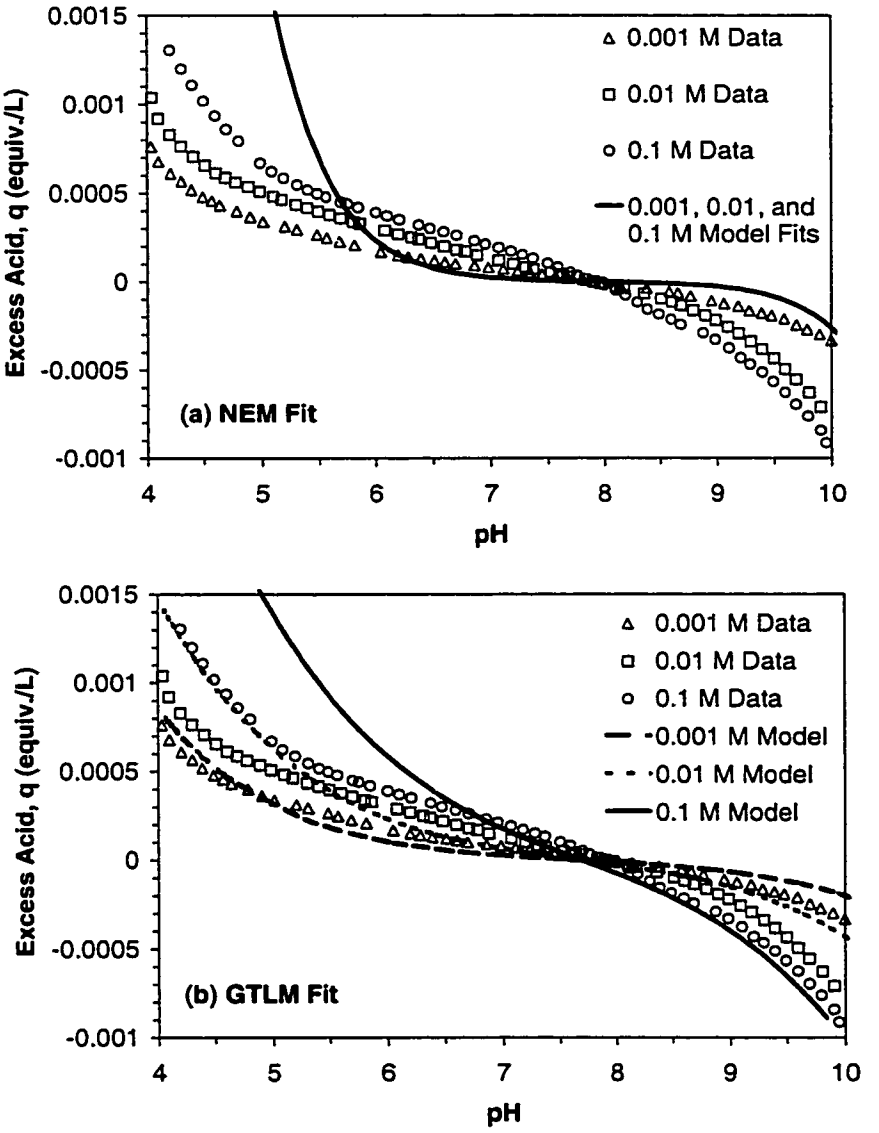

Figure 3.1 **Best fits of potentiometric titration data for 2-line ferrihydrite using the (a) nonelectrostatic model (NEM); (b) generalized two-layer model (GTLM); and (c) modified triple-layer model (TLM). Error bars/bands shown in (c) for experimental data and model predictions are +/- 2σ. Experimental conditions: 1 g ferrihydrite/L; 0.001, 0.01, and 0.1 M $NaNO_3$ electrolyte solutions; room temperature; N_2 glovebox; 1 L reactor; 2-minute equilibration time at each pH point; 0.1 M NaOH used to raise initial pH to ~ 10; 0.1 M HNO_3 used to titrate mixture downward to ~ pH 4.**

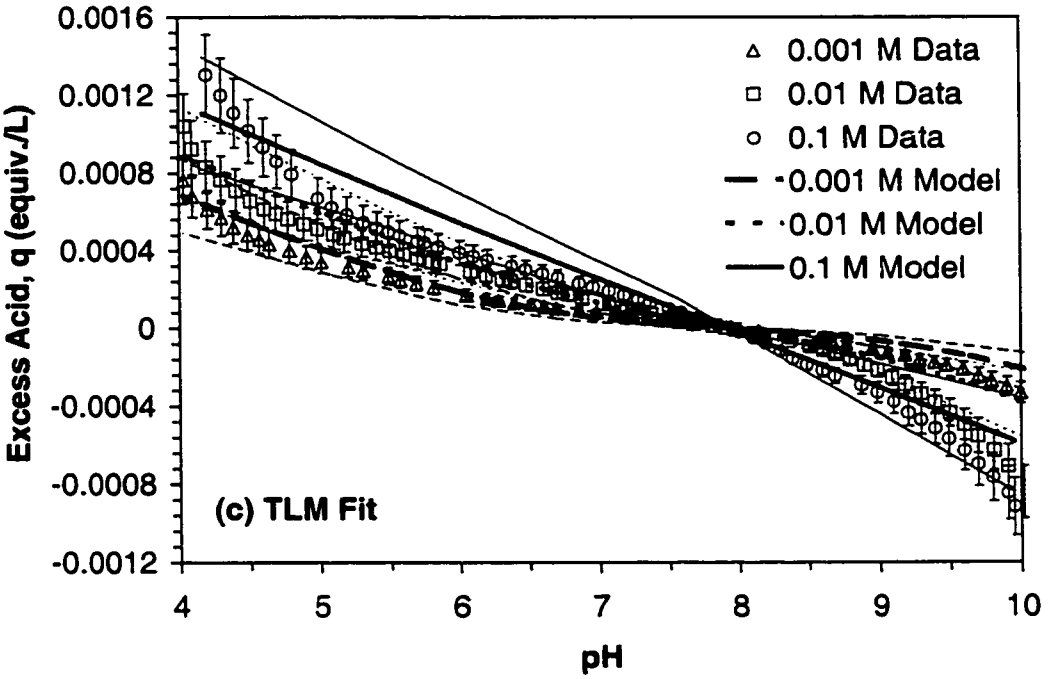

Figure 3.1 Continued.

curvature in the titration curves. The optimum fit shown in Figure 3.1c, along with the associated model parameters in Table 3.2, were obtained from the 3-factor, FCC, response-surface experimental design. As shown by the response surfaces in Figure 3.2, the quality of the fits based on R_{avg} was highly sensitive to the value of C_1. On the other hand, the impacts of ΔpK_a and N_s on R_{avg} were moderate and small, respectively. In all cases, the TLM could not reproduce the sharp increase (decrease) in proton surface charge at pH < 5 (> 9). In general, the quality of the TLM fit deteriorated at the pH extremes and as ionic strength increased. To validate the quality and consistency of the data, the ferrihydrite titration in 0.1 M $NaNO_3$ solution was repeated two more times in separate runs. These new titrations occurred one year after the original titrations used for the model regressions, used a different batch of ferrihydrite,

Table 3.2 Model parameters for the NEM, GTLM, and TLM based on regression of potentiometric titration data for 2-line ferrihydrite at room temperature in a N_2 atmosphere.

Model	N_s (mol/ mol)	C_1 (F/m^2)	C_2 (F/m^2)	log $K_{a1}^{int\ a}$	log $K_{a2}^{int\ b}$	log $K_{NO3-}^{int\ c}$	log $K_{Na+}^{int\ d}$	R_{avg}
NEM	0.8	N/A	N/A	-4.43	-11.52	N/A	N/A	6.0
GTLM	0.8	N/A	N/A	-6.49	-8.89	N/A	N/A	1.6
TLM	0.8	1.0	0.2	-5.56	-10.26	-7.48	8.36	1.3

[a] $\equiv FeOH_2^+ = \equiv FeOH + H^+$, where $K_{a1}^{int} = a_{H+}[\equiv FeOH]\exp(-F\Psi_o/RT)/[\equiv FeOH_2^+]$.

[b] $\equiv FeOH = \equiv FeO^- + H^+$, where $K_{a2}^{int} = a_{H+}[\equiv FeO^-]\exp(-F\Psi_o/RT)/[\equiv FeOH]$.

[c] $\equiv FeOH_2^+ - NO_3^- = \equiv FeOH + H^+ + NO_3^-$, where
$K_{NO3-}^{int} = a_{H+}a_{NO3-}[\equiv FeOH]\exp(F(\Psi_\beta - \Psi_o)/RT)/[\equiv FeOH_2^+ - NO_3^-]$.

[d] $\equiv FeO^- - Na^+ + H^+ = \equiv FeOH + Na^+$, where
$K_{Na+}^{int} = a_{Na+}[\equiv FeOH]\exp(F(\Psi_o - \Psi_\beta)/RT)/a_{H+}[\equiv FeO^- - Na^+]$.

were conducted over a narrower pH range (5 to 9 vs. pH 4 to 10), and were conducted from both low-to-high and high-to-low pH. Figure 3.3 shows excellent agreement between the triplicate 0.1 M $NaNO_3$ runs, indicating that the ferrihydrite-preparation and experimental-titration methods are reproducible. The results are also similar regardless of the initial conditions. The average coefficient of variation (1σ) for the ~ 100 titration steps between pH 5 and 9 was ~ 8%. Error bars (+/- 2σ) are shown in Figure 3.1c. In addition, independent solubility measurements for 2-line ferrihydrite in 0.01 M $NaNO_3$ solutions over the pH range 3 to 5 showed that sorbent dissolution could not account for the sharp increase in acid consumption between pH 5 and 4. Ferrihydrite solubility was nondetect, 1.7 ppb, and 6.5 ppb at pH 5, 4.5, and 4, respectively. It is possible that the sharp change in slope of the titration curves below

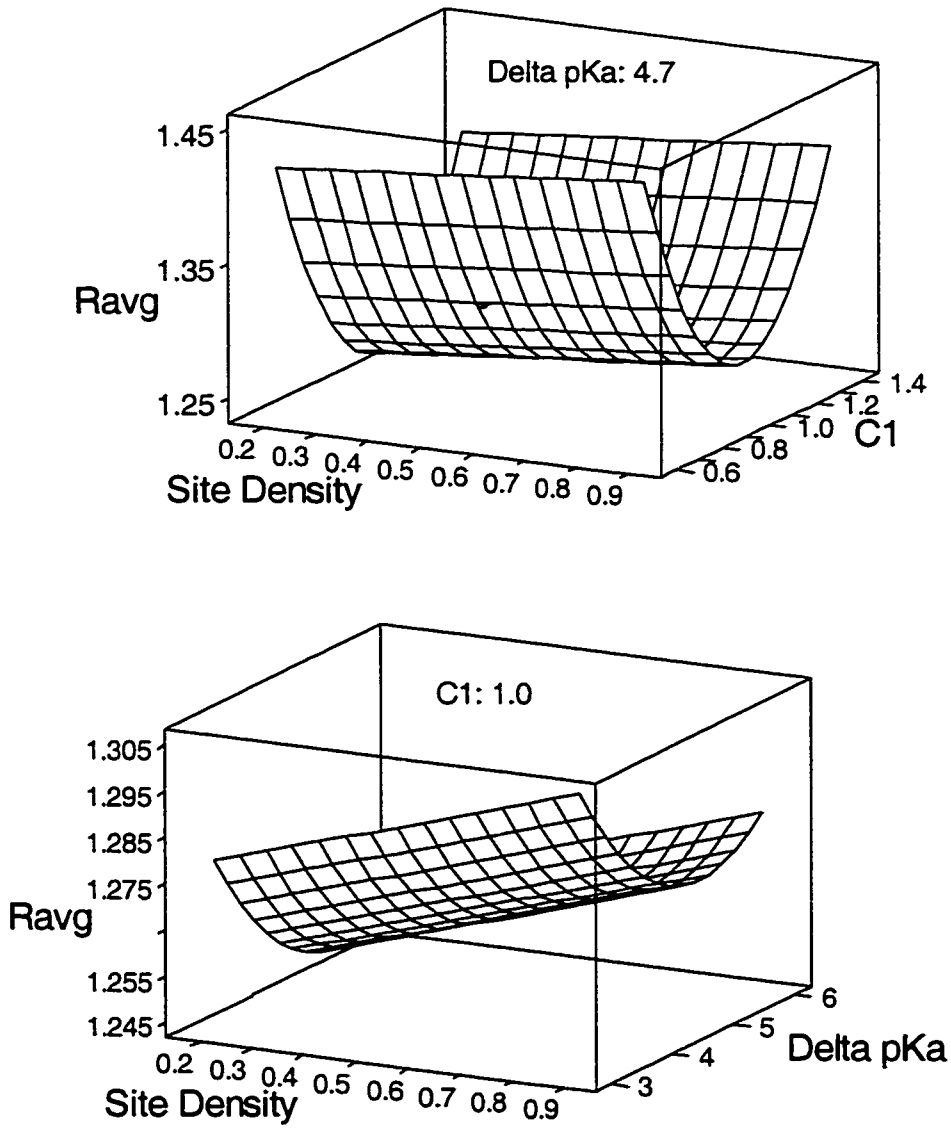

Figure 3.2 **Response surfaces from MINITAB™ Statistical Software for a 3-factor, face-centered-cube, response-surface experimental design used to determine the best-fit oxide surface parameters for the triple-layer model. The 3 factors studied were C_1, N_s, and ΔpK_a; the response, R_{avg}, is the arithmetic average of the nonlinear regression fit parameters (R_i) obtained from the OLI Software for all potentiometric titration data points.**

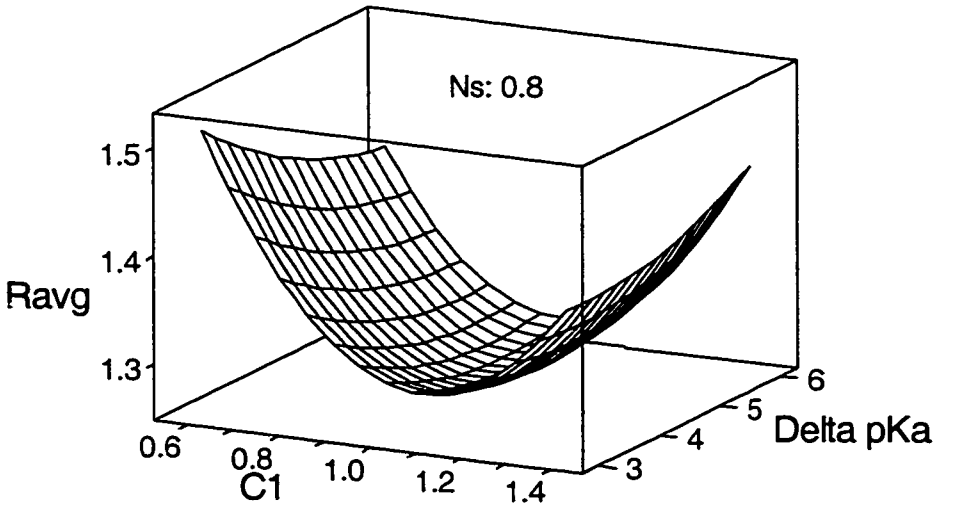

Figure 3.2 Continued.

pH 5 and above pH 9 was due to a fundamental change in ferrihydrite morphology and, hence, in the surface area available for reaction with acid or base.

While none of the SCMs could predict the shape of the titration curves over the entire pH range, the TLM provided the best fits of the ferrihydrite titration data over the pH range of environmental significance (5 to 9). There are several important points to keep in mind regarding the quality of the titration-data fits. First, while optimizing the model fit of the titration data over different pH ranges (5-8, 5-9, and 4-10) resulted in different sets of best-fit oxide surface parameters (i.e., C_1, log K^{int}_{NO3-}, and log K^{int}_{Na+}), these unique sets of parameters gave essentially identical fits of the constant-pH isotherm data (i.e., log Ks for the Pb(II) surface complexes). Second, the model predictions are also bounded by some level of uncertainty. Figure 3.1c displays the 95% prediction intervals for the model titration curves based on the results of a rigorous error propagation analysis using the uncertainty analysis module in the

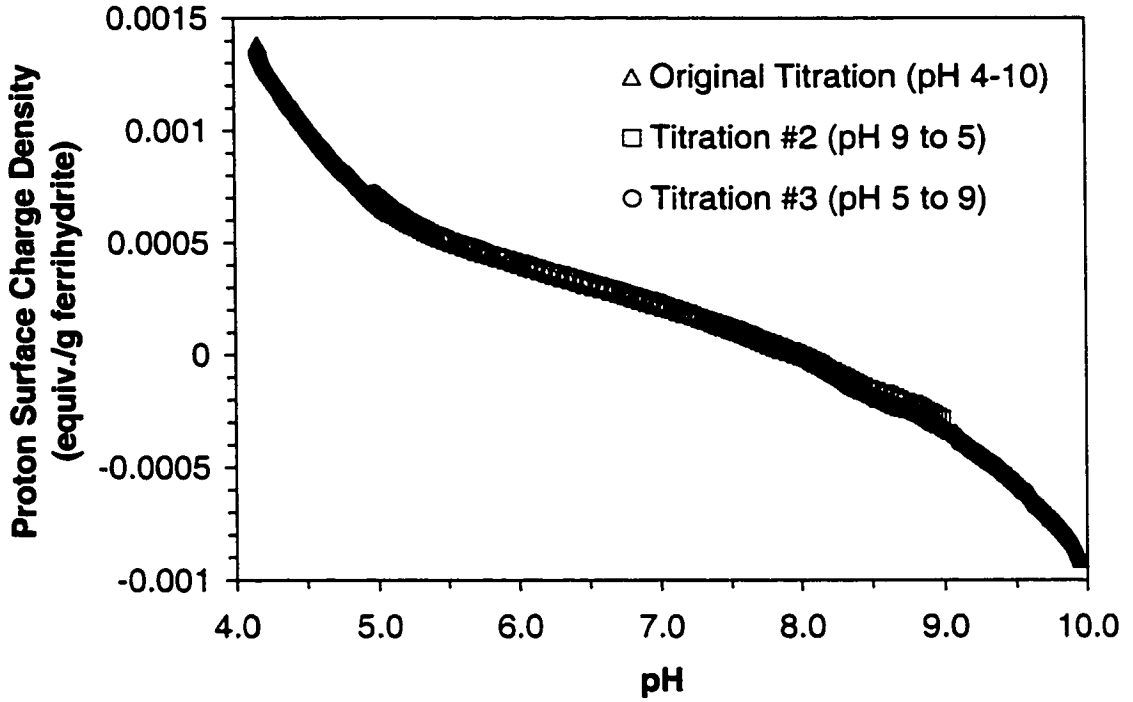

Figure 3.3 **Triplicate sets of potentiometric titration data for 2-line ferrihydrite in 0.1 M $NaNO_3$ electrolyte solution. Titrations #2 and #3 were conducted one year after the original set of titrations using a different batch of ferrihydrite and over the pH range 5 to 9 versus 4 to 10. The ferrihydrite was titrated downward in run #2 and upward in run #3. Experimental conditions: 1 g ferrihydrite/L; room temperature; N_2 glovebox; 1-L reactor; 2-minute equilibration time at each pH point; 0.1 M NaOH and 0.1 M HNO_3 used to titrate mixture upward or downward depending on run.**

OLI code. Assumed input/thermodynamic uncertainties (1σ) were C_1 (10%), C_2 (10%), pH (0.03 units), total ferrihydrite (10%), total H_2O (3%), total $NaNO_3$ (10%), total NaOH (2.5%), total HNO_3 (2.5%), log K_{a1}^{int} (0.125 log units), log K_{a2}^{int} (0.125 log units), log K_{NO3-}^{int} (0.125 log units), and log K_{Na+}^{int} (0.125 log units). When uncertainties in the data and model are both considered, the experimental data points fall within the uncertainty bands for the model curves, except for a handful of points at pH > 9.5. Third, extensive uncertainty analyses of the Pb(II) isotherm and pH-edge model fits revealed that input uncertainties in log K_{NO3-}^{int} and log K_{Na+}^{int} have little impact on the predicted output uncertainties in Pb(II) sorbed and Pb(II) in solution over the majority of the pH, Pb-concentration, and ionic-strength space covered by this study. Only in the narrow pH range 3.5-4.5 at low Pb(II) surface (< 10^{-3} mol/mol) and solution (< 1 ppm) concentrations, did uncertainty in the titration data fit have a significant impact on predicted Pb(II) partitioning. More importantly, this was true only when the 1σ uncertainties in log K_{NO3-}^{int} and log K_{Na+}^{int} were greater than 0.24 log units (i.e., a 2σ uncertainty > 148% in K space). In all other cases, uncertainties in Pb(II) concentrations were not sensitive to the fit of the titration data. Based on consideration of R_{avg}, visual inspection of the fits, extensive uncertainty analyses, and the results of past TLM modeling efforts with HFO (Davis and Leckie, 1978; Hsi and Langmuir, 1985; Cowan et al., 1991), Figure 3.1c was defined as the "best fit" to carry forward for the regression of the Pb sorption data.

3.4.2 Pb Sorption Isotherms and Edges

Analysis of macroscopic and spectroscopic data from Trivedi et al. (2002a) for Pb(II) sorption onto 2-line ferrihydrite provided several insights to help focus the SCM development. First, pH-edge data for 50 μM Pb(II) equilibrated with 1

g ferrihydrite/L in 0.001, 0.01, and 0.1 M $NaNO_3$ solutions showed only a small ionic-strength dependence, indicating the likelihood of inner-sphere surface complexes. Second, the slope of the constant-pH isotherms at low Pb(II) concentrations was approximately 1.0, suggesting that a one-site model would be adequate. Third, the unequal spacing between the pH 4.5, 5.5, and 6.5 isotherms (changing $d[pPb_{aq}]/d[pH]$ at a constant Pb(II) surface loading) suggested that a unique set of equilibrium constants and/or surface species would not fit all the data. Spectroscopic results, however, gave no indication that a change in surface speciation was the reason for this significant change in spacing between the isotherms. Fourth, the plateau in the pH 5.5 and 6.5 isotherm data suggested a maximum Pb(II) surface loading of approximately 0.35-0.40 moles Pb/mole Fe. Fifth, the spectroscopic data analysis indicated that a bidentate-mononuclear inner-sphere surface complex dominated at pH 5.5 and 6.5, while at pH 4.5, there was evidence for both inner-sphere monodentate-mononuclear and bidentate-mononuclear surface complexes. More specifically, XAFS (x-ray absorption fine-structure spectroscopy) studies over the pH range 4.5 to 6.5 revealed a first shell (Pb–O) composed of two oxygen atoms at an average radial distance of 2.28 Å. These radial distances are much shorter than first-shell distances reported for fully hydrated Pb(II) ions (2.47-2.49 Å), which suggests that Pb(II) ions do not retain their primary hydration sphere upon sorption onto ferrihydrite (i.e., an inner-sphere surface complex is formed). The second shell (Pb–Fe) was best fitted with two iron atoms at an average radial distance of 3.34 Å over the pH range 5.0 to 6.5. This fit was independent of Pb(II) concentration and is indicative of edge-sharing bidentate sorption. At pH 4.5, on the other hand, two distinct Pb–Fe bond distances of 3.34 Å and 3.89 Å are seen. The longer bond distance of 3.89 Å arises from either

monodentate or corner-sharing bridging-bidentate bonding of Pb(II) ions to the FeO_6 octahedra. At lower pH, therefore, at least two of the following distinct Pb-ferrihydrite sorption complexes coexist: mononuclear monodentate, mononuclear edge-sharing bidentate, and mononuclear corner-sharing bidentate. No meaningful contribution of Pb–Pb was seen in the second shell.

The constant-pH isotherm data are shown in Figure 3.4, along with fits obtained using the modified TLM for two different species pairs: $(\equiv FeO)_2Pb$ plus $\equiv FeOHPb^{2+}$ and $(\equiv FeO)_2Pb$ plus $\equiv FeOPb^{+}–NO_3^{-}$. Equilibrium constants, associated equilibrium reactions and mass law expressions, and R_{avg} values for the pH 4.5, 5.5, and 6.5 isotherm fits are summarized in Table 3.3 for both species pairs. Based on a maximum Pb(II) surface loading of 0.35-0.40 moles Pb/mole Fe, N_s was optimized at 0.80 moles sites/mole Fe. In general, as pH and surface loading increased, the bidentate-mononuclear surface complex became more dominant. The monodentate-mononuclear complexes were more important at lower pH and surface loading. Spectroscopic data were unable to distinguish between the monodentate-mononuclear complexes, $\equiv FeOHPb^{2+}$ and $\equiv FeOPb^{+}–NO_3^{-}$. Based on R_{avg} alone, the $(\equiv FeO)_2Pb/\equiv FeOHPb^{2+}$ species pair provided a better fit of the constant-pH isotherms. Regression of the isotherm data using only a one-species model gave inferior fits when compared to a two-species model (Figures 3.5 through 3.7). Although not supported by spectroscopic data, the species pair, $\equiv FeOPbOH$ plus $\equiv FeOPb^{+}$, provided essentially the same quality of fit as the bidentate-mononuclear species pairs (Figure 3.8). Mathematically, the mass-law expression for $\equiv FeOPbOH$ looks much the same as the mass-law expression for $(\equiv FeO)_2Pb$. In addition, the two-species, one-site TLM provided superior fits of the isotherm data when compared to the one-species, two-site

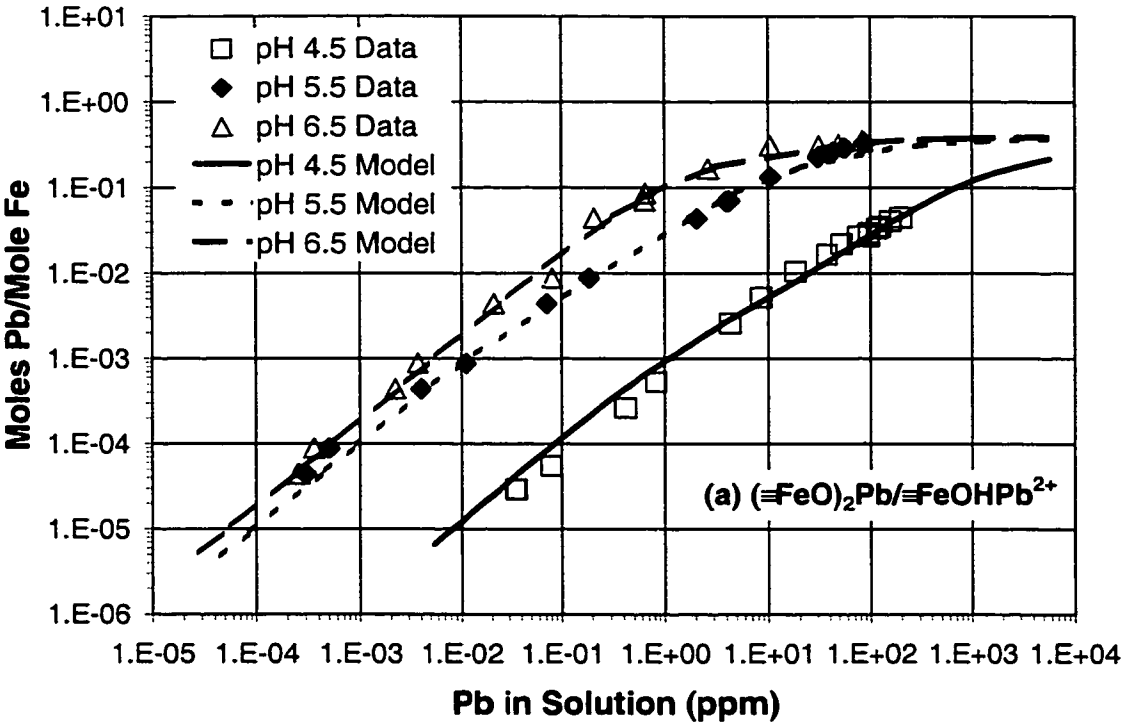

Figure 3.4 **Optimized triple-layer model fits of pH 4.5, 5.5, and 6.5 equilibrium isotherm data for single-solute Pb(II) sorption onto 2-line ferrihydrite assuming the species pairs (a) $(\equiv FeO)_2Pb/\equiv FeOHPb^{2+}$ [log $K_{(\equiv FeO)_2Pb}$ = 5.00 (pH 4.5, 5.5) and 6.16 (pH 6.5); log $K_{\equiv FeOHPb^{2+}}$ = -8.80 (pH 4.5, 5.5) and -5.33 (pH 6.5)] and (b) $(\equiv FeO)_2Pb/\equiv FeOPb^{+}–NO_3^{-}$ [log $K_{(\equiv FeO)_2Pb}$ = 5.04 (pH 4.5, 5.5) and 5.97 (pH 6.5); log $K_{\equiv FeOPb^{+}\text{-}NO_3^{-}}$ = -2.10 (pH 4.5, 5.5) and -0.16 (pH 6.5)].**

Experimental conditions: 0.1 and 1.0 g ferrihydrite/L in 0.01 M $NaNO_3$ solution; Pb(II) added as $Pb(NO_3)_2$; 4-hour equilibration time; room temperature; N_2 glovebox.

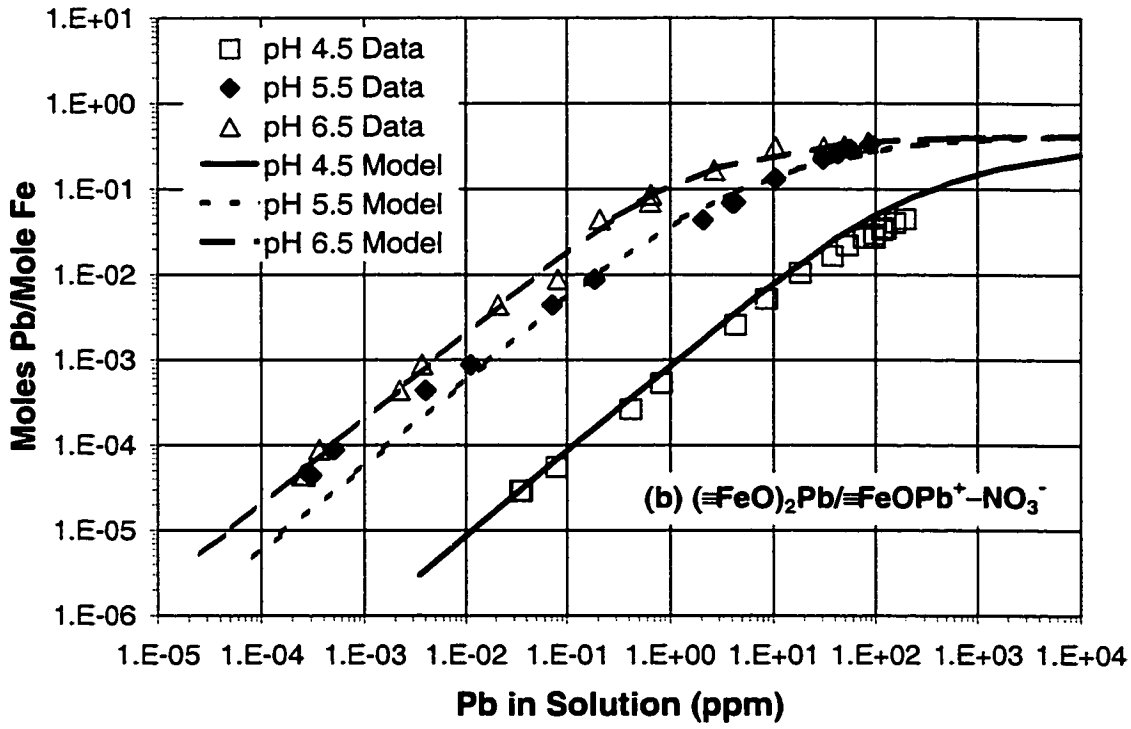

Figure 3.4 Continued.

Table 3.3 TLM parameters for single-solute Pb sorption onto 2-line ferrihydrite (fh) at room temperature in a N_2 atmosphere.

Species Pair	pH	log $K_{(\equiv FeO)_2Pb}$ @ 1 g fh/L [a, b]	log $K_{\equiv FeOHPb^{2+} \text{ or } \equiv FeOPb^{+}-NO_3^-}$ [c]	R_{avg} (Pb_{aq}) [d]	R_{avg} (Γ) [d]
$(\equiv FeO)_2Pb$/ $\equiv FeOHPb^{2+}$	4.5-5.5	5.00	-8.80	1.2	1.1
	6.5	6.16	-5.33	1.2	1.01
	3.0	2.44	-9.57	-	-
	3.5	3.39	-9.51	-	-
	4.0	4.28	-9.26	-	-
	6.0	5.67	-7.50	-	-
$(\equiv FeO)_2Pb$/ $\equiv FeOPb^{+}-NO_3^-$	4.5-5.5	5.04	-2.10	1.3	1.2
	6.5	5.97	-0.16	1.2	1.01
	3.0	9.00	-3.98	-	-
	3.5	3.69	-3.13	-	-
	4.0	5.04	-2.63	-	-
	6.0	5.68	-1.29	-	-

[a] $(\equiv FeO)_2Pb + 2H^+ = 2\equiv FeOH + Pb^{2+}$, where $K_{(\equiv FeO)_2Pb} = a_{Pb2+}[\equiv FeOH]^2/a_{H+}^2\gamma_s[(\equiv FeO)_2Pb]$. The γ_s correction applies for $(\equiv FeO)_2Pb/\equiv FeOHPb^{2+}$ only. [b] For bidentate-mononuclear surface complexes, K^{int} is actually a conditional K that depends on sorbent solids concentration, C_s, regardless. This peculiarity arises with multidentate complexes, because of the definition of the standard state for surface species in molality, rather than mole fraction. It can be shown that $K^{int} = K^{cond}/B$, where $B = N_s$ (sites/m^2) x A_s (m^2/g) x C_s (g/L) / N_A (6.02×10^{23} sites/mole sites). Hence, $K_2^{cond}/K_1^{cond} = C_{s2}/C_{s1}$ for the bidentate-mononuclear reactions written here as dissociation reactions. The bidentate-mononuclear Ks reported in the table are based on 1 g ferrihydrite/L. [c] $\equiv FeOHPb^{2+} = \equiv FeOH + Pb^{2+}$, where $K_{\equiv FeOHPb^{2+}} = a_{Pb2+}[\equiv FeOH]\exp(-2F\Psi_o/RT)/\gamma_s[\equiv FeOHPb^{2+}]$; and $\equiv FeOPb^{+}-NO_3^- + H^+ = \equiv FeOH + Pb^{2+} + NO_3^-$, where $K_{\equiv FeOPb^{+}-NO_3^-} = a_{Pb2+}a_{NO3-}[\equiv FeOH]\exp(F(\Psi_\beta - \Psi_o)/RT)/a_{H+}[\equiv FeOPb^{+}-NO_3^-]$. [d] R_{avg} reported for regressions of pH 4.5, 5.5, and 6.5 isotherm data only. Ks for other pH values are approximate based on regression of a few pH edge points only. The intent is to show how K varies with pH.

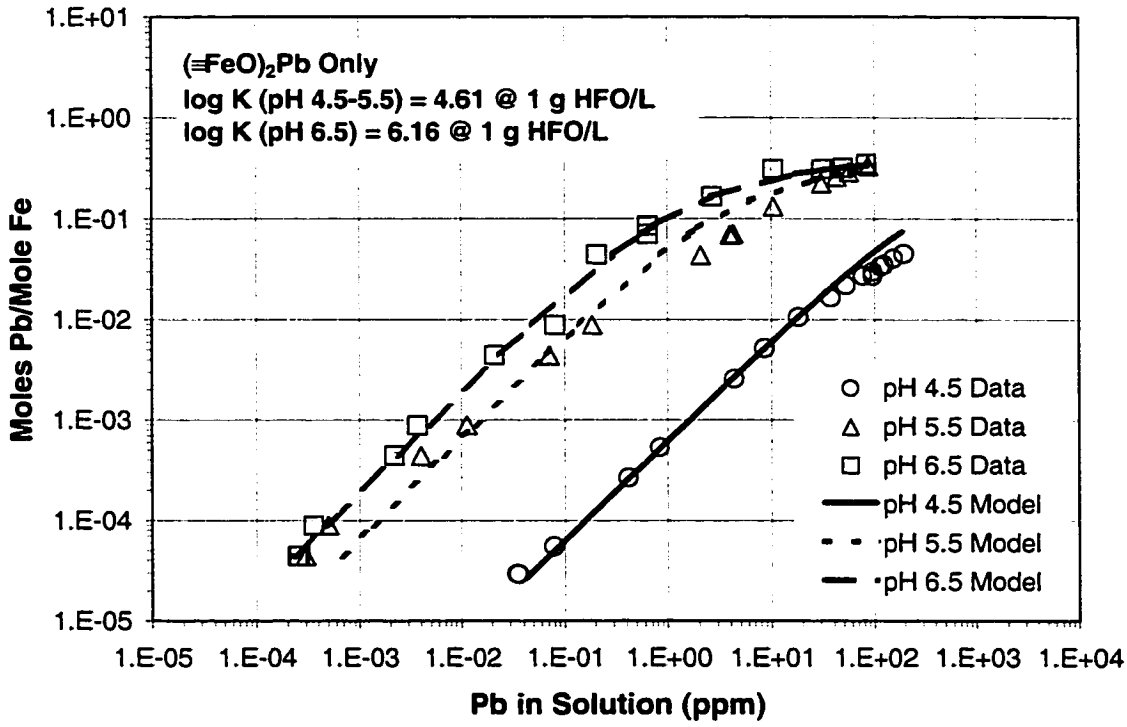

Figure 3.5 **Triple-layer model fits of pH 4.5, 5.5, and 6.5 equilibrium isotherm data for single-solute Pb sorption onto 2-line ferrihydrite using the bidentate-mononuclear species $(\equiv FeO)_2Pb$ only. Experimental conditions: 0.1 and 1.0 g ferrihydrite/L in 0.01 M $NaNO_3$; Pb added as $Pb(NO_3)_2$; 4-hour equilibration time; room temperature; N_2 glovebox. Surface activity coefficient correction ($\gamma_s=\gamma_{Pb2+}$) included in data regression. Model parameters are from Table 3.2.**

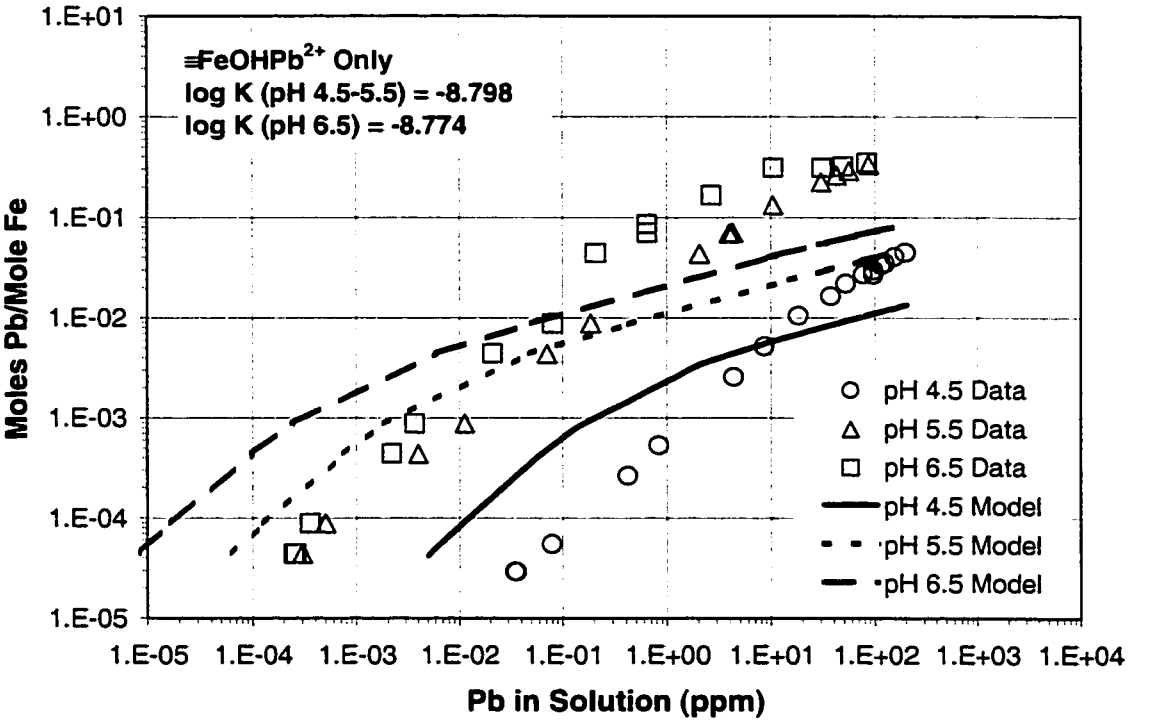

Figure 3.6 **Triple-layer model fits of pH 4.5, 5.5, and 6.5 equilibrium isotherm data for single-solute Pb sorption onto 2-line ferrihydrite using the monodentate-mononuclear species $\equiv FeOHPb^{2+}$ only. Experimental conditions: 0.1 and 1.0 g ferrihydrite/L in 0.01 M $NaNO_3$; Pb added as $Pb(NO_3)_2$; 4-hour equilibration time; room temperature; N_2 glovebox. Surface activity coefficient correction ($\gamma_s=\gamma_{Pb2+}$) included in data regression. Model parameters are from Table 3.2.**

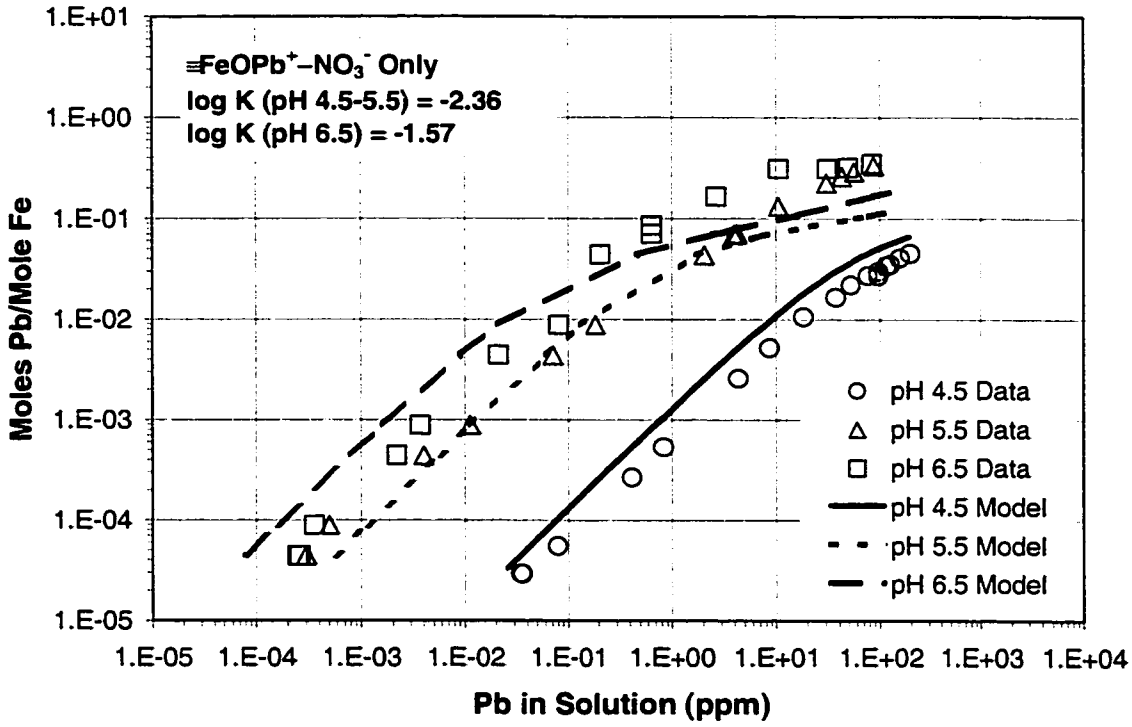

Figure 3.7 **Triple-layer model fits of pH 4.5, 5.5, and 6.5 equilibrium isotherm data for single-solute Pb sorption onto 2-line ferrihydrite using the monodentate-mononuclear species $\equiv FeOPb^{+}–NO_3^{-}$ only. Experimental conditions: 0.1 and 1.0 g ferrihydrite/L in 0.01 M $NaNO_3$; Pb added as $Pb(NO_3)_2$; 4-hour equilibration time; room temperature; N_2 glovebox. No surface activity coefficient correction included in data regression ($\gamma_s = 1.0$). Model parameters are from Table 3.2.**

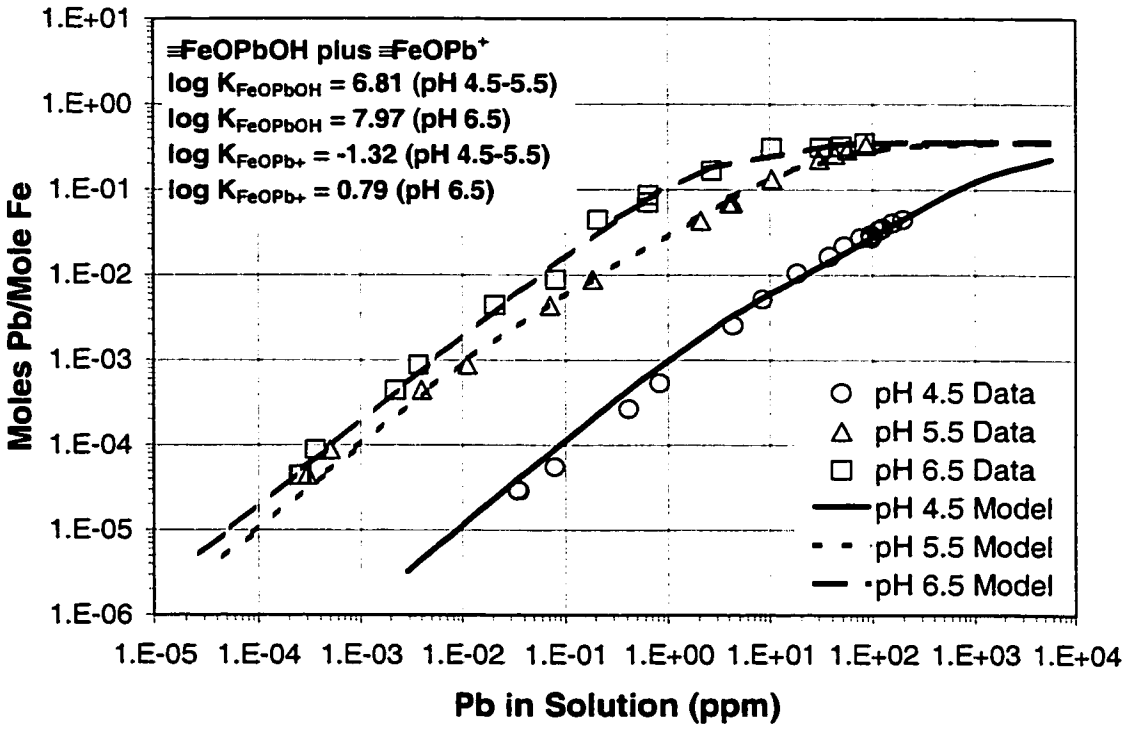

Figure 3.8 **Triple-layer model fits of pH 4.5, 5.5, and 6.5 equilibrium isotherm data for single-solute Pb sorption onto 2-line ferrihydrite using the species pair, ≡FeOPbOH and ≡FeOPb$^+$. Experimental conditions: 0.1 and 1.0 g ferrihydrite/L in 0.01 M $NaNO_3$; Pb added as $Pb(NO_3)_2$; 4-hour equilibration time; room temperature; N_2 glovebox. Surface activity coefficient correction ($\gamma_s=\gamma_{Pb2+}$) included in data regression. Model parameters: N_s = 0.36 moles sites/mole Fe; C_1 = 1.0 F/m^2; C_2 = 0.2 F/m^2; A_s = 600 m^2/g; log K_{a1}^{int} = -5.11; log K_{a2}^{int} = -10.71; log K_{NO3-}^{int} = -7.86; log K_{Na+}^{int} = 7.98.**

GTLM (Figures 3.9 and 3.10). The GTLM was evaluated for two cases—using the same site densities and log Ks for Pb(II) as proposed by Dzombak and Morel (1990) (Figure 3.9) and using modified Ks in combination with a much higher Type-2 site density of 0.9 moles sites/mole Fe (Figure 3.10).

As shown in Table 3.3, the same pair of equilibrium constants provided very good fits of both the pH 4.5 and 5.5 isotherm data over 5 orders of magnitude in Pb(II) concentration. At pH 6.5, however, the values of K^{int} for the Pb(II) surface complexes required adjustment; that is, the binding strength of the surface complexes was reduced. No change in surface speciation or N_s was necessary to fit the pH 6.5 data. For this reason, equilibrium constants for the Pb(II) surface complexes are reported as conditional Ks (K_i), rather than as intrinsic Ks (K_i^{int}). To explore this further, pH-sorption-edge data were plotted with isotherm data on the same graph. Figure 3.11 shows excellent agreement between the pH-edge and isotherm data, indicating that the data is internally consistent. Interestingly, Figure 3.11 suggests that a reduction in spacing between the constant-pH isotherms should be expected based on the inherent shape of a pH-sorption edge. More specifically, $d[pPb_{aq}]/d[pH]$ changes significantly over the course of a pH-sorption edge. At low and high values of % Pb sorbed, the change in sorbed Pb(II) and, hence, in total [Pb(II) (aq)] is relatively small for a unit change in pH (i.e., $d[pPb_{aq}]/d[pH]$ is small). However, over a narrow pH range, the change in sorbed Pb(II) with pH increases substantially (i.e., $d[pPb_{aq}]/d[pH]$ is large). For Pb(II), the steep slope of the pH-sorption edge occurs over the pH range 4 to 5.5 where $d[pPb_{aq}]/d[pH]$ peaks at about 2.0. By pH 6.5, however, the sorption edge has begun to plateau and $d[pPb_{aq}]/d[pH]$ is 0.5 or less. The constant-pH isotherm curves for pH 3, 3.5, 4, and 6 shown in Figure 3.11 represent model fits to the pH-edge

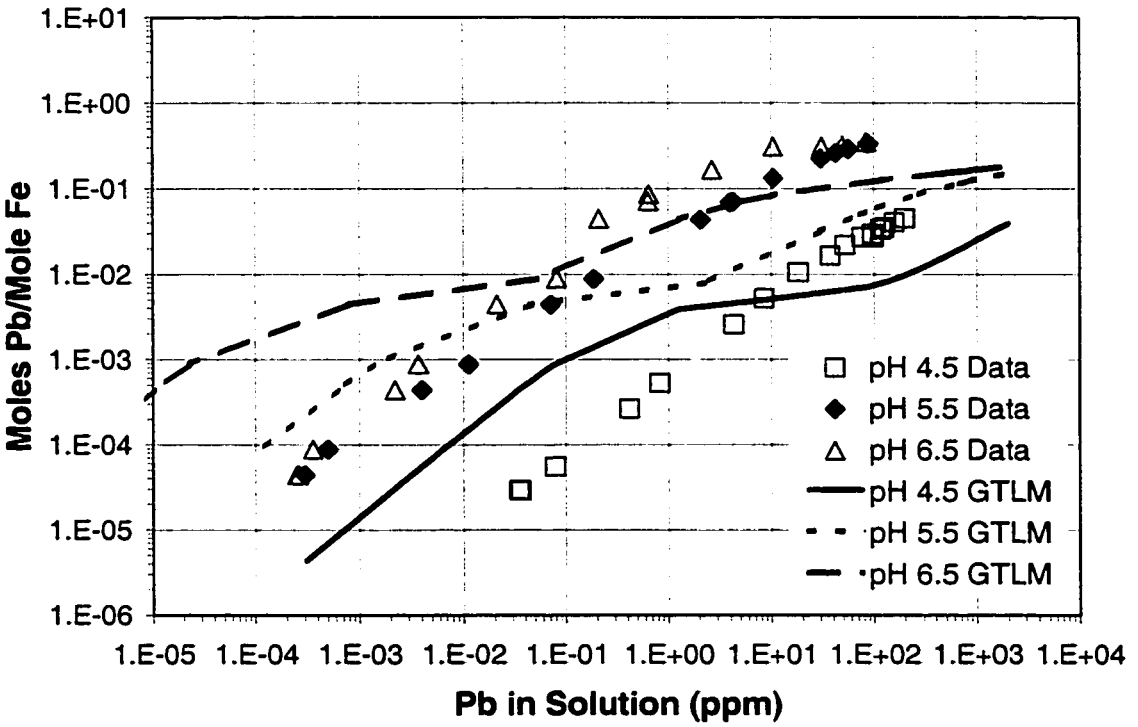

Figure 3.9 **Generalized two-layer model (GTLM) fits of pH 4.5, 5.5, and 6.5 equilibrium isotherm data for single-solute Pb sorption onto 2-line ferrihydrite using the same speciation assumptions, log K values, site types, and site densities reported in Dzombak and Morel (1990). Experimental data conditions: 0.1 and 1.0 g ferrihydrite/L in 0.01 M $NaNO_3$; Pb added as $Pb(NO_3)_2$; 4-hour equilibration time; room temperature; N_2 glovebox. Model parameters: $N_s = 0.005$ moles Type 1 sites/mole Fe and 0.2 moles Type 2 sites/mole Fe; $A_s = 600$ m^2/g; log $K_{a1}^{int} = -7.29$; log $K_{a2}^{int} = -8.93$; log $K_{1,Pb}^{int} = 4.65$; log $K_{2,Pb}^{int} = 0.3$. Reported log K values are for reactions as written using the convention of Dzombak and Morel (1990), rather than the OLI convention.**

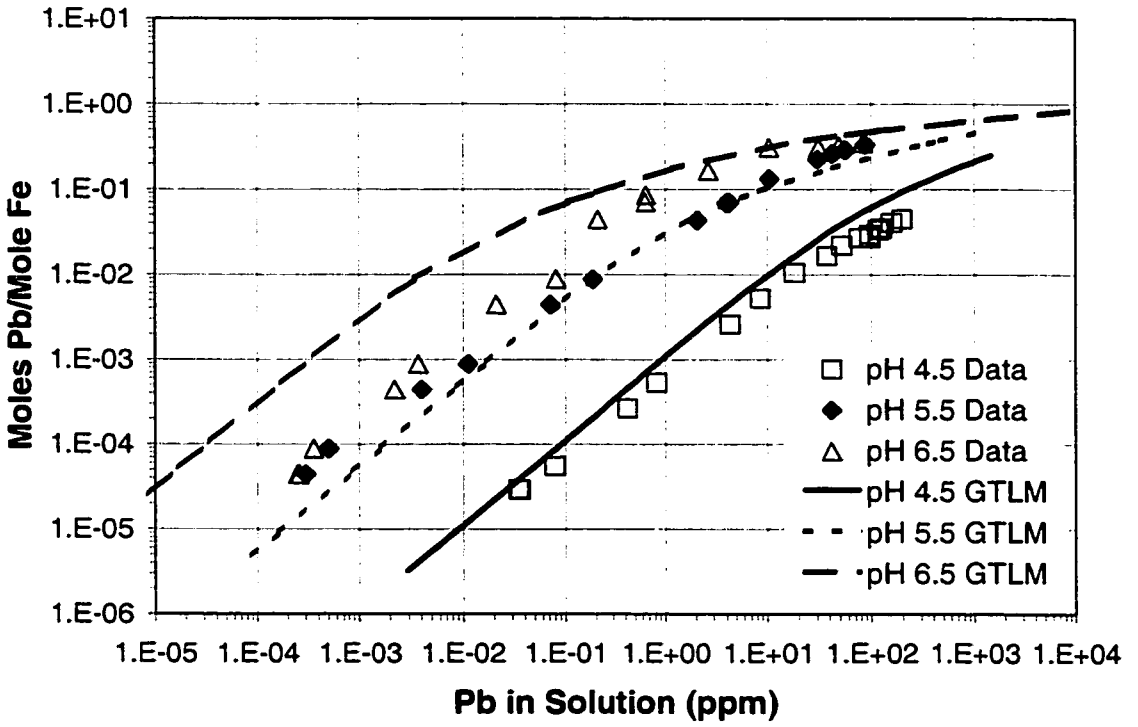

Figure 3.10 **Generalized two-layer model (GTLM) fits of pH 4.5, 5.5, and 6.5 equilibrium isotherm data for single-solute Pb sorption onto 2-line ferrihydrite using adjusted log K values and a much higher Type-2 site density. Experimental data conditions: 0.1 and 1.0 g ferrihydrite/L in 0.01 M $NaNO_3$; Pb added as $Pb(NO_3)_2$; 4-hour equilibration time; room temperature; N_2 glovebox. Model parameters: $N_s = 0.005$ moles Type 1 sites/mole Fe and 0.9 moles Type 2 sites/mole Fe; $A_s = 600$ m^2/g; log $K_{a1}^{int} = -6.43$; log $K_{a2}^{int} = -9.75$; log $K_{1,Pb}^{int} = 2.5$; log $K_{2,Pb}^{int} = 1.0$. Reported log K values are for reactions as written using the convention of Dzombak and Morel (1990), rather than the OLI convention.**

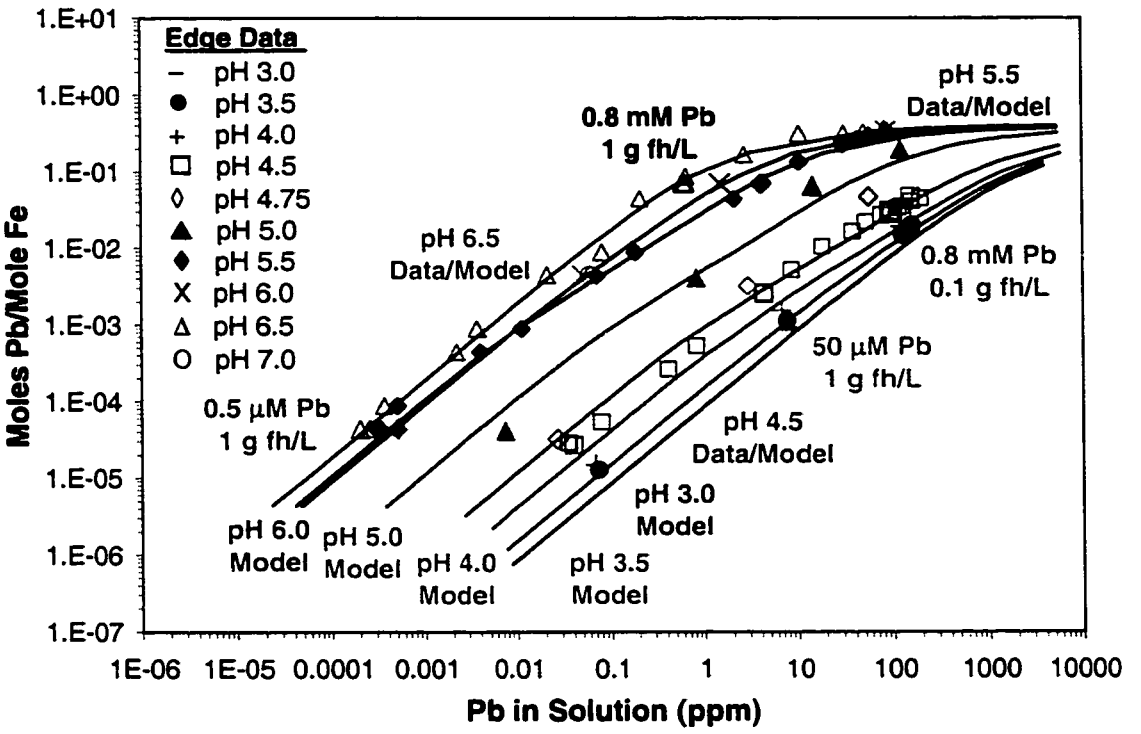

Figure 3.11 **Comparison of constant-pH-isotherm and pH-sorption-edge data to modified triple-layer model predictions for single-solute Pb(II) sorption onto 2-line ferrihydrite assuming the species pair $(\equiv FeO)_2Pb/\equiv FeOHPb^{2+}$ [log $K_{(\equiv FeO)_2Pb}$ = 2.44, 3.39, 4.28, 5.00, 5.67, & 6.16 and log $K_{\equiv FeOHPb^{2+}}$ = -9.57, -9.51, -9.26, -8.80, -7.50, & -5.33 at pH 3.0, 3.5, 4.0, 4.5-5.5, 6.0, & 6.5, respectively]. Experimental conditions: 0.1 and 1.0 g ferrihydrite/L; 0.01 M $NaNO_3$ background electrolyte for isotherms and edges; Pb(II) added as $Pb(NO_3)_2$; 4-hour equilibration time; room temperature; N_2 glovebox.**

data only for the species pair, $(\equiv FeO)_2Pb$ plus $\equiv FeOHPb^{2+}$. Oxide surface parameters for the TLM (Table 3.2) and the assumed surface speciation were the same as those used to regress the pH 4.5, 5.5, and 6.5 isotherm data. Conditional equilibrium constants for each pH value are given in Table 3.3. The pH-5 isotherm curve shown in Figure 3.11 was predicted using the best-fit log $K_{(\equiv FeO)_2Pb}$ and log $K_{\equiv FeOHPb^{2+}}$ values reported for pH 4.5-5.5 in Table 3.3. Although not shown, results for the $(\equiv FeO)_2Pb/\equiv FeOPb^{+}–NO_3^{-}$ species pair are very similar; conditional Ks as a function of pH are reported in Table 3.3 as well.

Figure 3.12 compares TLM predictions to pH-edge data (50 μM Pb(II); 1 g ferrihydrite/L; 0.001, 0.01, and 0.1 M $NaNO_3$) presented in Trivedi et al. (2002a) and Appendix A. Figure 3.12a displays model predictions for the $(\equiv FeO)_2Pb/\equiv FeOHPb^{2+}$ species pair using (1) best-fit equilibrium constants for the pH 4.5/5.5 data only, and (2) aqueous activity coefficient corrections for bulk solution ions only (i.e., the ratio of the surface activity coefficients is assumed to equal 1.0) (Sahai and Sverjensky, 1998). Note that the model significantly underpredicts Pb(II) sorption at pH < 4.0. Although not evident in the figure, the model also overpredicts Pb(II) sorption at pH > 6. The same was true for the $(\equiv FeO)_2Pb/\equiv FeOPb^{+}–NO_3^{-}$ species pair (Figure 3.12b). The nonzero plateau in the pH-edge data at low pH seems questionable at first; however, others have also reported pH edges for divalent metal sorption onto amorphous ferric hydroxides with this same phenomenon (Davis and Leckie, 1978; Swallow et al., 1980; Benjamin and Bloom, 1981; Benjamin, 1983; Harvey and Linton, 1984; Misak et al., 1996). This plateau seems to occur most often for HFO at low metal-to-sorbent ratios (i.e., in dilute systems). For example, note the difference in the pH edges for sorption of 800μM Pb(II) onto 1.0 g versus 0.1 g ferrihydrite/L (Figures 3.13 and

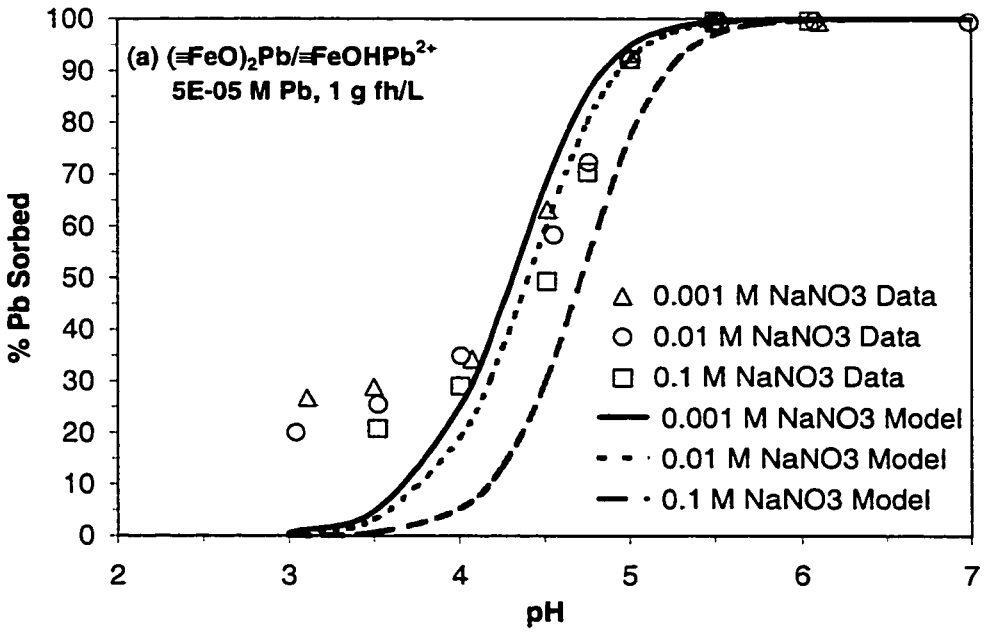

Figure 3.12 **Triple-layer model predictions of pH-sorption-edge data for single-solute Pb(II) sorption onto 2-line ferrihydrite. Fits for (a) $(\equiv FeO)_2Pb/\equiv FeOHPb^{2+}$ using $\gamma_s = 1.0$ and best-fit Ks for pH 4.5-5.5 data only [log $K_{(\equiv FeO)_2Pb} = 5.00$ & log $K_{\equiv FeOHPb^{2+}} = -8.80$]; (b) $(\equiv FeO)_2Pb/\equiv FeOPb^{+}–NO_3^{-}$ using $\gamma_s = 1.0$ and best-fit Ks for pH 4.5-5.5 data only [log $K_{(\equiv FeO)_2Pb} = 5.04$ & log $K_{\equiv FeOPb^{+}\text{-}NO_3^{-}} = -2.10$]; (c) $(\equiv FeO)_2Pb/\equiv FeOHPb^{2+}$ using $\gamma_s=\gamma_{Pb2+}$ correction and pH-adjusted Ks from Table 3.3 [log $K_{(\equiv FeO)_2Pb} = 2.44, 3.39, 4.28, 5.00, 5.67,$ & 6.16 and log $K_{\equiv FeOHPb^{2+}} = -9.57, -9.51, -9.26, -8.80, -7.50,$ & -5.33 at pH 3.0, 3.5, 4.0, 4.5-5.5, 6.0, & 6.5, respectively]; (d) $(\equiv FeO)_2Pb/\equiv FeOPb^{+}–NO_3^{-}$ using $\gamma_s = 1.0$ and pH-adjusted Ks from Table 3.3 [log $K_{(\equiv FeO)_2Pb} = 9.00, 3.69, 5.04, 5.04, 5.68,$ & 5.97 and log $K_{\equiv FeOPb^{+}\text{-}NO_3^{-}} = -3.98, -3.13, -2.63, -2.10, -1.29,$ & -0.16 at pH 3.0, 3.5, 4.0, 4.5-5.5, 6.0, & 6.5, respectively]. Experimental conditions: 1.0 g ferrihydrite/L; 0.001-0.1 M $NaNO_3$; 50 μM Pb(II) added as $Pb(NO_3)_2$; 4-hour equilibration time; room temperature; N_2 glovebox.**

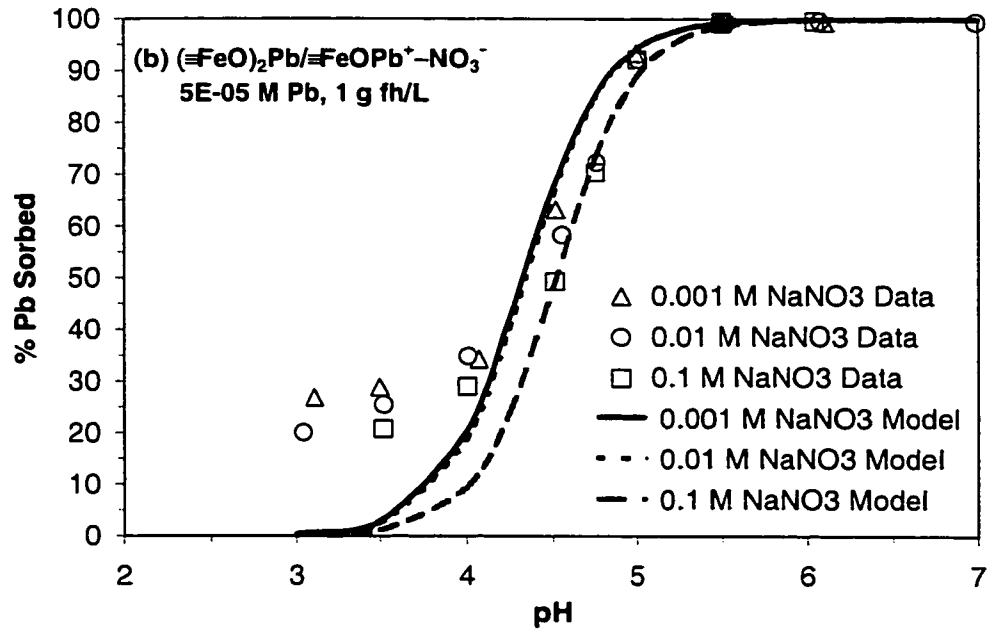

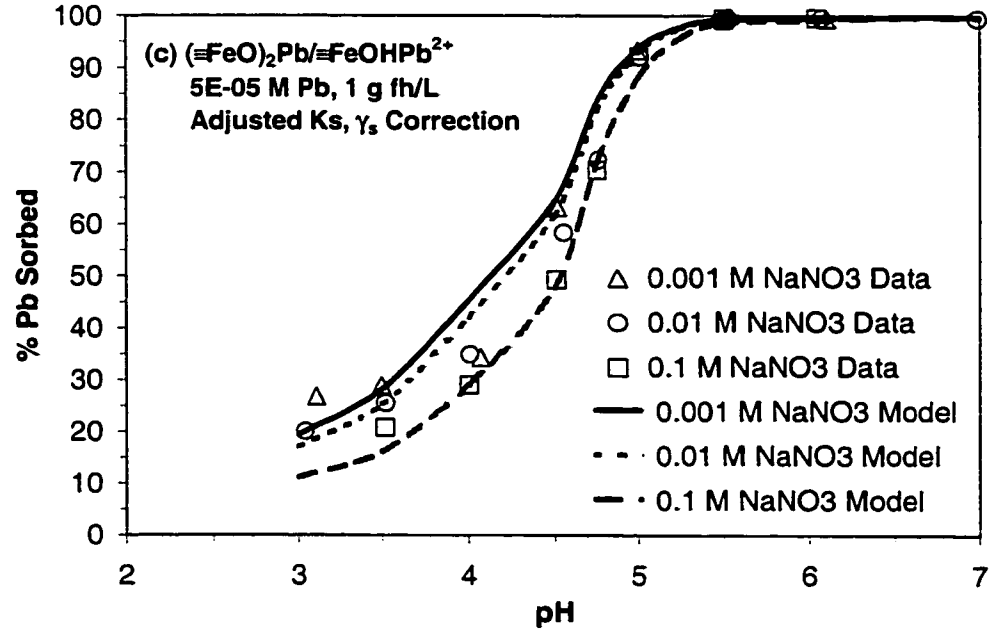

Figure 3.12 Continued.

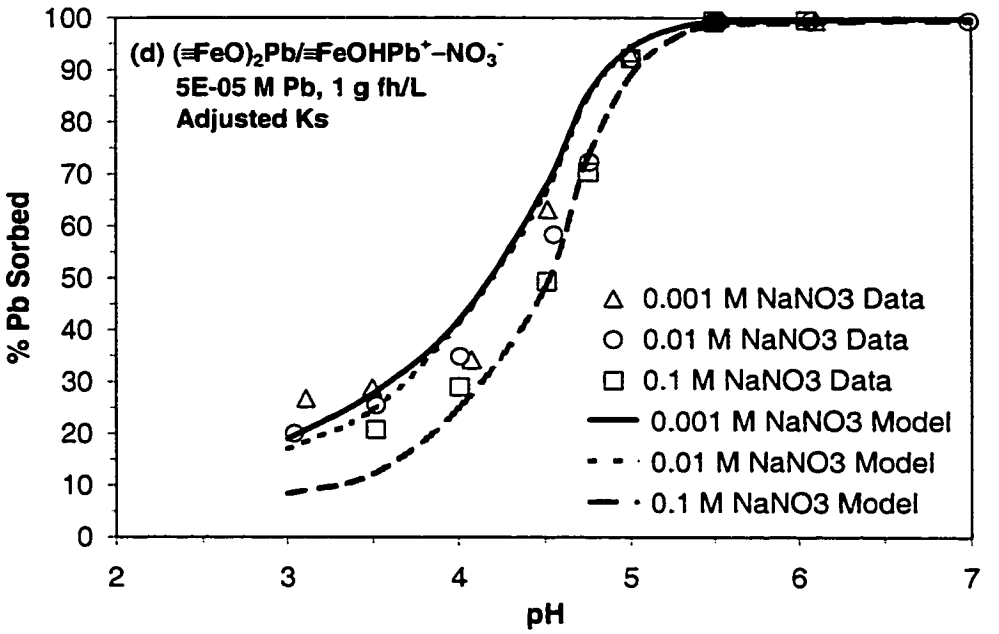

Figure 3.12 Continued.

3.14). The plateau is absent at 0.1 g ferrihydrite/L. Interestingly, Dzombak and Morel (1990) report no pH-edge data for divalent metals below pH 4.0-4.5.

Figure 3.12a also shows that model curves for the $(\equiv FeO)_2Pb/\equiv FeOHPb^{2+}$ species pair display a much stronger ionic-strength dependence than suggested by the 0.1 M $NaNO_3$ data. This is an artifact of the modified TLM thermodynamic framework itself. First, bulk solution concentrations and activity coefficients for the sorbing ions (i.e., H^+, NO_3^-, Na^+, and Pb^{2+}) are used in the mass-law expressions (because we know how to measure and estimate them, respectively), rather than true surface species activities themselves (Robertson and Leckie, 1997). Second, lacking a way to directly determine the activity of a surface complex as well as a predictive model for estimating surface activity coefficients, the ratio of the activity coefficients for the surface species (i.e., $(\equiv FeO)_2Pb$, $\equiv FeOHPb^{2+}$, and $\equiv FeOH$) is assumed to equal

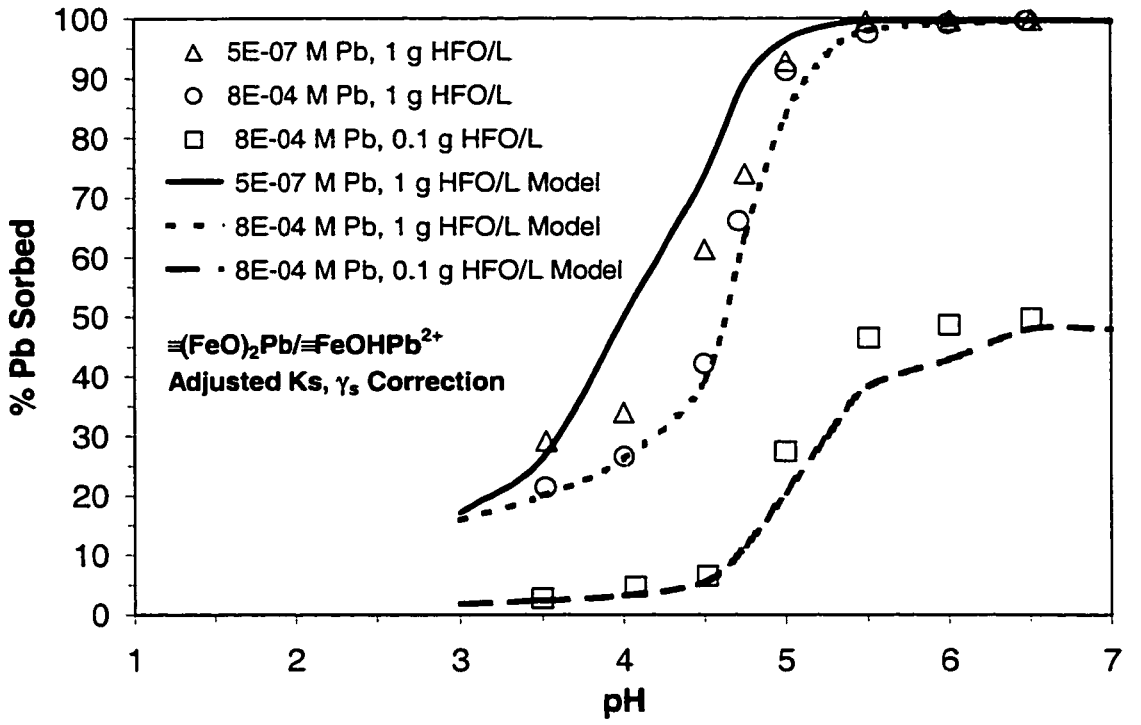

Figure 3.13 **Comparison of triple-layer model predictions to pH edge data for single-solute Pb sorption onto 2-line ferrihydrite assuming the species pair, $(\equiv FeO)_2Pb/\equiv FeOHPb^{2+}$, using pH-adjusted Ks from Table 3.3, and including a correction for surface activity coefficients ($\gamma_s=\gamma_{Pb2+}$). Experimental conditions: 1.0 g ferrihydrite/L; 0.01 M $NaNO_3$; Pb added as $Pb(NO_3)_2$; 4-hour equilibration time; room temperature; N_2 glovebox.**

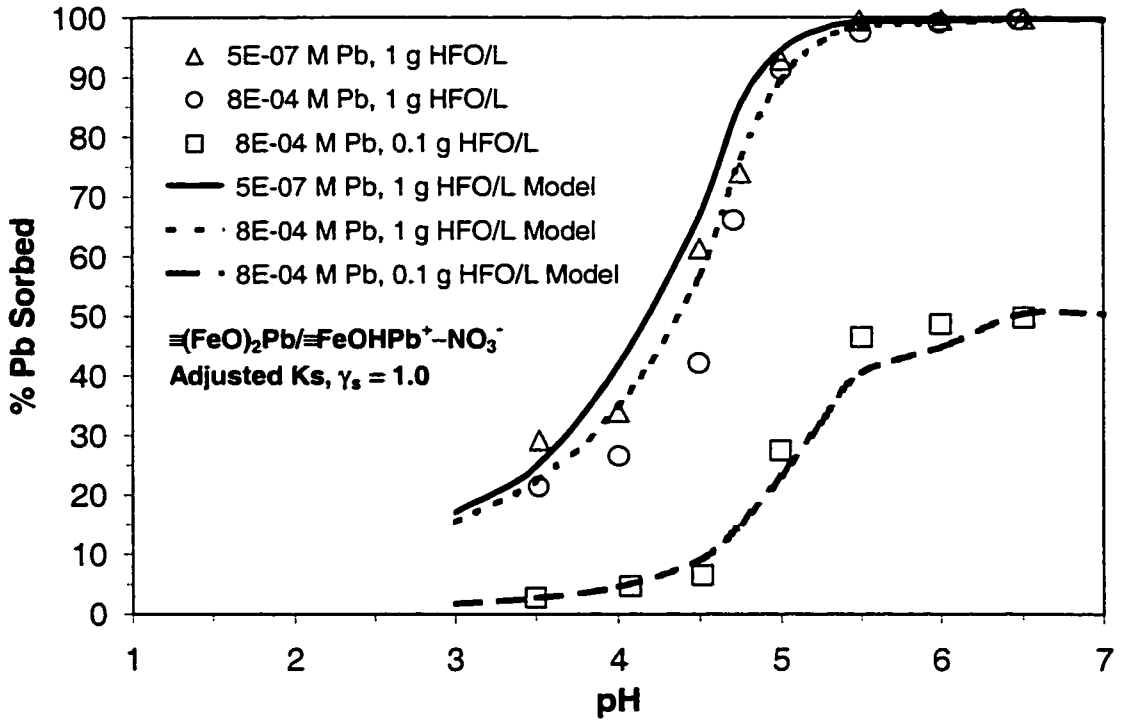

Figure 3.14 **Comparison of triple-layer model predictions to pH edge data for single-solute Pb sorption onto 2-line ferrihydrite assuming the species pair, $(\equiv FeO)_2Pb/\equiv FeOPb^+–NO_3^-$, using pH-adjusted Ks from Table 3.3, and including no correction for surface activity coefficients (γ_s=1.0). Experimental conditions: 1.0 g ferrihydrite/L; 0.01 M $NaNO_3$; Pb added as $Pb(NO_3)_2$; 4-hour equilibration time; room temperature; N_2 glovebox.**

1.0. In essence, this represents only a "partial correction" for nonidealities at the surface. To correct for the overprediction of the ionic-strength dependence, a surface activity term (γ_s) was used in the OLI model to better match the pH-edge data. Interestingly, the best agreement between the predicted curves and actual data was obtained when γ_s was set equal to γ_{Pb2+}, the bulk solution activity coefficient for the Pb^{2+} ion. The γ_s term was also used during regression of the isotherm data for the $(\equiv FeO)_2Pb/\equiv FeOHPb^{2+}$ species pair; therefore, the equilibrium constants given in Table 3.3 include this correction.

Interestingly, ionic-strength dependence is less with the species pair, $(\equiv FeO)_2Pb/\equiv FeOPb^{+}–NO_3^{-}$, as shown in Figure 3.12b. Criscenti and Sverjensky (1999) found that surface species of the form, $\equiv FeOPb^{+}–NO_3^{-}$, $\equiv FeOHPb^{2+}–NO_3^{-}$ and so on, better represented the ionic-strength dependence of metal sorption in nitrate solutions. At the present time, spectroscopy is unable to prove whether this type of surface species actually exists at the surface or whether it is necessary because of the construct of the TLM thermodynamic framework itself.

Figures 3.12c and 3.12d display TLM predictions for both species pairs when pH-adjusted Ks are used, rather than the best-fit equilibrium constants for pH 4.5/5.5 only. In other words, log K values for the Pb surface complexes in the model were adjusted with pH as reported in Table 3.3. In addition, Figure 3.12c includes the γ_s correction. Note the good agreement between the model curves and the actual data. The better fit at pH < 4 was accomplished without introducing a second, high-affinity site type or additional surface species as has often been done in past modeling studies that are based on pH-edge data only. Although not shown, introducing a second, high-affinity site to account for the elevated Pb(II) sorption at pH < 4 resulted in

unacceptable fits of the isotherm data at low Pb(II) concentrations. Instead, when considered together, the isotherm and edge data suggest that a one-site, two-species model is sufficient, but that the best-fit equilibrium constants are valid over a limited pH range only. Additional pH-edge data (Trivedi et al., 2002a; Appendix A) at different Pb(II):Fe ratios were also compared against the TLM-predicted edges (see Figures 3.13 and 3.14).

3.4.3 Implications for Surface Complexation Modeling

This study highlights the benefits of combining comprehensive molecular- and macroscopic-scale studies conducted by the same researcher in the same laboratory with surface complexation modeling. Regressing constant-pH isotherm data together with potentiometric-titration and pH-edge data is clearly a much more rigorous test of the SCM. When combined with spectroscopic data on surface speciation, the scope of feasible surface complexes and site types becomes much more limited. In this work, application of the triple-layer SCM led to the same conclusions about Pb(II) speciation on the ferrihydrite surface as did analysis of the spectroscopic data in Trivedi et al. (2002a). More specifically, the authors found that regressing pH-edge data in the absence of isotherm and spectroscopic data resulted in a much larger number of surface-species and site-type combinations that provided acceptable fits of the edge data. However, when these same assumptions were used to predict the constant-pH isotherms, the agreement between model and data was poor in most cases. In conclusion, the results of this research suggest that the ability of SCMs to predict single-solute sorption over a wide range of conditions is still not completely resolved. While many advances have been made over the past decade, much more work still needs to be done in fine-tuning the thermodynamic framework and databases.

3.5 References

Anderko A., Sanders S. J., and Young R. D. (1997) Real-solution stability diagrams: A thermodynamic tool for modeling corrosion in wide temperature and concentration ranges. *Corrosion* **53,** 43-53.

Balistrieri L. S. and Murray J. W. (1982) The adsorption of Cu, Pb, Zn, and Cd on goethite from major ion seawater. *Geochim. Cosmochim. Acta* **46,** 1253-1265.

Benjamin M. M. (1979) Effects of competing metals and complexing ligands on trace metal adsorption at the oxide/solution interface. Ph.D. dissertation. Stanford University.

Benjamin M. M. (1983) Adsorption and surface precipitation of metals on amorphous iron oxyhydroxide. *Environ. Sci. Technol.* **17,** 686-692.

Benjamin M. M. and Bloom N. S. (1981) Effects of strong binding of anionic adsorbates on adsorption of trace metals on amorphous iron oxyhydroxide. In *Adsorption From Aqueous Solutions* (ed. P.H. Tewari), pp. 41-60. Plenum Press.

Brown G. E. Jr., Parks G. A., Bargar J. R., and Towle S. N. (1998) Use of x-ray absorption spectroscopy to study reaction mechanisms at metal oxide-water interfaces. In *Mineral-Water Interfacial Reactions: Kinetics and Mechanisms* (eds. D.L. Sparks and T.J. Grundl), ACS Symposium Series 715, pp. 14-36. American Chemical Society.

Catts J. G. and Langmuir D. (1986) Adsorption of Cu, Pb, and Zn by δMnO_2: Applicability of the site binding-surface complexation model. *Appl. Geochem.* **1,** 255-264.

Chase M. W. Jr., Davies C. A., Downey J. R. Jr., Frurip D. J., McDonald R. A., and Syverud A. N. (1985) JANAF thermochemical tables. 3rd ed., Suppl. No. 1. *J. Phys. Chem. Ref. Data* **14,** 1-1856.

Christl I. and Kretzschmar R. (1999) Competitive sorption of copper and lead at the oxide-water interface: Implications for surface site density. *Geochim. Cosmochim. Acta* **63,** 2929-2938.

Cowan C. E., Zachara J. M., and Resch C. T. (1991) Cadmium adsorption on iron oxides in the presence of alkaline-earth elements. *Environ. Sci. Technol.* **25,** 437-446.

Criscenti L. J. and Sverjensky D. A. (1999) The role of electrolyte anions (ClO_4^-, NO_3^-, and Cl^-) in divalent metal (M^{2+}) adsorption on oxide and hydroxide surfaces in salt solutions. *Am. J. Sci.* **299,** 828-899.

Daubert T. E. and Danner R. P. (1989) *Physical and Thermodynamic Properties of Pure Chemicals: DIPPR Data Compilation.* Hemisphere Publishing Corp.

Davis J. A. and Leckie J. O. (1978) Surface ionization and complexation at the oxide/water interface. II. Surface properties of amorphous iron oxyhydroxide and adsorption of metal ions. *J. Colloid Interface Sci.* **67,** 90-107.

Dzombak D. A. and Morel F. M. M. (1990) *Surface Complexation Modeling: Hydrous Ferric Oxide.* John Wiley & Sons.

Glushko V. P., Medvedev V. A., Bergman G. A., Vasil'ev B. P., Kolesov W. P., Gurvich L. V., Yungmand V. S., Khodakovskii I. L., Resnitskii L. A., Smirnova N. L., Gal'chenko G. L., Alekseev V. I., Vorob'ev A. F., Baibuz V. F., Kostryukov B. N., and Biryokov B. P. (1965-1981) *Thermo Constants of Compounds.* Academy of Sciences, Moscow, USSR, vols. 1-10.

Gunneriusson L., Lovgren L., and Sjoberg S. (1994) Complexation of Pb(II) at the goethite (∝-FeOOH)/water interface: The influence of chloride. *Geochim. Cosmochim. Acta* **58,** 4973-4983.

Gurvich L.V., Veyts I. V., Medvedev V. A., Khachkuruzov G. A., Yungman V. S., Bergman G. A., Iorish V. S., Yurkov G. N., Gorbov S. I., Kuratova L. F., Trishcheva N. P., Przheval'skiy I. N., Leonidov V. Ya., Ezhov Yu. S., Tomberg S. E., Nazarenko I. I., Rogatskiy A. L., Dorofeyeva O. V., and Demidova M. S. (1989) *Thermodynamic Properties of Individual Substances.* 4th ed., USSR Academy of Sciences, Institute for High Temperatures and State Institute of Applied Chemistry, Hemisphere Publishing Corporation, vols. 1-5.

Harvey D. T. and Linton R. W. (1984) X-ray photoelectron spectroscopy (XPS) of adsorbed zinc on amorphous hydrous ferric oxide. *Colloids Surf.* **11,** 81-96.

Hayes K. F. (1987) Equilibrium, spectroscopic, and kinetic studies of ion adsorption at the oxide/aqueous interface. Ph.D. dissertation. Stanford University.

Hayes K. F. and Katz L. E. (1996) Application of x-ray absorption spectroscopy for surface complexation modeling of metal ion sorption. In *Physics and Chemistry of Mineral Surfaces* (ed. P.V. Brady), pp. 147-223. CRC Press.

Hsi C-K. D. and Langmuir D. (1985) Adsorption of uranyl onto ferric oxyhydroxides: Application of the surface complexation site-binding model. *Geochim. Cosmochim. Acta* **49,** 1931-1941.

Hunter K. A., Hawke D. J., and Choo L. K. (1988) Equilibrium adsorption of thorium by metal oxides in marine electrolytes. *Geochim. Cosmochim. Acta* **52,** 627-636.

Kanungo S. B. (1994) Adsorption of cations on hydrous oxides of iron. II. Adsorption of Mn, Co, Ni, and Zn onto amorphous FeOOH from simple electrolyte solutions as well as from a complex electrolyte solution resembling seawater in major ion content. *J. Colloid Interface Sci.* **162,** 93-102.

Katz L. E. and Boyle-Wight E. J. (2001) Application of spectroscopic methods to sorption model parameter estimation. In *Physical and Chemical Processes of Water and Solute Transport/Retention in Soil*, (eds. H.M. Selim and D.L. Sparks), SSSA Special Publication No. 56, pp. 213-255. Soil Science Society of America.

Katz L. E. and Hayes K. F. (1995a) Surface complexation modeling. I. Strategy for modeling monomer complex formation at moderate surface coverage. *J. Colloid Interface Sci.* **170,** 477-490.

Katz L. E. and Hayes K. F. (1995b) Surface complexation modeling. II. Strategy for modeling polymer and precipitation reactions at high surface coverage. *J. Colloid Interface Sci.* **170,** 491-501.

Kooner Z. S., Cox C. D., and Smoot J. L. (1995) Prediction of adsorption of divalent heavy metals at the goethite/water interface by surface complexation modeling. *Environ. Toxicol. Chem.* **14,** 2077-2083.

Koretsky C. (2000) The significance of surface complexation reactions in hydrologic systems: A geochemist's perspective. *J. Hydrol.* **230,** 127-171.

Koretsky C. M., Sverjensky D. A., and Sahai N. (1998) A model of surface site types on oxide and silicate minerals based on crystal chemistry: Implications for site types and densities, multi-site adsorption, surface infrared spectroscopy, and dissolution kinetics. *Am. J. Sci.* **298,** 349-438.

Kulik D. A. (2000) Thermodynamic properties of surface species at the mineral-water interface under hydrothermal conditions: A Gibbs energy minimization single-site $2pK_A$ triple-layer model of rutile in NaCl electrolyte to 250°C. *Geochim. Cosmochim. Acta* **64,** 3161-3179.

Kulik D. A. (2002) Gibbs energy minimization approach to modeling sorption equilibria at the mineral-water interface: Thermodynamic relations for multi-site-surface complexation. *Am. J. Sci.* **302,** 227-279.

Misak N. Z., Ghoneimy H. F., and Morcos T. N. (1996) Adsorption of Co^{2+} and Zn^{2+} ions on hydrous Fe(III), Sn(IV), and Fe(III)/Sn(IV) oxides. II. Thermal behavior of loaded oxides, isotopic exchange equilibria, and percentage adsorption-pH curves. *J. Colloid Interface Sci.* **184,** 31-43.

Oelkers E. H., Helgeson H. C., Shock E. L., Sverjensky D. A., Johnson J. W., and Pokrovskii V. A. (1995) Summary of the apparent standard partial molal gibbs free energies of aqueous species, minerals, and gases at pressures 1 to 5000 bars and temperatures 25 to 1000 °C. *J. Phys. Chem. Ref. Data* **24,** 1401-1560.

Rafal M., Berthold J. W., Scrivner N. C., and Grise S. L. (1994a) Models for electrolyte solutions. In *Models for Thermodynamic and Phase Equilibria Calculations* (ed. S. I. Sandler), pp. 601-670. Marcel Dekker, Inc.

Rafal M., Black P., Sanders S. J., Tolmach P. I., and Young R. D. (1994b) Development of a comprehensive environmental simulation program. Presented at the AIChE 1994 Spring National Meeting, April 17-21, Atlanta, Ga.

Robertson A. P. and Leckie J. O. (1997) Cation binding predictions of surface complexation models: Effects of pH, ionic strength, cation loading, surface complex, and model fit. *J. Colloid Interface Sci.* **188,** 444-472.

Robertson A. P. and Leckie J. O. (1998) Acid/base, copper binding, and Cu^{2+}/H^{+} exchange properties of goethite, an experimental and modeling study. *Environ. Sci. Technol.* **32,** 2519-2530.

Sahai N. and Sverjensky D. A. (1997) Solvation and electrostatic model for specific electrolyte adsorption. *Geochim. Cosmochim. Acta* **61,** 2827-2848.

Sahai N. and Sverjensky D. A. (1998) GEOSURF: A computer program for modeling adsorption on mineral surfaces from aqueous solution. *Comput. Geosci.* **24,** 853-873.

Sanders S. J., Rafal M., Clark D. M., Young R. D., Scrivner N. C., Pease R. A., Grise S. L., and Diemer R. B. (1988) Modeling the separation of amino acids by ion-exchange chromatography. *Chem. Eng. Prog.* **92,** 47-54.

Scheinost A. C., Abend S., Pandya K. I., and Sparks D. L. (2001) Kinetic controls on Cu and Pb sorption by ferrihydrite. *Environ. Sci. Technol.* **35,** 1090-1096.

Scrivner N. C., Butler P. B., and Karmazyn J. (1996) Modeling: An excellent solution for remediation. Presented at the 69th Annual Conference and Exposition of the Water Environment Federation, October 5-9, Session No. 5, Dallas, TX.

Shock E. L. and Helgeson H. C. (1988) Calculation of the thermodynamics and transport properties of aqueous species at high pressures and temperatures: Correlation algorithms for ionic species and equation of state predictions to 5 kbar and 1000 °C. *Geochim. Cosmochim. Acta* **52,** 2009-2036.

Sparks D. L. (1995) *Environmental Soil Chemistry.* Academic Press.

Sverjensky D. A. (2001) Interpretation and prediction of triple-layer model capacitances and the structure of the oxide-electrolyte-water interface. *Geochim. Cosmochim. Acta* **65,** 3643-3655.

Sverjensky D. A. and Sahai N. (1996) Theoretical prediction of single-site surface-protonation equilibrium constants for oxides and silicates in water. *Geochim. Cosmochim. Acta* **60,** 3773-3797.

Swallow K. C., Hume D. N., and Morel F. M. M. (1980) Sorption of copper and lead by hydrous ferric oxide. *Environ. Sci. Technol.* **14,** 1326-1331.

Trivedi P., Dyer J. A., and Sparks D. L. (2002a) Lead sorption onto ferrihydrite. 1. A macroscopic and spectroscopic assessment. *Environ. Sci. Technol.* (In press).

Wagman D. D., Evans W. H., Parker V. B., Schumm R. H., Halow I., Bailey S. M., Churney K. L., and Nuttall R. L. (1982) The NBS tables of chemical thermodynamic properties. Selected values for inorganics and C1 and C2 organic substances in SI units. Suppl. No. 2. *J. Phys. Chem. Ref. Data* **11,** 1-392.

Zemaitis J. F. Jr., Clark D. M., Rafal M., and Scrivner N. C. (1986) *Handbook of Aqueous Electrolyte Thermodynamics: Theory and Application. Design Institute for Physical Property Data.* American Institute of Chemical Engineers, Inc.

Chapter 4

LEAD SORPTION ONTO FERRIHYDRITE: MULTISTAGE CONTACTING

4.1 Abstract

Few studies have demonstrated the practical application of surface complexation models, calibrated with fundamental macroscopic and spectroscopic metal sorption data, in helping to solve industrial trace-metal emissions problems. In this work, multistage ferrihydrite sorption systems are evaluated for their effectiveness in reducing single-solute lead (Pb) concentrations in contaminated water streams to very low levels. Experimental data and modeling results indicate that a multistage sorption system can significantly reduce Pb effluent concentrations for the same total amount of sorbent or, alternatively, dramatically lower total sorbent consumption for the same effluent Pb concentration. Model predictions were generated using a steady-state, multistage, equilibrium adsorber model that was specifically developed for and integrated into OLI Systems' Environmental Simulation Program (ESP). The modified triple-layer model was used to simulate Pb surface-liquid equilibria within the adsorber model. Engineering screening evaluations indicate that a 2- to 3-stage sorption process can provide significant economic savings when compared to a 1-stage process operating with the same target effluent Pb concentration. Additional equilibrium stages beyond 2 or 3 provide diminishing economic returns. The major economic driver for multiple contacting stages is reduced capital investment and operating costs for sludge handling. dewatering, and disposal.

4.2 Introduction

Trace-metal discharges from industrial manufacturing processes are being increasingly scrutinized and regulated as new, revised, and proposed regulations are pushing metal effluent limits to part-per-billion (ppb) and lower levels (U. S. EPA, 2000; Gurian et al., 2001; U. S. EPA, 2001a, b; Wenning, 2001). Alkaline precipitation has historically been the technology of choice for meeting part-per-million regulatory levels for metals in direct-discharge wastewater point sources; however, this technology is limited to $\geq$ 1 ppm effluent concentrations due to the inherent solubility of amorphous metal hydroxide phases and inefficiencies in commercial solid-liquid separation devices (Dyer et al., 1998). On the other hand, much lower effluent levels are possible by taking advantage of the large sorptive capacity of amorphous, high-surface-area solids, such as hydrous iron and aluminum oxides.

Merrill et al. (1985) examined the technical and economic feasibility of removing inorganic trace elements, such as arsenic (As) and selenium (Se), from coal-fired power plant wastewater streams via coprecipitation with hydrous ferric oxide (HFO) in a single contacting stage. Removal efficiencies of 80-99% were achieved for 5-140 ppb As(III), As(V), and Se(IV) feed concentrations at pH 7.5-8.5; however, Se(VI) removal was only 5-15%. Testing results showed that optimum metals removal occurred at pH < 9 for As(V), pH 8-9 for As(III), pH < 7 for Se(IV), and pH < 4 for Se(VI). On the other hand, a two-stage crossflow process (i.e., separate fresh-HFO feeds to each stage) might allow for satisfactory removal of all four contaminants if the two stages are controlled at different pH values (e.g., 4.5 and 8.5).

Schultz et al. (1987) examined the feasibility of a closed-loop, one-stage process that consisted of metal sorption onto ferrihydrite from dilute solutions at pH 9,

followed by desorption into a more concentrated regenerant solution at pH 4.5. Reaction times were 1-3 hr in each step. Except for cadmium, a measurable fraction of the bound metals were not easily desorbed. This slowly reversible fraction increased with increasing pH and duration of the high-pH sorption stage, and increased more or less continuously in subsequent cycles. Interestingly, the metals retained in the ferrihydrite lattice did not affect metals removal in 5 subsequent cycles for the concentration range studied. Edwards and Benjamin (1989) extended the work of Schultz et al. (1987) by considering the performance of the regenerated ferrihydrite sorbent over 50 cycles, rather than just six. Removal efficiency remained > 98% when treating both synthetic and real plating wastes containing 1-3 ppm each of six metals. Adsorption and desorption cycle times were reduced from 1-3 hours to 10 and 10-30 minutes, respectively. Preformed ferrihydrite solids (0.45 g/L) were found to aid removal of 90% of the suspended sorbent solids within 3 minutes; only 4% remained suspended after 50 minutes.

An alternative to batch or continuous stirred-tank reactor configurations for the ex situ treatment of metal-contaminated waters is a fixed-bed column containing a granular sorbent that can be regenerated over many cycles (Theis et al., 1992; Gao et al., 1995; Fan and Anderson, 1996; Smith, 1998; Smith and Amini, 2000). Advocates of this alternative approach argue that dynamic flow in fixed beds is preferred over a continuous stirred-tank configuration, because it eliminates the need for potentially expensive solid-liquid separation facilities. For example, Smith and Amini (2000) investigated removal of 10 ppm lead (Pb) from a wastewater stream at pH 5.5 in fixed-bed columns containing a recycled, granular, iron-bearing material recovered from surface finishing operations in cast-iron manufacture. While treatment

was effective initially, efforts to regenerate the sorbent with aqueous EDTA and DTPA chloride salt solutions resulted in relatively low Pb recovery (40-50%) and a subsequent loss of adsorption efficiency. Interestingly, Smith (1998) and Smith and Amini (2000) used the modified triple-layer model (TLM) to predict metal sorption equilibria onto the recycled iron-bearing sorbents; the iron sorbent was treated as a hydrous ferric oxide in aqueous solution. The modified TLM was integrated into a dual-resistance mass-transport model to simulate the performance of the fixed-bed columns.

There is essentially no discussion in the peer-reviewed literature of using a high-surface-area sorbent, such as HFO or ferrihydrite, to treat metals-contaminated wastewater streams to ppb levels in a multistage crossflow or countercurrent-flow reaction system. However, treatment with any high-surface-area sorbent in two or more equilibrium contacting stages will (1) reduce metal effluent concentrations to much lower levels than can be achieved in one stage using an equivalent amount of sorbent; or (2) reduce total sorbent consumption and disposal for the same target effluent concentration. In addition, staging can be used in a crossflow configuration to optimize the removal of several trace metals and metalloids whose pH ranges for optimum treatment are much different. Experience in the chemical engineering field has shown that 2 to 4 contacting stages often provide significant improvement over a single contacting stage in chemical reaction, leaching, and extraction systems, while additional stages beyond 4 or so often lead to diminishing economic returns (Zomosa, 1990; Reyes-Labarta and Grossmann, 2001; Van Vliet et al., 2001). A decision on the number of contacting stages often becomes an economic trade-off between the

incremental capital investment for the additional equipment and the savings in raw material, energy, and waste disposal costs.

In this chapter, one-, two-, three-, and four-stage ferrihydrite sorption systems are evaluated for their effectiveness in reducing single-solute Pb concentrations to very low levels in contaminated water streams. The objectives of the research were three-fold. First, to demonstrate how a multistage sorption process can significantly reduce trace-metal effluent concentrations for the same total amount of sorbent or, alternatively, dramatically lower total sorbent consumption for the same metal effluent concentration. Second, to develop and validate a steady-state, multistage, adsorber model for treating a Pb-contaminated water stream to part-per-billion levels. In the process, demonstrate the integration of a surface complexation model (SCM), such as the modified TLM, into a steady-state equilibrium process flowsheet simulator to predict metals removal efficiency and sorbent requirements. Third, to conduct engineering screening evaluations to highlight the economic drivers for equilibrium staging.

4.3 Methods

4.3.1 Ferrihydrite Preparation

The 2-line ferrihydrite was synthesized, washed, and aged for 48 hours according to the procedures described in Trivedi et al. (2002a).

4.3.2 Multistage Pb Sorption Experiments

Sorption studies were conducted with preformed ferrihydrite solids at room temperature in a N_2 glovebox using 1-liter, well-mixed reaction vessels containing a 0.01 M $NaNO_3$ background electrolyte solution. All studies were

conducted in triplicate at the same time using the same batch of ferrihydrite. Equilibration time was 4 hours for each contacting stage, and pH was controlled at 5.5 using 0.1 M HNO_3 or NaOH. Lead was added as $Pb(NO_3)_2$ using a 1 M stock solution. All chemicals were ACS reagent-grade; ultrapure water (Micropore SA) was used throughout. Equilibrated ferrihydrite solids were separated from the aqueous phase using a RC5 Sorvall centrifuge operating at 12,000 rpm for 20 minutes. Graphite furnace, atomic absorption spectroscopy (Perkin-Elmer Analyst 800) was used to analyze the centrates for total soluble Pb. The multistage, crossflow sorption experiments were batch equilibration studies; the experimental conditions for each case are summarized in Table 4.1. For example, in a two-stage system, such as Case 1B, 0.5 g "fresh" ferrihydrite sorbent was first equilibrated with 0.5 millimoles $Pb(NO_3)_2$ dissolved in 1 L of a 0.01 M $NaNO_3$ background solution (103.6 ppm Pb). After 4 hours, the mixture was centrifuged, and the resulting centrate was analyzed for residual Pb in solution. The bulk of the remaining centrate (~ 0.9 L) was then added to a second 1-L reaction vessel, where it was equilibrated again for 4 hours with 0.5 g/L of "fresh" ferrihydrite sorbent. The resulting centrate was analyzed for residual Pb. More background on the experimental protocol used in this study can be found in Trivedi et al. (2002a). Raw data for the multistage studies are reported in Appendix B.

4.3.3 Geochemical Modeling Software

The OLI Software (OLI Systems, Inc., Morris Plains, NJ) was used to perform the multistage, steady-state simulations. Details on the thermodynamic databank and framework, the equation solvers, and the SCMs used in the OLI Software are presented in Chapter 2. More specifically, the Environmental Simulation Program (ESP) was used for this study, because it is designed for steady-state

Table 4.1 Definition of and results for Pb/ferrihydrite (fh) multistage sorption case studies.[a]

Case	Stg. #	g fh/L in each stage	Stg. 1 Pb Feed Conc. (ppm)	Pb Effluent Measured[b]	95% C. I. Pb Effluent Measured[c]	Pb Effluent Model	95% C. I. Pb Effluent Model[c]
1A	1	1.0	103.6	2.1 ppm	2.04-2.15 ppm	1.8 ppm	0.97-3.3 ppm
1B	1	0.5	103.6	10.0 ppm	9.3-10.7 ppm	4.5 ppm	2.5-8.5 ppm
	2	0.5		128 ppb	122-132 ppb	57 ppb	12.3-148.6 ppb
2A	1	4.65	10.36	13.7 ppb	10.9-15.5 ppb	10 ppb	5.9-19.8 ppb
2B	1	0.253	10.36	323 ppb	310-340 ppb	462 ppb	272-827 ppb
	2	0.253		5.3 ppb	4.3-6.3 ppb	8 ppb	1.9-20.7 ppb
2C[d]	1	0.08	10.36	N/A	N/A	1.8 ppm	N/A
	2	0.08		N/A	N/A	183 ppb	N/A
	3	0.08		N/A	N/A	10 ppb	N/A
3A	1	0.4	103.6	11.6 ppm	11.1-12.1 ppm	6.2 ppm	3.4-11.5 ppm
3B	1	0.2	103.6	22.0 ppm	21.8-22.6 ppm	17.8 ppm	10.8-31.2 ppm
	2	0.2		1.6 ppm	1.6-1.64 ppm	1.3 ppm	0.39-3.1 ppm

Table 4.1 Continued.

Case	Stg. #	g fh/L in each stage	Stg. 1 Pb Feed Conc. (ppm)	Pb Effluent Measured[b]	95% C. I. Pb Effluent Measured[c]	Pb Effluent Model	95% C. I. Pb Effluent Model[c]
3C	1	0.1	103.6	41.0 ppm	40.6-41.3 ppm	44.3 ppm	34.9-59.1 ppm
	2	0.1		8.2 ppm	8.0-8.3 ppm	10.9 ppm	5.7-20.1 ppm
	3	0.1		0.395 ppm	0.39-0.4 ppm	1.6 ppm	0.35-3.8 ppm
	4	0.1		6.1 ppb	5.8-6.3 ppb	115 ppb	8.1-378 ppb

[a] All experiments were conducted at room temperature in a N_2 glovebox using a 0.01 M $NaNO_3$ background electrolyte solution. The pH in each stage was controlled at 5.5 using 0.1 M HNO_3 or NaOH. [b] Mean of triplicate studies. [c] See Dyer et al. (2002c) and Chapter 5 for more details on how the 95% confidence intervals (C. I.) were generated. C. I. for the measured values reflect "same-batch" variation displayed by the triplicate studies. C. I. for the model values reflect "between-batch" uncertainties in input parameters (i.e., pH, Pb, ferrihydrite, and $NaNO_3$ feed concentrations, and mass H_2O) as well as uncertainties in the thermodynamic parameters (i.e., surface complexation Ks). [d] ESP simulation only for inclusion in engineering evaluations.

simulation of vapor, liquid, and solid interphase and intraphase equilibria occurring within multistage chemical process flowsheets. The modified TLM was utilized in this work, having provided best fits of the Pb/ferrihydrite isotherm and pH-edge data presented in Appendix A and Trivedi et al. (2002a) and subsequently analyzed in Chapter 3 and Dyer et al. (2002b).

4.3.4 Modeling Protocol

Examples of two-stage crossflow and two-stage countercurrent-flow sorption systems for treating a metals-contaminated wastewater stream are shown schematically in Figures 4.1a and 4.1b, respectively. In a crossflow system, fresh sorbent is added to each reaction vessel or stage, equilibrated with the contaminated wastewater, and then removed for dewatering and disposal. This contrasts with a true countercurrent-flow system (Figure 4.1b), where fresh sorbent is added to the final sorption stage, and partially spent sorbent is subsequently reused in the upstream stages (i.e., the flow of sorbent is countercurrent to the flow of wastewater). A true countercurrent-flow system represents the minimum-sorbent-consumption case for a specified metals effluent concentration. For solids handling reasons, a crossflow arrangement will probably be more practical for amorphous materials, such as ferrihydrite, in most industrial situations. In addition, to simplify the process, most full-scale industrial systems would likely be operated in a coprecipitation mode, rather than a sorption (onto preformed floc) mode as shown in Figure 4.1. The experimental and modeling studies in this work are based on Pb sorption onto preformed ferrihydrite in order to utilize the triple-layer modeling results from Chapter 3 and Dyer et al. (2002b). Operation in a coprecipitation mode would likely lead to lower Pb effluent concentrations and sorbent requirements; however, the benefits of staging will be

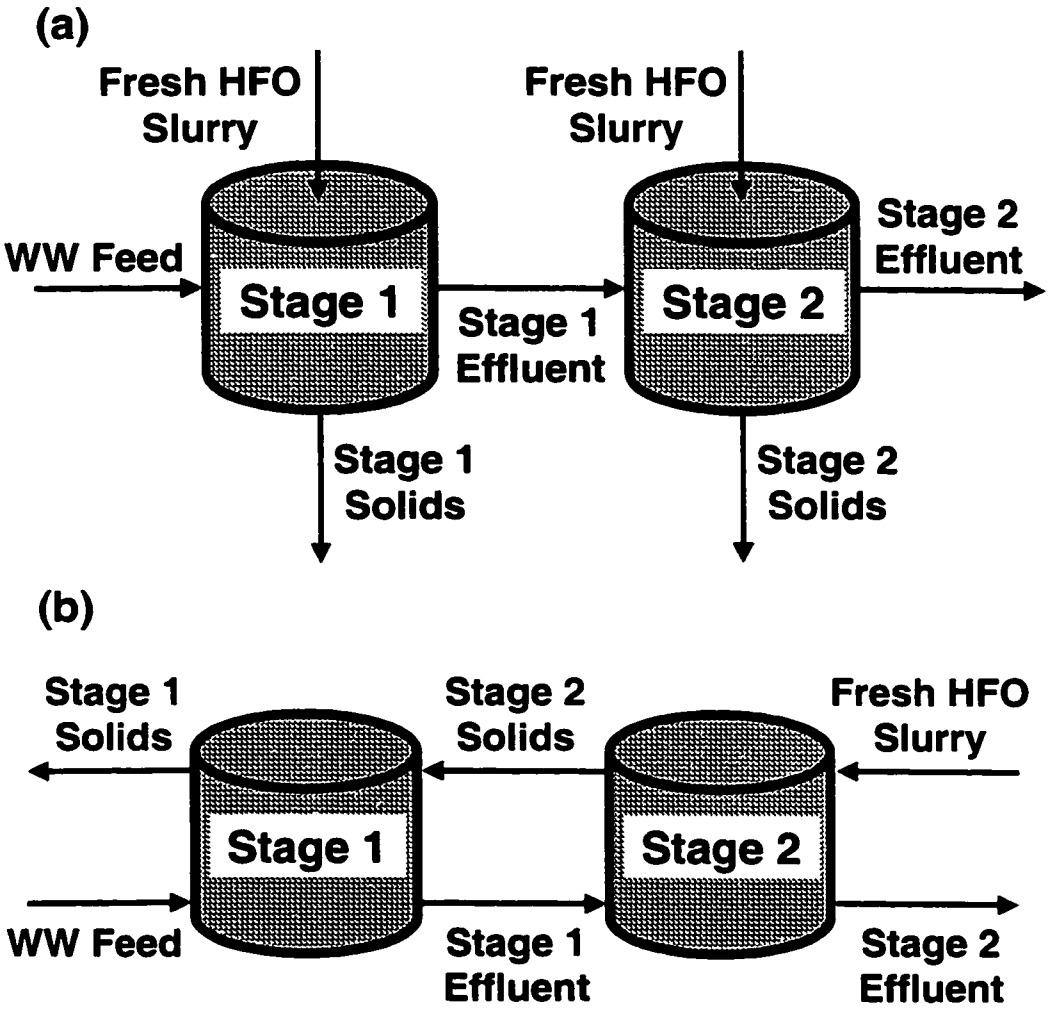

Figure 4.1 Schematic flow diagrams for two-stage crossflow (a) and countercurrent-flow (b) sorption systems.

realized in either mode. As a result, model predictions based on a sorption process will be conservative for environmental compliance purposes.

Steady-state process flowsheets were constructed in ESP using the appropriate combination of unit operations (separator, pH controller, acid/base manipulator, and sensitivity blocks) and feed/effluent streams (wastewater feed, sorbent feed, NaOH feed, stage 1 effluent, stage 1 solids, and so on). Separator blocks served as the isothermal reaction vessels. The efficiency of the solid-liquid separation was also specified in this block. An acid/base manipulator block and a pH controller were linked to each separator block to regulate the flow of mineral acid or base to each reaction vessel, so as to control pH at 5.5. The sensitivity block was used to perform multiple-case runs. The TLM functioned within all blocks containing sorbing solids. An example of a block flow diagram for a two-stage ESP crossflow sorption model is shown in Figure 4.2.

TLM parameters and associated Pb surface speciation assumptions used in this work were obtained from Tables 3.2 and 3.3 (see also Dyer et al., 2002b). They are summarized again in Table 4.2. ESP simulations were made for each of the cases listed in Table 4.1. The objective was to compare model predictions based on the single-solute Pb sorption data reported in Appendix A and Trivedi et al. (2002a) to the results of the bench-scale multistage experiments (Appendix B). In theory, the results should not be statistically different when taking into account experimental and model uncertainties. In addition, generalized sensitivity studies were conducted to understand the impact of pH, Pb feed concentration, number of stages, perfect vs. imperfect solid-liquid separations, and crossflow vs. countercurrent-flow arrangement

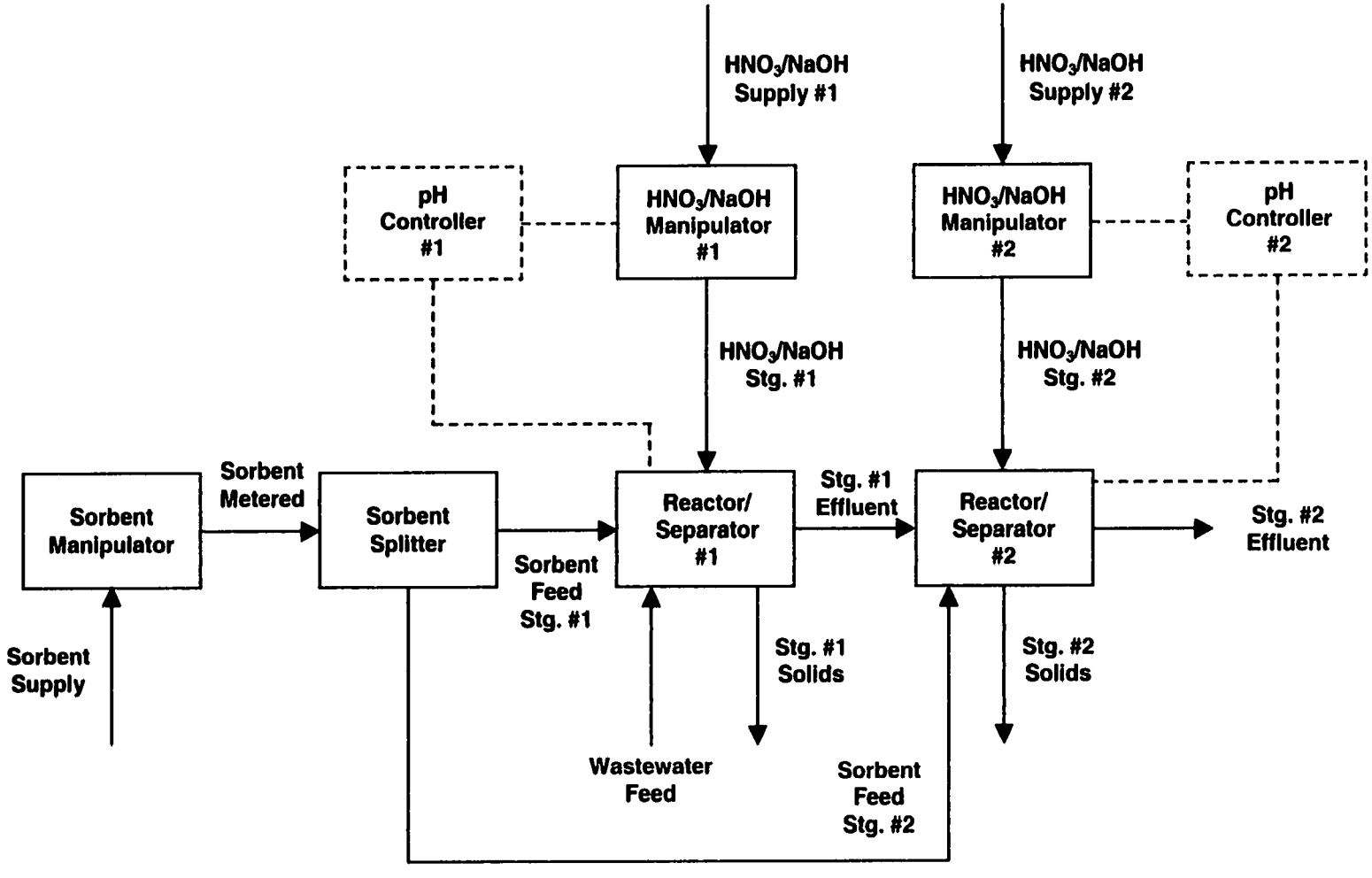

Figure 4.2 Block flow diagram for a two-stage ESP crossflow sorption model.

Table 4.2 Triple-layer model parameters used in ESP simulations of multistage Pb sorption onto 2-line ferrihydrite.[a]

Parameter	Value
Pb Surface Species	$(\equiv FeO)_2Pb$ and $\equiv FeOHPb^{2+}$
N_s (mol /mol)	0.8
A_s (m^2/g)	600
C_1 (F/m^2)	1.0
C_2 (F/m^2)	0.2
log K_{a1}^{int}	-5.56
log K_{a2}^{int}	-10.26
log K_{NO3-}^{int}	-7.48
log K_{Na+}^{int}	8.36
log $K_{(\equiv FeO)_2Pb}^{int}$ @ 1 g solids/L[b]	5.00 (pH 4.5-5.5)
	6.16 (pH 6.5)
log $K_{\equiv FeOHPb^{2+}}^{int}$	-8.80 (pH 4.5-5.5)
	-5.33 (pH 6.5)
γ_s	$\gamma_s = \gamma_{Pb2+}$

[a] Refer to Tables 3.2 and 3.3 as well as Dyer et al. (2002b) for details on the chemical reactions and mass law expressions corresponding to each of the equilibrium constants given above. Definitions for each of the parameters can be found in the nomenclature section. [b] For bidentate surface complexes, K^{int} is really a conditional K that depends on sorbent solids concentration. The value for K in this table is based on 1 g ferrihydrite/L. See Table 3.3 for additional explanation.

on the predicted Pb effluent concentration at a fixed sorbent dose and the predicted sorbent requirement at a specified Pb effluent concentration.

4.3.5 Engineering Evaluations

High-spot engineering evaluations (+/- 30%) were completed for each of the cases in Table 4.1 to assess the relative economic incentive/penalty for additional equilibrium sorption stages. There are two key differences between the treatment process assumed in the engineering evaluations and that used in the experimental and modeling studies—use of $FeCl_3$, rather than $Fe(NO_3)_2$, and operation in a coprecipitation mode, rather than a sorption mode. Investment, costs, and economics should not be used on an absolute basis to compare to other technology alternatives, such as ion exchange, alkaline precipitation, and so on; however, they can be safely used for a relative ranking of the multistage process alternatives.

The evaluations are based on the 10-step engineering evaluations methodology outlined in detail in Mulholland and Dyer (1999). For each case, a process flow diagram was developed, showing the necessary equipment pieces (pumps, tanks, clarifiers, filter presses, etc.) and process interconnections. From the process flow diagrams, facility scopes-of-work (i.e., a description of the physical facilities required to build the process) were developed and operating requirements were defined (i.e., annual requirements for 50 wt % NaOH, 30 wt% $FeCl_3$, electricity, sludge disposal, etc.). Based on the facility scopes-of-work, capital investment was then estimated for each case using a factored, research-guidance-appraisal technique that is widely used within the chemical industry. Finally, armed with estimates for new capital investment and operating requirements, a 10-year cash flow analysis was completed for each case to estimate annual cash operating cost and net present cost at

both a 12% and 25% discount rate. Net present cost (NPC) was the economic measure of merit used to rank alternatives, because it incorporates the effects of both new capital investment and on-going cash operating costs over the life of the facility. A discount rate of 25% was chosen to rank the alternatives, because it better reflects the opportunity cost of capital in situations where the supply of capital dollars is limited and other viable projects are competing for the same dollars (which is almost always the case in the chemical industry).

Table 4.3 summarizes the major assumptions used in the engineering evaluations. Bare equipment, raw material, utility, and waste disposal costs were obtained from various reliable sources (Gumerman et al., 1986; DuPont Investment Technologies, 1998; Mulholland and Dyer, 1999; DuPont Sourcing, 2002; Schnell Publishing, 2002). Process flow diagrams for one- and two-stage, crossflow, coprecipitation processes are shown in Figures 4.3 and 4.4. Facility scopes-of-work, operating requirements, factored investment estimates, and 10-year cash flow analyses are included in Appendix C.

4.4 Results and Discussion

4.4.1 Multistage Sorption Case Studies

Experimental data (Pb Effluent Measured) and ESP modeling results (Pb Effluent Model) for the multistage sorption case studies are summarized in Table 4.1. Experimental data are the arithmetic average of the effluent Pb concentrations measured in the three replicate studies for each stage of each case. Model data are ESP predictions based on the modified triple-layer model and the parameters summarized in Table 4.2. To better assess the agreement between the measured and

Table 4.3 Major assumptions and bases used in engineering evaluations.

Assumption/Basis	Value	Assumption/Basis	Value
Raw Material Costs		Cash Flow Analysis	
30% $FeCl_3$	\$0.15/lb[a]	Plant Utility	90%
50% NaOH	\$0.15/lb[a]	Escalation Rate	2.5%/yr
Emulsion Polymer	\$1.50/lb[a]	Years of Operation	10 yr
Filter Aid	\$0.165/lb[a]	Income Tax Rate	40%
Filter Cloth	\$0.095/ft^2	Creep Investment	1.5%
Filtered Water	\$0.15/lb	NPC[b] Discount Rates	12% and 25%
Hazardous Waste Landfill Disposal	\$0.085/lb wet sludge	Depreciation (6-year)	20%, 32%, 19%, 12%, 12%, 5%
Electricity	\$0.045/kWh	Δ Working Capital	60 days cash costs
Other Cash Costs		Capital Investment Factors	
General Plant Overheads	0.5% replacement inv. + 24% salaries, wages, & benefits	Misc. Equipment/ Foundations, Supports, Platforms	5%/7%
Maintenance	4% replacement inv.	Field Material, Labor, Insulation	17%
Property Taxes & Insurance	0.75% replacement inv.	Piping/Instrument/ Electrical	45%/16%/11%
Operations (round-the-clock shift coverage)	\$430,000/yr	Minor Changes/ Working Conditions	2%/10%
Technical Exempt	\$160,000/yr	PG&S[c]/D&R[d]	10%
Startup/Project Liaison	10%/2% new inv.	Contingencies	25%
		MCC/ICR/ECR[e]	6%
		Freight/QA/Sales Tax/Procurement	11%
		Engineering & Home Office/Field Indirects	20%/8%

[a] 100% basis. [b] Net present cost. [c] Power, general, and service facilities. [d] Dismantlement and rearrangement. [e] Motor control center/instrument control center/electrical control center.

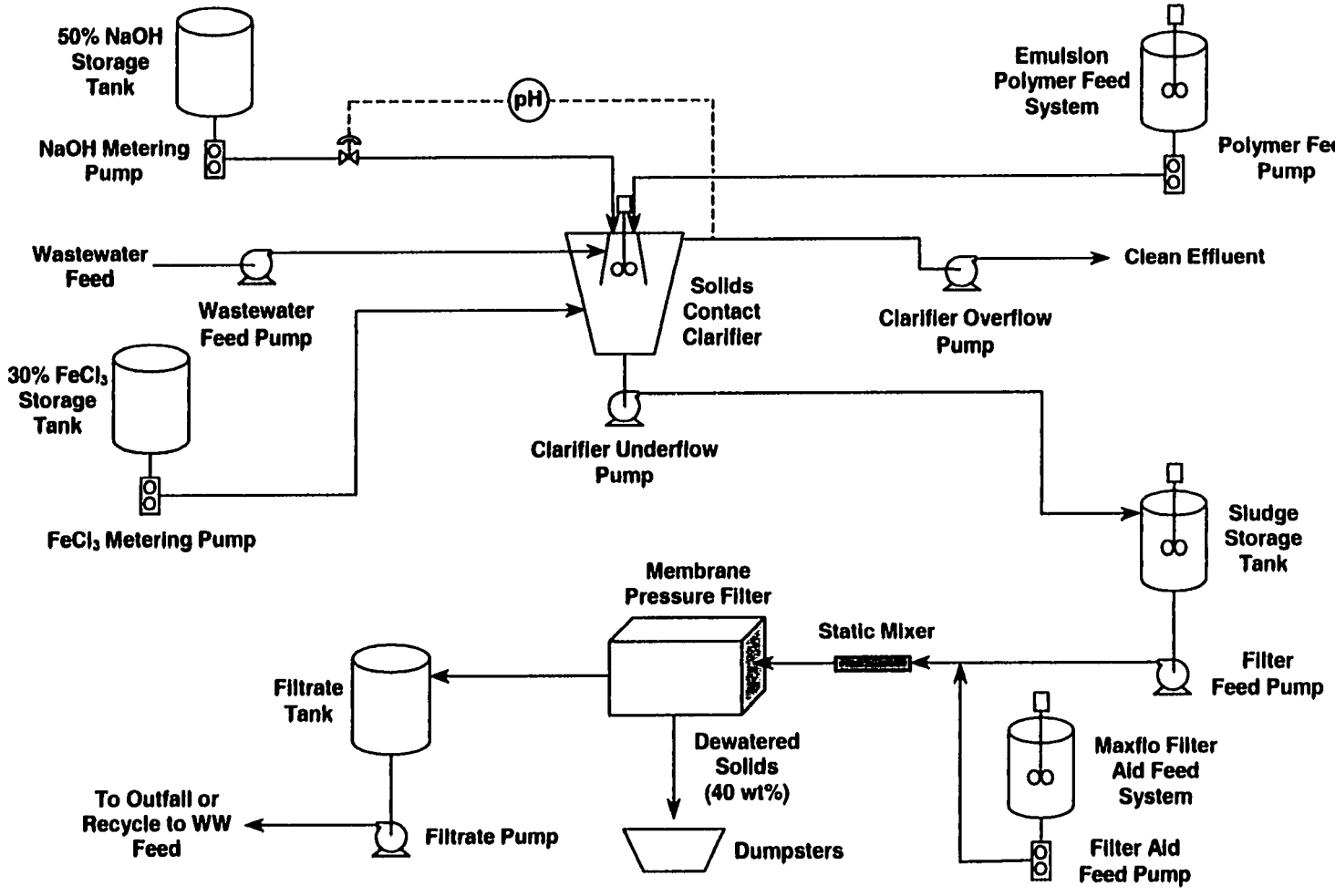

Figure 4.3 **Process flow diagram for a one-stage ferrihydrite coprecipitation process used in the engineering evaluations.**

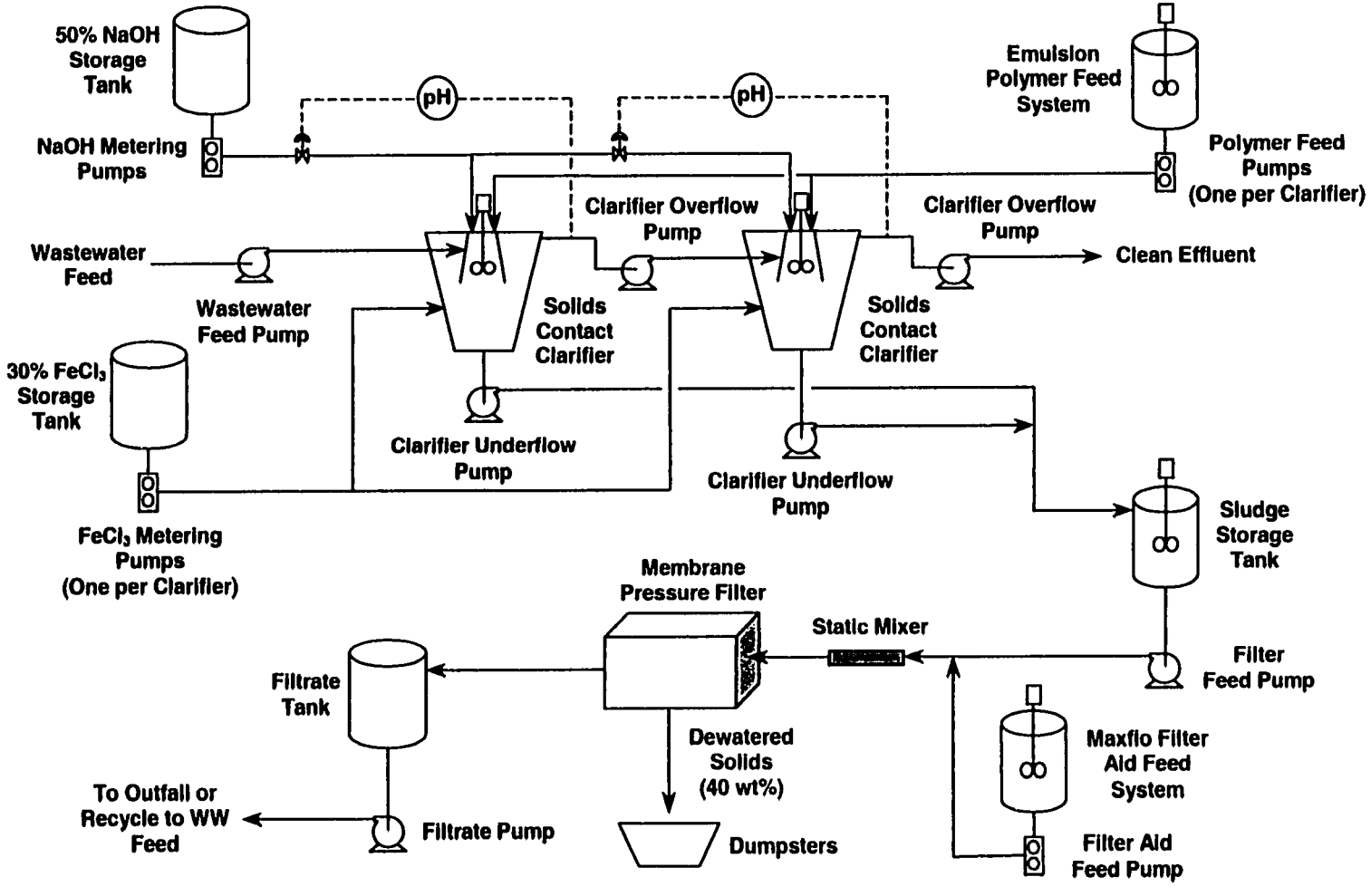

Figure 4.4 **Process flow diagram for a two-stage ferrihydrite coprecipitation process used in the engineering evaluations.**

model data, 95% confidence intervals were generated for each data point, and are reported in Table 4.1. Details on the statistical tools, methodology, and uncertainty assumptions used to calculate the 95% confidence intervals are described in Chapter 5 and Dyer et al. (2002c).

Briefly, confidence intervals for the measured values reflect the variation in or, more specifically, the *repeatability* of the 3 replicate studies for each stage of each case. Hence, the confidence intervals account for "within-the-same-batch" uncertainties in analytical/experimental procedures and equipment for the same operator conducting experiments with the same batch of ferrihydrite on the same day. These include analytical equipment, sample collection, sample handling, and sample processing errors as well as errors in pH calibration/control, reagent doses, and so on. The Resampling Stats for Windows software (Resampling Stats, Inc., Arlington, Virginia) was used to estimate the 95% confidence intervals for the measured values. This software uses a bootstrap procedure (Diaconis and Efron, 1983; Simon, 1997) to randomly generate with replacement N new samples of size, n, directly from the original sample. The number of new samples (N) is usually set at 10,000 or more, while the sample size (n), in this case, was 3. For this study, N was set equal to 10,000. The bootstrap procedure effectively creates a hypothetical "infinite" population that represents one's best guess about the real population.

The 95% confidence intervals for the ESP model predictions, on the other hand, attempt to account for "between-batch" uncertainties in the model input parameters (i.e., pH, Pb feed concentration, ferrihydrite dose, $NaNO_3$ concentration, and the mass of H_2O) as well as uncertainties in the regressed thermodynamic parameters (i.e., surface complexation equilibrium constants). Examples of between-

batch uncertainties include differences in sorbent properties, reagent concentrations, and pH measurement equipment as compared to the original isotherm and edge studies used to determine the best-fit model parameters. Hence, the confidence intervals attempt to reflect the *reproducibility* of Pb/ferrihydrite sorption studies on different days using different batches of ferrihydrite/reagents as well as the quality of the model fits of the acid-base titration and Pb sorption data used to estimate the thermodynamic parameters in the first place. As described in Dyer et al. (2002c), the OLI Software's error analysis tool was first used to propagate input and thermodynamic parameter uncertainties through the multistage sorption model, yielding local extrapolation models that approximated the value of each output parameter of interest (i.e., effluent Pb concentration and Pb surface loading). Monte Carlo simulations ($N = 10{,}000$) of the OLI-generated local extrapolation models were then conducted with the Resampling Stats software to estimate the 95% confidence intervals for the model predictions.

In principle, the greater the overlap of the confidence intervals for the measured and model values, the higher the probability that the two values are the same. That is, one cannot say with confidence that the model and measured values are statistically different. Based on the 95% confidence intervals reported in Table 4.1 (i.e., when model and experimental uncertainties are taken into account), the agreement between the model-predicted and measured effluent Pb concentrations is very good. In all cases but three (Stage 1 of Case Studies 1B and 3A and Stage 4 of Case Study 3C), there is significant overlap of the 95% confidence intervals. More rigorous hypothesis testing using Resampling Stats indicated that the difference between the measured and model values was statistically significant ($p < 0.05$) in only

two cases (Stage 1 of Case Studies 1B and 3A). Based on these results, the ESP model does an adequate job of predicting the expected Pb removal efficiency in a multistage operation.

4.4.2 Generalized Multistage Sensitivity Studies

Figure 4.5 shows the effects of influent Pb concentration, pH, and number of equilibrium stages on the predicted effluent Pb concentration from a multistage crossflow adsorber operating with a total ferrihydrite dose of 1 g/L, equally split across the stages (i.e., 1 g/L in a one-stage system vs. 0.5 g/L in each stage of a two-stage system). Figure 4.5a assumes perfect solid-liquid separations, while Figure 4.5b highlights the impact of 20 ppm suspended solids in the clarified effluent and 30 wt% solids in the settled iron sludge on effluent Pb levels at pH 5.5. In both scenarios, the impact of pH and number of stages on Pb removal is significant. For example, as shown in Figure 4.5a, a 10-ppm Pb-containing water stream can be treated to only 80 ppb Pb using a one-stage adsorber at pH 5.5; however, the addition of a second stage at the same pH will reduce the effluent Pb concentration to approximately 2 ppb. On the other hand, adding a second stage and raising the pH to 6.5 will lower the effluent Pb concentration another order of magnitude to approximately 0.2 ppb. The benefit realized by adding a second stage is most significant at low Pb feed concentrations and at pH 5.5 and 6.5, where sorption of Pb is highly favored. At pH 5.5 and 6.5, adding a second stage lowers the effluent Pb concentration by 30- to 100-fold. The minimal impact of a second stage at pH 4.5 is the result of operating along the lower portion of the pH sorption edge for Pb.

The impact of solids carryover in the clarified effluent is to reduce Pb removal efficiency. As shown in Figure 4.5b, predicted effluent Pb concentrations at

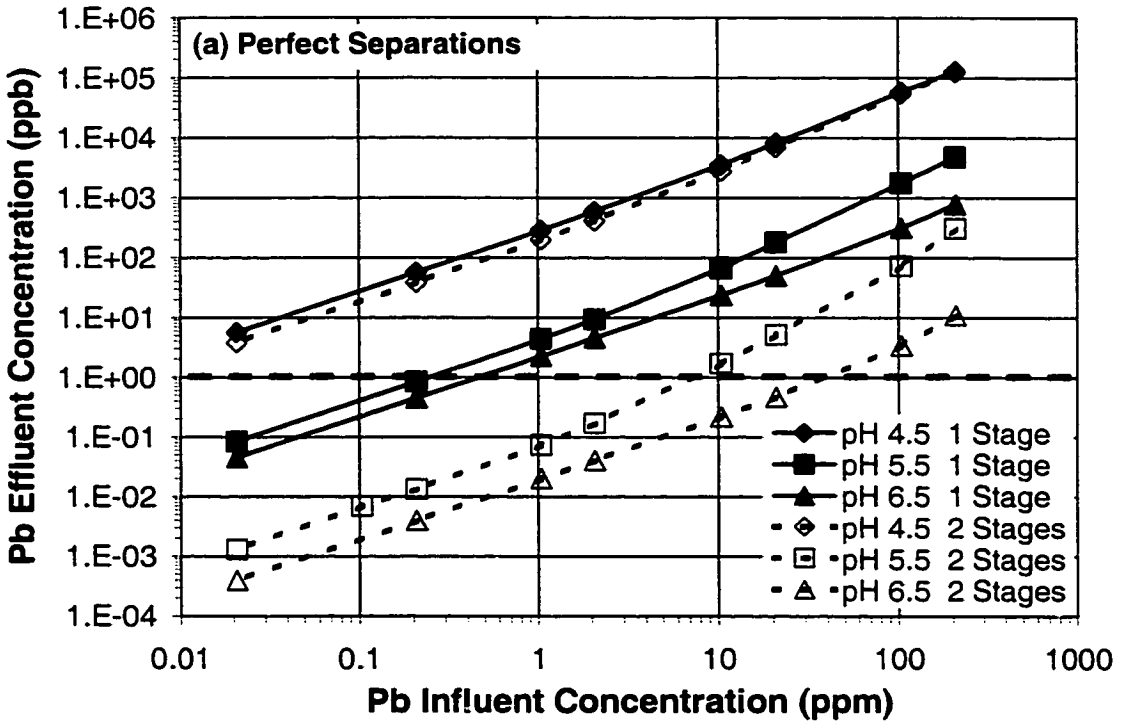

Figure 4.5 **Impact of influent Pb concentration, pH, and number of equilibrium stages on the effluent Pb concentration in one- and two-stage crossflow adsorbers operating with a fixed total ferrihydrite dose of 1 g/L (1 g/L equally split between stages in two-stage system). In (a), perfect solid-liquid separations are assumed. In (b), the impact of imperfect solid-liquid separations (20 ppm suspended solids in clarified effluent and 30 wt% solids in the settled sludge) on Pb removal at pH 5.5 is shown. Model predictions are based on the modified triple-layer model using a 0.01 M $NaNO_3$ background electrolyte solution and parameters summarized in Table 4.2.**

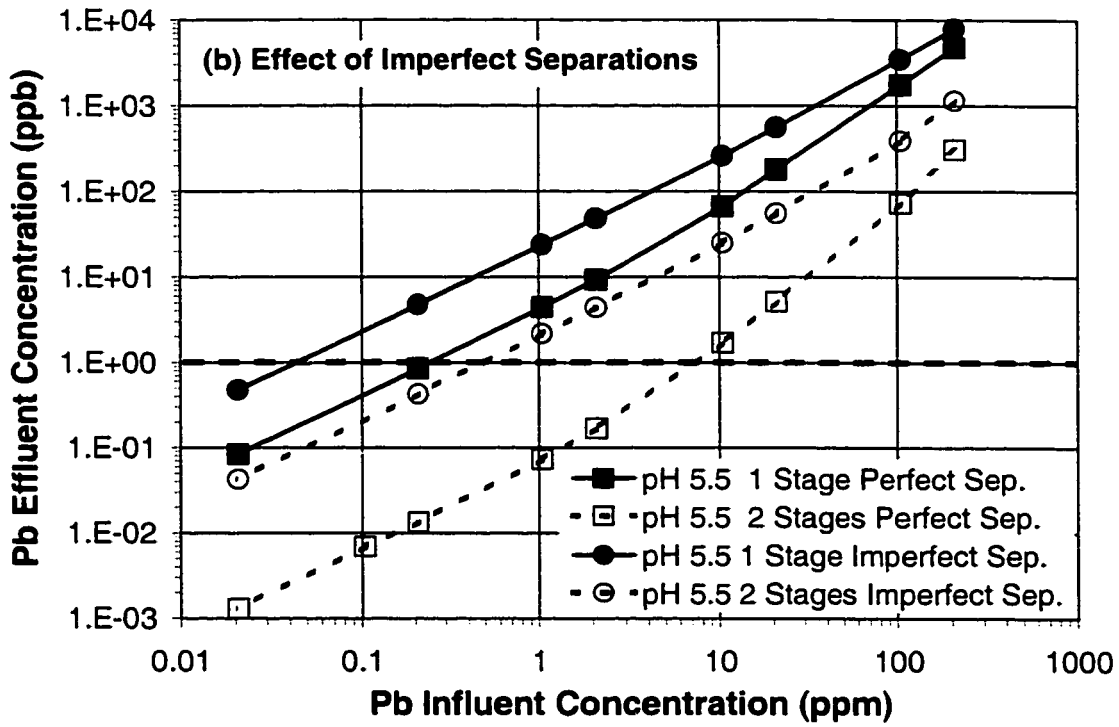

Figure 4.5 Continued.

pH 5.5 increase by 2- to 50-fold when compared to the model predictions based on perfect solid-liquid separations. As might be expected, the benefit gained by adding a second equilibrium stage is diminished as solids carryover increases. Consider the same 10-ppm Pb-containing water stream discussed above for Figure 4.5a. Based on Figure 4.5b, the predicted effluent Pb concentration for a two-stage adsorber operating at pH 5.5 is about 30 ppb (instead of 2 ppb) when more realistic solid-liquid separation efficiencies are assumed (20 ppm suspended solids in the clarified effluent and 30 wt% solids in the settled iron sludge).

Similarly, Figures 4.6a and 4.6b display the impacts of influent Pb concentration, pH, and number of equilibrium stages on the total required ferrihydrite dose in multistage crossflow Pb adsorbers operating with a fixed effluent Pb concentration of 1 ppb. Figure 4.6a assumes perfect solid-liquid separations; Figure 4.6b highlights the impact of 20 ppm suspended solids in the clarified effluent and 30 wt% solids in the settled iron sludge on effluent Pb concentration at pH 5.5. As in Figure 4.5, the impact of pH and number of stages on Pb removal efficiency is significant. For example, as shown in Figure 4.6a, total ferrihydrite consumption for the same hypothetical 10-ppm Pb-containing water stream can be reduced from approximately 40 g/L using a one-stage adsorber at pH 5.5, to ~ 1.2 g/L using a two-stage adsorber at pH 5.5, to ~ 0.45 g/L using a two-stage adsorber at pH 6.5. In this case, the beneficial impact of adding a second stage is most significant at higher Pb feed concentrations and pH.

The negative impact of solids carryover in the clarified effluent is displayed in Figure 4.6b. Predicted total ferrihydrite doses at pH 5.5 increase by 4- to 7-fold when compared to the predicted doses assuming perfect solid-liquid

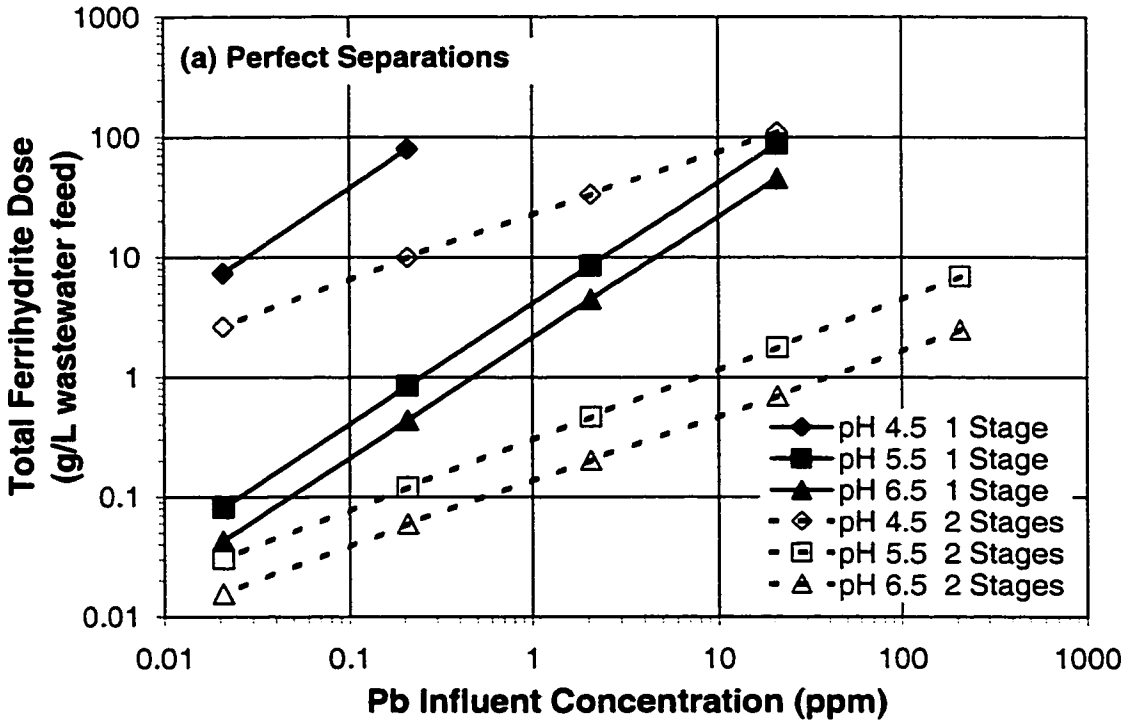

Figure 4.6 **Impact of influent Pb concentration, pH, and number of equilibrium stages on total ferrihydrite consumption in one- and two-stage crossflow adsorbers operating with a fixed effluent Pb concentration of 1 ppb. Ferrihydrite is equally split between stages in the two-stage system. In (a), perfect solid-liquid separations are assumed. In (b), the impact of imperfect solid-liquid separations (20 ppm suspended solids in clarified effluent and 30 wt% solids in the settled sludge) on ferrihydrite consumption at pH 5.5 is shown. Model predictions are based on the modified triple-layer model using a 0.01 M $NaNO_3$ background electrolyte solution and parameters summarized in Table 4.2.**

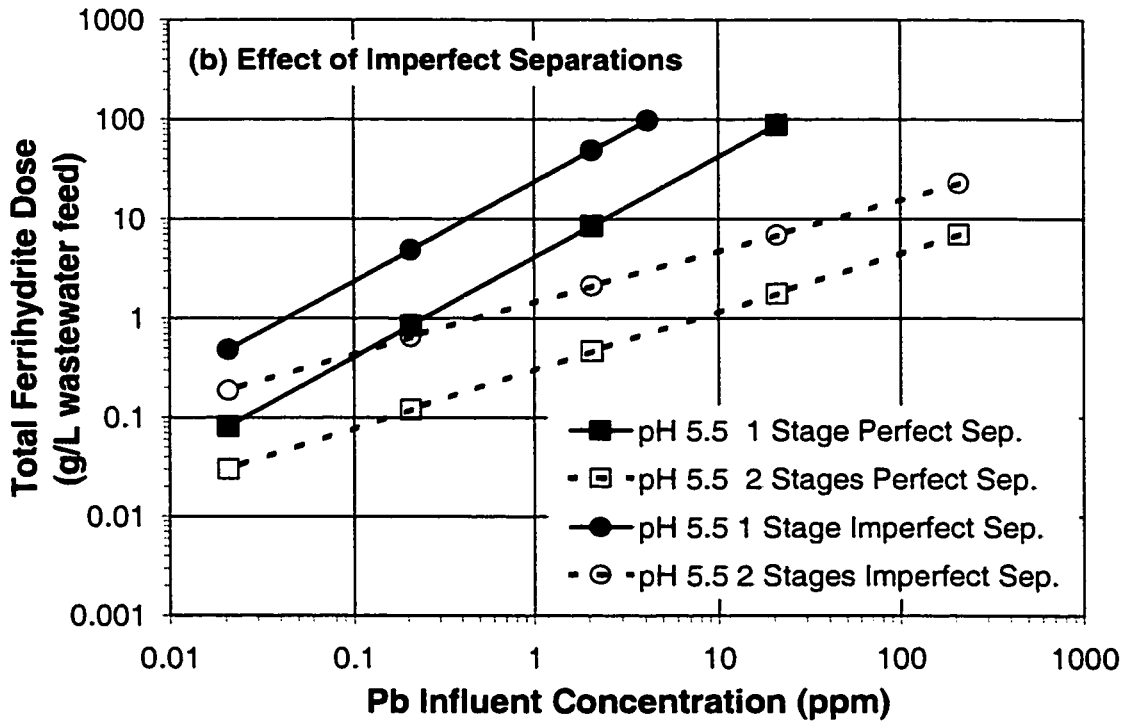

Figure 4.6 Continued.

separations. For the same 10-ppm Pb-containing water stream discussed above for Figure 4.6a, the required total ferrihydrite dose for a two-stage adsorber operating at pH 5.5 is about 5 g/L (instead of 1.2 g/L) when more realistic solid-liquid separation efficiencies are assumed.

Finally, Figure 4.7 shows the impact of the number of equilibrium stages on total ferrihydrite dose as a function of Pb feed concentration for both crossflow (Figure 4.1a) and true countercurrent-flow (Figure 4.1b) arrangements. Figure 4.7 assumes operation at pH 5.5, 10 ppb Pb total in the clarified effluent, 20 ppm suspended solids carryover, and 30 wt% solids in the iron sludge. It is apparent from Figure 4.7 that the benefits of staging diminish as the number of equilibrium stages increases. By 3 to 4 stages, the dose curves begin to level out. Figure 4.7 also highlights the ferrihydrite-consumption penalty realized by operating in a crossflow arrangement instead of a true countercurrent-flow arrangement. Total ferrihydrite doses are 2 to 4 times higher for the crossflow arrangement for 2 or more equilibrium stages.

4.4.3 Economic Benefits of Staging

Table 4.4 presents the results of engineering evaluations for the multistage sorption case studies summarized in Table 4.1. A key principle of engineering evaluations is that process flowsheets and scopes-of-work should be based on equivalent outcomes (i.e., the same effluent Pb concentration) in order to fairly compare alternatives. Case Studies 2A through 2C adhere to this principle, having been designed to achieve an effluent Pb concentration of ~ 10 ppb from the final stage. For this reason, $NPC_{25\%}$ values for each of these cases can be compared to choose the

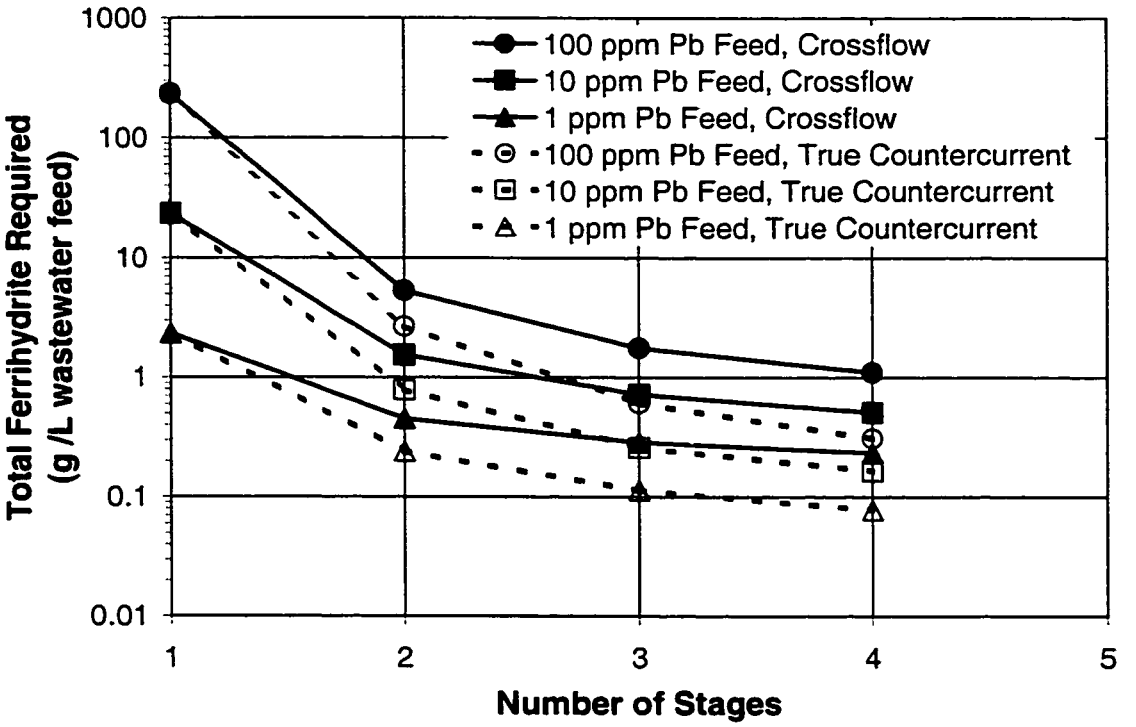

Figure 4.7 **Impact of the number of equilibrium stages and influent Pb concentration on total ferrihydrite consumption in crossflow and true countercurrent-flow adsorbers operating at pH 5.5 with a fixed effluent Pb concentration of 10 ppb, 20 ppm suspended solids in clarified effluent, and 30 wt% solids in the settled sludge. Ferrihydrite is equally split between stages in the multistage systems. Model predictions are based on the modified triple-layer model using a 0.01 M $NaNO_3$ background electrolyte solution and parameters summarized in Table 4.2.**

Table 4.4 Engineering evaluation results for multistage Pb sorption case studies.

Case	# Stgs.	g fh/L in each stage	Pb Feed Conc. (ppm)	2002 Investment ($1000)	2004 Cash Operating Cost ($1000/yr)	2002 NPC @ 12% ($1000)	2002 NPC @ 25% ($1000)
1A	1	1.0	103.6	2,400	710	4,900	3,200
1B	2	0.5	103.6	2,800	770	5,500	3,600
2A	1	4.65	10.36	4,100	2,180	12,600	7,400
2B	2	0.253	10.36	2,500	540	4,300	2,900
2C	3	0.08	10.36	2,800	500	4,400	3,000
3A	1	0.4	103.6	2,000	450	3,500	2,400
3B	2	0.2	103.6	2,500	520	4,200	2,900
3C	4	0.1	103.6	3,400	640	5,400	3,800

most cost-effective alternative(s). In other words, they can provide insight on the economic benefit of additional equilibrium stages. Case Studies 1 and 3, on the other hand, are not based on equivalent outcomes (i.e., the effluent Pb concentration varies between alternatives). However, they do provide valuable insights on the incremental investment and net present cost associated with adding equilibrium stages to lower the effluent Pb concentration at a fixed total ferrihydrite dose.

The results for Case Studies 2A through 2C in Table 4.4 clearly show that the addition of a second equilibrium stage makes economic sense ($NPC_{25\%}$ of $2,900,000 for 2 stages versus $7,400,000 for 1 stage). The additional investment and ongoing operating costs associated with handling, dewatering, and disposing of an order of magnitude more iron sludge (4.65 g/L for Case 2A vs. 0.506 g/L total for Case 2B) are substantial. On the other hand, the addition of a third stage just about breaks even ($NPC_{25\%}$ of $3,000,000 for 3 stages versus $2,900,000 for 2 stages); therefore, the additional operational complexity associated with three stages versus two is probably not justified. In this case, the reduction in sludge from Case 2B to 2C is only about 2-fold (0.506 g/L vs. 0.24 g/L total). The use of 4 or more stages would almost certainly result in an $NPC_{25\%} > \$3,000,000$.

The results for Case Studies 1 and 3 indicate that the incremental investment and $NPC_{25\%}$ for moving to a multistage operation are both on the order of $400,000-$500,000 per added stage. This compares to one-stage (i.e., base case) $NPC_{25\%}$ values of $3,200,000 and $2,400,000 for Case Studies 1A and 3A, respectively. In other words, the incremental $NPC_{25\%}$ for an additional stage is approximately 15-20% of the base-case $NPC_{25\%}$. For Case Study 1, a second stage at the same total ferrihydrite dose results in more than an order-of-magnitude reduction

in effluent Pb concentration. For Case Study 3, each incremental stage provides about an order-of-magnitude reduction in effluent Pb concentration based on the experimental data reported in Table 4.1.

In summary, as regulated trace-metal concentrations in water discharges are pushed to part-per-billion and lower levels, multistage contacting schemes will likely provide substantial economic benefits when sorption onto or coprecipitation with amorphous materials, such as ferrihydrite, are being considered. Table 4.4 shows that a 2- to 3-stage sorption process can provide significant economic savings when compared to a 1-stage process operating with the same target effluent Pb concentration. In addition, this research has shown that a steady-state process flowsheet simulator, such as OLI Systems' ESP software, can adequately predict Pb removal in a multistage ferrihydrite adsorber using the triple-layer surface complexation model calibrated with macroscopic and spectroscopic Pb sorption data. More importantly, however, this study helps to show how fundamental macroscopic and spectroscopic metal sorption data, coupled with surface complexation models, can be practically used to help solve industrial trace-metal emissions problems.

4.5 References

Diaconis P. and Efron B. (1983) Computer-intensive methods in statistics. *Sci. Am.* **248**(5), 116-130.

DuPont Investment Technologies. (1998) *RGA Software, Version 3.1*. DuPont Company.

DuPont Sourcing (2002) Personal communications.

Dyer J. A., Scrivner N. C., and Dentel S. K. (1998) A practical guide for determining the solubility of metal hydroxides and oxides in water. *Environ. Prog.* **17**, 1-7.

Dyer J. A., Trivedi P., Scrivner N. C., and Sparks D. L. (2002b) Lead sorption onto ferrihydrite. 2. New modeling insights. *Environ. Sci. Technol.* (In press).

Dyer J. A., Trivedi P., Scrivner N. C., and Sparks D. L. (2002c) Lead sorption onto ferrihydrite. 4. Uncertainty analysis. *Environ. Sci. Technol.* (In press).

Edwards M. and Benjamin M. M. (1989) Regeneration and reuse of iron hydroxide adsorbents in treatment of metal-bearing wastes. *J. Water Pollut. Control Fed.* **61,** 481-490.

Fan H. and Anderson P. R. (1996) Development and evaluation of Mn oxide-coated composite adsorbent for the removal and recovery of heavy metals from metal contaminated wastewater. *Proceedings of the 50th Industrial Waste Conference*, pp. 217-226. Ann Arbor Press.

Gao Y., Sengupta A. K., and Simpson D. (1995) A new hybrid inorganic sorbent for heavy metals removal. *Water Res.* **29,** 2195-2205.

Gumerman R. C., Burris B. E., and Hansen S. P. (1986) *Small Water System Treatment Costs*. Noyes Data Corporation.

Gurian P. L., Small M. J., Lockwood J. R., and Schervish M. J. (2001) Addressing uncertainty and conflicting cost estimates in revising the arsenic MCL. *Environ. Sci. Technol.* **35,** 4414-4420.

Merrill D. T., Maroney P. M., and Parker D. S. (1985) *Trace Element Removal by Coprecipitation with Amorphous Iron Oxyhydroxide: Engineering Evaluation.* CS-4087, Electric Power Research Institute, Palo Alto, California.

Mulholland K. L. and Dyer J. A. (1999) *Pollution Prevention: Methodology, Technologies and Practices*. American Institute of Chemical Engineers.

Reyes-Labarta J. A. and Grossmann I. E. (2001) Disjunctive optimization design models for complex liquid-liquid multistage extractors. *AIChE J.* **47,** 2243-2252.

Schnell Publishing (2002) *Chemical Market Reporter* **261**(12), 16-19.

Schultz M. F., Benjamin M. M., and Ferguson J. F. (1987) Adsorption and desorption of metals on ferrihydrite: Reversibility of the reaction and sorption properties of the regenerated solid. *Environ. Sci. Technol.* **21,** 863-869.

Simon J. L. (1997) *Resampling: The New Statistics*. Resampling Stats, Inc.

Smith E. H. (1998) Surface complexation modeling of metal removal by recycled iron sorbent. *J. Environ. Eng.* **124,** 913-920.

Smith E. H. and Amini A. (2000) Lead removal in fixed beds by recycled iron sorbent. *J. Environ. Eng.* **126,** 58-65.

Theis T. L., Iyer R., and Ellis S. K. (1992) Evaluating a new granular iron oxide for removing lead from drinking water. *J. Am. Water Works Assoc.* **84,** 101-105.

Trivedi P., Dyer J. A., and Sparks D. L. (2002a) Lead sorption onto ferrihydrite. 1. A macroscopic and spectroscopic assessment. *Environ. Sci. Technol.* (In press).

U. S. EPA. (2000) Revisions to the water quality planning and management regulation and revisions to the national pollutant discharge elimination system program in support of revisions to the water quality planning and management regulation. *Fed. Regist.* **65**(135), 43586-43670.

U. S. EPA. (2001a) National primary drinking water regulations; arsenic and clarifications to compliance and new source contaminants monitoring. *Fed. Regist.* **66**(14), 6976-7066.

U. S. EPA. (2001b) Effective date of revisions to the water quality planning and management regulation and revisions to the national pollutant discharge elimination system program in support of revisions to the water quality planning and management regulations; and revision of the date for state submission of the 2002 list of impaired waters. *Fed. Regist.* **66**(202), 53044-53048.

Van Vliet R. E., Tiemersma T. P., Krooshof G. J., and Iedema P. D. (2001) The use of liquid-liquid extraction in the EPDM solution polymerization process. *Ind. Eng. Chem. Res.* **40,** 4586-4595.

Wenning R. J. (2001) USEPAs forum on managing contaminated sediments at hazardous waste sites: Summary of policy discussions. *Contaminated Soil Sediment & Water* (June/July), 49-54.

Zomosa A. (1990) Calculating optimum number of stages in continuous countercurrent decantation (CCD). *Miner. Metall. Process.* **7,** 118-120.

Chapter 5

LEAD SORPTION ONTO FERRIHYDRITE: UNCERTAINTY ANALYSIS

5.1 Abstract

Few studies over the years have addressed error propagation through surface complexation models (SCMs). Yet, outputs from SCMs, such as trace-metal partition coefficients, are frequently used as input parameters in contaminant fate and transport models to predict trace-metal mobility in aqueous environmental systems. The reality is that SCMs are often fit to limited set(s) of metal sorption data using input parameters with large uncertainties. As a result, it is important to quantify the impact of input-parameter uncertainty on model output-parameter uncertainty as well as to identify the input parameter(s) that have a dominant influence on output uncertainty. This chapter presents a methodology for quantifying the impact of analytical, thermodynamic, and SCM input-parameter uncertainties on the uncertainty in output parameters, such as metal surface loading and soluble metal concentration, as well as for identifying the input parameters that have the most significant impact on output uncertainty. Using a novel uncertainty analysis module in the OLI Software (OLI Systems, Inc., Morris Plains, NJ), error propagation through the modified triple-layer model was studied using previously published constant-pH isotherm, pH sorption edge, and multistage crossflow treatment data for lead (Pb) sorption onto 2-line ferrihydrite. When coupled with the nonlinear equation solver's gain matrix, the linearized local extrapolation and error propagation models in the OLI ElectroChem

code provide a satisfactory alternative to a more rigorous, time-consuming Monte Carlo simulation.

5.2 Introduction

Crumbling et al. (2001) contend that most environmental decision makers assume that the quality of data pertaining to a contaminated site is mainly determined by the analytical methods used, ignoring the importance of uncertainties in the techniques used to collect samples in the first place. As a result, efforts to improve data quality have centered on increasing analytical laboratory oversight, rather than on developing better approaches to manage the largest sources of uncertainty, which are field sampling issues. Choosing the right solution to a problem, therefore, depends on one's ability to identify the largest component(s) of the overall environmental-decision uncertainty up front.

In surface complexation models (SCMs), uncertainty in the predicted partitioning of trace metals between the solid and aqueous phases depends on uncertainties in both analytical (e.g., pH, temperature, reagent weights/volumes, impurity levels, etc.) and model (e.g., site density, capacitance values, equilibrium constants, etc.) parameters. For this reason, it is equally important for users of SCMs to understand which parameters contribute most to the overall uncertainty in a particular system over a range of conditions. Studies dealing with uncertainty in SCMs are limited (Goldberg, 1991; Hayes et al., 1991; Lumsdon and Evans, 1994; Robertson and Leckie, 1997). In reality, these studies deal more with sensitivity analyses (some qualitative; some quantitative) than with true uncertainty analyses. For example, Goldberg (1991) found that the ability of the constant capacitance model (CCM) and the modified triple-layer model (TLM) to describe anion sorption onto

goethite using both inner- and outer-sphere surface complexes was highly sensitive to the value of the site density parameter, N_s. A low site density led to the choice of an inner-sphere complex, while a high value for N_s led to the choice of an outer-sphere complex. Hayes et al. (1991) evaluated the sensitivity of proton- and electrolyte-binding constants to changes in model input parameters (N_s, C_1, and ΔpK_a) for the CCM, TLM, and diffuse-layer model (DLM) using potentiometric titration data for three oxides. For changes in relative and absolute errors in total acid added of 0.0 to 0.5 and 2.0E-06 to 0.0 M, respectively, the impact on best-fit equilibrium constants was < 0.2 log units. Similarly, for an absolute error in measured pH of 0.25 units, the best-fit log K values changed by < 0.1 log units. Robertson and Leckie (1997) conducted an extensive analysis of the effects of pH, ionic strength, cation loading, model type, model fit, and surface complex type on model-predicted cation partitioning and proton release using the DLM and two versions of the TLM. For the same SCM, significant response differences could exist between different surface complexes; still several surface complexes or combinations of complexes were able to fit the data equally well. Between SCMs, the responses of comparable surface complexes could differ substantially. The authors concluded that several SCMs can provide good fits of metal sorption data, although the optimum surface complexes may differ between the models.

Looking beyond the community of SCM practitioners, there is increased discussion of error propagation through geochemical and contaminant-fate codes (Schecher and Driscoll, 1987, 1988; Nordstrom and Ball, 1989; Criscenti et al., 1996; Goovaerts et al., 2001). Criscenti et al. (1996) note that most standard geochemical codes are not designed for rigorous error propagation. In fact, sensitivity analyses are

typically performed by varying input variables one at a time and performing a separate equilibrium calculation for each case. This is cumbersome for more than a few input variables. As an alternative, they present a methodology for propagating uncertainty through geochemical equilibrium speciation code calculations using Monte Carlo simulation and Generalized Sensitivity Analysis (GSA). Overall uncertainty was determined by first propagating analytical and thermodynamic uncertainties generated by Monte Carlo simulation through the geochemical code, thereby generating probability distributions for the calculated output parameters. In the second step, GSA was employed to determine the relative contribution of the uncertainty associated with each input variable to the output uncertainty. The use of Monte Carlo simulation in combination with GSA helped to focus attention on the key parameters and uncertainties in the system. Goovaerts et al. (2001) also used Monte Carlo analysis to analyze error propagation through the Michaelis-Menten equation. They noted that models of microbial activity are typically fit to few data, which can lead to large errors in parameter estimates and uncertain prediction of reaction rates and degradation times. This is true for SCMs as well, which are often fit to few sorption data using input parameters with large uncertainties. The output parameters from SCMs, such as metal partition coefficients, are then used downstream as input parameters in fate and transport models to predict metal mobility. For this reason, it is important to be able to quantify the impact of input-parameter uncertainty on SCM output-parameter uncertainty as well as to identify which input parameter(s) contribute most to the output uncertainty.

This chapter presents a methodology for quantifying the impact of analytical, thermodynamic, and SCM input-parameter uncertainties on the predicted

values of output parameters (e.g., % metal sorbed, surface charge, soluble metal concentration, etc.) as well as for identifying the input parameters that have the most impact on the output uncertainty. Using the uncertainty analysis module in the OLI Software (OLI Systems, Inc., Morris Plains, NJ), error propagation through the modified TLM was studied using previously published data for lead (Pb) sorption onto 2-line ferrihydrite (Trivedi et al., 2002a; Dyer et al., 2002b).

5.3 Uncertainty Analysis Methodology

A key objective of quantitative uncertainty analyses is to identify the input variables that drive the overall uncertainty in the output variable(s). Uncertainty in an output variable is due to two components: the sensitivity of the model output to the input variables and the uncertainty in the input variables themselves. As an alternative to a more rigorous and computationally intensive Monte Carlo approach, Robinson and Hurst (1997) advocate that a simple measure of the uncertainty importance of each input variable is to consider both the sensitivity $(\partial y/\partial x_i)$ and the uncertainty (σ_{xi}) in the value of x_i. A first-order or linearized approximation of the uncertainty importance of an input variable is given by the equation

$$\text{Uncertainty importance of } x_i = \left(\frac{\partial y}{\partial x_i}\right)\sigma_{x_i} \qquad [5.1]$$

where σ_{xi} is the sample standard deviation of x_i. First-order (or linearized) means that only the first-order (or linear) terms from the Taylor series expansion of the multivariable function $y = y\ (x_1, x_2, \ldots, x_n)$ are retained in the general error propagation equation (Coleman and Steele, 1989). When the function $y = y\ (x_1, x_2, \ldots, x_n)$ is also linear, the sample output variance, σ_y^2, is given by

$$\sigma_y^2 = \left(\frac{\partial y}{\partial x_1}\right)^2 \sigma_{x_1}^2 + \left(\frac{\partial y}{\partial x_2}\right)^2 \sigma_{x_2}^2 + \ldots + \left(\frac{\partial y}{\partial x_n}\right)^2 \sigma_{x_n}^2 \qquad [5.2]$$

Equation [5.2], therefore, identifies which input variables contribute the most to the output variance based on the magnitude of $(\partial y/\partial x_i)^2 \sigma_{x_i}^2$. This simplified first-order approach is a local approach, because it assumes that the response surface is a plane over the domain of interest (i.e., $(\partial y/\partial x)$ is constant). This linear response will not occur in many cases, however, such as in chemical equilibrium problems. In linear Cartesian-coordinate space, local will translate to a very narrow range of x_i values unless a strong linear correlation can be found between the output and input variables. Even then, the values of $\partial y/\partial x_i$ are estimates, only as good as the quality of the linear regression.

A more robust approach for situations where the relationship between the input and output variables is nonlinear has been developed and implemented within the OLI Software's ElectroChem solver. While the methodology is similar to that found in Robinson and Hurst (1997), it does not require a linear relationship between x_i and y in order to estimate $\partial y/\partial x_i$ and, hence, validate the use of Eq. [5.2]. There are two key differences between the two approaches. First, a good estimate of $\partial y/\partial x_i$ for each input variable is provided by the Newton-Raphson method that is used to solve the set of nonlinear equations in an ElectroChem model. A linear regression of the output vs. input variables, therefore, is not required. Second, the nonlinear relationship between x_i and y is assumed to be of the form $y = x_1^{a_1} x_2^{a_2} x_3^{a_3} \ldots x_n^{a_n}$, where the exponents are positive or negative constants. This functional form is advantageous for two reasons. First, it can be linearized in $\log_e$-$\log_e$ space, meaning that a first-order Taylor series expansion in $\log_e$-$\log_e$ space results in a fairly simple local extrapolation model (i.e., an approximate model) that greatly extends the range of x_i values for

which the approximate equation is valid. Experience has shown that the functional form $y = x_1^{a_1} x_2^{a_2} x_3^{a_3} \ldots x_n^{a_n}$, coupled with linearization in $\log_e$-$\log_e$ space, results in a more robust extrapolation tool for the nonlinear equations encountered in chemical equilibrium problems. Second, the partial derivative of y with respect to x_i $(\partial y/\partial x_i)$ is equal to $a_i(y/x_i)$, which nicely simplifies the linearized error propagation equation derived below.

5.3.1 The Gain Matrix

In the ElectroChem code, a normalized sensitivity or gain matrix is generated that is comprised of j rows of output variables (OV_j) by i columns of input variables (IV_i). Given that $(\partial \ln y/\partial \ln x_i) = (\partial y/\partial x_i)(x_i/y) = (\partial \% y/\partial \% x_i)$ and redefining $(\partial y_j/\partial x_i)$ as $(\partial OV_j/\partial IV_i)$, the gain ($G_{ji}$) of each output variable (OV_j) for a 1% change in an input variable (IV_i) is given by:

$$G_{ji} = \left(\frac{IV_i}{OV_j}\right)\left(\frac{\partial OV_j}{\partial IV_i}\right) = \left(\frac{\partial \ln OV_j}{\partial \ln IV_i}\right) = \left(\frac{\partial \% OV_j}{\partial \% IV_i}\right) \qquad [5.3]$$

The gain matrix, however, provides only half the input needed to assess the uncertainty importance of each input variable; that is, the sensitivity of the model output to the input variable(s). Inspection of the gain matrix alone does not tell which x values contribute the most to the uncertainty in the output parameters. The next step is to derive the uncertainty analysis or error propagation equation using a local extrapolation model that will be developed below. This will provide the other half of the input needed to assess the uncertainty importance of each input variable.

5.3.2 Local Extrapolation Model

For a multivariable function of the form $y_j = x_1^{a_1} x_2^{a_2} x_3^{a_3} \ldots x_n^{a_n}$, it can be shown that the constants $a_1, a_2, a_3, \ldots, a_n$ are equal in value and sign to the gain matrix values, $G_{j1}, G_{j2}, G_{j3}, \ldots, G_{jn}$ (see proof in Appendix D). Hence, the multivariable function, $y = x_1^{a_1} x_2^{a_2} x_3^{a_3} \ldots x_n^{a_n}$, can be rewritten as

$$y_j = x_1^{G_{j1}} x_2^{G_{j2}} x_3^{G_{j3}} \ldots x_n^{G_{jn}} \qquad [5.4]$$

where G_{j1}, G_{j2}, and so on are given by Eq. [5.3]. Linearizing Eq. [5.4] by taking the natural logarithm of both sides, followed by a first-order Taylor series expansion (Ang and Tang, 1975) to approximate the resulting multivariable function, leads to the equation

$$\ln y_j - \ln y_{j_o} = G_{j1}(\ln x_1 - \ln x_{1_o}) + G_{j2}(\ln x_2 - \ln x_{2_o}) + \ldots + G_{jn}(\ln x_n - \ln x_{n_o}) \qquad [5.5]$$

where the subscript *o* denotes the base case where the value of the function is known. Equation [5.5] simplifies to

$$\ln\left(\frac{y_j}{y_{j_o}}\right) = \sum_{i=1}^{n} G_{ji} \ln\left(\frac{x_i}{x_{i_o}}\right) \qquad [5.6]$$

Rewriting Eq. [5.6] in terms of the ElectroChem gain matrix nomenclature given in Eq. [5.3] leads to

$$\ln\left(\frac{OV_{j_N}}{OV_{j_B}}\right) = \sum_{i=1}^{n} G_{ji} \ln\left(\frac{IV_{i_N}}{IV_{i_B}}\right) \qquad [5.7]$$

where the subscripts *N* and *B* refer to the new case and base case, respectively. Finally, transforming Eq. [5.7] back into linear *x*-*y* space gives the general form of the local extrapolation model equation used in ElectroChem.

$$\left(\frac{OV_{j_N}}{OV_{j_B}}\right)=\prod_i\left(\frac{IV_{i_N}}{IV_{i_B}}\right)^{G_{ji}} \qquad [5.8]$$

In most cases, Eq. [5.8] has been found to be valid for an approximately ten-fold range in values for the input variables (i.e., the values of G_{ji} will eventually change, but they are approximately constant over a wide range). For the case of trace-metal sorption onto ferrihydrite, Eq. [5.8] might take the form

$$\left(\frac{(\%\text{Sorbed})_N}{(\%\text{Sorbed})_B}\right)=\left(\frac{pH_N}{pH_B}\right)^{0.1}\times\left(\frac{Pb_{TOT\,N}}{Pb_{TOT\,B}}\right)^{0.002}\times\ldots\times\left(\frac{(HFO_{IN})_N}{(HFO_{IN})_B}\right)^{0.005} \qquad [5.9]$$

5.3.3 Error Propagation Equation

For $y = y(x_1, x_2)$, the general form of the linearized error propagation equation (Coleman and Steele, 1989) is given by:

$$\sigma_y^2=\left(\frac{\partial y}{\partial x_1}\right)^2\sigma_{x_1}^2+\left(\frac{\partial y}{\partial x_2}\right)^2\sigma_{x_2}^2+2\left(\frac{\partial y}{\partial x_1}\right)\left(\frac{\partial y}{\partial x_2}\right)\sigma_{x_1,x_2} \qquad [5.10]$$

where σ_{x_1,x_2} is the covariance. When x_1 and x_2 are statistically independent, σ_{x_1,x_2} goes to zero. Assuming σ_{x_1,x_2} equals zero and dividing both sides of Eq. [5.10] by y leads to

$$\left(\frac{\sigma_y}{y}\right)^2=\left(\frac{\partial y}{\partial x_1}\right)^2\left(\frac{\sigma_{x_1}}{y}\right)^2+\left(\frac{\partial y}{\partial x_2}\right)^2\left(\frac{\sigma_{x_2}}{y}\right)^2=\sum_{i=1}^{N}\left(\frac{\partial y}{\partial x_i}\frac{\sigma_{x_i}}{y}\right)^2 \qquad [5.11]$$

The assumption that σ_{x_1,x_2} equals zero will not be a good assumption, of course, if there is significant correlation between the variables. As in Eqs. [5.1] and [5.2], only the first-order (linear) terms from the Taylor series expansion of the multivariable function $y = y(x_1, x_2)$ have been retained in Eqs. [5.10] and [5.11].

When the local extrapolation model equation is of the functional form given by Eq. [5.4], the linearized error propagation equation simplifies to

$$\left(\frac{\sigma_y}{y}\right)^2 = \sum_{i=1}^{N}\left(\frac{G_i\sigma_{x_i}}{x_i}\right)^2 \qquad [5.12]$$

by substituting G_i/x_i for $(\partial y/\partial x_i)(1/y)$ as derived in Eqs. D7 through D9, Appendix D. A nice feature of this substitution is that it leads to dimensionless variables on both sides of the equation (i.e., σ_y/y and σ_{x_i}/x_i). Equation [5.12] assumes that the relationship given by Eqs. [5.4] and [5.8] is continuous and has continuous derivatives in the domain of interest, that the measured variables x_i are independent of each another, and that the uncertainties in the measured variables, σ_{x_i}, are also independent of each other. Rewriting Eq. [5.12] in terms of the OLI gain matrix nomenclature given in Eq. [5.3] leads to

$$\left(\frac{\sigma_{OV_j}}{OV_j}\right)^2 = \sum_{i=1}^{N}\left(\frac{G_{ji}\sigma_{IV_i}}{IV_i}\right)^2 \qquad [5.13]$$

The coefficient of variation (COV) of variable r is defined as σ_r/r. Rewriting Eq. [5.13] in terms of COV variables gives

$$(COV\_OV_j)^2 = \sum_{i=1}^{N}(G_{ji}\times COV\_IV_i)^2 = \sum_{i=1}^{N} U_{ji} \qquad [5.14]$$

where $U_{ji} = (G_{ji}\times COV\_IV_i)^2$. It follows, then, that the fraction of the output uncertainty attributable to the uncertainty in a specific input variable can be approximated by

$$\text{Fraction of Total Uncertainty} = FRAC_{U_{ji}} =$$

$$U_{ji}\Big/\sum_{i=1}^{N} U_{ji} = U_{ji}/(COV\_OV_j)^2 \qquad [5.15]$$

The input variables with the largest values of U_{ji} will contribute the most variance to the overall output variance. A more complete derivation can be found in Appendix D.

5.4 Modeling Protocol and Validation

5.4.1 Pb/Ferrihydrite Sorption Data

The 2-line ferrihydrite was prepared according to procedures described in Trivedi et al. (2002a). Constant-pH isotherm and pH edge data for single-solute Pb sorption onto ferrihydrite are reported in Appendix A and Trivedi et al. (2002a). Analysis of the sorption data using the modified TLM is summarized in Chapter 3 and Dyer et al. (2002b). Application of the TLM regression results to predict Pb sorption in multistage crossflow contacting systems (pH 5.5, 0.01 M $NaNO_3$) is described in Chapter 4 and Dyer et al. (2002a).

5.4.2 Geochemical Modeling Software

The ElectroChem solver within the OLI Software was used to conduct the uncertainty analyses using the methodology outlined above. Equations [5.3] and [5.13] through [5.15] have been incorporated into the uncertainty analysis module in ElectroChem; this module has also been linked to the SCMs. For every input variable where σ_{IV_i} is specified, the uncertainty analysis module will report values for the following parameters: IV_i, σ_{IV_i}, COV_IV_i, G_{ji}, OV_j, σ_{OV_j}, COV_OV_j, U_{ji}, and $FRAC_{U_{ji}}$. Details on the thermodynamic databank and framework, the equation solvers, and the SCMs used in the OLI Software are presented in Chapter 2 and Dyer et al. (2002b). The modified TLM was utilized in this work, having provided best fits of the Pb/ferrihydrite sorption data. Steady-state predictions for the multistage, crossflow Pb/ferrihydrite sorption studies were generated using OLI's Environmental Simulation Program (ESP) as described in Chapter 4 and Dyer et al. (2002a). The multistage results were then further analyzed using the uncertainty analysis module in ElectroChem to obtain 95% confidence intervals.

5.4.3 Input Variable Uncertainty Assumptions

Scouting runs using ElectroChem's uncertainty analysis module for one-stage, single-solute Pb sorption onto ferrihydrite over a wide range of conditions identified which input and thermodynamic parameters determined the majority of the uncertainty in the output variables of interest—total Pb in solution (Pb_{aq}) and Pb surface loading (Pb_{sorb}). Table 5.1 summarizes these parameters and their corresponding uncertainty values, which were used throughout this study. Input/thermodynamic uncertainties are reported as either absolute values (standard deviation) or relative values (coefficient of variation). Uncertainty assumptions for input parameters, such as pH, Total Pb, Total H_2O, etc., are based on experience and a review of the literature. Uncertainty assumptions for the thermodynamic parameters were determined by estimating the 95% prediction intervals ($\pm 2\sigma$) for the potentiometric titration and constant-pH lead isotherm data reported in Appendix A and Dyer et al. (2002b).

5.4.4 Test of Local Extrapolation and Error Propagation Models

Significant time was spent understanding the range over which the local extrapolation model (Eq. [5.8]) was valid, in addition to testing the implementation of both the local extrapolation and error propagation models in ElectroChem. The validity range for the local extrapolation model was tested in two ways. First, the variability in gain matrix values for Pb_{aq} and Pb_{sorb}, based on uncertainties in the input/thermodynamic parameters given in Table 5.1, was examined as a function of pH, total ferrihydrite, and total Pb. The more constant the gain matrix values, the wider the range over which the local extrapolation model is valid. Results of the

Table 5.1 Input/thermodynamic parameters and corresponding uncertainty assumptions used throughout this study.[a]

Parameter	Standard Deviation (σ_i)	Coefficient of Variation (COV_i)[b]
Total Pb		0.02
Total Ferrihydrite		0.10
Total H_2O		0.03
Total $NaNO_3$		0.10
pH	0.03 pH units	
log K^{int}_{NO3-}	0.36 log units	
log K^{int}_{Na+}	0.36 log units	
log $K^{int}_{(\equiv FeO)_2 Pb}$	0.12 log units	
log $K^{int}_{\equiv FeOHPb^{2+}}$	0.12 log units	

[a] Refer to Tables 3.2 and 3.3 in Chapter 3 for details on the chemical reactions and mass-law expressions corresponding to each of the equilibrium constants given above. Definitions for each of the parameters can be found in the nomenclature section. [b] $COV_i = \sigma_{Yi}/Y_i$.

analysis showed that the gains varied some, but were of the same order of magnitude over a 5- to 10-fold range in model input and output values. The gains varied more significantly with pH (especially on the steep part of the pH sorption edge) and at high Pb/Fe ratios (i.e., approaching site saturation). Second, estimates for Pb_{aq} and Pb_{sorb} using the local extrapolation model (Eq. [5.8]) and gain matrix values from ElectroChem's uncertainty analysis module were compared to actual predictions from a one-stage ESP Pb/ferrihydrite model as a function of pH, total Pb, total ferrihydrite, and log $K^{int}_{(\equiv FeO)_2 Pb}$. The base case was a one-equilibrium-stage simulation at pH 5.5 using 0.5 mM Pb, 0.4 g L^{-1} ferrihydrite, and 0.01 M $NaNO_3$. Plots of estimated vs. predicted values for Pb_{aq} and Pb_{sorb} showed that the local model was valid to within ± 20% in most cases and to within ± 50% in all cases over a 10- to 100-fold range in input and output values. Figure 5.1 shows two examples of these parity plots for changes in total ferrihydrite dose (see Figures D1 through D6, Appendix D, for additional plots).

Implementation of the overall uncertainty analysis methodology was also tested in two ways for the base case above. In the first test, a Monte Carlo simulation of ElectroChem's local extrapolation model was performed using the Resampling Stats for Windows software (Resampling Stats, Inc., Arlington, Virginia) to estimate the sample means ($\overline{X}$), sample standard deviations (s), and 95% confidence intervals for Pb_{aq} and Pb_{sorb}. Normal distributions for the input/thermodynamic parameters in Table 5.1 were randomly sampled 10,000 times with replacement to generate distributions for the two output values. Agreement between the actual ElectroChem output and the results of the Monte Carlo simulation of the local extrapolation model was excellent for sample standard deviation (Table 5.2), indicating that

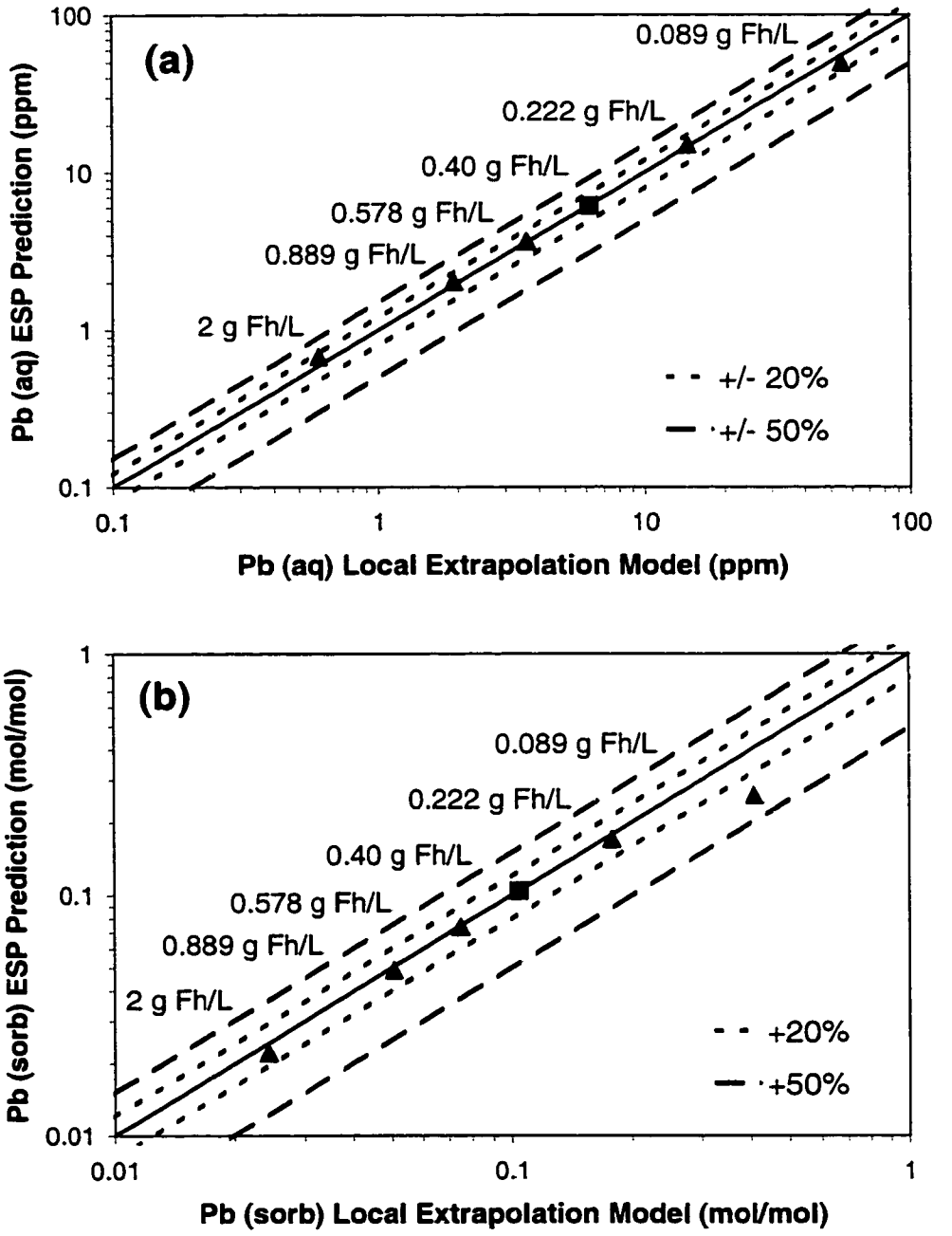

Figure 5.1 **Comparison of local extrapolation model estimates to ESP model predictions for (a) Pb_{aq} and (b) Pb_{sorb} as a function of ferrihydrite (Fh) dose for one-stage, single-solute sorption of 0.5 mM Pb onto 0.4 g L^{-1} ferrihydrite (base case) at pH 5.5 in 0.01 M $NaNO_3$ solution.**

Table 5.2 Results of validity tests of the local extrapolation and error propagation models in ElectroChem.

Parameter	ElectroChem Uncertainty Analysis	Monte Carlo Simulation of Local Extrap. Model	ESP Monte Carlo Simulation + Resampling Stats
Pb_{aq} (ppm)			
Sample Mean ($\overline{X}$)	6.2[a]	6.5	6.4
Sample Std. Deviation (s)	2.1	2.1	1.8
95% Confidence Interval	2.0-10.4[b]	3.4-11.5	3.4-10.7
Pb_{sorb} (mol Pb/mol Fe)			
Sample Mean ($\overline{X}$)	0.104[a]	0.105	0.106
Sample Std. Deviation (s)	0.0099	0.0102	0.0100
95% Confidence Interval	0.085-0.124[b]	0.088-0.129	0.085-0.127

[a] Actual model prediction (i.e., point value, rather than mean). [b] Assumes normal distribution; calculated as $\overline{X} \pm 1.96s$.

implementation of the local extrapolation and error propagation models was correct. The discrepancy in the 95% confidence intervals for Pb_{aq} arises from the fact that Resampling Stats provides the interval that literally contains 95% of the sampled data points, while the confidence interval for ElectroChem was calculated using the output standard deviation and assuming a normal distribution of values (± 1.96s). The confidence interval from Resampling Stats, therefore, is a better representation of the real population. In this case, the results suggest that the probability distribution for Pb_{aq} is slightly skewed to higher Pb concentrations (−1.5s to +2.35s) and, hence, is not normal. The values for Pb_{sorb}, on the other hand, are much closer to being normally distributed about the mean.

In the second test, a 100-run Monte Carlo simulation was performed for the base case with ESP. Using the uncertainties in Table 5.1 and assuming normal distributions, the MINITAB™ Statistical Software v. 13.30 (Minitab, Inc., State College, PA) was used to generate 100 random sets of input variables for the ESP runs. Results from the Monte Carlo simulations were then analyzed using the bootstrap procedure in the Resampling Stats software. Background on the bootstrap procedure can be found in Diaconis et al. (1983) and Simon (1997). The bootstrap procedure effectively creates a hypothetical "infinite" population that represents one's best guess about the real population. In this case, 10,000 new samples of size 100 were randomly generated with replacement directly from the original sample of 100 runs. The real benefit of this approach is that it made it unnecessary to perform several thousand Monte Carlo simulations in ESP. As shown in Table 5.2, the "ESP Monte Carlo Simulation + Resampling Stats" results agree well with both the "ElectroChem Uncertainty Analysis" and "Monte Carlo Simulation of Local Extrap.

Model" results. The ESP Monte Carlo simulation predicts a slightly lower sample standard deviation for Pb_{aq} than does the ElectroChem model. The ESP Monte Carlo simulation results also reaffirm that the 95% confidence interval for Pb_{aq} is skewed somewhat to higher Pb concentrations, while the confidence interval for Pb_{sorb} is essentially normally distributed about the mean.

In summary, thorough testing of the uncertainty analysis module in ElectroChem has shown that the simplified methodology described above is a satisfactory substitute for more rigorous Monte Carlo simulations of the triple-layer SCM.

5.4.5 Isotherm and pH-Edge Data Analysis

ElectroChem was used to identify uncertainty bands for the constant-pH isotherm and pH sorption edge data using the input/thermodynamic parameter uncertainty assumptions in Table 5.1. The uncertainty bands for Pb_{aq} (ppm), Pb_{sorb} (mol Pb/mol Fe), and % Pb_{sorb} were calculated using the ElectroChem uncertainty analysis module output for OV_j and σ_{OV_j}. Based on the Monte Carlo simulation results shown in Table 5.2 and described below for the multistage crossflow sorption case studies, a normal distribution of data was assumed for Pb_{sorb} ($OV_j \pm 1.96\,\sigma_{OV_j}$) and skewed distributions were assumed for Pb_{aq} ($OV_j - 1.5\,\sigma_{OV_j}$ to $OV_j + 2.35\,\sigma_{OV_j}$) and % Pb_{sorb} ($OV_j - 2.35\,\sigma_{OV_j}$ to $OV_j + 1.5\,\sigma_{OV_j}$). The ElectroChem results for Eq. [5.15] (fraction of the total output uncertainty attributable to specific input variables) were also analyzed to identify the input variables that had a dominant influence on the output uncertainty.

5.4.6 Multistage Crossflow Sorption Data Analysis

The multistage crossflow sorption case studies presented in Chapter 4 and Dyer et al. (2002a) were also analyzed using ElectroChem's uncertainty analysis module. The uncertainty analysis methodology was applied in two ways. First, the input variables that had the most influence on the output uncertainty in Pb_{aq} and Pb_{sorb} for each stage of the multistage crossflow sorption systems were identified as given by Eq. [5.15]. Second, for each stage of the multistage sorption systems, the Resampling Stats software was used to conduct a Monte Carlo simulation of the local extrapolation model from ElectroChem to estimate the 95% confidence interval for the model-predicted effluent Pb concentration. The 95% confidence intervals are presented in Table 4.1 and Dyer et al. (2002a). As for the base-case results in Table 5.2, 95% confidence intervals for Pb_{aq} for the multistage crossflow cases were all skewed toward higher Pb concentrations (i.e., ~ -1.5s to ~ +2.35s).

5.5 Results and Discussion

5.5.1 Uncertainty in Isotherm and pH-Edge Data

Constant-pH isotherm data, TLM-predicted isotherm curves (solid/dashed lines), and uncertainty bars for the model predictions are shown in Figure 5.2 for single-solute Pb sorption onto ferrihydrite. Uncertainty bars are not shown for every data point for clarity. The experimental data points fall comfortably within the uncertainty bars for the model predictions in all cases. As shown in the figure, the uncertainty ranges for Pb_{aq} are much wider than those for Pb_{sorb}, especially in the concentration region where the isotherm curves begin to flatten out. In this transition region, the gains for Pb_{aq} with respect to total ferrihydrite and log $K^{int}_{(\equiv FeO)_2Pb}$ (Eq. [5.3])

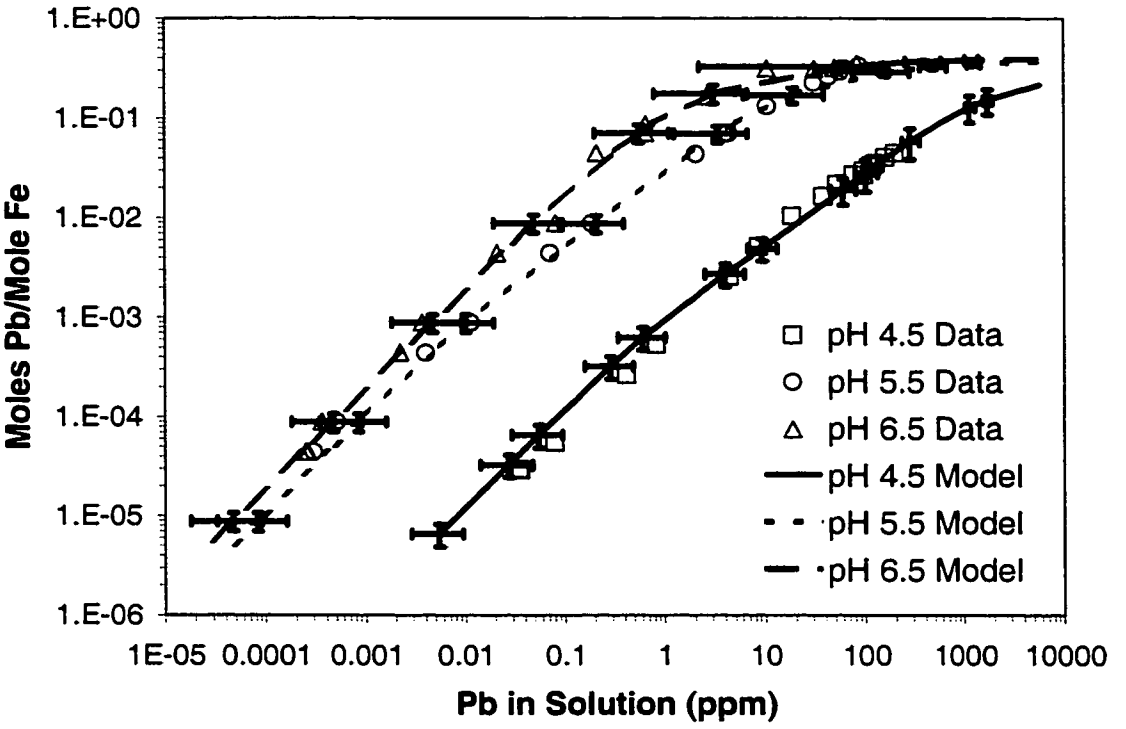

Figure 5.2 **ElectroChem-predicted uncertainties in triple-layer model fits of the pH 4.5, 5.5, and 6.5 equilibrium isotherm data for single-solute Pb sorption onto 2-line ferrihydrite assuming the species pair, $(\equiv FeO)_2Pb/\equiv FeOHPb^{2+}$. Experimental conditions: 0.1 and 1.0 g ferrihydrite/L in 0.01 M $NaNO_3$; Pb added as $Pb(NO_3)_2$; 4-hour equilibration time; room temperature; N_2 glovebox. See Chapter 3 and Dyer et al. (2002b) for TLM regression assumptions and results.**

increase significantly, meaning that a small change in surface loading will result in a large change in Pb_{aq}.

For select isotherm data points, Tables 5.3 and 5.4 show the fraction of the total output uncertainty in Pb_{aq} and Pb_{sorb}, respectively, that is attributable to specific input/thermodynamic parameters. The values in the tables for each input/thermodynamic parameter represent the fraction of the output COV squared (Eq. [5.15]). As shown in Table 5.3, at lower pH and Pb surface loading, uncertainties in log K^{int}_{NO3-} and log $K^{int}_{\equiv FeOHPb^{2+}}$ dominate the output uncertainty in Pb_{aq}. However, as pH and Pb surface loading increase, uncertainties in total ferrihydrite and log $K^{int}_{(\equiv FeO)_2Pb}$ begin to dominate the uncertainty in Pb_{aq}. Near site saturation, uncertainty in total ferrihydrite dominates the output uncertainty in Pb_{aq}, along with increasing contributions from total Pb and total H_2O as pH decreases. For sorbed Pb, Table 5.4 shows that the uncertainty in total ferrihydrite dominates the output uncertainty in Pb_{sorb} at pH 5.5 and 6.5, except near site saturation where log $K^{int}_{(\equiv FeO)_2Pb}$ and, to a lesser extent, log K^{int}_{NO3-} dominate the output uncertainty. At pH 4.5, on the other hand, uncertainties in log $K^{int}_{(\equiv FeO)_2Pb}$ and pH dominate the uncertainty in Pb_{sorb}, except at the lowest Pb surface loadings where uncertainties in log K^{int}_{NO3-} and log $K^{int}_{\equiv FeOHPb^{2+}}$ are the most important. Input/thermodynamic parameters listed in Table 5.1, but not shown in Tables 5.3 and 5.4, had a negligible impact on the output uncertainty under all conditions. The input variables (pH, total ferrihydrite, total Pb, and total H_2O) generally accounted for 45-60% of the output uncertainty in Pb_{aq} at the lowest Pb surface loadings and 90-100% of the output uncertainty at the highest Pb surface loadings. The balance of the output uncertainty was due to uncertainties in the thermodynamic parameters (log $K^{int}_{(\equiv FeO)_2Pb}$, log K^{int}_{NO3-}, and log $K^{int}_{\equiv FeOHPb^{2+}}$). For Pb_{sorb},

Table 5.3 **Input/thermodynamic parameters dominating output uncertainty in Pb_{aq} (ppm) for the Pb/ferrihydrite constant-pH isotherms shown in Figure 5.2.**

pH	Pb Total (M)	Fraction of Output COV Squared for Pb_{aq}						
		Total Pb	Total Ferri-hydrite	pH	Total H_2O	log $K^{int}_{(\equiv FeO)_2Pb}$	log $K^{int}_{\equiv FeOHPb^{2+}}$	log $K^{int}_{NO3^-}$
4.5	1E-02	0.19	**0.27**	0.05	**0.25**	**0.24**	–	–
	2E-03	0.04	**0.31**	0.10	0.02	**0.50**	–	0.02
	1E-04	0.02	**0.29**	0.12	–	**0.30**	0.07	0.19
	1E-06	–	0.08	0.10	–	0.03	**0.34**	**0.45**
5.5	1E-02	0.16	**0.69**	–	0.12	0.02	–	–
	2E-03	–	**0.50**	0.08	–	**0.40**	–	0.01
	1E-04	–	**0.31**	0.13	–	**0.45**	0.03	0.07
	1E-06	–	0.11	0.11	–	0.05	**0.35**	**0.38**
6.5	1E-02	0.15	**0.74**	–	0.11	–	–	–
	2E-03	–	**0.51**	0.08	–	**0.40**	–	–
	1E-04	–	0.25	0.12	–	**0.62**	–	–
	1E-06	–	0.25	0.12	–	**0.63**	–	–

Table 5.4 **Input/thermodynamic parameters dominating output uncertainty in Pb_{sorb} (mol Pb/mol Fe) for the Pb/ferrihydrite constant-pH isotherms shown in Figure 5.2.**

pH	Pb Total (M)	Fraction of Output COV Squared for Pb_{sorb}						
		Total Pb	Total Ferri-hydrite	pH	Total H_2O	log $K^{int}_{(\equiv FeO)_2 Pb}$	log $K^{int}_{\equiv FeOHPb^{2+}}$	log K^{int}_{NO3-}
4.5	1E-02	–	0.05	0.15	0.02	**0.74**	–	0.04
	2E-03	–	0.02	0.16	0.02	**0.76**	–	0.03
	1E-04	0.02	0.03	0.17	0.01	**0.41**	0.10	**0.26**
	1E-06	0.02	**0.27**	0.08	–	–	**0.26**	**0.34**
5.5	1E-02	–	–	0.13	0.02	**0.62**	–	**0.22**
	2E-03	0.04	**0.93**	–	–	0.02	–	–
	1E-04	0.04	**0.96**	–	–	–	–	–
	1E-06	0.04	**0.96**	–	–	–	–	–
6.5	1E-02	–	–	0.13	0.02	**0.64**	–	**0.21**
	2E-03	0.04	**0.96**	–	–	–	–	–
	1E-04	0.04	**0.96**	–	–	–	–	–
	1E-06	0.04	**0.96**	–	–	–	–	–

the input variables generally accounted for 60-100% and 40-50% of the output uncertainty at the lowest and highest Pb surface loadings, respectively.

Figures 5.3a through 5.3d display the uncertainty bars for three TLM-predicted pH sorption edges for single-solute Pb sorption onto ferrihydrite in 0.01 M NaNO3 solution. Figures 5.3b and 5.3c display the same data for 50 μM total Pb, but Figure 5.3c is plotted on a compressed pH scale to highlight the region of maximum Pb sorption. Once again, the experimental data fall well within the uncertainty bars for the model predictions. Note the large uncertainty in percent Pb sorbed over most of the pH range of the edges. This reinforces one of the major conclusions from Chapter 3 and Dyer et al. (2002b); that is, regression of pH sorption edge data alone is not a sufficient test of the predictive capability of a SCM. Regression of constant-pH isotherm data at multiple pH values, together with pH edge data at several ionic strengths and metal/sorbent molar ratios, is a much more rigorous test of the model.

For select pH edge points, Table 5.5 shows the fraction of the total output uncertainty in % Pb_{sorb} that is attributable to specific input/thermodynamic parameters. At higher pH and Pb surface loadings, uncertainties in total ferrihydrite and log $K^{int}_{(\equiv FeO)_2Pb}$ dominate the output uncertainty in % Pb_{sorb}. As pH and surface loading decrease, however, the importance of uncertainties in log $K^{int}_{NO3^-}$ and log $K^{int}_{\equiv FeOHPb^{2+}}$ increases. This trend is similar to what was observed for the constant-pH-isotherm Pb_{aq} data in Table 5.3. At all pH and Pb surface loadings, the impact of uncertainties in pH on the uncertainty in % Pb_{sorb} is about the same (10-15%). Input/thermodynamic parameters listed in Table 5.1, but not shown in Table 5.5, had a negligible impact on the output uncertainty under all conditions. The input variables

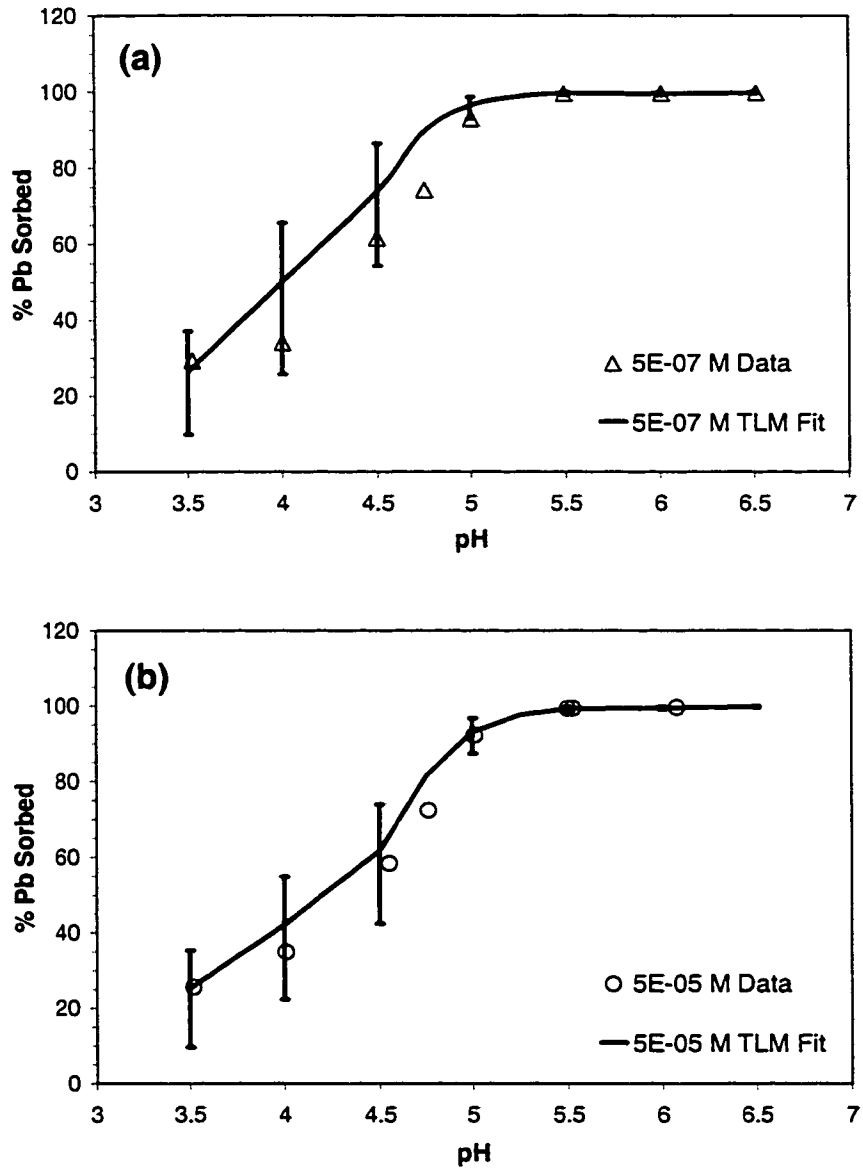

Figure 5.3 **ElectroChem-predicted uncertainties in triple-layer model fits of the pH sorption edge data for single-solute sorption of (a) 0.5 μM, (b) 50 μM, (c) 50 μM (compressed pH scale), and (d) 800 μM Pb onto 2-line ferrihydrite assuming the species pair, $(\equiv FeO)_2Pb/\equiv FeOHPb^{2+}$. Experimental conditions: 1.0 g ferrihydrite/L; 0.01 M $NaNO_3$; Pb added as $Pb(NO_3)_2$; 4-hour equilibration time; room temperature; N_2 glovebox. See Chapter 3 and Dyer et al. (2002b) for TLM regression assumptions and results.**

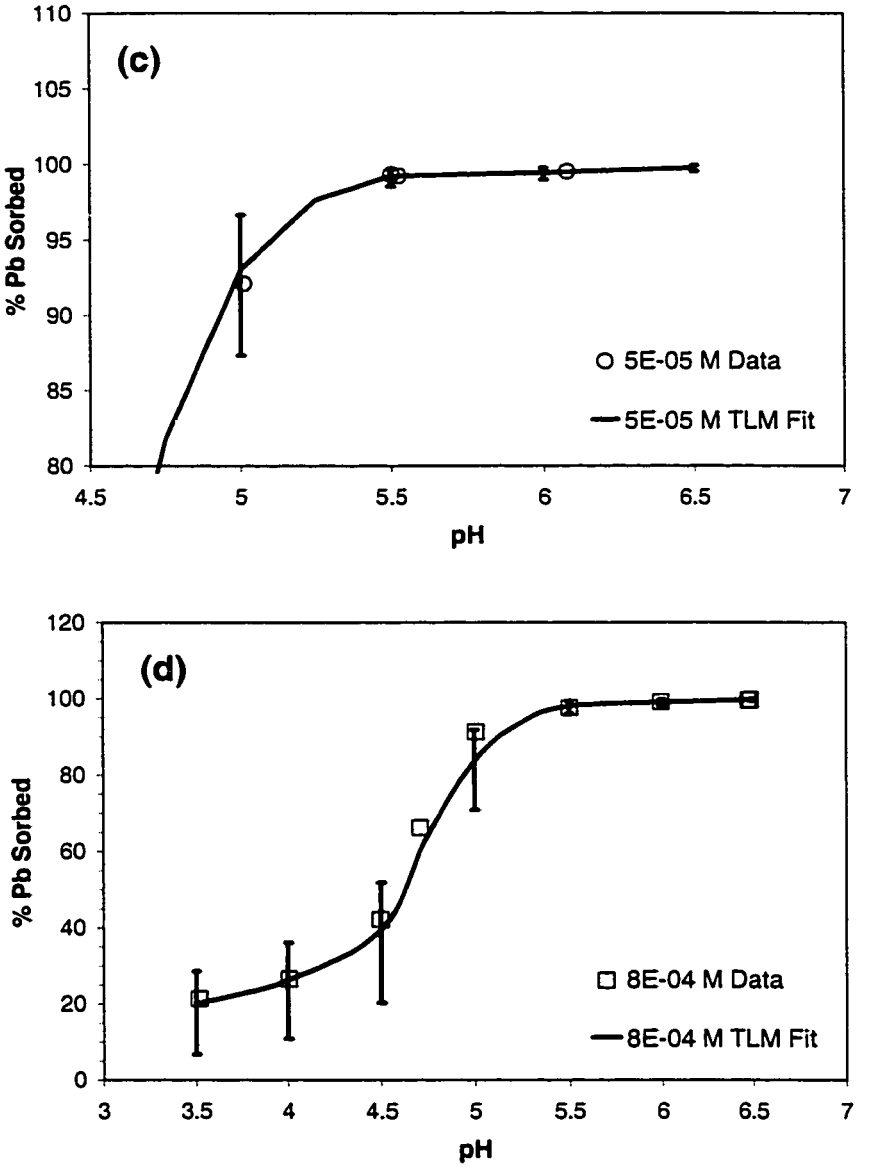

Figure 5.3 Continued.

Table 5.5 **Input/thermodynamic parameters dominating output uncertainty in percent Pb sorbed for the Pb/ferrihydrite pH sorption edges shown in Figure 5.3.**

pH	Pb Total (M)	Fraction of Output COV Squared for % Pb_{sorb}				
		Total Ferri-hydrite	pH	log $K^{int}_{(\equiv FeO)_2Pb}$	log $K^{int}_{\equiv FeOHPb^{2+}}$	log $K^{int}_{NO3^-}$
3.5	5E-07	0.20	0.15	**0.31**	0.11	**0.22**
	5E-05	**0.23**	0.14	**0.37**	0.07	0.17
	8E-04	**0.27**	0.12	**0.54**	–	0.05
4.5	5E-07	0.08	0.10	0.03	**0.34**	**0.45**
	5E-05	**0.23**	0.12	0.17	0.15	**0.31**
	8E-04	**0.30**	0.12	**0.53**	–	0.03
5.5	5E-07	0.10	0.11	0.04	**0.35**	**0.38**
	5E-05	**0.29**	0.13	**0.32**	0.08	0.15
	8E-04	**0.34**	0.11	**0.53**	–	0.01
6.5	5E-07	**0.24**	0.11	**0.62**	–	–
	5E-05	**0.25**	0.11	**0.62**	–	–
	8E-04	**0.32**	0.10	**0.55**	–	–

(pH and total ferrihydrite) generally accounted for 60-70% of the output uncertainty, except at the lowest Pb surface loadings where they accounted for 50-60% of the uncertainty in % Pb_{sorb}. The balance of the output uncertainty was due to uncertainties in the thermodynamic parameters (log $K^{int}_{(\equiv FeO)_2Pb}$, log $K^{int}_{NO3^-}$, and log $K^{int}_{\equiv FeOHPb^{2+}}$).

5.5.2 Uncertainty in Multistage Crossflow Sorption Data

In all cases, the uncertainty analysis results for the first stage (Stage 1) of a one-stage or multistage crossflow sorption system paralleled the results for the constant-pH isotherm data at pH 5.5 (Tables 5.3 and 5.4). At moderate Pb concentrations and surface loadings, uncertainty in log $K^{int}_{(\equiv FeO)_2Pb}$ accounted for more than 60% of the output uncertainty in Pb_{aq}, with secondary contributions from total ferrihydrite and pH. On the other hand, uncertainties in log $K^{int}_{NO3^-}$ and log $K^{int}_{\equiv FeOHPb^{2+}}$ dominated the output uncertainty in Pb_{aq} at very low Pb concentrations and surface loadings, while uncertainty in total ferrihydrite had the most influence on output uncertainty in Pb_{aq} near site saturation. For sorbed Pb, uncertainty in total ferrihydrite accounted for more than 90% of the output uncertainty in Pb_{sorb}, except at high Pb surface loadings where log $K^{int}_{(\equiv FeO)_2Pb}$ dominated the output uncertainty. In Stages 2 through 4, on the other hand, uncertainty in the total Pb feed concentration to each stage dictated the output uncertainties in both Pb_{aq} and Pb_{sorb}. For Pb_{aq} only, secondary contributions were made by log $K^{int}_{NO3^-}$ and log $K^{int}_{\equiv FeOHPb^{2+}}$ at very low Pb concentrations and surface loadings and by log $K^{int}_{(\equiv FeO)_2Pb}$ at moderate to high Pb surface loadings. Quantitative uncertainty analysis results for the multistage crossflow sorption case studies are summarized in Tables 5.6 and 5.7.

In this chapter, a simplified uncertainty analysis methodology was successfully integrated with the triple-layer surface complexation model to (1) quantify

Table 5.6 Input/thermodynamic parameters dominating output uncertainty in Pb_{aq} (ppm) for the multistage crossflow Pb/ferrihydrite sorption case studies (pH 5.5, 0.01 M $NaNO_3$).

Case	Stg. #	Pb Outlet Conc. (ppm)[a]	Surface Loading (mol Pb /mol Fe)	Fraction of Output COV Squared for Pb_{aq}					
				Total Pb	Total Ferri.	pH	log $K^{int}_{(\equiv FeO)_2Pb}$	log $K^{int}_{\equiv FeOHPb^{2+}}$	log K^{int}_{NO3-}
1A	1	1.8	0.044	–	0.15	0.15	**0.63**	–	0.05
1B	1	4.5	0.085	–	0.16	0.14	**0.65**	–	0.04
	2	0.057	0.004	**0.62**	0.05	0.05	0.04	0.10	0.14
2A	1	0.01	9.6E-04	–	0.08	0.12	0.04	**0.39**	**0.35**
2B	1	0.462	0.017	–	0.17	0.16	**0.49**	0.05	0.12
	2	0.008	7.8E-04	**0.55**	0.04	0.055	–	0.18	0.16
3A	1	6.2	0.104	–	0.18	0.14	**0.64**	–	0.04
3B	1	17.8	0.184	–	**0.29**	0.11	**0.54**	–	0.045
	2	1.3	0.036	**0.60**	0.06	0.06	**0.25**	–	0.024
3C	1	44.3	0.253	0.06	**0.46**	0.065	**0.34**	–	0.055
	2	10.9	0.145	**0.45**	0.12	0.07	**0.34**	–	–
	3	1.6	0.041	**0.70**	0.045	0.05	0.19	–	–
	4	0.115	0.0064	**0.84**	0.03	0.025	0.04	0.03	–

[a] ESP model prediction.

Table 5.7 Input/thermodynamic parameters dominating output uncertainty in Pb_{sorb} (mol Pb/mol Fe) for the multistage crossflow Pb/ferrihydrite sorption case studies (pH 5.5, 0.01 M $NaNO_3$).

Case	Stg. #	Pb Outlet Conc. (ppm)[a]	Surface Loading (mol Pb /mol Fe)	Fraction of Output COV Squared for Pb_{aq}					
				Total Pb	Total Ferri.	pH	log $K^{int}_{(\equiv FeO)_2Pb}$	log $K^{int}_{\equiv FeOHPb^{2+}}$	log K^{int}_{NO3-}
1A	1	1.8	0.044	0.04	**0.96**	–	–	–	–
1B	1	4.5	0.085	0.04	**0.94**	–	–	–	–
	2	0.057	0.004	**0.93**	0.07	–	–	–	–
2A	1	0.01	9.6E-04	0.04	**0.96**	–	–	–	–
2B	1	0.462	0.017	0.04	**0.94**	–	–	–	–
	2	0.008	7.8E-04	**0.94**	0.06	–	–	–	–
3A	1	6.2	0.104	0.04	**0.92**	–	–	0.04	–
3B	1	17.8	0.184	0.04	**0.62**	0.05	**0.27**	–	–
	2	1.3	0.036	**0.90**	0.09	–	–	–	–
3C	1	44.3	0.253	–	0.105	0.125	**0.65**	–	0.105
	2	10.9	0.145	**0.61**	0.17	0.04	0.17	–	–
	3	1.6	0.041	**0.92**	0.06	–	–	–	–
	4	0.115	0.0064	**0.97**	0.03	–	–	–	–

[a] ESP model prediction.

the level of uncertainty in key output variables (i.e., output standard deviation and 95% confidence interval); and (2) identify which input variables and thermodynamic parameters control the uncertainty in the output variables of interest. When coupled with the nonlinear equation solver's gain matrix, the linearized local extrapolation and error propagation models in the ElectroChem code provide a satisfactory alternative to a more rigorous, time-consuming Monte Carlo simulation.

5.6 References

Ang A. H-S. and Tang W. H. (1975) *Probability Concepts in Engineering Planning and Design. Volume I. Basic Principles*. John Wiley & Sons.

Coleman H. W. and Steele W. G. (1989) *Experimentation and Uncertainty Analysis for Engineers*. John Wiley & Sons.

Criscenti L. J., Laniak G. F., and Erikson R. L. (1996) Propagation of uncertainty through geochemical calculations. *Geochim. Cosmochim. Acta* **60,** 3551-3568.

Crumbling D. M., Groenjes C., Lesnik B., Lynch K., Shockley J., van EE J., Howe R., Keith L., and McKenna J. (2001) Managing uncertainty in environmental decisions. *Environ. Sci. Technol.* **35,** 404A-409A.

Diaconis P. and Efron B. (1983) Computer-intensive methods in statistics. *Sci. Am.* **248**(5), 116-130.

Dyer J. A., Trivedi P., Sanders S. J., Scrivner N. C., and Sparks D. L. (2002a) Lead sorption onto ferrihydrite. 3. Multistage contacting. *Environ. Sci. Technol.* (In press).

Dyer J. A., Trivedi P., Scrivner N. C., and Sparks D. L. (2002b) Lead sorption onto ferrihydrite. 2. New modeling insights. *Environ. Sci. Technol.* (In press).

Goldberg S. (1991) Sensitivity of surface complexation modeling to the surface site density parameter. *J. Colloid Interface Sci.* **145,** 1-9.

Goovaerts P., Semrau J., and Lontoh S. (2001) Monte carlo analysis of uncertainty attached to microbial pollutant degradation rates. *Environ. Sci. Technol.* **35,** 3924-3930.

Hayes K. F., Redden G., Ela W., and Leckie J. O. (1991) Surface complexation models: An evaluation of model parameter estimation using FITEQL and oxide mineral titration data. *J. Colloid Interface Sci.* **142,** 448-469.

Lumsdon D. G. and Evans L. J. (1994) Surface complexation model parameters for goethite (α-FeOOH). *J. Colloid Interface Sci.* **164,** 119-125.

Nordstrom D. K. and Ball J. W. (1989) Mineral saturation states in natural waters and their sensitivity to thermodynamic and analytic errors. *Sci. Geol. Bull.* **42,** 269-280.

Robertson A. P. and Leckie J. O. (1997) Cation binding predictions of surface complexation models: Effects of pH, ionic strength, cation loading, surface complex, and model fit. *J. Colloid Interface Sci.* **188,** 444-472.

Robinson R. B. and Hurst B. T. (1997) Statistical quantification of the sources of variance in uncertainty analyses. *Risk Anal.* **17,** 447-453.

Schecher W. D. and Driscoll C. T. (1987) An evaluation of uncertainty associated with aluminum equilibrium calculations. *Water Resour. Res.* **23,** 525-534.

Schecher W. D. and Driscoll C. T. (1988) An evaluation of the equilibrium calculations within acidification models: The effect of uncertainty in measured chemical components. *Water Resour. Res.* **24,** 533-540.

Simon J. L. (1997) *Resampling: The New Statistics*. Resampling Stats, Inc.

Trivedi P., Dyer J. A., and Sparks D. L. (2002a) Lead sorption onto ferrihydrite. 1. A macroscopic and spectroscopic assessment. *Environ. Sci. Technol.* (In press).

Chapter 6

ZINC SORPTION ONTO FERRIHYDRITE: NEW MODELING INSIGHTS

6.1 Abstract

A previous study involving lead (Pb) sorption onto ferrihydrite over a wide range of conditions highlighted the new insights gained when molecular- and macroscopic-scale investigations are combined with surface complexation model (SCM) development to predict Pb speciation and partitioning in aqueous systems. In this work, an extensive collection of new macroscopic and spectroscopic data was used to assess the ability of the modified triple-layer model (TLM) to predict single-solute zinc (Zn) sorption onto 2-line ferrihydrite in $NaNO_3$ solutions as a function of pH, ionic strength, and concentration. The results for Zn reported in this chapter nicely corroborate the results reported previously for Pb sorption onto ferrihydrite. Regression of constant-pH isotherm data, together with potentiometric titration and pH edge data, was a much more rigorous test of the SCM than fitting pH edge data alone. When coupled with valuable input from spectroscopic analyses, excellent fits of the isotherm data were obtained with a one-species, one-Zn-sorption-site model using the bidentate-mononuclear surface complex, $(\equiv FeO)_2Zn$. No evidence was found for surface precipitation at high loadings over the pH range 4.5 to 7.5. Regressing edge data in the absence of isotherm and spectroscopic data resulted in a fair number of surface-species/site-type combinations that provided acceptable fits of the edge data, but unacceptable fits of the isotherm data. Surprisingly, however, both the density of

Zn sorption sites and the value of the best-fit equilibrium "constant" for the bidentate-mononuclear complex had to be varied with pH to fit the isotherm data. A linear relationship between log $K_{(\equiv FeO)2Zn}$ and pH was found as given by: log $K_{(\equiv FeO)2Zn\ @1\ g/L}$ = 2.058(pH) – 6.131. In addition, a surface activity coefficient term was used in the model to reduce the ionic-strength dependence of sorption. In light of this and previous work, much work still needs to be done in fine-tuning the thermodynamic framework and databases for the SCMs.

6.2 Introduction

Numerous commercial and public-domain geochemical codes exist for predicting trace-metal speciation in aqueous systems; however, the existing surface complexation models (SCMs) in these codes often prove inadequate for simulating multisolute sorption reactions in complex industrial systems. One contributing factor is that many published equilibrium constants for surface complexes are based on regressions of a handful of pH sorption edges covering a narrow range of conditions, without the aid of state-of-the-art spectroscopic techniques to confirm surface speciation.

Extensive studies of metal cation and anion sorption onto amorphous iron (hydr)oxides have been conducted over the years. Dzombak and Morel (1990) critically reviewed pre-1990 single-solute sorption data for hydrous ferric oxide (HFO); this data was regressed to obtain best-fit intrinsic equilibrium constants (K^{int}) for the Generalized Two-Layer Model (GTLM). Interestingly, only 17% of 184 cation/anion data sets were equilibrium isotherms. This suggests that these equilibrium constants will have limited applicability if the pH edges used to determine them did not cover a wide enough range of conditions. Constant-pH equilibrium

isotherms, on the other hand, often cover 5 to 8 orders of magnitude in metal concentration. If generated at multiple pH values, regression of constant-pH isotherm data, along with pH sorption edge data, is a much more rigorous test of the SCM.

Zinc (Zn) is a common constituent found in contaminated soils, sediments, and wastewater and groundwater streams. Unlike for lead (Dyer et al., 2002b), a reasonable blend of edge and isotherm data was found in the peer-reviewed literature for Zn sorption onto various forms of HFO. Many of the studies report pH edge data only (Gadde and Laitinen, 1974; Kinniburgh et al., 1976; Leckie et al., 1980; Benjamin and Bloom, 1981; Benjamin, 1983; Schultz et al., 1987; Crawford et al., 1993; Misak et al., 1996); however, a fair number of studies present both isotherm and edge data (Kinniburgh et al., 1977; Benjamin, 1979; Dempsey and Singer, 1980; Kinniburgh and Jackson, 1982; Harvey and Linton, 1984; Kanungo, 1994; Trivedi and Axe, 2000). Benjamin (1979) published a pH-6.4 isotherm spanning 3 orders of magnitude in Zn concentration, while Kinniburgh and Jackson's (1982) isotherm data cover 4 log units in Zn concentration at pH 5.5 and 6.5. Harvey and Linton (1984) provide isotherms at pH 6.25, 6.5, 6.75, 7.0, and 7.25 covering 3-3.5 orders of magnitude in Zn concentration. Trivedi and Axe (2000) present isotherms at pH 6, 7, and 8 that span 3-4 log units in Zn concentration. The three remaining isotherm data sets (Kinniburgh et al., 1977; Dempsey and Singer, 1980; Kanungo, 1994) cover only 1-2 orders of magnitude in Zn concentration. Dzombak and Morel (1990) used a blend of Zn edges and isotherms to determine the best-fit surface complexation constants for both Type 1 and Type 2 sites. Preferred data sets included Kinniburgh et al. (1977), Benjamin (1979), Dempsey and Singer (1980), Leckie et al. (1980), and Kinniburgh and Jackson (1982). Surface precipitation reactions were included by

Dzombak and Morel (1990) in the GTLM only to fit the pH-6.5 isotherm data from Kinniburgh and Jackson (1982) at high surface loading. Otherwise, only adsorption reactions were required to fit the data. None of these studies, however, benefited from spectroscopic analyses of the sorbent surface to help confirm surface speciation. In addition, while the collective data set for Zn sorption onto HFO is more impressive than for lead (Pb), the fact remains that the studies were performed by different researchers in different labs under different conditions.

Chapters 1 and 3 provide more detailed discussion on the evolution of surface complexation modeling as it pertains to justifying this specific research project. In short, an in-depth literature review highlighted only a few studies where molecular- and macroscopic-scale data have been coupled with surface complexation model development to predict metal-cation sorption over a wide range of conditions (Hayes, 1987; Brown et al., 1998; Katz and Boyle-Wight, 2001). None were found for Zn sorption onto HFO/ferrihydrite. Appendix E and Trivedi et al. (2002b) present comprehensive single-solute macroscopic and spectroscopic data for Zn sorption onto 2-line ferrihydrite. This chapter will highlight the insights that come from integrating spectroscopic data on surface speciation with macroscopic isotherm and pH sorption edge data covering a wide range of conditions. In addition, it will point to potential limitations in using existing SCMs to determine an optimal set of surface complexation modeling parameters for single-solute Zn sorption onto 2-line ferrihydrite.

6.3 Methods

6.3.1 Potentiometric Titration and Zn Sorption Data

Modeling studies were based on macroscopic and spectroscopic data for single-solute Zn sorption onto 2-line ferrihydrite (N_2 atmosphere, room temperature, and 4-hour equilibration time) that are reported in Appendix E and discussed in Trivedi et al. (2002b). In addition, Appendix A and Trivedi et al. (2002a) report potentiometric titration data for 2-line ferrihydrite in 0.001, 0.01, and 0.1 M $NaNO_3$ solutions (N_2 atmosphere and room temperature). Analysis of the potentiometric titration data is described in Chapter 3 and Dyer et al. (2002b).

6.3.2 Geochemical Modeling Software

The OLI Software (OLI Systems, Inc., Morris Plains, NJ) was used to perform the simulations in this study. Details on the thermodynamic databank and framework, the equation solvers, and the SCMs used in the OLI Software are presented in Chapter 2 and Dyer et al. (2002b). More specifically, the ElectroChem solver was used in this study because it performs single-point aqueous equilibrium calculations at steady state (Sanders et al., 1988).

6.3.3 Surface Complexation Models

Four different surface complexation models are available in the OLI Software—the nonelectrostatic model (NEM), the constant capacitance model (CCM), the GTLM, and the modified triple-layer model (TLM). In this study, the modified TLM was employed, having provided best fits of the Pb/ferrihydrite isotherm and pH-edge data presented and analyzed in Chapter 3 as well as Trivedi et al. (2002a) and

Dyer et al. (2002b). The thermodynamic framework for the modified TLM is described in Sahai and Sverjensky (1998).

6.3.4 Modeling Protocol

Hayes and Katz (1996) served as a basis for the modeling protocol used in this study. First, the OLI Software's nonlinear regression routine was used to determine a valid set(s) of metal hydroxide surface parameters for the modified TLM using potentiometric titration data for 2-line ferrihydrite at three different ionic strengths as reported in Appendix A and Trivedi et al. (2002a). Hayes and Katz (1996) showed that various combinations of $N_{s,\,total}$, C_1, and ΔpK_a will provide adequate fits of potentiometric titration data for mineral oxides. As detailed in Chapter 3 and Dyer et al. (2002b), a 3-factor, face-centered-cube (FCC), response-surface experimental design was previously used to determine the values of $N_{s,\,total}$, C_1, and ΔpK_a that provide the best fit of the titration data (A_s and C_2 were held constant in the model). The criterion for judging the quality of fit was the value of R_{avg} obtained from the OLI code's nonlinear regression program, in addition to visual inspection of a plot of the model titration curves with the actual data. For each experimental data point, the nonlinear regression program calculates the ratio of the experimental value to the model-calculated value (or vice versa), such that R is always ≥ 1.0. A perfect fit is defined as R equal to 1.0. R_{avg} represents the arithmetic average of the R-values for all the data points comprising a set of regressed titration data. Dyer et al. (2002b) found that the quality of the fit was largely determined by the value of C_1 and, to a lesser extent, by ΔpK_a. The impact of $N_{s,\,total}$ was very small. Based on these results, the values of C_1 and ΔpK_a (as well as A_s and C_2) were fixed at the same values as those used in the Pb/ferrihydrite modeling studies summarized in Chapter 3 and Dyer

et al. (2002b). $N_{s,\,total}$ was initially set at 0.8 moles sites/mole Fe based on the Pb /ferrihydrite modeling results. If $N_{s,\,total}$ had to be adjusted to fit the Zn isotherm data, then the potentiometric titration data was re-regressed using the new value of $N_{s,\,total}$.

Next, spectroscopic results and the impact of ionic strength on Zn sorption were used to guide the selection of the Zn surface complexation reactions at low to moderate surface coverage. Hayes and Katz (1996) note that past x-ray absorption fine structure spectroscopy (XAFS) studies have suggested that mononuclear species predominate at low to moderate surface coverage (0.1 to 10%) for strongly sorbing metals and at all coverages for weakly sorbing metals. Ionic-strength dependence has also been used historically to infer the presence of inner- versus outer-sphere surface complexes (Sparks, 1995). In this study, pH edges generated at 3 different ionic strengths were used to assess the ionic-strength dependence of Zn sorption. Spectroscopic results are summarized in Trivedi et al. (2002b).

Spectroscopic results and the shape of the constant-pH equilibrium isotherms were used to determine the need for multinuclear surface complexation reactions at higher surface coverage (i.e., surface polymers and/or surface precipitates). The constant-pH isotherms were also used to determine a reasonable starting point for site density and to assess the possibility of site heterogeneity (i.e., the need for more than one site type). Robertson and Leckie (1997) found that site heterogeneity is likely if the slope of a constant-pH isotherm curve is less than 1.0 at low surface coverage.

Based on the above analyses of the macroscopic and spectroscopic data, an appropriate set of oxide surface-parameters ($N_{s,\,total}$, C_1, C_2, ΔpK_a, and A_s) and Zn surface complex species were assumed for the TLM. These surface parameters/species were used to regress the constant-pH isotherm data to obtain a set

of best-fit equilibrium constants for single-solute Zn sorption. The best-fit Ks were then used to assess how the model predicted the pH edge data at multiple ionic strengths and initial Zn concentrations. Various combinations of viable Zn surface complexes were considered to evaluate the sensitivity of the model fits to the speciation assumptions. The minimum numbers of site and species types that provided the best fit of the isotherm and pH edge data were considered the optimum. Again, R_{avg} values for both the *x* [total Zn (aq)] and *y* [moles Zn/mole Fe] data from the nonlinear regression program, together with visual inspection of graphical output, were used to judge the quality of the fits. This step was an iterative process, whereby the oxide surface parameters were adjusted if $N_{s,\,total}$ was altered.

6.3.5 Uncertainty Analysis

Screening simulations using ElectroChem's uncertainty analysis module for one-stage, single-solute Zn sorption onto ferrihydrite over a wide range of conditions identified which input and thermodynamic parameters determined the majority of the uncertainty in the output variables of interest—total Zn (aq) [Zn_{aq}] and Zn surface loading [Zn_{sorb}]. Table 6.1 summarizes these model input parameters and their corresponding uncertainty values. Input/thermodynamic uncertainties are reported as either absolute values (standard deviation, σ_i) or relative values (coefficient of variation, COV_i). The bases for the input-parameter uncertainty assumptions are described in detail in Chapter 5 and Dyer et al. (2002c). Based on the uncertainty assumptions in Table 6.1, ElectroChem's uncertainty analysis module and the Resampling Stats for Windows software (Resampling Stats, Inc., Arlington, Virginia) were then utilized to estimate 95% confidence intervals for the constant-pH-

Table 6.1 Input/thermodynamic parameters and corresponding uncertainty assumptions.[a]

Parameter	Standard Deviation (σ_i)	Coefficient of Variation (COV_i)[b]
Total Zn		0.02
Total Ferrihydrite		0.10
Total H_2O		0.03
Total $NaNO_3$		0.10
pH	0.03 pH units	
log K^{int}_{NO3-}	0.36 log units	
log K^{int}_{Na+}	0.36 log units	
log $K^{int}_{(\equiv FeO)_2Zn}$	0.12 log units	

[a] Refer to Tables 6.2 and 6.3 for details on the chemical reactions and mass-law expressions corresponding to each of the equilibrium constants given above. Definitions for each of the parameters can be found in the nomenclature section.
[b] $COV_i = \sigma_{Yi}/Y_i$.

isotherm and pH-sorption-edge model predictions. Details on the Monte Carlo simulation methodology used to generate these confidence intervals can be found in Chapter 5 and Dyer et al. (2002c). ElectroChem's uncertainty analysis module also provides quantitative results on the fraction of the total output uncertainty that is attributable to specific input variables. These results were also analyzed to identify the input variables that had a dominant influence on the output uncertainty in Zn_{aq} and Zn_{sorb}.

6.4 Results and Discussion

6.4.1 Potentiometric Titration Data

The point of zero net proton charge (PZNPC) for 2-line ferrihydrite was determined to be 7.91 as reported previously (Dyer et al., 2002b; Trivedi et al. 2002a). This falls within the range of point of zero charge values reported by others (Dzombak and Morel, 1990). Detailed results of the 3-factor, FCC, response-surface experimental design are reported in Chapter 3 and Dyer et al. (2002b). Figure 6.1 provides the best fit of the potentiometric titration data using the TLM. As discussed below, the density of proton-active sites ($N_{s,\,total}$) was increased from 0.8 moles sites/mole Fe (the value used in the Pb/ferrihydrite studies) to 1.2 moles sites/mole Fe in order to fit the pH-7.5 Zn isotherm data at maximum loading using a bidentate-mononuclear surface complex. Model parameters corresponding to this fit are given in Table 6.2, along with the value of R_{avg} from the nonlinear regression. A discussion of the discrepancies between the experimental data and model predictions is given in Chapter 3 and Dyer et al. (2002b).

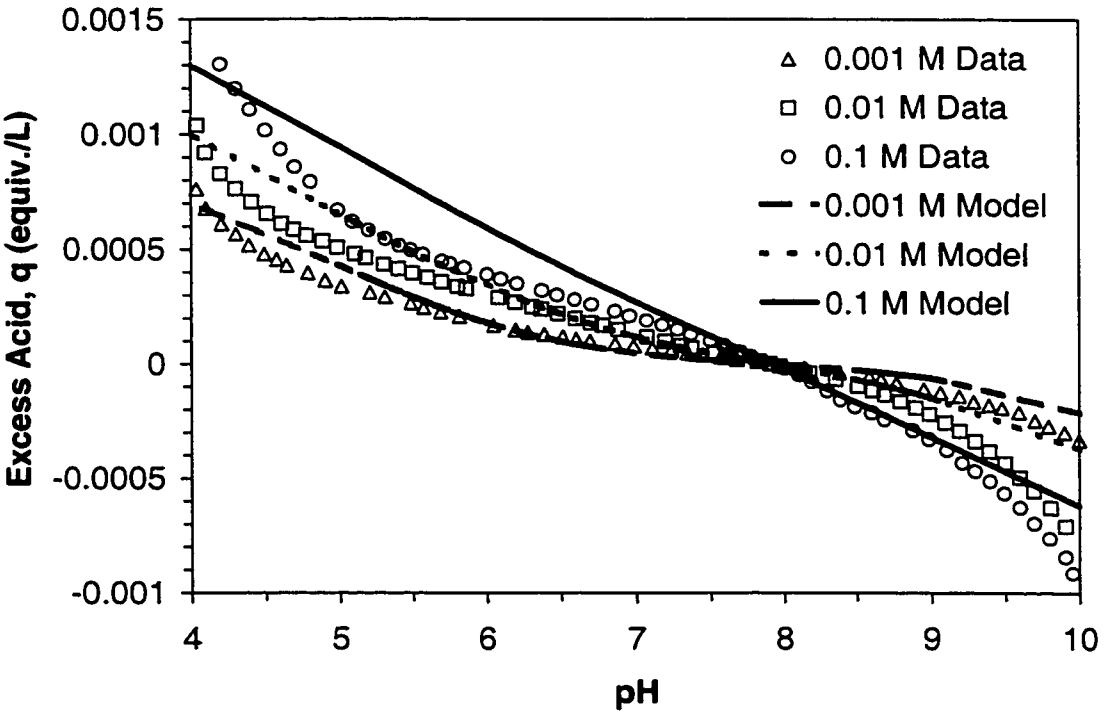

Figure 6.1 **Best fit of potentiometric titration data for 2-line ferrihydrite using the modified triple-layer model. Experimental conditions: 1 g ferrihydrite/L; 0.001, 0.01, and 0.1 M $NaNO_3$ electrolyte solutions; room temperature; N_2 glovebox; 1 L reactor; 2-minute equilibration time at each pH point; 0.1 M NaOH used to raise initial pH to ~ 10; 0.1 M HNO_3 used to titrate mixture downward to ~ pH 4.**

Table 6.2 Best-fit oxide surface parameters for the TLM based on regression of potentiometric titration data for 2-line ferrihydrite at room temperature in a N_2 atmosphere.

Parameter	Value
$N_{s,\,total}$ (mol /mol)	1.2
A_s (m^2/g)	600
C_1 (F/m^2)	1.0
C_2 (F/m^2)	0.2
log $K_{a1}^{int\,a}$	-5.56
log $K_{a2}^{int\,b}$	-10.26
log $K_{NO3-}^{int\,c}$	-7.154
log $K_{Na+}^{int\,d}$	8.69
R_{avg}	1.3

[a] $\equiv FeOH_2^+ = \equiv FeOH + H^+$, where
$K_{a1}^{int} = a_{H+}[\equiv FeOH]\exp(-F\Psi_o/RT)/[\equiv FeOH_2^+]$.

[b] $\equiv FeOH = \equiv FeO^- + H^+$, where
$K_{a2}^{int} = a_{H+}[\equiv FeO^-]\exp(-F\Psi_o/RT)/[\equiv FeOH]$.

[c] $\equiv FeOH_2^+ - NO_3^- = \equiv FeOH + H^+ + NO_3^-$, where
$K_{NO3-}^{int} = a_{H+}a_{NO3-}[\equiv FeOH]\exp(F(\Psi_\beta - \Psi_o)/RT)/[\equiv FeOH_2^+ - NO_3^-]$.

[d] $\equiv FeO^- - Na^+ + H^+ = \equiv FeOH + Na^+$, where
$K_{Na+}^{int} = a_{Na+}[\equiv FeOH]\exp(F(\Psi_o - \Psi_\beta)/RT)/a_{H+}[\equiv FeO^- - Na^+]$.

6.4.2 Zn Sorption Isotherms and Edges

Analysis of macroscopic and spectroscopic data from Trivedi et al. (2002b) for Zn sorption onto 2-line ferrihydrite provided several insights to help focus the SCM development. First, pH edge data for 50 μM Zn equilibrated with 1 g ferrihydrite/L in 0.001, 0.01, and 0.1 M $NaNO_3$ solutions showed only a small ionic-strength dependence, indicating the likelihood of inner-sphere surface complexes. Second, the slopes of the constant-pH isotherms at low Zn concentrations were approximately 1.0, suggesting that a one-Zn-sorption-site model would be adequate. Third, the unequal spacing between the pH 4.5, 5.5, 6.5, and 7.5 isotherms (changing $d[pZn_{aq}]/d[pH]$ at a constant Zn surface loading) suggested that a unique set of equilibrium constants and/or surface species would not fit the entire data set. The spectroscopic results, however, gave no indication that a change in surface speciation was the reason for this significant change in spacing between the isotherms. Fourth, the maximum surface loading of Zn for each of the constant-pH isotherms changes with pH, suggesting that the TLM assumption for the site density of available Zn sorption sites needs to be adjusted with pH. As shown in Figure 6.2, maximum Zn sorption capacity on 2-line ferrihydrite is approximately 0.04, 0.13, 0.31, and 0.46 moles Zn/mole Fe at pH 4.5, 5.5, 6.5, and 7.5, respectively. As pH increases, the isotherm data clearly appear to plateau at higher surface loadings. This is in contrast to the Pb/ferrihydrite sorption data reported in Chapter 3 and Dyer et al. (2002b) where the pH 5.5 and 6.5 isotherm data appear to converge at the same maximum sorption capacity of 0.35-0.40 moles Pb/mole Fe. Fifth, the spectroscopic data analysis indicated that a bidentate-mononuclear inner-sphere surface complex dominated over the pH range 4.5 to 7.5 (Trivedi et al., 2002b). More specifically, XAFS (x-ray

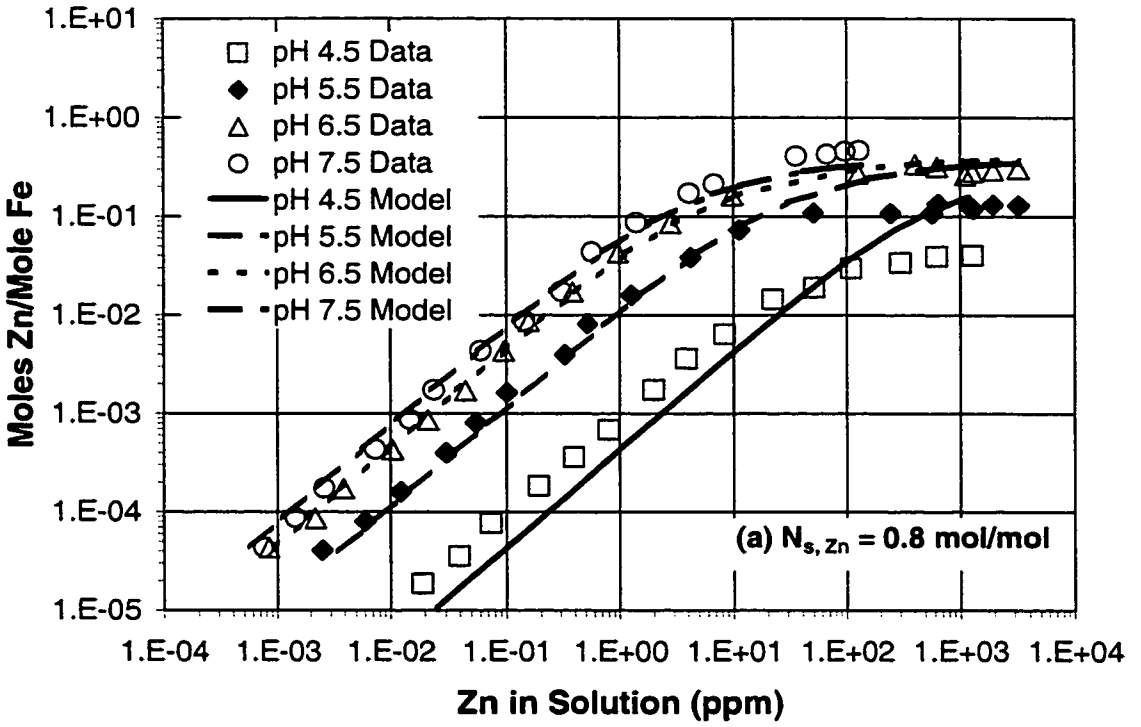

Figure 6.2 **Optimized triple-layer model fits of pH 4.5, 5.5, 6.5, and 7.5 equilibrium isotherm data for single-solute Zn sorption onto 2-line ferrihydrite using the bidentate-mononuclear surface complex, $(\equiv FeO)_2Zn$. In (a), $N_{s, Zn}$ was fixed at 0.8 moles sites/mole Fe; in (b), $N_{s, Zn}$ was varied with pH. Ninety-five percent confidence intervals for the model predictions are also shown in (b). Experimental conditions: 0.1 and 1.0 g ferrihydrite/L in 0.01 M $NaNO_3$ solution; Zn added as $Zn(NO_3)_2$; 4-hour equilibration time; room temperature; N_2 glovebox.**

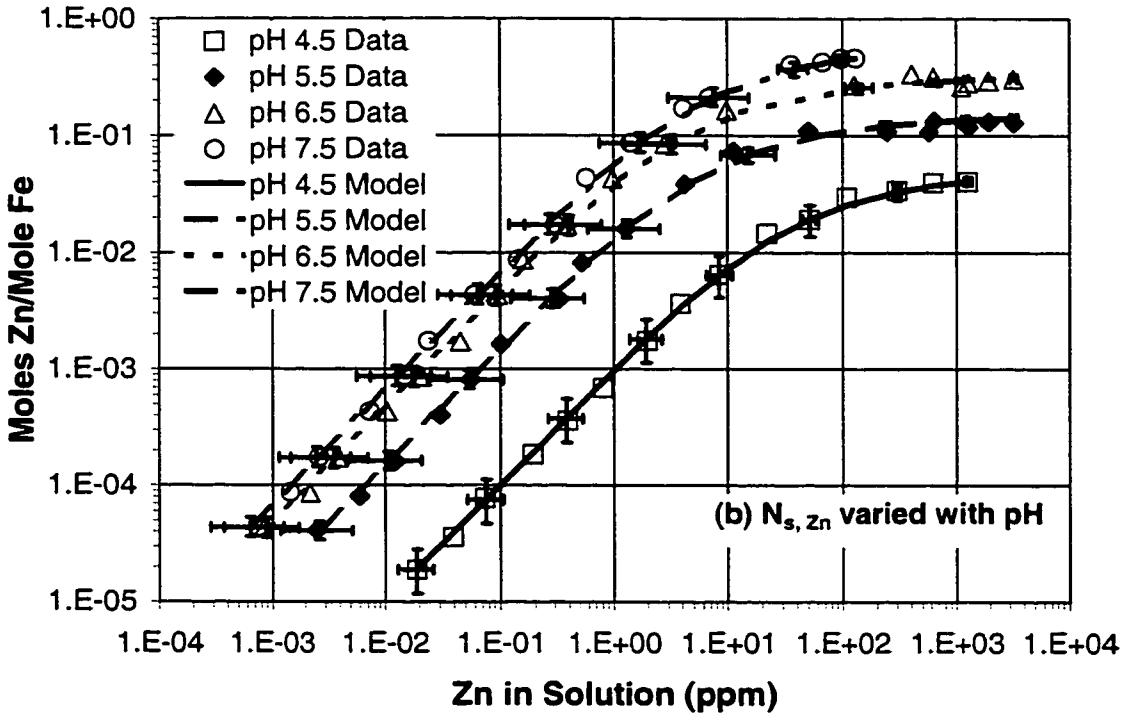

Figure 6.2 Continued.

absorption fine-structure spectroscopy) studies over the pH range 4.5 to 7.5 revealed a first shell (Zn–O) composed of four oxygen atoms at an average radial distance of 1.98 Å (i.e., tetrahedral coordination). These radial distances are much shorter than first-shell distances reported for fully hydrated Zn(II) ions, which suggests that Zn(II) ions do not retain their primary hydration sphere upon sorption onto ferrihydrite (i.e., an inner-sphere surface complex is formed). The second shell (Zn–Fe) was best fitted with two iron atoms at an average radial distance of 3.48 Å over the pH range 4.5 to 7.5. This fit was independent of Zn(II) concentration and is indicative of edge-sharing bidentate sorption. At pH $\geq$ 6.5 and approaching site saturation, however, a fit based on a Zn–Fe bond distance of 3.48 Å (CN = 1.4-1.8) and a Zn–Zn bond distance of 3.53 Å (CN = 0.17-0.31) was found to be a possible alternative. This suggests that a small contribution from multinuclear Zn complexes is possible at higher pH and Zn loadings.

The constant-pH isotherm data are shown in Figure 6.2, along with modified TLM fits obtained using the bidentate-mononuclear surface complex $(\equiv FeO)_2Zn$. In Figure 6.2a, the density of Zn-active sites ($N_{s,\,Zn}$) was fixed at 0.8 moles sites/mole Fe for all pH; in Figure 6.2b, the value of $N_{s,\,Zn}$ was adjusted with pH to properly capture the variable maximum Zn sorption capacity. In both cases, the nonlinear regression fits of the isotherm data are based on a total density of proton-active sites ($N_{s,\,total}$) of 1.2 moles sites/mole Fe. It is clear from Figure 6.2b that adjusting $N_{s,\,Zn}$ results in excellent fits of the Zn/ferrihydrite sorption data over 6 orders of magnitude in Zn concentration. Equilibrium constants, Zn-active site densities, associated equilibrium reactions and mass law expressions, and R_{avg} values for the preferred pH 4.5, 5.5, 6.5 and 7.5 isotherm fits (Figure 6.2b) are summarized in

Table 6.3. Equilibrium constants for the bidentate-mononuclear Zn surface complex are reported as conditional Ks (K_i), rather than as intrinsic Ks (K_i^{int}) because of the dependence on pH and site density. Regression of the isotherm data using multispecies and/or multi-Zn-sorption-site models (data not given) resulted in inferior fits when compared to the one-Zn-sorption-site bidentate-mononuclear model. Although not supported by spectroscopic data, the species ≡FeOZnOH provided essentially the same quality of fit as the bidentate-mononuclear surface complex (see Figure 6.3). Mathematically, the mass-law expression for ≡FeOZnOH looks very similar to the mass-law expression for $(\equiv FeO)_2Zn$.

To explore the issue of a "nonconstant" equilibrium constant further, pH sorption edge data were plotted with isotherm data on the same graph. Figure 6.4 shows very good agreement between the edge and isotherm data, indicating that the data are internally consistent. Interestingly, Figure 6.4 suggests that a reduction in spacing between the constant-pH isotherms should be expected based on the inherent shape of a pH sorption edge. More specifically, $d[pZn_{aq}]/d[pH]$ changes significantly over the course of a pH sorption edge. At low and high values of % Zn sorbed, the change in sorbed Zn and, hence, in total Zn_{aq} is relatively small for a unit change in pH (i.e., $d[pZn_{aq}]/d[pH]$ is small). However, over a narrow pH range, the change in sorbed Zn with pH increases substantially (i.e., $d[pZn_{aq}]/d[pH]$ is large). For Zn, the steep slope of the pH sorption edge occurs over the pH range 4.5 to 5.5 where $d[pZn_{aq}]/d[pH]$ peaks at about 1.3. By pH 6, however, the sorption edge has begun to plateau and $d[pZn_{aq}]/d[pH]$ is 0.5 or less. The constant-pH isotherm curves for pH 4, 5, 6, 7, and 8 shown in Figure 6.4 represent TLM fits to the pH edge data only. Oxide surface parameters and the assumed surface speciation were the same as those used to

Table 6.3 TLM parameters for single-solute Zn sorption onto 2-line ferrihydrite (fh) at room temperature in a N_2 atmosphere using a bidentate-mononuclear surface complex.

pH	$N_{s,Zn}$ (mol/mol)[a]	log $K_{(\equiv FeO)_2Zn}$ @ 1 g fh/L[b, c]	R_{avg} (Zn_{aq})[d]	R_{avg} (Γ)[d]
4.5	0.10	3.17	1.02	1.05
5.5	0.30	4.95	1.08	1.05
6.5	0.65	7.15	1.11	1.04
7.5	1.20	9.52	1.11	1.01
4.0	0.075	2.18	-	-
5.0	0.21	4.35	-	-
6.0	0.43	6.01	-	-
7.0	0.90	8.31	-	-
8.0	1.20	10.32	-	-

[a] $N_{s,total}$ set at 1.2 moles proton-active sites/mole Fe. [b] $(\equiv FeO)_2Zn + 2H^+ = 2\equiv FeOH + Zn^{2+}$, where $K_{(\equiv FeO)_2Zn} = a_{Zn2+}[\equiv FeOH]^2/a_{H+}^2\gamma_s[(\equiv FeO)_2Zn]$. A γ_s correction was used, whereby $\gamma_{(\equiv FeO)2Zn} = \gamma_{Zn++}$. [c] For bidentate-mononuclear surface complexes, K^{int} is actually a conditional K that depends on sorbent solids concentration (C_s) regardless. This peculiarity arises with multidentate complexes, because of the definition of the standard state for surface species in molality, rather than mole fraction. It can be shown that
$K^{int} = K^{cond}/B$, where $B = N_s$ (sites/m^2) x A_s (m^2/g) x C_s (g/L) / N_A (6.02×10^{23} sites/mole sites). Hence, $K_2^{cond}/K_1^{cond} = C_{s2}/C_{s1}$ for the bidentate-mononuclear reaction written here as a dissociation reaction. The bidentate-mononuclear Ks reported in the table are based on 1 g ferrihydrite/L. [d] R_{avg} reported for regressions of pH 4.5, 5.5, 6.5, and 7.5 isotherm data only. Ks for other pH values are approximate based on regression of a few pH edge points only. The intent is to show how K varies with pH.

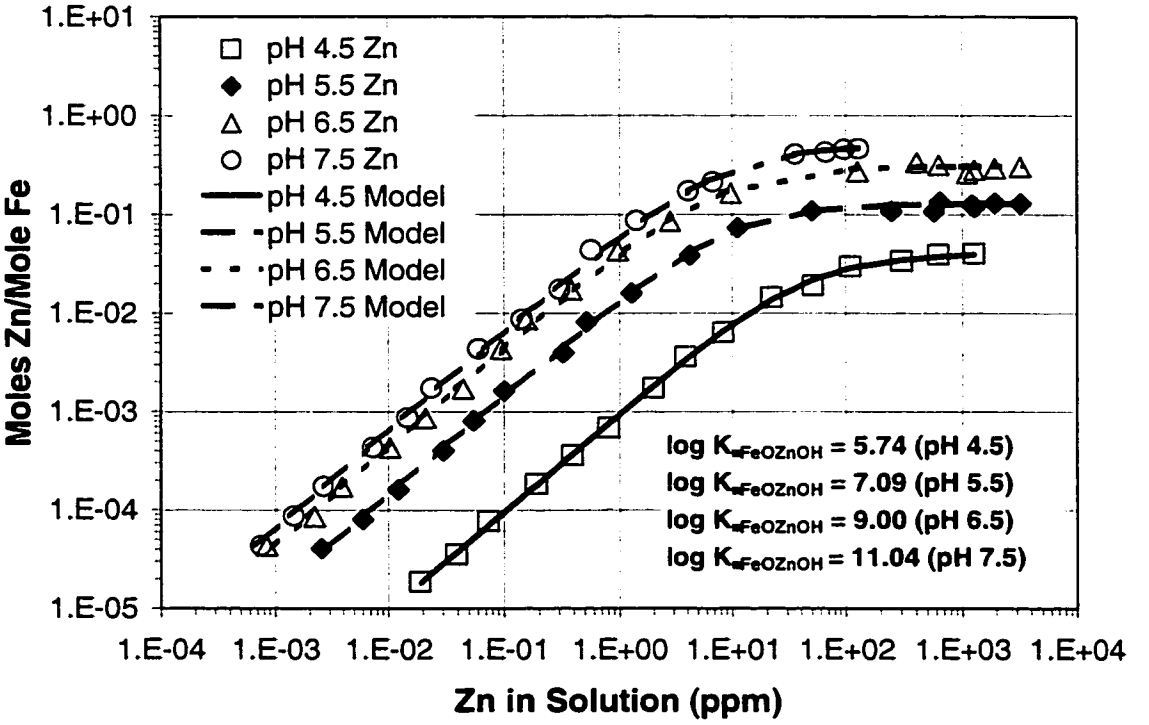

Figure 6.3 **Triple-layer model fits of pH 4.5, 5.5, 6.5, and 7.5 equilibrium isotherm data for single-solute Zn sorption onto 2-line ferrihydrite using the monodentate-mononuclear species, ≡FeOZnOH. Experimental conditions: 0.1 and 1.0 g ferrihydrite/L in 0.01 M $NaNO_3$; Zn added as $Zn(NO_3)_2$; 4-hour equilibration time; room temperature; N_2 glovebox. Surface activity coefficient correction ($\gamma_s=\gamma_{Zn2+}$) included in data regression. $N_{s,\,Zn}$ was varied with pH. Model parameters: $C_1 = 1.0$ F/m^2; $C_2 = 0.2$ F/m^2; $A_s = 600$ m^2/g; log $K_{a1}^{int} = -5.56$; log $K_{a2}^{int} = -10.26$; log $K_{NO3-}^{int} = -7.699$; log $K_{Na+}^{int} = 8.137$; $N_{s,\,total} = 0.50$ moles proton-active sites/mole Fe; $N_{s,\,Zn} = 0.04$, 0.13, 0.31, and 0.50 moles Zn-active sites/mole Fe at pH 4.5, 5.5, 6.5, and 7.5, respectively.**

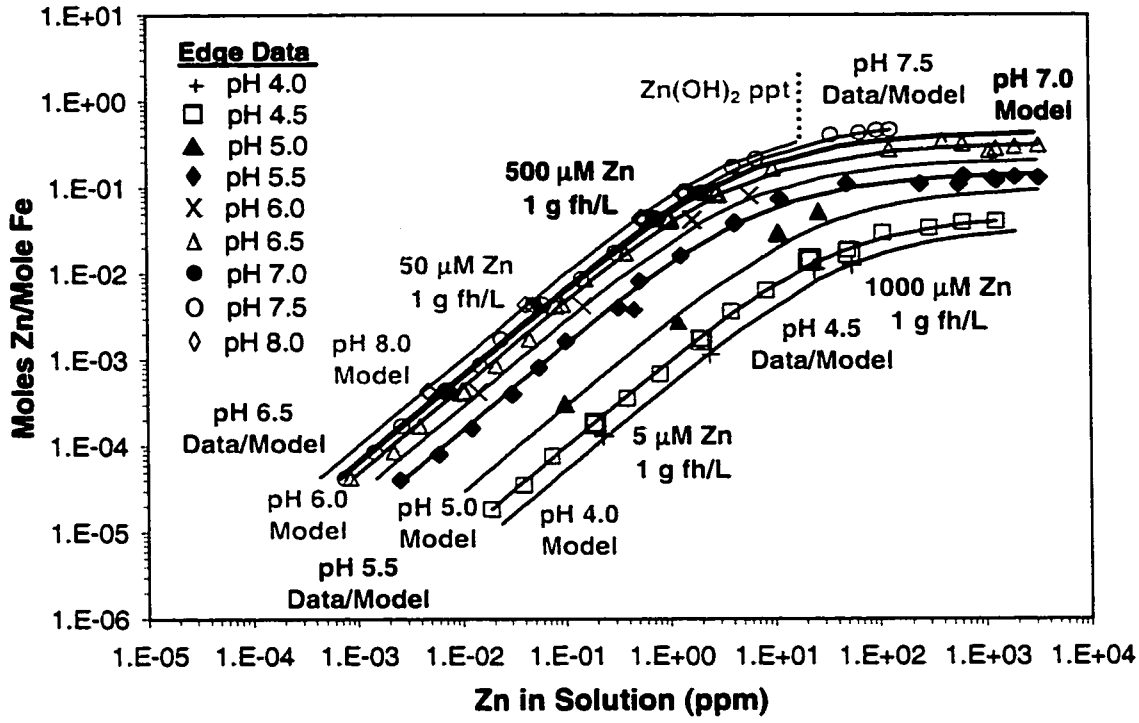

Figure 6.4 **Comparison of equilibrium isotherm and pH-edge data for single-solute Zn sorption onto 2-line ferrihydrite to modified triple-layer model predictions using the bidentate-mononuclear surface complex, $(\equiv FeO)_2Zn$. Experimental conditions: 0.1 and 1.0 g ferrihydrite/L; 0.01 M $NaNO_3$ background electrolyte for isotherms and edges; Zn added as $Zn(NO_3)_2$; 4-hour equilibration time; room temperature; N_2 glovebox.**

regress the pH 4.5, 5.5, 6.5, and 7.5 data. Equilibrium constants for the bidentate-mononuclear Zn surface complex and estimated values for $N_{s,Zn}$ for each of these fits are reported in Table 6.3.

Figure 6.5 compares TLM predictions for the bidentate-mononuclear Zn surface complex to pH edge data presented in Appendix E and Trivedi et al. (2002b). Figure 6.5a displays model predictions for 50 μM Zn, 1 g ferrihydrite/L, and 0.001, 0.01, and 0.1 M $NaNO_3$ using (1) the best-fit equilibrium constant and Zn-active site density for the pH 5.5 isotherm data only, and (2) aqueous activity coefficient corrections for bulk solution ions only (i.e., the ratio of the surface activity coefficients is assumed to equal 1.0 (Sahai and Sverjensky, 1998)). Note that the model significantly underpredicts Zn sorption at pH < 5.0. Although not obvious in the figure, the model also overpredicts Zn sorption at pH ≥ 6. In addition, Figure 6.5a shows that model curves display a much stronger ionic-strength dependence than suggested by the 0.1 M $NaNO_3$ data. This is an artifact of the modified TLM thermodynamic framework itself. First, bulk solution concentrations and activity coefficients for the sorbing ions (i.e., H^+, NO_3^-, Na^+, and Zn^{2+}) are used in the mass law expressions (because we know how to measure and estimate them, respectively), rather than true surface species activities themselves (Robertson and Leckie, 1997). Second, lacking a way to directly determine the activity of a surface complex as well as a predictive model for estimating surface activity coefficients, the ratio of the activity coefficients for the surface species (i.e., $(\equiv FeO)_2Zn$ and $\equiv FeOH$) is assumed to equal 1.0. In essence, this represents only a "partial correction" for nonidealities at the surface. To correct for the overprediction of the ionic-strength dependence, a surface activity coefficient term (γ_s) was introduced to the OLI model to better match the pH

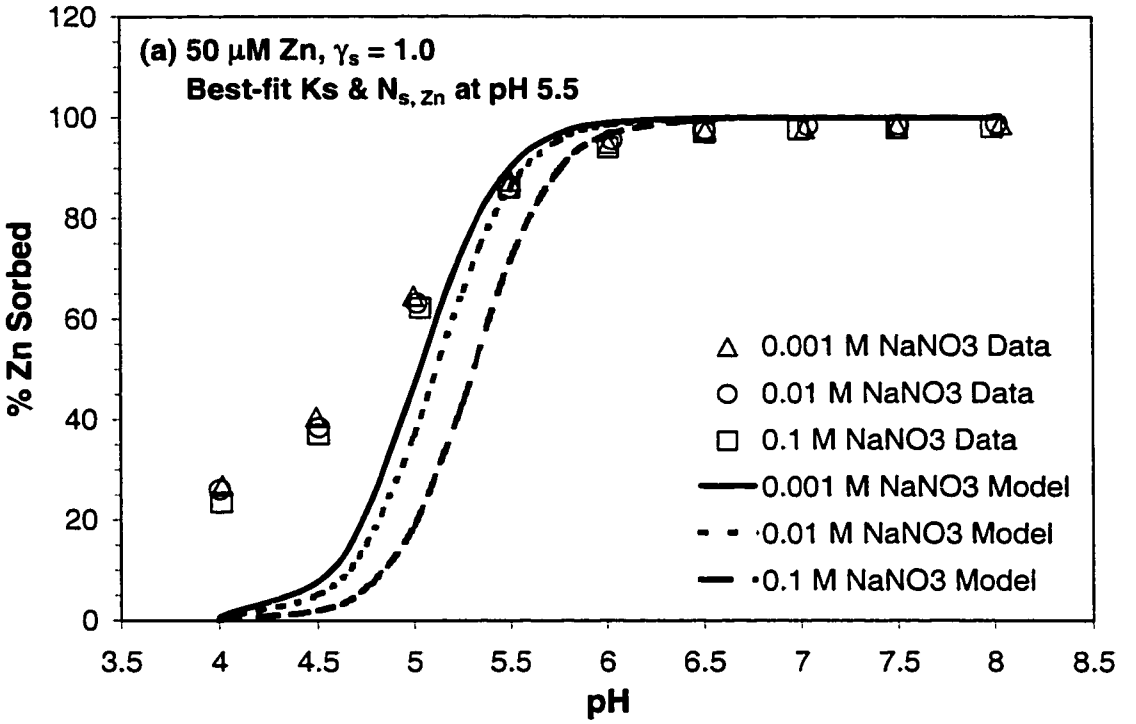

Figure 6.5 **Triple-layer model predictions of pH sorption edge data for single-solute Zn sorption onto 2-line ferrihydrite using the bidentate-mononuclear surface complex, $(\equiv FeO)_2Zn$. Plots for (a) 50 μM Zn in 0.001-0.1 M $NaNO_3$ using the best-fit K and $N_{s,Zn}$ for pH 5.5 isotherm data only and assuming $\gamma_s = 1.0$; (b) 50 μM Zn in 0.001-0.1 M $NaNO_3$ using pH-adjusted Ks and $N_{s,Zn}$ values from Table 6.3 and $\gamma_s=\gamma_{Zn2+}$ correction; (c) 5, 500, and 1000 μM Zn in 0.01 M $NaNO_3$ using pH-adjusted Ks and $N_{s,Zn}$ values from Table 6.3 and $\gamma_s=\gamma_{Zn2+}$ correction. Ninety-five percent confidence intervals for the model predictions are also shown in (b) and (c). Experimental conditions: 1.0 g ferrihydrite/L; Zn added as $Zn(NO_3)_2$; 4-hour equilibration time; room temperature; N_2 glovebox.**

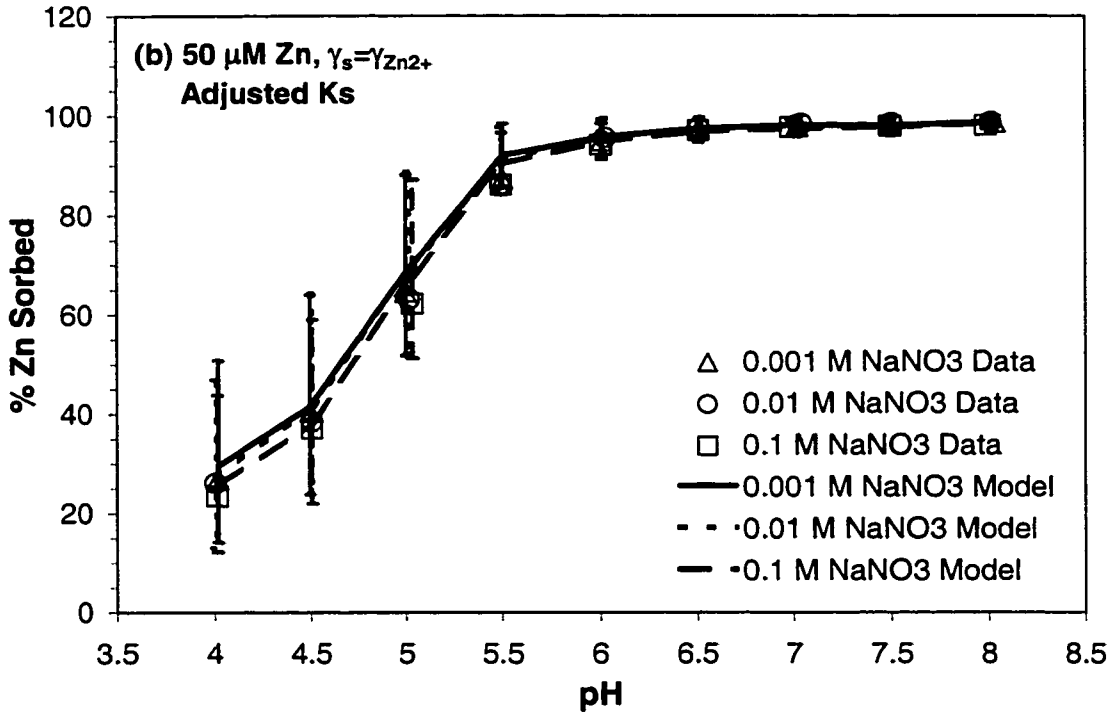

Figure 6.5 Continued.

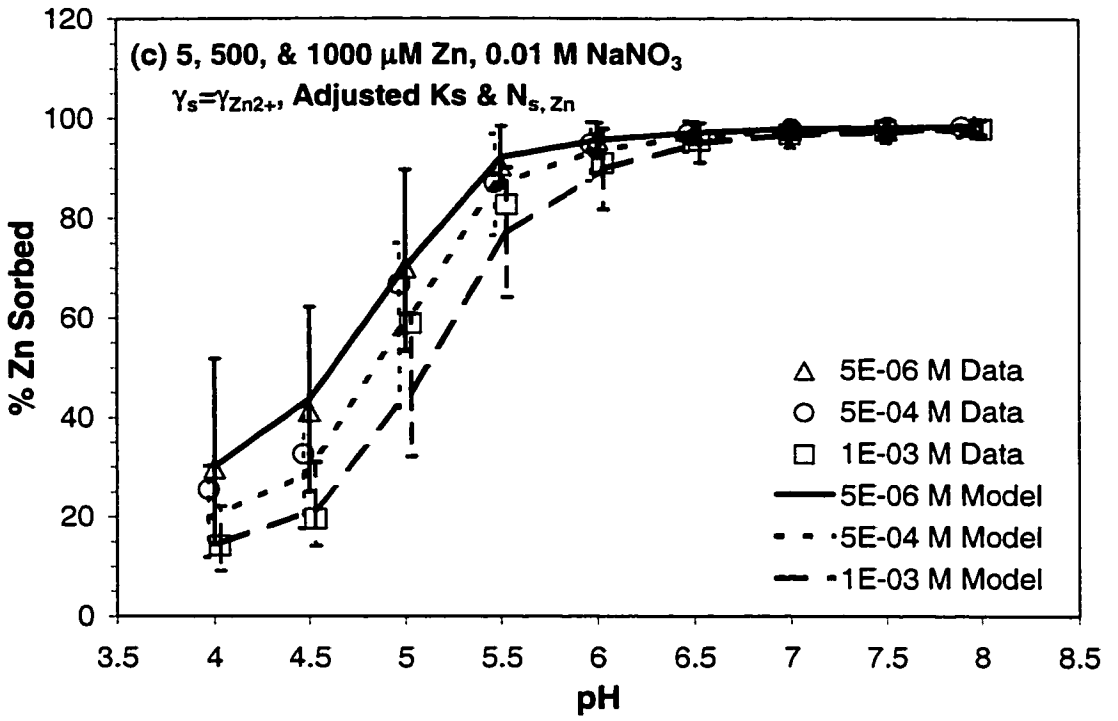

Figure 6.5 Continued.

edge data. Interestingly, the best agreement between the predicted curves and the actual data was obtained when γ_s was set equal to γ_{Zn2+}, the bulk solution activity coefficient for the Zn^{2+} ion. This was also found to be true for the Pb/ferrihydrite system (Dyer et al., 2002b). The γ_s term was used during regression of the constant-pH isotherm data shown in Figures 6.2 and 6.4; therefore, the equilibrium constants given in Table 6.3 include this correction.

Figures 6.5b and 6.5c display TLM predictions for the bidentate-mononuclear surface complex when pH-adjusted Ks and site densities ($N_{s,\,Zn}$) are used in addition to the γ_s correction. Note the good agreement between the model curves and the actual data. The better fit at pH < 4.5 was accomplished without introducing a second, high-affinity site type for Zn or additional surface species as has often been done in past modeling studies that are based on pH edge data only. Although not shown, introducing a second, high-affinity site for Zn to account for elevated Zn sorption at pH < 4.5 resulted in unacceptable fits of the isotherm data at low Zn concentrations. Instead, when considered together, the isotherm and edge data suggest that a one-Zn-sorption-site, one-species model is sufficient.

The downside of this investigation is that the best-fit equilibrium constants and site densities appear to be functions of pH as the TLM is currently constructed. Interestingly, Figure 6.6 shows that there is a linear relationship between log $K_{(\equiv FeO)2Zn}$ and pH. The same was found to be true for model regressions using the surface complex, ≡FeOZnOH (Figure 6.7). The reason for this linear relationship is not totally understood at the present time; however, it does provide a useful engineering tool to estimate the conditional equilibrium constant for the bidentate-mononuclear complex.

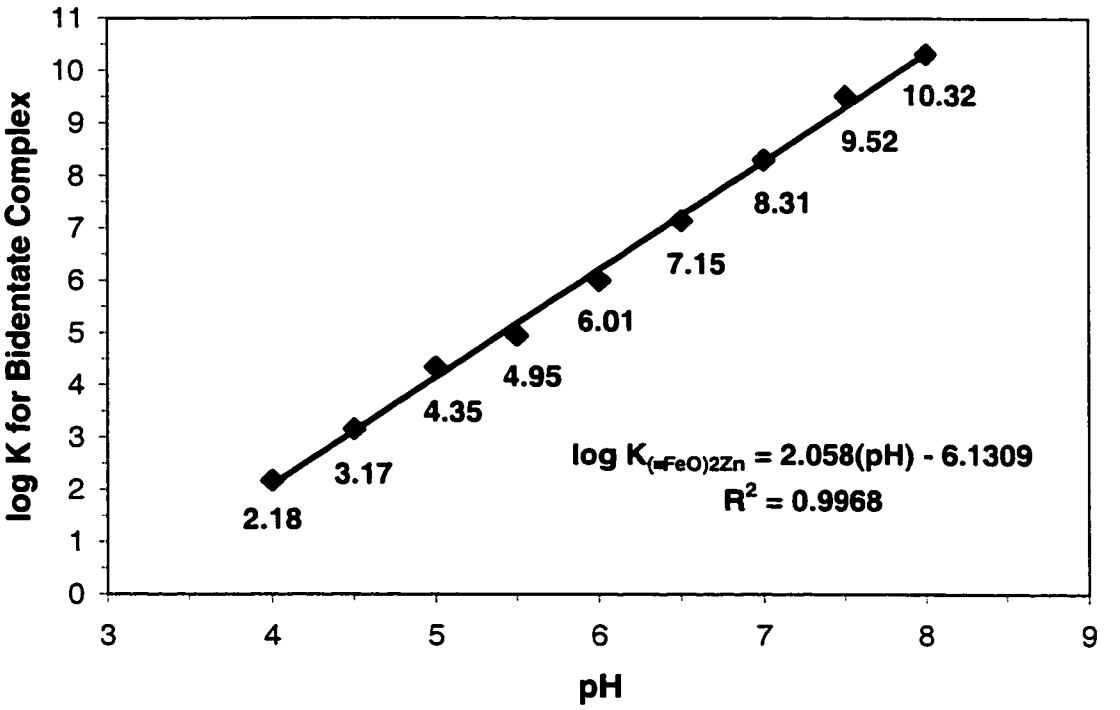

Figure 6.6 **Linear relationship between log K (@ 1 g ferrihydrite/L) and pH for the bidentate-mononuclear Zn surface complex, $(\equiv FeO)_2Zn$. Experimental conditions: 1.0 g ferrihydrite/L; Zn added as $Zn(NO_3)_2$; 4-hour equilibration time; room temperature; N_2 glovebox.**

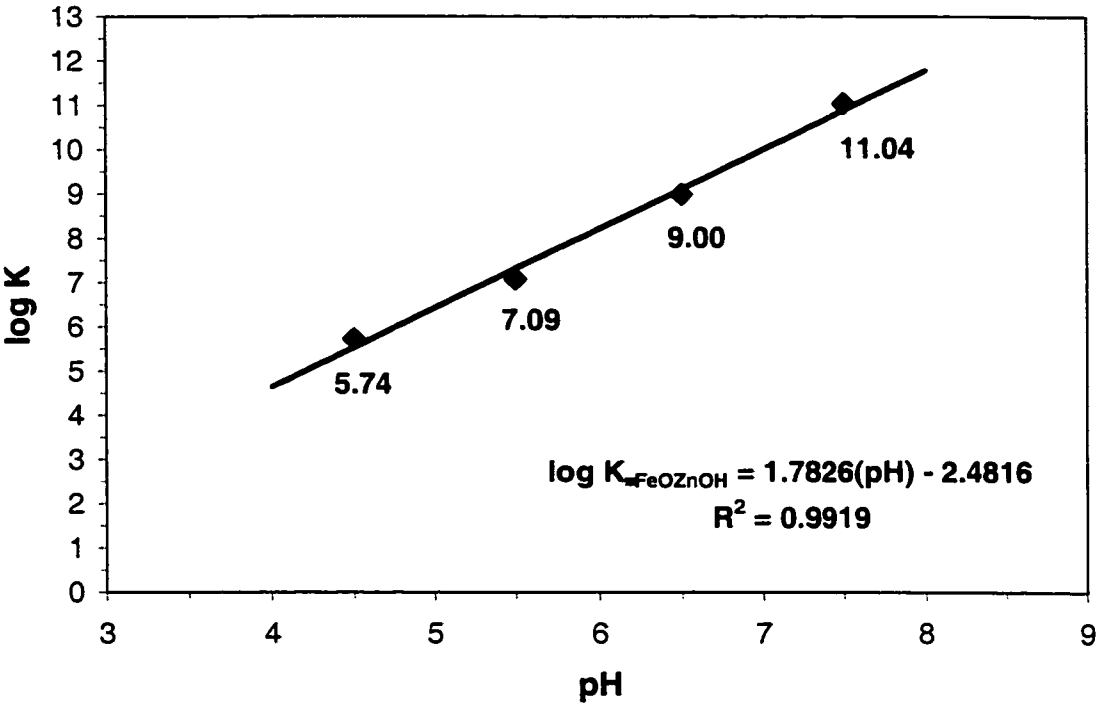

Figure 6.7 **Linear relationship between log K and pH for the monodentate-mononuclear Zn surface complex, ≡FeOZnOH. Experimental conditions: 1.0 g ferrihydrite/L; Zn added as $Zn(NO_3)_2$; 4-hour equilibration time; room temperature; N_2 glovebox.**

6.4.3 Uncertainty in Isotherm and pH-Edge Data

Uncertainty bars (95% confidence intervals) for the constant-pH-isotherm model predictions are shown in Figure 6.2b. Uncertainty bars are not shown for every data point for clarity. The experimental data points fall comfortably within the uncertainty bars in all cases. As shown in the figure, the uncertainty ranges for Zn_{aq} tend to be much wider than those for Zn_{sorb}, especially at pH 5.5 and above.
For select isotherm data points, Tables 6.4 and 6.5 show the fraction of the total output uncertainty in Zn_{aq} and Zn_{sorb}, respectively, that is attributable to specific input/thermodynamic parameters. The values in the tables for each input/thermodynamic parameter represent the fraction of the output COV squared (Dyer et al., 2002c). As shown in Table 6.4, at Zn surface loadings lower than those approaching site saturation, uncertainties in log $K^{int}_{(\equiv FeO)_2Zn}$ and, to a lesser degree, total ferrihydrite dominate the output uncertainty in Zn_{aq} for all pH. As surface loading increases, the relative importance of total ferrihydrite increases relative to log $K^{int}_{(\equiv FeO)_2Zn}$. On the other hand, as site saturation is approached, uncertainties in total H_2O, total Zn, and, at higher pH, total ferrihydrite dominate the uncertainty in Zn_{aq}.
For sorbed Zn, Table 6.5 shows that the uncertainty in total ferrihydrite dominates the output uncertainty in Zn_{sorb} at pH 5.5 and above, except near site saturation where log $K^{int}_{(\equiv FeO)_2Zn}$ and, to a lesser extent, pH dominate the output uncertainty. At pH 4.5, on the other hand, uncertainties in log $K^{int}_{(\equiv FeO)_2Zn}$ and, to a lesser extent, log $K^{int}_{NO3^-}$ and pH dominate the uncertainty in Zn_{sorb}. Input/thermodynamic parameters listed in Table 6.1, but not shown in Tables 6.4 and 6.5, had a negligible impact on the output uncertainty under all conditions.

Figures 6.5b and 6.5c display the uncertainty bars (95% confidence

Table 6.4 **Input/thermodynamic parameters dominating output uncertainty in Zn_{aq} (ppm) for the Zn/ferrihydrite constant-pH isotherms shown in Figure 6.2b (1 g ferrihydrite/L except where noted).**

pH	Zn Total (M)	Fraction of Output COV Squared for Zn_{aq}					
		Total H_2O	Total Zn	Total Ferri-hydrite	pH	log $K^{int}_{(\equiv FeO)_2Zn}$	log K^{int}_{NO3-}
4.5	2E-02	**0.68**	**0.32**	–	–	–	–
	1E-03	0.13	0.13	**0.31**	0.06	**0.30**	0.07
	2E-04	–	0.03	**0.26**	0.09	**0.51**	0.11
	2E-06	–	0.01	**0.22**	0.11	**0.55**	0.11
5.5	2E-02	**0.62**	**0.33**	0.05	–	–	–
	1E-03	–	0.02	**0.50**	0.07	**0.38**	0.03
	2E-04	–	–	**0.28**	0.11	**0.57**	0.03
	2E-06	–	–	**0.24**	0.12	**0.61**	0.03
6.5	2E-02	**0.46**	**0.30**	**0.23**	–	–	–
	1E-03	–	–	**0.37**	0.10	**0.52**	–
	2E-04	–	–	**0.26**	0.12	**0.61**	–
	2E-06	–	–	**0.24**	0.12	**0.63**	–
7.5	2E-03 (0.1 g/L)	**0.25**	**0.22**	**0.45**	–	0.08	–
	1E-03	–	–	**0.31**	0.11	**0.58**	–
	2E-04	–	–	**0.26**	0.11	**0.62**	–
	2E-06	–	–	**0.25**	0.11	**0.63**	–

Table 6.5 **Input/thermodynamic parameters dominating output uncertainty in Zn_{sorb} (mol Zn/mol Fe) for the Zn/ferrihydrite constant-pH isotherms shown in Figure 6.2b (1 g ferrihydrite/L except where noted).**

pH	Zn Total (M)	Fraction of Output COV Squared for Zn_{sorb}					
		Total H_2O	Total Zn	Total Ferri-hydrite	pH	log $K^{int}_{(\equiv FeO)_2Zn}$	log K^{int}_{NO3-}
4.5	2E-02	0.02	–	0.06	0.11	**0.59**	**0.22**
	1E-03	0.02	–	0.03	0.13	**0.66**	0.15
	2E-04	0.02	–	0.01	0.13	**0.68**	0.14
	2E-06	0.02	–	–	0.13	**0.69**	0.14
5.5	2E-02	0.02	–	0.06	0.13	**0.67**	0.12
	1E-03	0.02	0.04	**0.27**	0.10	**0.53**	0.04
	2E-04	–	0.05	**0.79**	0.02	0.13	–
	2E-06	–	0.05	**0.85**	0.02	0.08	–
6.5	2E-02	0.02	–	0.05	0.14	**0.74**	0.05
	1E-03	–	0.05	**0.92**	–	0.03	–
	2E-04	–	0.04	**0.95**	–	0.01	–
	2E-06	–	0.04	**0.95**	–	–	–
7.5	2E-03 (0.1 g/L)	0.03	–	0.03	0.14	**0.79**	–
	1E-03	–	0.04	**0.95**	–	–	–
	2E-04	–	0.04	**0.95**	–	–	–
	2E-06	–	0.04	**0.95**	–	–	–

intervals) for six TLM-predicted pH sorption edges for single-solute Zn sorption onto ferrihydrite. Once again, the experimental data fall well within the uncertainty bars for the model predictions. Note the large uncertainty in percent Zn sorbed over most of the pH range of the edges. This reinforces the point that regression of pH sorption edge data alone is not a sufficient test of the predictive capability of the SCM. Regression of constant-pH isotherm data at multiple pH values, together with pH edge data at several ionic strengths and metal/sorbent molar ratios, is a necessary approach.

For select pH edge points, Table 6.6 shows the fraction of the total output uncertainty in % Zn_{sorb} that is attributable to specific input/thermodynamic parameters. For Zn surface loadings less than those approaching site saturation, uncertainties in log $K^{int}_{(\equiv FeO)_2Zn}$ and, to a lesser degree, total ferrihydrite and pH dominate the output uncertainty in % Zn_{sorb}. As surface loading decreases, the importance of log $K^{int}_{(\equiv FeO)_2Zn}$ relative to total ferrihydrite increases for all pH. Conversely, as surface loading increases and pH decreases, the importance of total ferrihydrite relative to log $K^{int}_{(\equiv FeO)_2Zn}$ increases. Uncertainties in log $K^{int}_{NO3^-}$ are only of secondary importance at pH < 4.5. This trend is similar to what was observed for the constant-pH-isotherm Zn_{aq} data in Table 6.4. At all pH and Zn surface loadings, the impact of uncertainties in pH on the uncertainty in % Zn_{sorb} is about the same (8-12%). Input/thermodynamic parameters listed in Table 6.1, but not shown in Table 6.6, had a negligible impact on the output uncertainty under all conditions.

6.4.4 Implications for Surface Complexation Modeling

As was found for single-solute Pb sorption onto ferrihydrite in Chapter 3, new insights arise when a comprehensive collection of potentiometric-titration, constant-pH-isotherm, and pH-sorption-edge data from the same laboratory are

Table 6.6 **Input/thermodynamic parameters dominating output uncertainty in percent Zn sorbed for the Zn/ferrihydrite pH sorption edges shown in Figures 6.5b and 6.5c (1 g ferrihydrite/L).**

pH	Zn Total (M)	Fraction of Output COV Squared for % Zn_{sorb}				
		Total H_2O	Total Ferri-hydrite	pH	log $K^{int}_{(\equiv FeO)_2Zn}$	log K^{int}_{NO3-}
4.0	5E-06	0.02	**0.21**	0.10	**0.53**	0.14
	5E-05	0.02	**0.22**	0.10	**0.52**	0.14
	1E-03	0.01	**0.37**	0.08	**0.41**	0.13
5.0	5E-06	0.02	**0.23**	0.11	**0.59**	0.05
	5E-05	0.02	**0.24**	0.11	**0.58**	0.05
	1E-03	0.01	**0.43**	0.08	**0.42**	0.05
6.0	5E-06	0.02	**0.24**	0.12	**0.61**	0.01
	5E-05	0.02	**0.24**	0.12	**0.61**	0.01
	1E-03	0.01	**0.44**	0.09	**0.45**	0.01
7.0	5E-06	0.02	**0.24**	0.12	**0.62**	–
	5E-05	0.02	**0.25**	0.12	**0.61**	–
	1E-03	0.02	**0.33**	0.10	**0.55**	–
8.0	5E-06	0.02	**0.25**	0.10	**0.63**	–
	5E-05	0.02	**0.25**	0.10	**0.63**	–
	1E-03	0.02	**0.31**	0.09	**0.58**	–

analyzed together with spectroscopic data to develop a surface complexation model. Clearly, regressing constant-pH isotherm data, together with potentiometric titration and pH edge data, is a more rigorous test of a surface complexation model. When combined with spectroscopic data on surface speciation, the scope of feasible surface complexes and site types becomes much more limited. The results for Zn reported in this chapter corroborate the results for Pb sorption onto ferrihydrite reported in Chapter 3 and Dyer et al. (2002b). First, application of the triple-layer SCM leads to the same conclusions about Zn and Pb speciation on the ferrihydrite surface as did independent analyses of spectroscopic data presented in Trivedi et al. (2002a, b). Second, regression of pH edge data in the absence of isotherm and spectroscopic data results in a much larger number of surface species and site type combinations that provide acceptable fits of the edge data. However, when these same assumptions are used to predict the constant-pH isotherms, the agreement between model and data is poor in most cases. Third, a unique set of surface complexation equilibrium constants and corresponding site densities is unable to describe Zn and Pb sorption onto ferrihydrite. In both cases, the regressed equilibrium constants for the Pb and Zn surface complexes were functions of pH. For Zn, the density of Zn sorption sites was also found to vary with pH.

In conclusion, the results for both Zn and Pb sorption onto ferrihydrite suggest that the ability of SCMs to predict single-solute metal sorption over a wide range of conditions is still not completely resolved. While many advances have been made over the past decade, much more work still needs to be done in fine-tuning the thermodynamic framework and databases.

6.5 References

Benjamin M. M. (1979) Effects of competing metals and complexing ligands on trace metal adsorption at the oxide/solution interface. Ph.D. dissertation. Stanford University.

Benjamin M. M. (1983) Adsorption and surface precipitation of metals on amorphous iron oxyhydroxide. *Environ. Sci. Technol.* **17,** 686-692.

Benjamin M. M. and Bloom N. S. (1981) Effects of strong binding of anionic adsorbates on adsorption of trace metals on amorphous iron oxyhydroxide. In *Adsorption From Aqueous Solutions* (ed. P.H. Tewari), pp. 41-60. Plenum Press.

Brown G. E. Jr., Parks G. A., Bargar J. R., and Towle S. N. (1998) Use of x-ray absorption spectroscopy to study reaction mechanisms at metal oxide-water interfaces. In *Mineral-Water Interfacial Reactions: Kinetics and Mechanisms* (eds. D.L. Sparks and T.J. Grundl), ACS Symposium Series 715, pp. 14-36. American Chemical Society.

Crawford R. J., Harding I. H., and Mainwaring D. E. (1993) Adsorption and coprecipitation of single heavy metal ions onto the hydrated oxides of iron and chromium. *Langmuir* **9,** 3050-3056.

Dempsey B. A. and Singer P. C. (1980) The effects of calcium on the adsorption of zinc by MnO_x (s) and $Fe(OH)_3$ (am). In *Contaminants and Sediments, Volume 2, Analysis, Chemistry, and Biology* (ed. R.A. Baker), Chapter 18, pp. 333-352. Ann Arbor Science.

Dyer J. A., Trivedi P., Scrivner N. C., and Sparks D. L. (2002b) Lead sorption onto ferrihydrite. 2. New modeling insights. *Environ. Sci. Technol.* (In press).

Dyer J. A., Trivedi P., Scrivner N. C., and Sparks D. L. (2002c) Lead sorption onto ferrihydrite. 4. Uncertainty analysis. *Environ. Sci. Technol.* (In press).

Dzombak D. A. and Morel F. M. M. (1990) *Surface Complexation Modeling: Hydrous Ferric Oxide.* John Wiley & Sons.

Gadde R. R. and Laitinen H. A. (1974) Studies of heavy metal adsorption by hydrous iron and manganese oxides. *Anal. Chem.* **46,** 2022-2026.

Harvey D. T. and Linton R. W. (1984) X-ray photoelectron spectroscopy (XPS) of adsorbed zinc on amorphous hydrous ferric oxide. *Colloids Surf.* **11,** 81-96.

Hayes K. F. (1987) Equilibrium, spectroscopic, and kinetic studies of ion adsorption at the oxide/aqueous interface. Ph.D. dissertation. Stanford University.

Hayes K. F. and Katz L. E. (1996) Application of x-ray absorption spectroscopy for surface complexation modeling of metal ion sorption. In *Physics and Chemistry of Mineral Surfaces* (ed. P.V. Brady), pp. 147-223. CRC Press.

Kanungo S. B. (1994) Adsorption of cations on hydrous oxides of iron. II. Adsorption of Mn, Co, Ni, and Zn onto amorphous FeOOH from simple electrolyte solutions as well as from a complex electrolyte solution resembling seawater in major ion content. *J. Colloid Interface Sci.* **162,** 93-102.

Katz L. E. and Boyle-Wight E. J. (2001) Application of spectroscopic methods to sorption model parameter estimation. In *Physical and Chemical Processes of Water and Solute Transport/Retention in Soil*, (eds. H.M. Selim and D.L. Sparks), SSSA Special Publication No. 56, pp. 213-255. Soil Science Society of America.

Kinniburgh D. G. and Jackson M. L. (1982) Concentration and pH dependence of calcium and zinc adsorption by iron hydrous oxide gel. *Soil Sci. Soc. Am. J.* **46,** 56-61.

Kinniburgh D. G., Jackson M. L., and Syers J. K. (1976) Adsorption of alkaline earth, transition, and heavy metal cations by hydrous oxide gels of iron and aluminum. *Soil Sci. Soc. Am. J.* **40,** 796-799.

Kinniburgh D. G., Sridhar K., and Jackson M. L. (1977) Specific adsorption of zinc and cadmium by iron and aluminum hydrous oxides. Proceedings of the 15th Hanford Life Sciences Symposium on Biological Implications of Metals in the Environment, Hanford, Washington, pp. 231-239.

Leckie J. O., Benjamin M. M., Hayes K. F., Kaufman G., and Altmann S. (1980) *Adsorption/Coprecipitation of Trace Elements from Water with Iron Oxyhydroxide.* CS-1513, Electric Power Research Institute, Palo Alto, California.

Misak N. Z., Ghoneimy H. F., and Morcos T. N. (1996) Adsorption of Co^{2+} and Zn^{2+} ions on hydrous Fe(III), Sn(IV), and Fe(III)/Sn(IV) oxides. II. Thermal behavior of loaded oxides, isotopic exchange equilibria, and percentage adsorption-pH curves. *J. Colloid Interface Sci.* **184,** 31-43.

Robertson A. P. and Leckie J. O. (1997) Cation binding predictions of surface complexation models: Effects of pH, ionic strength, cation loading, surface complex, and model fit. *J. Colloid Interface Sci.* **188,** 444-472.

Sahai N. and Sverjensky D. A. (1998) GEOSURF: A computer program for modeling adsorption on mineral surfaces from aqueous solution. *Comput. Geosci.* **24,** 853-873.

Sanders S. J., Rafal M., Clark D. M., Young R. D., Scrivner N. C., Pease R. A., Grise S. L., and Diemer R. B. (1988) Modeling the separation of amino acids by ion-exchange chromatography. *Chem. Eng. Prog.* **92,** 47-54.

Schultz M. F., Benjamin M. M., and Ferguson J. F. (1987) Adsorption and desorption of metals on ferrihydrite: Reversibility of the reaction and sorption properties of the regenerated solid. *Environ. Sci. Technol.* **21,** 863-869.

Sparks D. L. (1995) *Environmental Soil Chemistry.* Academic Press.

Trivedi P. and Axe L. (2000) Modeling Cd and Zn sorption to hydrous metal oxides. *Environ. Sci. Technol.* **34,** 2215-2223.

Trivedi P., Dyer J. A., and Sparks D. L. (2002a) Lead sorption onto ferrihydrite. 1. A macroscopic and spectroscopic assessment. *Environ. Sci. Technol.* (In press).

Trivedi P., Dyer J. A., and Sparks D. L. (2002b) Zinc sorption onto ferrihydrite. 1. A spectroscopic understanding of macroscopic results. *Environ. Sci. Technol.* (In review).

Chapter 7

ZINC SORPTION ONTO FERRIHYDRITE: MULTISTAGE CONTACTING

7.1 Abstract

Previous studies demonstrated the environmental and economic benefits of treating lead-contaminated water streams with ferrihydrite in multiple equilibrium sorption stages. In this work, multistage ferrihydrite sorption systems were evaluated for their effectiveness in reducing single-solute zinc (Zn) concentrations in contaminated water streams to very low levels. As for lead (Pb), experimental data and modeling results indicate that a multistage sorption system can significantly reduce Zn effluent concentrations for the same total amount of sorbent or, alternatively, dramatically lower total sorbent consumption for the same effluent Zn concentration. Compared to Pb, however, Zn removal requires on the order of 10 times more sorbent to achieve the same target effluent concentration for the same pH and number of stages. Model predictions were made using a steady-state, multistage, equilibrium adsorber model that was previously developed for and integrated into OLI Systems' Environmental Simulation Program (ESP). The modified triple-layer model was used to simulate Zn surface-liquid equilibria within the adsorber model. Engineering screening evaluations again indicate that a 2- to 3-stage sorption process can provide significant economic savings when compared to a 1-stage process operating with the same target effluent Zn concentration. Additional equilibrium stages beyond 2 or 3 provide diminishing economic returns. The major economic

driver for multiple contacting stages is reduced capital investment and operating costs for sludge handling. dewatering, and disposal.

7.2 Introduction

Trace-metal discharges from industrial manufacturing processes are being increasingly scrutinized and regulated as new, revised, and proposed regulations are pushing metal effluent limits to part-per-billion (ppb) and lower levels (U. S. EPA, 2000; Gurian et al., 2001; U. S. EPA, 2001a, b; Wenning, 2001). Alkaline precipitation has historically been the technology of choice for meeting part-per-million (ppm) regulatory levels for metals in direct-discharge wastewater point sources; however, this technology is limited to $\geq$ 1 ppm effluent concentrations due to the inherent solubility of amorphous metal hydroxide phases and inefficiencies in commercial solid-liquid separation devices (Dyer et al., 1998). On the other hand, much lower effluent levels are possible by taking advantage of the large sorptive capacity of amorphous, high-surface-area solids, such as hydrous iron and aluminum oxides.

As previously reviewed by Dyer et al. (2002a), the scientific and engineering literature is devoid of experimental and modeling studies demonstrating the use of a high-surface-area sorbent, such as ferrihydrite, to treat metals-contaminated wastewater streams to ppb levels in a multistage crossflow or countercurrent-flow reaction system. Previous research by other groups has focused on one-stage treatment using amorphous metal oxides (Merrill et al., 1985; Schultz et al., 1987; Edwards and Benjamin, 1989) or multi-equilibrium-stage treatment in fixed-bed columns using a granular sorbent that can be regenerated over many cycles (Theis et al., 1992; Gao et al., 1995; Fan and Anderson, 1996; Smith, 1998; Smith and Amini,

2000). More background on these previous studies can be found in Chapter 4. The various technologies for sorbing trace metals onto metal-oxide sorbents each fill a niche, and each technology presents its own advantages and disadvantages. The niche for multistage sorption onto ferrihydrite appears to be for the ex-situ treatment of contaminated wastewater streams in existing or new wastewater treatment facilities that must comply with ppb regulatory levels for trace metals. Treatment at the process source, prior to dilution with the rest of the manufacturing site's wastewater, will result in a more economical treatment process with less sludge generation and a smaller environmental footprint.

Dyer et al. (2002a) showed for lead (Pb) that treatment with a high-surface-area sorbent, such as ferrihydrite, in two or more equilibrium contacting stages will (1) reduce metal effluent concentrations to much lower levels than can be achieved in one stage using an equivalent amount of sorbent; or (2) reduce total sorbent consumption and disposal for the same target effluent concentration. In theory, then, equilibrium staging can be used in a crossflow configuration to optimize the removal of several trace metals and metalloids whose pH ranges for optimum treatment are much different. Experience in the chemical engineering field has shown that 2 to 4 contacting stages often provide significant improvement over a single contacting stage in chemical reaction, leaching, and extraction systems, while additional stages beyond 4 or so often lead to diminishing economic returns (Zomosa, 1990; Reyes-Labarta and Grossmann, 2001; Van Vliet et al., 2001). A decision on the number of contacting stages often becomes an economic trade-off between the incremental capital investment for the additional equipment and the savings in raw material, energy, and waste disposal costs.

In this study, one-, two-, three-, and four-stage ferrihydrite sorption systems were evaluated for their effectiveness in reducing single-solute zinc (Zn) concentrations to very low levels in contaminated water streams. The objectives of the research were three-fold. First, to demonstrate for another trace metal how a multistage sorption process can significantly reduce trace-metal effluent concentrations for the same total amount of sorbent or, alternatively, dramatically lower total sorbent consumption for the same metal effluent concentration. Second, to develop and validate a steady-state, multistage, adsorber model for treating a Zn-contaminated water stream to part-per-billion levels. In the process, demonstrate the integration of a surface complexation model (SCM), such as the modified triple-layer model (TLM), into a steady-state equilibrium process flowsheet simulator to predict metals removal efficiency and sorbent requirements. Third, to conduct engineering screening evaluations to verify the economic drivers for equilibrium staging.

7.3 Methods

7.3.1 Ferrihydrite Preparation

The 2-line ferrihydrite was synthesized, washed, and aged for 48 hours according to the procedures described in Trivedi et al. (2002a).

7.3.2 Multistage Zn Sorption Experiments

Sorption studies were conducted with preformed ferrihydrite solids at room temperature in a N_2 glovebox using 1-liter, well-mixed reaction vessels containing a 0.01 M $NaNO_3$ background electrolyte solution. All studies were conducted in triplicate at the same time using the same batch of ferrihydrite. Equilibration time was 4 hours for each contacting stage, and pH was controlled at 6.5

using 0.1 M HNO_3 or NaOH. Zinc was added as $Zn(NO_3)_2$ using a 1 M stock solution. All chemicals were ACS reagent-grade; ultrapure water (Micropore SA) was used throughout. Equilibrated ferrihydrite solids were separated from the aqueous phase using a RC5 Sorvall centrifuge operating at 12,000 rpm for 20 minutes. Graphite furnace, atomic absorption spectroscopy (Perkin-Elmer Analyst 800) was used to analyze the centrates for total soluble Zn. The multistage, crossflow sorption experiments were batch equilibration studies; the experimental conditions for each case are summarized in Table 7.1. For example, in a two-stage system, such as Case 1B, 0.5 g "fresh" ferrihydrite sorbent was first equilibrated with 0.6 millimoles $Zn(NO_3)_2$ dissolved in 1 L of a 0.01 M $NaNO_3$ background solution (39.23 ppm Zn). After 4 hours, the mixture was centrifuged, and the resulting centrate was analyzed for residual Zn in solution. The bulk of the remaining centrate (~ 0.9 L) was then added to a second 1-L reaction vessel, where it was equilibrated again for 4 hours with 0.5 g/L of "fresh" ferrihydrite sorbent. The resulting centrate was analyzed for residual Zn. More background on the experimental protocol used in this study can be found in Trivedi et al. (2002b). Raw data for the multistage studies are reported in Appendix F.

7.3.3 Geochemical Modeling Software

The OLI Software (OLI Systems, Inc., Morris Plains, NJ) was used to perform the multistage, steady-state simulations. Details on the thermodynamic databank and framework, the equation solvers, and the SCMs used in the OLI Software are presented in Chapter 2. More specifically, the Environmental Simulation Program (ESP) was used for this study, because it is designed for steady-state

Table 7.1 Definition of and results for Zn/ferrihydrite (fh) multistage sorption case studies.[a]

Case	Stg. #	g fh/L in each stage	Stg. 1 Zn Feed Conc. (ppm)	Zn Effluent Measured[b]	95% C. I. Zn Effluent Measured[c]	Zn Effluent Model	95% C. I. Zn Effluent Model[c]
1A	1	1.0	39.23	1.2 ppm	1.1-1.3 ppm	1.4 ppm	0.73-2.6 ppm
1B	1	0.5	39.23	3.4 ppm	3.2-3.5 ppm	3.2 ppm	1.8-5.9 ppm
	2	0.5		108.6 ppb	102-117 ppb	189.2 ppb	55-426 ppb
2A	1	5.12	1.63	8.3 ppb	7.8-9.0 ppb	9.6 ppb	5.1-18.6 ppb
2B	1	0.34	1.63	110.7 ppb	106-114 ppb	136.5 ppb	76-249 ppb
	2	0.34		7.1 ppb	6.9-7.4 ppb	11.2 ppb	3.4-24.9 ppb
2C	1	0.15	1.63	301.4 ppb	293-309 ppb	283.9 ppb	169-491 ppb
	2	0.15		50.3 ppb	49.4-51.0 ppb	48.1 ppb	17.8-97.1 ppb
	3	0.15		7.3 ppb	7.0-7.4 ppb	8.1 ppb	1.6-18.5 ppb
3A	1	0.4	16.35	1.2 ppm	1.1-1.2 ppm	1.4 ppm	0.76-2.5 ppm
3B	1	0.2	16.35	3.4 ppm	3.39-3.41 ppm	2.9 ppm	1.8-4.9 ppm
	2	0.2		413.1 ppb	408-418 ppb	402.4 ppb	140-848 ppb

Table 7.1 Continued.

Case	Stg. #	g fh/L in each stage	Stg. 1 Zn Feed Conc. (ppm)	Zn Effluent Measured[b]	95% C. I. Zn Effluent Measured[c]	Zn Effluent Model	95% C. I. Zn Effluent Model[c]
3C	1	0.1	16.35	6.2 ppm	6.1-6.3 ppm	5.9 ppm	4.2-8.4 ppm
	2	0.1		1.8 ppm	1.7-1.8 ppm	1.6 ppm	0.8-2.9 ppm
	3	0.1		425.4 ppb	422-430 ppb	391.8 ppb	111-808 ppb
	4	0.1		82.3 ppb	81.7-83.4 ppb	92.4 ppb	19-210 ppb

[a] All experiments were conducted at room temperature in a N_2 glovebox using a 0.01 M $NaNO_3$ background electrolyte solution. The pH in each stage was controlled at 6.5 using 0.1 M HNO_3 or NaOH. [b] Mean of triplicate studies. [c] See Dyer et al. (2002c) and Chapter 5 for more details on how the 95% confidence intervals (C. I.) were generated. C. I. for the measured values reflect "same-batch" variation displayed by the triplicate studies. C. I. for the model values reflect "between-batch" uncertainties in input parameters (i.e., pH, Zn, ferrihydrite, and $NaNO_3$ feed concentrations, and mass H_2O) as well as uncertainties in the thermodynamic parameters (i.e., surface complexation Ks).

simulation of vapor, liquid, and solid interphase and intraphase equilibria occurring within multistage chemical process flowsheets. The modified TLM was utilized in this work, having provided best fits of the Zn/ferrihydrite isotherm and pH-edge data presented in Appendix E and Trivedi et al. (2002b) and subsequently analyzed in Chapter 6 and Dyer et al. (2002d).

7.3.4 Modeling Protocol

Examples of two-stage crossflow and two-stage countercurrent-flow sorption systems for treating a metals-contaminated wastewater stream are shown schematically in Figures 4.1a and 4.1b, respectively (Chapter 4). In a crossflow system, fresh sorbent is added to each reaction vessel or stage, equilibrated with the contaminated wastewater, and then removed for dewatering and disposal. This contrasts with a true countercurrent-flow system (Figure 4.1b), where fresh sorbent is added to the final sorption stage, and partially spent sorbent is subsequently reused in the upstream stages (i.e., the flow of sorbent is countercurrent to the flow of wastewater). A true countercurrent-flow system represents the minimum-sorbent-consumption case for a specified metals effluent concentration. For solids handling reasons, a crossflow arrangement will probably be more practical for amorphous materials, such as ferrihydrite, in most industrial situations. In addition, to simplify the process, most full-scale industrial systems would likely be operated in a coprecipitation mode, rather than a sorption (onto preformed floc) mode as shown in Figure 4.1. The experimental and modeling studies in this work are based on Zn sorption onto preformed ferrihydrite in order to utilize the triple-layer modeling results from Chapter 6 and Dyer et al. (2002d). Operation in a coprecipitation mode would likely lead to lower Zn effluent concentrations and sorbent requirements; however, the

benefits of staging will be realized in either mode. As a result, model predictions based on a sorption process will be conservative for environmental compliance purposes.

Steady-state process flowsheets were constructed in ESP using the appropriate combination of unit operations (separator, pH controller, acid/base manipulator, and sensitivity blocks) and feed/effluent streams (wastewater feed, sorbent feed, NaOH feed, stage 1 effluent, stage 1 solids, and so on). Separator blocks served as the isothermal reaction vessels. The efficiency of the solid-liquid separation was also specified in this block. An acid/base manipulator block and a pH controller were linked to each separator block to regulate the flow of mineral acid or base to each reaction vessel, so as to control pH at 6.5. The sensitivity block was used to perform multiple-case runs. The TLM functioned within all blocks containing sorbing solids. An example of a block flow diagram for a two-stage ESP crossflow sorption model is shown in Figure 4.2 (Chapter 4).

TLM parameters and associated Zn surface speciation assumptions used in this work were obtained from Tables 6.2 and 6.3 in Chapter 6 (see also Dyer et al., 2002d) and are summarized in Table 7.2. ESP simulations were made for each of the cases listed in Table 7.1. The objective was to compare model predictions based on the single-solute Zn sorption data reported in Appendix E and Trivedi et al. (2002b) to the results of the bench-scale multistage experiments (Appendix F). In theory, the results should not be statistically different when taking into account experimental and model uncertainties. In addition, generalized sensitivity studies were conducted to understand the impact of pH, Zn feed concentration, number of stages, perfect vs. imperfect solid-liquid separations, and crossflow vs. countercurrent-flow arrangement

Table 7.2 Triple-layer model parameters used in ESP simulations of multistage Zn sorption onto 2-line ferrihydrite.[a]

Parameter	Value
Zn Surface Species	$(\equiv FeO)_2Zn$
N_s for H^+ (mol /mol)	1.2
N_s for Zn^{2+} (mol /mol)	0.3, 0.65, 1.2 (pH 5.5, 6.5, 7.5)
A_s (m^2/g)	600
C_1 (F/m^2)	1.0
C_2 (F/m^2)	0.2
$\log K_{a1}^{int}$	-5.56
$\log K_{a2}^{int}$	-10.26
$\log K_{NO3-}^{int}$	-7.154
$\log K_{Na+}^{int}$	8.69
$\log K_{(\equiv FeO)_2Zn}^{int}$ @ 1 g solids/L[b]	4.954, 7.147, 9.523 (pH 5.5, 6.5, 7.5)
γ_s	$\gamma_s = \gamma_{Zn2+}$

[a] Refer to Tables 6.2 and 6.3 as well as Dyer et al. (2002d) for details on the chemical reactions and mass law expressions corresponding to each of the equilibrium constants given above. Definitions for each of the parameters can be found in the nomenclature section. [b] For bidentate surface complexes, K^{int} is really a conditional K that depends on sorbent solids concentration. The value for K in this table is based on 1 g ferrihydrite/L. See Table 6.3 for additional explanation.

on the predicted Zn effluent concentration at a fixed sorbent dose and the predicted sorbent requirement at a specified Zn effluent concentration.

7.3.5 Engineering Evaluations

High-spot engineering evaluations (+/- 30%) were completed for each of the cases in Table 7.1 to assess the relative economic incentive/penalty for additional equilibrium sorption stages. There are two key differences between the treatment process assumed in the engineering evaluations and that used in the experimental and modeling studies—use of $FeCl_3$, rather than $Fe(NO_3)_2$, and operation in a coprecipitation mode, rather than a sorption mode. Investment, costs, and economics should not be used on an absolute basis to compare to other technology alternatives, such as ion exchange, alkaline precipitation, and so on; however, they can be safely used for a relative ranking of the multistage process alternatives.

The evaluations are based on the 10-step engineering evaluations methodology outlined in detail in Mulholland and Dyer (1999). For each case, a process flow diagram was developed, showing the necessary equipment pieces (pumps, tanks, clarifiers, filter presses, etc.) and process interconnections. From the process flow diagrams, facility scopes-of-work (i.e., a description of the physical facilities required to build the process) were developed and operating requirements were defined (i.e., annual requirements for 50 wt % NaOH, 30 wt% $FeCl_3$, electricity, sludge disposal, etc.). Based on the facility scopes-of-work, capital investment was then estimated for each case using a factored, research-guidance-appraisal technique that is widely used within the chemical industry. Finally, armed with estimates for new capital investment and operating requirements, a 10-year cash flow analysis was completed for each case to estimate annual cash operating cost and net present cost at

both a 12% and 25% discount rate. Net present cost (NPC) was the economic measure of merit used to rank alternatives, because it incorporates the effects of both new capital investment and on-going cash operating costs over the life of the facility. A discount rate of 25% was chosen to rank the alternatives, because it better reflects the opportunity cost of capital in situations where the supply of capital dollars is limited and other viable projects are competing for the same dollars (which is almost always the case in the chemical industry).

Table 4.3 (Chapter 4) summarizes the major assumptions used in the engineering evaluations. Bare equipment, raw material, utility, and waste disposal costs were obtained from various reliable sources (Gumerman et al., 1986; DuPont Investment Technologies, 1998; Mulholland and Dyer, 1999; DuPont Sourcing, 2002; Schnell Publishing, 2002). Process flow diagrams for one- and two-stage, crossflow, coprecipitation processes are shown in Figures 4.3 and 4.4 (Chapter 4). Process flow diagrams, facility scopes-of-work, operating requirements, factored investment estimates, and 10-year cash flow analyses are included in Appendix G.

7.4 Results and Discussion

7.4.1 Multistage Sorption Case Studies

Experimental data (Zn Effluent Measured) and ESP modeling results (Zn Effluent Model) for the multistage sorption case studies are summarized in Table 7.1. Experimental data are the arithmetic average of the effluent Zn concentrations measured in the three replicate studies for each stage of each case. Model data are ESP predictions based on the modified triple-layer model and the parameters summarized in Table 7.2. To better assess the agreement between the measured and

model data, 95% confidence intervals were generated for each data point, and are reported in Table 7.1. Details on the statistical tools, methodology, and uncertainty assumptions used to calculate the 95% confidence intervals are described in Chapter 5 and Dyer et al. (2002c).

Briefly, confidence intervals for the measured values reflect the variation in or, more specifically, the *repeatability* of the 3 replicate studies for each stage of each case. Hence, the confidence intervals account for "within-the-same-batch" uncertainties in analytical/experimental procedures and equipment for the same operator conducting experiments with the same batch of ferrihydrite on the same day. These include analytical equipment, sample collection, sample handling, and sample processing errors as well as errors in pH calibration/control, reagent doses, and so on. The Resampling Stats for Windows software (Resampling Stats, Inc., Arlington, Virginia) was used to estimate the 95% confidence intervals for the measured values. This software uses a bootstrap procedure (Diaconis and Efron, 1983; Simon, 1997) to randomly generate with replacement N new samples of size, n, directly from the original sample. The number of new samples (N) is usually set at 10,000 or more, while the sample size (n), in this case, was 3. For this study, N was set equal to 10,000. The bootstrap procedure effectively creates a hypothetical "infinite" population that represents one's best guess about the real population.

The 95% confidence intervals for the ESP model predictions, on the other hand, attempt to account for "between-batch" uncertainties in the model input parameters (i.e., pH, Zn feed concentration, ferrihydrite dose, $NaNO_3$ concentration, and the mass of H_2O) as well as uncertainties in the regressed thermodynamic parameters (i.e., surface complexation equilibrium constants). Examples of between-

batch uncertainties include differences in sorbent properties, reagent concentrations, and pH measurement equipment as compared to the original isotherm and edge studies used to determine the best-fit model parameters. Hence, the confidence intervals attempt to reflect the *reproducibility* of Zn/ferrihydrite sorption studies on different days using different batches of ferrihydrite/reagents as well as the quality of the model fits of the acid-base titration and Zn sorption data used to estimate the thermodynamic parameters in the first place. As described in Dyer et al. (2002c), the OLI Software's error analysis tool was first used to propagate input and thermodynamic parameter uncertainties through the multistage sorption model, yielding local extrapolation models that approximated the value of each output parameter of interest (i.e., effluent Zn concentration and Zn surface loading). Monte Carlo simulations (N = 10,000) of the OLI-generated local extrapolation models were then conducted with the Resampling Stats software to estimate the 95% confidence intervals for the model predictions.

In principle, the greater the overlap of the confidence intervals for the measured and model values, the higher the probability that the two values are the same. That is, one cannot say with confidence that the model and measured values are statistically different. Based on the 95% confidence intervals reported in Table 7.1 (i.e., when model and experimental uncertainties are taken into account), the agreement between the model-predicted and measured effluent Zn concentrations is excellent. In all cases, there is significant overlap of the 95% confidence intervals. More rigorous hypothesis testing using Resampling Stats indicated that the difference between the measured and model values was not statistically significant ($p < 0.05$) in

any cases. Based on these results, the ESP model does a satisfactory job of predicting the expected Zn removal efficiency in a multistage operation.

Another useful product of the error analysis tool in the OLI Software is a quantitative analysis of which input/thermodynamic parameter uncertainties dominate the uncertainty in the output variables (Dyer et al., 2002c). In all cases, the output uncertainty in effluent Zn concentration (Zn_{aq}) from the first equilibrium sorption stage was dominated by the input uncertainty in log $K^{int}_{(\equiv FeO)_2Zn}$ (i.e., 60-70% of the output coefficient of variation squared). The balance was split between input uncertainties in pH and total ferrihydrite concentration. The importance of total ferrihydrite concentration relative to pH increased as Zn surface loading increased. On the other hand, the output uncertainty in Zn_{aq} from the second and subsequent stages was dominated by the input uncertainty in total Zn feed concentration (i.e., 45-75% of the output coefficient of variation squared). The balance was mainly due to input uncertainties in log $K^{int}_{(\equiv FeO)_2Zn}$, followed by pH and total ferrihydrite concentration. Due to error propagation downstream, the dominance of total Zn feed concentration increased with stage number. Quantitative uncertainty analysis results for the multistage crossflow sorption case studies are summarized in Table 7.3. The results in Table 7.3 are based on the same input/thermodynamic parameter uncertainty assumptions reported in Chapter 5 and Dyer et al. (2002c) for Pb.

7.4.2 Generalized Multistage Sensitivity Studies

Figure 7.1 shows the effects of influent Zn concentration, pH, and number of equilibrium stages on the predicted effluent Zn concentration from a multistage crossflow adsorber operating with a total ferrihydrite dose of 1 g/L, equally split across the stages (i.e., 1 g/L in a one-stage system vs. 0.5 g/L in each stage of a two-stage

Table 7.3 **Input/thermodynamic parameters dominating output uncertainty in Zn_{aq} (ppm) for the multistage crossflow Zn/ferrihydrite sorption case studies (pH 6.5, 0.01 M $NaNO_3$).**

Case	Stg. #	Zn Outlet Conc. (ppm)[a]	Surface Loading (mol Zn /mol Fe)	Fraction of Output COV Squared for Zn_{aq}			
				Total Zn	Total Ferri-hydrite	pH	log $K^{int}_{(\equiv FeO)_2Zn}$
1A	1	1.38	0.0514	–	0.10	0.14	**0.74**
1B	1	3.21	0.0979	–	0.15	0.13	**0.70**
	2	0.189	0.0082	**0.51**	0.04	0.07	**0.38**
2A	1	0.0096	4.3E-04	–	0.08	0.15	**0.77**
2B	1	0.136	0.006	–	0.08	0.15	**0.77**
	2	0.011	5.0E-04	**0.50**	0.04	0.07	**0.39**
2C	1	0.284	0.012		0.08	0.14	**0.76**
	2	0.048	0.0021	**0.50**	0.04	0.07	**0.39**
	3	0.008	3.6E-04	**0.67**	0.02	0.05	**0.26**
3A	1	1.36	0.05	–	0.10	0.14	**0.74**
3B	1	2.9	0.091	–	0.14	0.13	**0.71**
	2	0.402	0.017	**0.49**	0.04	0.07	**0.39**
3C	1	5.89	0.142	0.02	**0.21**	0.12	**0.63**
	2	1.61	0.058	**0.45**	0.06	0.08	**0.41**
	3	0.392	0.0166	**0.63**	0.03	0.05	**0.28**
	4	0.092	0.0041	**0.73**	0.02	0.04	**0.21**

[a] ESP model prediction.

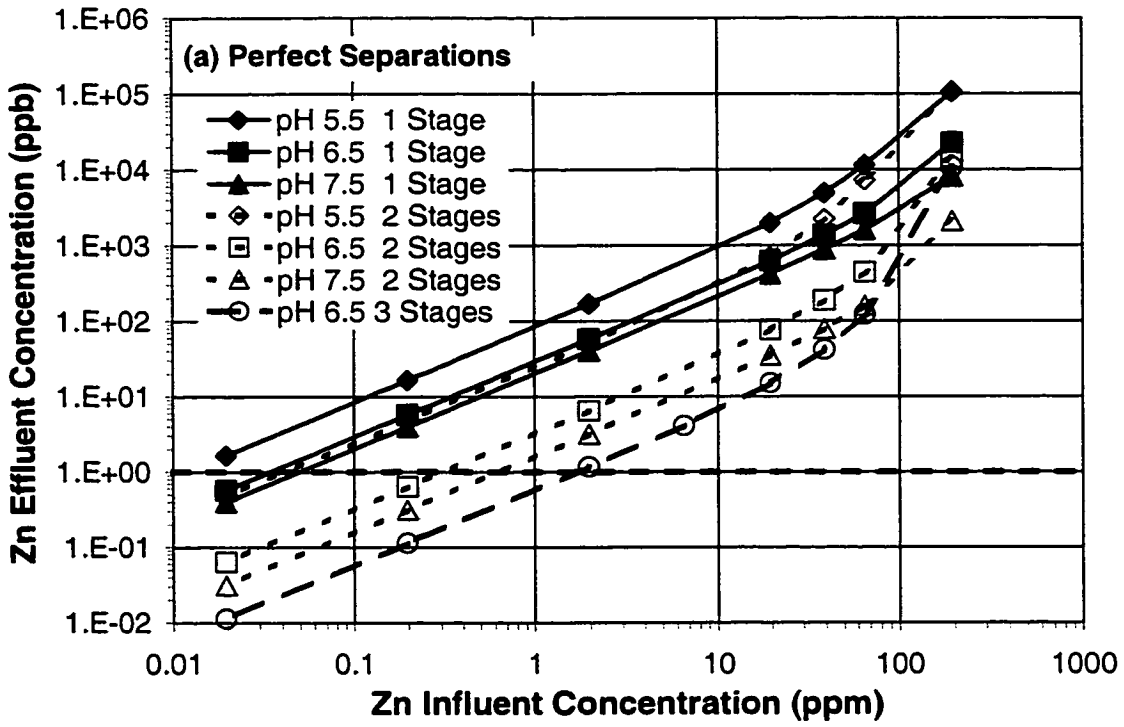

Figure 7.1 **Impact of influent Zn concentration, pH, and number of equilibrium stages on the effluent Zn concentration in one- and two-stage crossflow adsorbers operating with a fixed total ferrihydrite dose of 1 g/L (1 g/L equally split between stages in two-stage system). In (a), perfect solid-liquid separations are assumed. In (b), the impact of imperfect solid-liquid separations (20 ppm suspended solids in clarified effluent and 30 wt% solids in the settled sludge) on Zn removal at pH 6.5 is shown. Model predictions are based on the modified triple-layer using a 0.01 M $NaNO_3$ background electrolyte solution and parameters summarized in Table 7.2.**

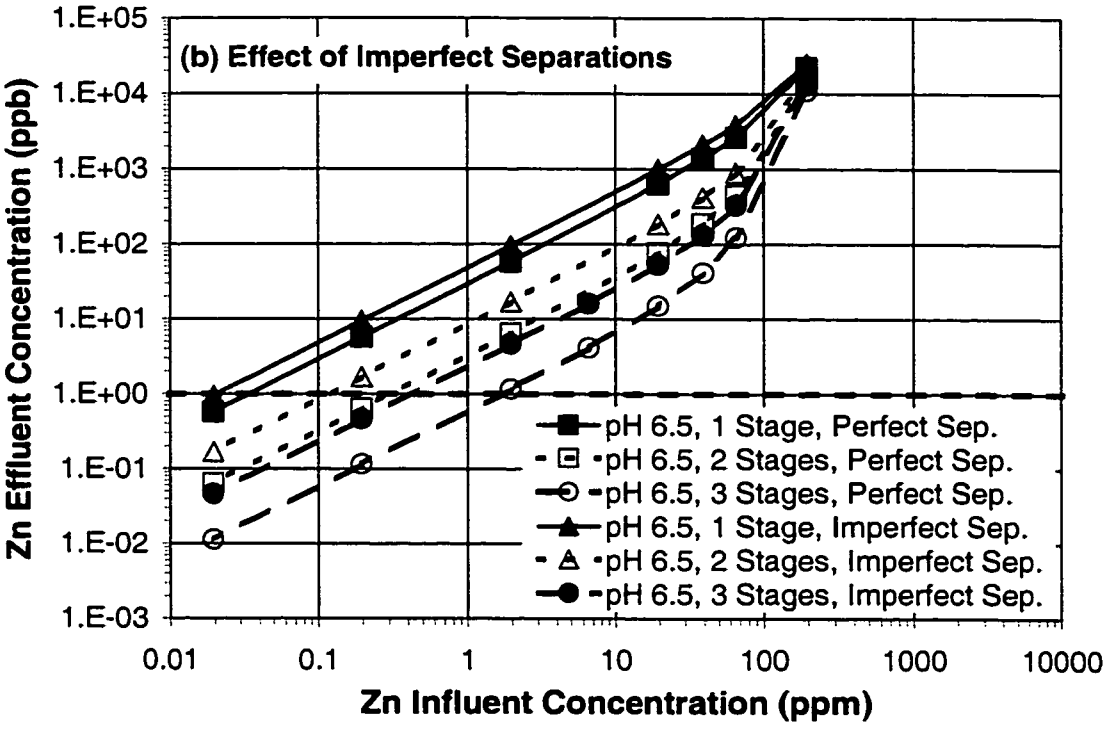

Figure 7.1 Continued.

system). Figure 7.1a assumes perfect solid-liquid separations, while Figure 7.1b highlights the impact of 20 ppm suspended solids in the clarified effluent and 30 wt% solids in the settled iron sludge on effluent Zn levels at pH 6.5. In both scenarios, the combined impact of pH and number of stages on Zn removal is significant. For example, as shown in Figure 7.1a, a 10-ppm Zn-containing water stream can be treated to only 300 ppb Zn using a one-stage adsorber at pH 6.5; however, the addition of a second and third stage at the same pH will reduce the effluent Zn concentration to approximately 35 and 7 ppb, respectively. On the other hand, raising the pH from 6.5 to 7.5 at constant number of stages will lower the effluent Zn concentration from 300 ppb to only 200 ppb for a one-stage process and from 35 ppb to only 20 ppb for a two-stage process. In this case, the beneficial impact of adding equilibrium stages is more significant than the impact of raising the pH from 6.5 to 7.5. The benefit realized from adding a second stage is most significant at low Zn feed concentrations and at pH 6.5 and 7.5, where sorption of Zn is highly favored. At pH 6.5 and 7.5, adding a second stage lowers the effluent Zn concentration by 4- to 15-fold for a Zn feed concentration of 100 ppm or less. This is substantially lower than the 30- to 100-fold reduction realized for Pb at pH 5.5 and 6.5 (Chapter 4 and Dyer et al., 2002a). The diminishing impact of additional equilibrium stages at high Zn feed concentrations (> 100 ppm) is the result of operating closer to site saturation (i.e., the systems are closer to being sorbent-limited).

The impact of solids carryover in the clarified effluent is to reduce Zn removal efficiency. As shown in Figure 7.1b, predicted effluent Zn concentrations at pH 6.5 increase by 1.5- to 4-fold when compared to the model predictions based on perfect solid-liquid separations. As might be expected, the benefit gained by adding a

second equilibrium stage is diminished as solids carryover increases. Consider the same 10-ppm Zn-containing water stream discussed above for Figure 7.1a. Based on Figure 7.1b, the predicted effluent Zn concentration for a two-stage adsorber operating at pH 6.5 is about 95 ppb (instead of 35 ppb) when more realistic solid-liquid separation efficiencies are assumed (20 ppm suspended solids in the clarified effluent and 30 wt% solids in the settled iron sludge).

Similarly, Figures 7.2a and 7.2b display the impacts of influent Zn concentration, pH, and number of equilibrium stages on the total required ferrihydrite dose in multistage crossflow Zn adsorbers operating with a fixed effluent Zn concentration of 1 ppb. Figure 7.2a assumes perfect solid-liquid separations; Figure 7.2b highlights the impact of 20 ppm suspended solids in the clarified effluent and 30 wt% solids in the settled iron sludge on effluent Zn concentration at pH 6.5. As in Figure 7.1, the combined impact of pH and number of stages on Zn removal efficiency is significant. For example, as shown in Figure 7.2a, total ferrihydrite consumption for the same hypothetical 10-ppm Zn-containing water stream can be reduced from approximately 300 g/L using a one-stage adsorber at pH 6.5 to ~ 6 g/L using a two-stage adsorber at pH 6.5. Further reductions in ferrihydrite consumption can be achieved by raising the pH in a two-stage adsorber to 7.5 (~ 4 g/L) or, alternatively, by adding a third stage at pH 6.5 (~ 2 g/L). In this case, the beneficial impact of adding a second stage is most significant at higher Zn feed concentrations and is uniform with pH. An approximately 2 order-of-magnitude reduction in ferrihydrite dose was also seen for Pb in moving from a one-stage system at pH 5.5 to a two-stage system at pH 6.5 (Chapter 4 and Dyer et al., 2002a).

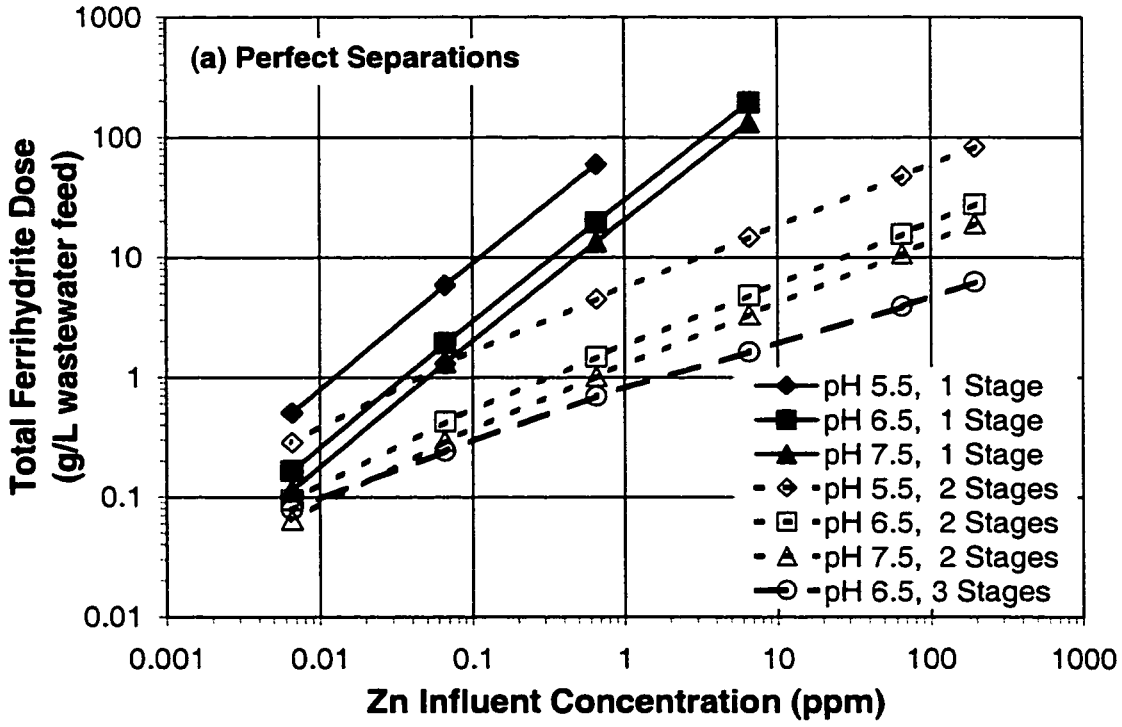

Figure 7.2 **Impact of influent Zn concentration, pH, and number of equilibrium stages on total ferrihydrite consumption in one- and two-stage crossflow adsorbers operating with a fixed effluent Zn concentration of 1 ppb. Ferrihydrite is equally split between stages in the two-stage system. In (a), perfect solid-liquid separations are assumed. In (b), the impact of imperfect solid-liquid separations (20 ppm suspended solids in clarified effluent and 30 wt% solids in the settled sludge) on ferrihydrite consumption at pH 6.5 is shown. Model predictions are based on the modified triple-layer using a 0.01 M $NaNO_3$ background electrolyte solution and parameters summarized in Table 7.2.**

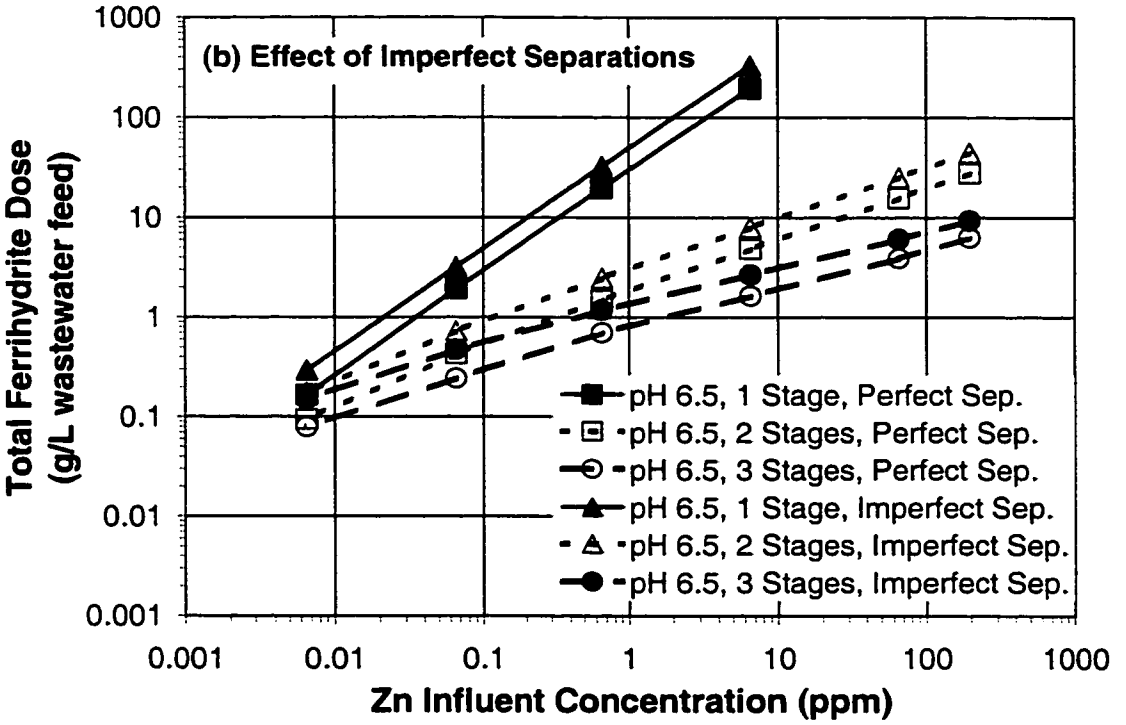

Figure 7.2 Continued.

The negative impact of solids carryover in the clarified effluent is displayed in Figure 7.2b. Predicted total ferrihydrite doses at pH 6.5 increase by 1.5- to 2-fold when compared to the predicted doses assuming perfect solid-liquid separations. For the same 10-ppm Zn-containing water stream discussed above for Figure 7.2a, the required total ferrihydrite dose for a two-stage adsorber operating at pH 6.5 is about 10 g/L (instead of 6 g/L) when more realistic solid-liquid separation efficiencies are assumed.

Finally, Figure 7.3 shows the impact of the number of equilibrium stages on total ferrihydrite dose as a function of Zn feed concentration for both crossflow (Figure 4.1a) and true countercurrent-flow (Figure 4.1b) arrangements. Figure 7.3 assumes operation at pH 6.5, 10 ppb Zn total in the clarified effluent, 20 ppm suspended solids carryover, and 30 wt% solids in the iron sludge. It is apparent from Figure 7.3 that the benefits of staging diminish as the number of equilibrium stages increases. By 3 to 4 stages, the dose curves begin to level out. This agrees with the results for multistage Pb sorption as well (Chapter 4 and Dyer et al., 2002a). Figure 7.3 also highlights the ferrihydrite-consumption penalty realized by operating in a crossflow arrangement instead of a true countercurrent-flow arrangement. As was the case for Pb, total ferrihydrite doses are 2 to 4 times higher for the crossflow arrangement for 2 or more equilibrium stages.

7.4.3 Economic Benefits of Staging

Table 7.4 presents the results of engineering evaluations for the multistage sorption case studies summarized in Table 7.1. A key principle of engineering evaluations is that process flowsheets and scopes-of-work should be based on equivalent outcomes (i.e., the same effluent Zn concentration) in order to fairly

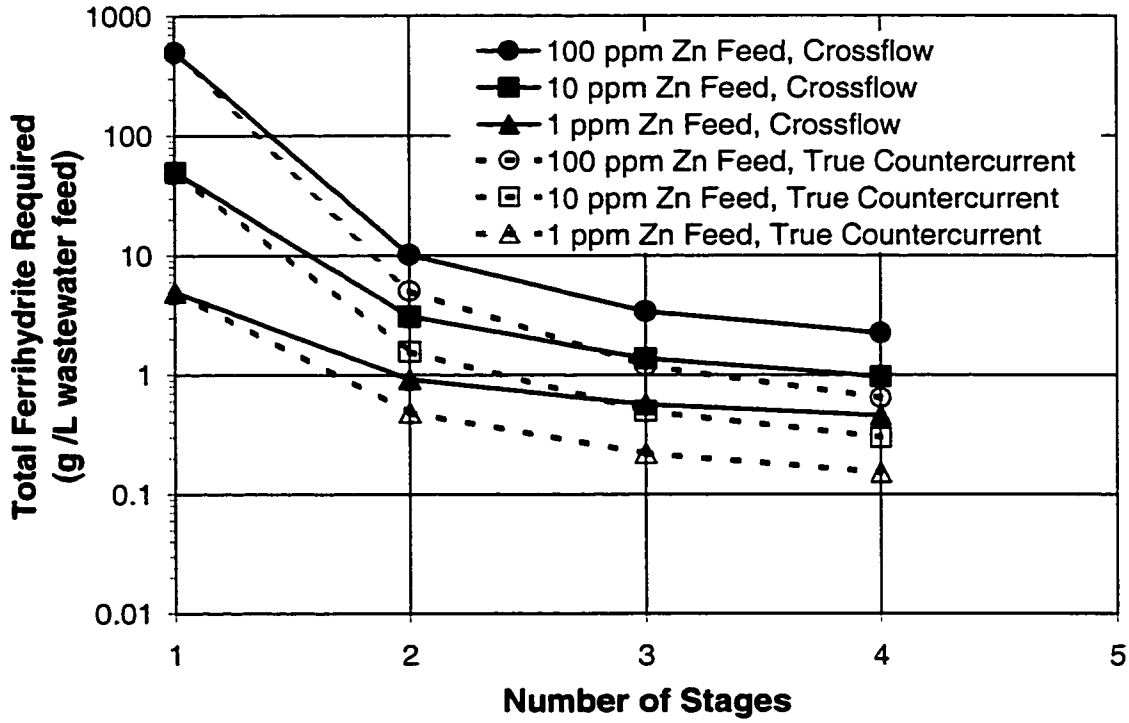

Figure 7.3 **Impact of the number of equilibrium stages and influent Zn concentration on total ferrihydrite consumption in crossflow and true countercurrent-flow adsorbers operating at pH 6.5 with a fixed effluent Zn concentration of 10 ppb, 20 ppm suspended solids in clarified effluent, and 30 wt% solids in the settled sludge. Ferrihydrite is equally split between stages in the multistage systems. Model predictions are based on the modified triple-layer using a 0.01 M $NaNO_3$ background electrolyte solution and parameters summarized in Table 7.2.**

Table 7.4 Engineering evaluation results for multistage Zn sorption case studies.

Case	# Stgs.	g fh/L in each stage	Zn Feed Conc. (ppm)	2002 Investment ($1000)	2004 Cash Operating Cost ($1000/yr)	2002 NPC @ 12% ($1000)	2002 NPC @ 25% ($1000)
1A	1	1.0	39.23	2,300	690	4,800	3,100
1B	2	0.5	39.23	2,800	760	5,500	3,600
2A	1	5.12	1.63	4,300	2,360	13,500	7,900
2B	2	0.34	1.63	2,600	600	4,600	3,100
2C	3	0.15	1.63	2,900	580	4,800	3,300
3A	1	0.4	16.35	1,900	420	3,300	2,200
3B	2	0.2	16.35	2,400	490	4,000	2,700
3C	4	0.1	16.35	3,300	620	5,300	3,600

compare alternatives. Case Studies 2A through 2C adhere to this principle, having been designed to achieve an effluent Zn concentration of ~ 10 ppb from the final stage. For this reason, $NPC_{25\%}$ values for each of these cases can be compared to choose the most cost-effective alternative(s). In other words, they can provide insight on the economic benefit of additional equilibrium stages. Case Studies 1 and 3, on the other hand, are not based on equivalent outcomes (i.e., the effluent Zn concentration varies between alternatives). However, they do provide valuable insights on the incremental investment and net present cost associated with adding equilibrium stages to lower the effluent Zn concentration at a fixed total ferrihydrite dose.

The results for Case Studies 2A through 2C in Table 7.4 clearly show that the addition of a second equilibrium stage makes economic sense ($NPC_{25\%}$ of $3,100,000 for 2 stages versus $7,900,000 for 1 stage). The additional investment and ongoing operating costs associated with handling, dewatering, and disposing of an order of magnitude more iron sludge (5.12 g/L for Case 2A vs. 0.68 g/L total for Case 2B) are substantial. On the other hand, the addition of a third stage just about breaks even ($NPC_{25\%}$ of $3,300,000 for 3 stages versus $3,100,000 for 2 stages); therefore, the additional operational complexity associated with three stages versus two is probably not justified. In this case, the reduction in sludge from Case 2B to 2C is only about 33% (0.68 g/L vs. 0.45 g/L total). The use of 4 or more stages would almost certainly result in an $NPC_{25\%} > \$3,300,000$. Very similar results were obtained for the multistage Pb sorption studies (Chapter 4 and Dyer et al., 2002a).

The results for Case Studies 1 and 3 indicate that the incremental investment and $NPC_{25\%}$ for moving to a multistage operation are both on the order of $450,000-$500,000 per added stage. This compares to one-stage (i.e., base case)

$NPC_{25\%}$ values of $3,100,000 and $2,200,000 for Case Studies 1A and 3A, respectively. In other words, the incremental $NPC_{25\%}$ for an additional stage is approximately 15-20% of the base-case $NPC_{25\%}$. For Case Study 1, a second stage at the same total ferrihydrite dose results in an order-of-magnitude reduction in effluent Zn concentration. For Case Study 3, each incremental stage provides a 4- to 8-fold reduction in effluent Zn concentration based on the experimental data reported in Table 7.1.

In summary, as regulated trace-metal concentrations in water discharges are pushed to part-per-billion and lower levels, multistage contacting schemes will likely provide substantial economic benefits when sorption onto or coprecipitation with amorphous materials, such as ferrihydrite, are being considered. Table 7.4 shows that a 2- to 3-stage sorption process can provide significant economic savings when compared to a 1-stage process operating with the same target effluent Zn concentration. These results corroborate the findings reported in Chapter 4 and Dyer et al. (2002a) for multistage Pb sorption. In addition, this research has again confirmed that a steady-state process flowsheet simulator, such as OLI Systems' ESP software, can adequately predict Zn removal in a multistage ferrihydrite adsorber using the triple-layer surface complexation model calibrated with macroscopic and spectroscopic Zn sorption data. More importantly, however, this study helps to show how fundamental macroscopic and spectroscopic metal sorption data, coupled with surface complexation models, can be practically used to help solve industrial trace-metal emissions problems.

7.5 References

Diaconis P. and Efron B. (1983) Computer-intensive methods in statistics. *Sci. Am.* **248**(5), 116-130.

DuPont Investment Technologies. (1998) *RGA Software, Version 3.1.* DuPont Company.

DuPont Sourcing (2002) Personal communications.

Dyer J. A., Scrivner N. C., and Dentel S. K. (1998) A practical guide for determining the solubility of metal hydroxides and oxides in water. *Environ. Prog.* **17,** 1-7.

Dyer J. A., Trivedi P., Sanders S. J., Scrivner N. C., and Sparks D. L. (2002a) Lead sorption onto ferrihydrite. 3. Multistage contacting. *Environ. Sci. Technol.* (In press).

Dyer J. A., Trivedi P., Scrivner N. C., and Sparks D. L. (2002c) Lead sorption onto ferrihydrite. 4. Uncertainty analysis. *Environ. Sci. Technol.* (In press).

Dyer J. A., Trivedi P., Scrivner N. C., and Sparks D. L. (2002d) Zinc sorption onto ferrihydrite. 2. New modeling insights. *Environ. Sci. Technol.* (In review).

Edwards M. and Benjamin M. M. (1989) Regeneration and reuse of iron hydroxide adsorbents in treatment of metal-bearing wastes. *J. Water Pollut. Control Fed.* **61,** 481-490.

Fan H. and Anderson P. R. (1996) Development and evaluation of Mn oxide-coated composite adsorbent for the removal and recovery of heavy metals from metal contaminated wastewater. *Proceedings of the 50th Industrial Waste Conference*, pp. 217-226. Ann Arbor Press.

Gao Y., Sengupta A. K., and Simpson D. (1995) A new hybrid inorganic sorbent for heavy metals removal. *Water Res.* **29,** 2195-2205.

Gumerman R. C., Burris B. E., and Hansen S. P. (1986) *Small Water System Treatment Costs.* Noyes Data Corporation.

Gurian P. L., Small M. J., Lockwood J. R., and Schervish M. J. (2001) Addressing uncertainty and conflicting cost estimates in revising the arsenic MCL. *Environ. Sci. Technol.* **35,** 4414-4420.

Merrill D. T., Maroney P. M., and Parker D. S. (1985) *Trace Element Removal by Coprecipitation with Amorphous Iron Oxyhydroxide: Engineering Evaluation.* CS-4087, Electric Power Research Institute, Palo Alto, California.

Mulholland K. L. and Dyer J. A. (1999) *Pollution Prevention: Methodology, Technologies and Practices*. American Institute of Chemical Engineers.

Reyes-Labarta J. A. and Grossmann I. E. (2001) Disjunctive optimization design models for complex liquid-liquid multistage extractors. *AIChE J.* **47,** 2243-2252.

Schnell Publishing (2002) *Chemical Market Reporter* **261**(12), 16-19.

Schultz M. F., Benjamin M. M., and Ferguson J. F. (1987) Adsorption and desorption of metals on ferrihydrite: Reversibility of the reaction and sorption properties of the regenerated solid. *Environ. Sci. Technol.* **21,** 863-869.

Simon J. L. (1997) *Resampling: The New Statistics*. Resampling Stats, Inc.

Smith E. H. (1998) Surface complexation modeling of metal removal by recycled iron sorbent. *J. Environ. Eng.* **124,** 913-920.

Smith E. H. and Amini A. (2000) Lead removal in fixed beds by recycled iron sorbent. *J. Environ. Eng.* **126,** 58-65.

Theis T. L., Iyer R., and Ellis S. K. (1992) Evaluating a new granular iron oxide for removing lead from drinking water. *J. Am. Water Works Assoc.* **84,** 101-105.

Trivedi P., Dyer J. A., and Sparks D. L. (2002a) Lead sorption onto ferrihydrite. 1. A macroscopic and spectroscopic assessment. *Environ. Sci. Technol.* (In press).

Trivedi P., Dyer J. A., and Sparks D. L. (2002b) Zinc sorption onto ferrihydrite. 1. A spectroscopic understanding of macroscopic results. *Environ. Sci. Technol.* (In review).

U. S. EPA. (2000) Revisions to the water quality planning and management regulation and revisions to the national pollutant discharge elimination system program in support of revisions to the water quality planning and management regulation. *Fed. Regist.* **65**(135), 43586-43670.

U. S. EPA. (2001a) National primary drinking water regulations; arsenic and clarifications to compliance and new source contaminants monitoring. *Fed. Regist.* **66**(14), 6976-7066.

U. S. EPA. (2001b) Effective date of revisions to the water quality planning and management regulation and revisions to the national pollutant discharge elimination system program in support of revisions to the water quality planning and management regulations; and revision of the date for state submission of the 2002 list of impaired waters. *Fed. Regist.* **66**(202), 53044-53048.

Van Vliet R. E., Tiemersma T. P., Krooshof G. J., and Iedema P. D. (2001) The use of liquid-liquid extraction in the EPDM solution polymerization process. *Ind. Eng. Chem. Res.* **40**, 4586-4595.

Wenning R. J. (2001) USEPAs forum on managing contaminated sediments at hazardous waste sites: Summary of policy discussions. *Contaminated Soil Sediment & Water* (June/July), 49-54.

Zomosa A. (1990) Calculating optimum number of stages in continuous countercurrent decantation (CCD). *Miner. Metall. Process.* **7**, 118-120.

Chapter 8

CONCLUSIONS

8.1 Summary of Research

The objectives of this research project were three-fold. First, to demonstrate how the integration of spectroscopic data on surface speciation with macroscopic sorption data covering a wide range of conditions leads to the determination of an optimum set(s) of surface complexation modeling parameters for both single-solute Pb and Zn sorption onto 2-line ferrihydrite. Second, to demonstrate an industrial application for these calibrated surface complexation models by developing and validating a steady-state, multistage, ferrihydrite adsorber model for treating a Pb-contaminated water stream to part-per-billion levels. Third, using state-of-the-art uncertainty analysis techniques, to demonstrate a methodology for quantifying the impact of analytical, thermodynamic, and SCM input-parameter uncertainties on the predicted output parameters (e.g., % metal sorbed, soluble metal concentration, etc.) as well as for identifying which input parameters have the most impact on the output uncertainty. While all three objectives were successfully met, the results were not always as expected.

Chapters 3 and 6 showed that regression of constant-pH isotherm data, together with potentiometric titration and pH edge data, is a much more rigorous test of a SCM than fitting pH edge data alone. When combined with spectroscopic data, the choices of feasible surface species/site types are limited to a few. For Pb, very

good fits of the isotherm data were obtained with a two-species, one-site model using the bidentate/monodentate species pair $(\equiv FeO)_2Pb/\equiv FeOHPb^{2+}$ or $(\equiv FeO)_2Pb/\equiv FeOPb^{+}–NO_3^{-}$. For Zn, on the other hand, a one-species, one-Zn-sorption-site model using the bidentate surface complex, $(\equiv FeO)_2Zn$, provided excellent fits of the data. There was no evidence for surface precipitation at high loadings over the pH range 4.5 to 7.5 for either metal. Regressing edge data in the absence of isotherm and spectroscopic data resulted in a fair number of surface-species/site-type combinations that provided acceptable fits of the edge data, but unacceptable fits of the isotherm data. Surprisingly, best-fit equilibrium "constants" for the Pb and Zn surface complexes required adjustment with pH in order to fit the isotherm data. For Zn, the density of Zn sorption sites also had to be varied with pH to fit the data. Finally, a surface activity coefficient term had to be introduced into the TLM for both metals to reduce the ionic-strength dependence of sorption.

Experimental data and modeling results in Chapters 4 and 7 showed that a multistage sorption system can significantly reduce Pb and Zn effluent concentrations for the same total amount of sorbent or, alternatively, dramatically lower total sorbent consumption for the same effluent concentration. Model predictions were made using the modified TLM, which was integrated into a steady-state, multistage, equilibrium adsorber model within the OLI Software's Environmental Simulation Program. Engineering screening evaluations indicated that a 2- to 3-stage sorption process can provide significant economic savings when compared to a 1-stage process operating with the same target effluent metal concentration. Additional equilibrium stages beyond 2 or 3 provide diminishing economic returns. The major economic driver for

multiple contacting stages was found to be reduced capital investment and operating costs for sludge handling. dewatering, and disposal.

Finally, Chapter 5 presented and validated a novel uncertainty analysis methodology within the OLI Software for propagating input- and thermodynamic-parameter errors through a surface complexation model. When coupled with the nonlinear equation solver's gain matrix, the linearized local extrapolation and error propagation models in the OLI ElectroChem code provided a satisfactory alternative to a more rigorous, time-consuming Monte Carlo simulation. Using isotherm, pH edge, and multistage treatment data for both metals, 95% confidence intervals were determined for all model predictions. In all cases but a few, the actual data points fell comfortably within the uncertainty bands. In addition, the analyses showed that the input- and thermodynamic-parameter uncertainties that dominated the output uncertainty varied with output parameter type (e.g., Pb_{aq} vs. Pb_{sorb}), pH, and metal surface loading. For one-stage equilibrium calculations for both metals, total ferrihydrite added and log K for the bidentate surface complex were the dominant variables controlling the output uncertainties in Me_{aq} and Me_{sorb} in most cases. Exceptions were at low pH and near site saturation. In addition, for multistage sorption, uncertainties in Me_{aq} and Me_{sorb} for Stages 2 and higher were dominated by the uncertainty in the inlet Pb or Zn concentration to that stage.

This research project, therefore, has shown that existing SCMs appear unable to predict single-solute metal sorption onto 2-line ferrihydrite over a wide range of conditions using a single set of best-fit thermodynamic equilibrium constants. As the models are currently constructed, the surface complexation equilibrium constants and, for Zn, site density must be varied with pH in order to fit the isotherm and pH

edge data. Despite this apparent limitation, however, SCMs will still be valuable tools, for example, in predicting trace metal speciation and removal in multistage ferrihydrite treatment systems.

8.2 Future Research Needs

While many advances have been made over the past decade, much work still needs to be done in fine-tuning the thermodynamic framework and databases for the SCMs. First, additional single-solute metal/ferrihydrite systems should be studied (e.g., Ni, Cr, Cu, etc.) to see if the one-stage and multistage modeling results observed for Pb and Zn are valid for a broad range of metal types. Second, bisolute and trisolute ferrihydrite systems should be investigated in more depth to see if the model parameters for single-solute systems are valid for multisolute systems. The capability to simulate competitive metal sorption in a multistage, flowing system is absent from both commercial and public-domain chemical equilibrium codes. A key objective should also be to determine the range of conditions for which competition for the ferrihydrite surface needs to be considered. Third, more comprehensive data-gathering and modeling studies like the ones described in this dissertation for Pb and Zn are needed for other metal/sorbent systems to test the ability of SCMs to predict metal speciation over a wide range of environmental conditions. Fourth, the inability of a single set of thermodynamic parameters to simulate single-solute Pb and Zn sorption over a wide range of conditions suggests that additional research is needed to validate and, if necessary, modify the thermodynamic framework for the SCMs. This should include a critical review of (1) the definition of standard states for the surface species and surface sites; (2) the approach needed to properly estimate activity coefficients for the surface species as well as for the bulk solution ions; and (3) the apparent need for a

variable site density in some cases. Fifth, technological breakthroughs are needed that will allow for spectroscopic determinations of metal surface speciation at surface loadings that are more typical of the dilute systems encountered in nature and in many industrial systems. Sixth, predictive models must ultimately be developed that will account for the dynamics or time dependency of metal ion movement through a soil or sediment column. The integration of equilibrium SCMs into reactive solute transport models has been rare to-date due to the computational challenges involved.

Appendix A

FERRIHYDRITE POTENTIOMETRIC TITRATION DATA AND SINGLE-SOLUTE LEAD SORPTION DATA

Table A.1 **Raw potentiometric titration data for 2-line ferrihydrite in 0.001 M $NaNO_3$ solution (1 g ferrihydrite/L, 25°C, N_2 glovebox, 1-L reactor, 2-minute equilibration time at each pH point, turbulent hydraulic conditions, $[pH]_o$ = 7.85, 9.3 ml of 0.1-M NaOH used to raise starting pH to 10.415, 0.1 M HNO_3 used to titrate mixture downward to pH ~ 4).**

pH	Acid (ml)	Acid (Equiv.)	pH	Acid (ml)	Acid (Equiv.)
10.415	0	0.00E+00	10.153	3.5	3.50E-04
10.414	0.1	1.00E-05	10.144	3.6	3.60E-04
10.414	0.2	2.00E-05	10.134	3.7	3.70E-04
10.411	0.3	3.00E-05	10.12	3.8	3.80E-04
10.408	0.4	4.00E-05	10.104	3.9	3.90E-04
10.403	0.5	5.00E-05	10.096	4	4.00E-04
10.398	0.6	6.00E-05	10.084	4.1	4.10E-04
10.394	0.7	7.00E-05	10.072	4.2	4.20E-04
10.389	0.8	8.00E-05	10.064	4.3	4.30E-04
10.385	0.9	9.00E-05	10.046	4.4	4.40E-04
10.381	1	1.00E-04	10.031	4.5	4.50E-04
10.375	1.1	1.10E-04	10.019	4.6	4.60E-04
10.368	1.2	1.20E-04	10.007	4.7	4.70E-04
10.36	1.3	1.30E-04	9.997	4.8	4.80E-04
10.353	1.4	1.40E-04	9.98	4.9	4.90E-04
10.345	1.5	1.50E-04	9.959	5	5.00E-04
10.336	1.6	1.60E-04	9.947	5.1	5.10E-04
10.328	1.7	1.70E-04	9.934	5.2	5.20E-04
10.319	1.8	1.80E-04	9.913	5.3	5.30E-04
10.311	1.9	1.90E-04	9.897	5.4	5.40E-04
10.301	2	2.00E-04	9.876	5.5	5.50E-04
10.291	2.1	2.10E-04	9.852	5.6	5.60E-04
10.28	2.2	2.20E-04	9.84	5.7	5.70E-04
10.272	2.3	2.30E-04	9.812	5.8	5.80E-04
10.261	2.4	2.40E-04	9.79	5.9	5.90E-04
10.253	2.5	2.50E-04	9.771	6	6.00E-04
10.243	2.6	2.60E-04	9.745	6.1	6.10E-04
10.234	2.7	2.70E-04	9.722	6.2	6.20E-04
10.225	2.8	2.80E-04	9.698	6.3	6.30E-04
10.216	2.9	2.90E-04	9.674	6.4	6.40E-04
10.207	3	3.00E-04	9.652	6.5	6.50E-04
10.198	3.1	3.10E-04	9.631	6.6	6.60E-04
10.187	3.2	3.20E-04	9.612	6.7	6.70E-04
10.174	3.3	3.30E-04	9.591	6.8	6.80E-04
10.164	3.4	3.40E-04	9.556	6.9	6.90E-04

Table A.1 Continued.

pH	Acid (ml)	Acid (Equiv.)	pH	Acid (ml)	Acid (Equiv.)
9.532	7	7.00E-04	6.111	11	1.10E-03
9.477	7.1	7.10E-04	6.048	11.1	1.11E-03
9.435	7.2	7.20E-04	5.972	11.2	1.12E-03
9.389	7.3	7.30E-04	5.933	11.3	1.13E-03
9.347	7.4	7.40E-04	5.877	11.4	1.14E-03
9.284	7.5	7.50E-04	5.818	11.5	1.15E-03
9.252	7.6	7.60E-04	5.743	11.6	1.16E-03
9.215	7.7	7.70E-04	5.689	11.7	1.17E-03
9.187	7.8	7.80E-04	5.622	11.8	1.18E-03
9.117	7.9	7.90E-04	5.574	11.9	1.19E-03
9.062	8	8.00E-04	5.538	12	1.20E-03
9.027	8.1	8.10E-04	5.485	12.1	1.21E-03
8.952	8.2	8.20E-04	5.415	12.2	1.22E-03
8.883	8.3	8.30E-04	5.376	12.3	1.23E-03
8.832	8.4	8.40E-04	5.308	12.4	1.24E-03
8.768	8.5	8.50E-04	5.247	12.5	1.25E-03
8.726	8.6	8.60E-04	5.203	12.6	1.26E-03
8.662	8.7	8.70E-04	5.131	12.7	1.27E-03
8.581	8.8	8.80E-04	5.07	12.8	1.28E-03
8.445	8.9	8.90E-04	5.011	12.9	1.29E-03
8.381	9	9.00E-04	4.969	13	1.30E-03
8.255	9.1	9.10E-04	4.932	13.1	1.31E-03
8.141	9.2	9.20E-04	4.901	13.2	1.32E-03
7.97	9.3	9.30E-04	4.878	13.3	1.33E-03
7.901	9.4	9.40E-04	4.85	13.4	1.34E-03
7.813	9.5	9.50E-04	4.822	13.5	1.35E-03
7.677	9.6	9.60E-04	4.784	13.6	1.36E-03
7.57	9.7	9.70E-04	4.752	13.7	1.37E-03
7.451	9.8	9.80E-04	4.711	13.8	1.38E-03
7.344	9.9	9.90E-04	4.679	13.9	1.39E-03
7.238	10	1.00E-03	4.641	14	1.40E-03
7.111	10.1	1.01E-03	4.611	14.1	1.41E-03
6.984	10.2	1.02E-03	4.589	14.2	1.42E-03
6.861	10.3	1.03E-03	4.572	14.3	1.43E-03
6.696	10.4	1.04E-03	4.533	14.4	1.44E-03
6.606	10.5	1.05E-03	4.512	14.5	1.45E-03
6.513	10.6	1.06E-03	4.489	14.6	1.46E-03
6.391	10.7	1.07E-03	4.468	14.7	1.47E-03
6.282	10.8	1.08E-03	4.446	14.8	1.48E-03
6.194	10.9	1.09E-03	4.424	14.9	1.49E-03

Table A.1 Continued.

pH	Acid (ml)	Acid (Equiv.)	pH	Acid (ml)	Acid (Equiv.)
4.41	15	1.50E-03	4.162	16.7	1.67E-03
4.389	15.1	1.51E-03	4.15	16.8	1.68E-03
4.375	15.2	1.52E-03	4.137	16.9	1.69E-03
4.361	15.3	1.53E-03	4.128	17	1.70E-03
4.344	15.4	1.54E-03	4.11	17.1	1.71E-03
4.328	15.5	1.55E-03	4.098	17.2	1.72E-03
4.314	15.6	1.56E-03	4.085	17.3	1.73E-03
4.302	15.7	1.57E-03	4.077	17.4	1.74E-03
4.285	15.8	1.58E-03	4.064	17.5	1.75E-03
4.268	15.9	1.59E-03	4.055	17.6	1.76E-03
4.249	16	1.60E-03	4.047	17.7	1.77E-03
4.235	16.1	1.61E-03	4.042	17.8	1.78E-03
4.221	16.2	1.62E-03	4.038	17.9	1.79E-03
4.205	16.3	1.63E-03	4.036	18	1.80E-03
4.194	16.4	1.64E-03	4.034	18.1	1.81E-03
4.186	16.5	1.65E-03	4.034	18.2	1.82E-03
4.175	16.6	1.66E-03			

Table A.2 **Raw potentiometric titration data for 2-line ferrihydrite in 0.01 M $NaNO_3$ solution (1 g ferrihydrite/L, 25°C, N_2 glovebox, 1-L reactor, 2-minute equilibration time at each pH point, turbulent hydraulic conditions, $[pH]_o$ = 7.85, 9.5 ml of 0.1-M NaOH used to raise starting pH to 10.019, 0.1 M HNO_3 used to titrate mixture downward to pH ~ 4).**

pH	Acid (ml)	Acid (Equiv.)	pH	Acid (ml)	Acid (Equiv.)
10.019	0	0	9.691	3.5	0.00035
10.016	0.1	0.00001	9.681	3.6	0.00036
10.012	0.2	0.00002	9.667	3.7	0.00037
10.005	0.3	0.00003	9.652	3.8	0.00038
10	0.4	0.00004	9.64	3.9	0.00039
9.995	0.5	0.00005	9.627	4	0.0004
9.989	0.6	0.00006	9.614	4.1	0.00041
9.98	0.7	0.00007	9.596	4.2	0.00042
9.973	0.8	0.00008	9.581	4.3	0.00043
9.961	0.9	0.00009	9.566	4.4	0.00044
9.955	1	0.0001	9.551	4.5	0.00045
9.948	1.1	0.00011	9.539	4.6	0.00046
9.938	1.2	0.00012	9.525	4.7	0.00047
9.929	1.3	0.00013	9.512	4.8	0.00048
9.921	1.4	0.00014	9.497	4.9	0.00049
9.912	1.5	0.00015	9.478	5	0.0005
9.904	1.6	0.00016	9.463	5.1	0.00051
9.894	1.7	0.00017	9.444	5.2	0.00052
9.884	1.8	0.00018	9.426	5.3	0.00053
9.875	1.9	0.00019	9.407	5.4	0.00054
9.865	2	0.0002	9.392	5.5	0.00055
9.853	2.1	0.00021	9.372	5.6	0.00056
9.844	2.2	0.00022	9.355	5.7	0.00057
9.834	2.3	0.00023	9.336	5.8	0.00058
9.825	2.4	0.00024	9.316	5.9	0.00059
9.813	2.5	0.00025	9.295	6	0.0006
9.804	2.6	0.00026	9.277	6.1	0.00061
9.792	2.7	0.00027	9.252	6.2	0.00062
9.782	2.8	0.00028	9.231	6.3	0.00063
9.769	2.9	0.00029	9.211	6.4	0.00064
9.754	3	0.0003	9.189	6.5	0.00065
9.74	3.1	0.00031	9.167	6.6	0.00066
9.727	3.2	0.00032	9.142	6.7	0.00067
9.717	3.3	0.00033	9.123	6.8	0.00068
9.705	3.4	0.00034	9.094	6.9	0.00069

Table A.2 Continued.

pH	Acid (ml)	Acid (Equiv.)	pH	Acid (ml)	Acid (Equiv.)
9.066	7	0.0007	6.946	11	0.0011
9.04	7.1	0.00071	6.882	11.1	0.00111
9.015	7.2	0.00072	6.833	11.2	0.00112
8.988	7.3	0.00073	6.78	11.3	0.00113
8.957	7.4	0.00074	6.706	11.4	0.00114
8.929	7.5	0.00075	6.652	11.5	0.00115
8.897	7.6	0.00076	6.599	11.6	0.00116
8.863	7.7	0.00077	6.533	11.7	0.00117
8.829	7.8	0.00078	6.481	11.8	0.00118
8.793	7.9	0.00079	6.422	11.9	0.00119
8.755	8	0.0008	6.373	12	0.0012
8.722	8.1	0.00081	6.31	12.1	0.00121
8.685	8.2	0.00082	6.249	12.2	0.00122
8.645	8.3	0.00083	6.194	12.3	0.00123
8.606	8.4	0.00084	6.14	12.4	0.00124
8.562	8.5	0.00085	6.082	12.5	0.00125
8.508	8.6	0.00086	6.031	12.6	0.00126
8.464	8.7	0.00087	5.965	12.7	0.00127
8.41	8.8	0.00088	5.92	12.8	0.00128
8.357	8.9	0.00089	5.864	12.9	0.00129
8.3	9	0.0009	5.807	13	0.0013
8.246	9.1	0.00091	5.749	13.1	0.00131
8.178	9.2	0.00092	5.698	13.2	0.00132
8.111	9.3	0.00093	5.656	13.3	0.00133
8.043	9.4	0.00094	5.6	13.4	0.00134
7.972	9.5	0.00095	5.541	13.5	0.00135
7.904	9.6	0.00096	5.496	13.6	0.00136
7.832	9.7	0.00097	5.454	13.7	0.00137
7.747	9.8	0.00098	5.4	13.8	0.00138
7.673	9.9	0.00099	5.347	13.9	0.00139
7.607	10	0.001	5.3	14	0.0014
7.526	10.1	0.00101	5.264	14.1	0.00141
7.456	10.2	0.00102	5.22	14.2	0.00142
7.375	10.3	0.00103	5.174	14.3	0.00143
7.304	10.4	0.00104	5.137	14.4	0.00144
7.259	10.5	0.00105	5.1	14.5	0.00145
7.198	10.6	0.00106	5.069	14.6	0.00146
7.139	10.7	0.00107	5.019	14.7	0.00147
7.073	10.8	0.00108	4.983	14.8	0.00148
7.018	10.9	0.00109	4.944	14.9	0.00149

Table A.2 Continued.

pH	Acid (ml)	Acid (Equiv.)	pH	Acid (ml)	Acid (Equiv.)
4.912	15	0.0015	4.266	18.1	0.00181
4.885	15.1	0.00151	4.251	18.2	0.00182
4.85	15.2	0.00152	4.238	18.3	0.00183
4.811	15.3	0.00153	4.219	18.4	0.00184
4.774	15.4	0.00154	4.207	18.5	0.00185
4.742	15.5	0.00155	4.196	18.6	0.00186
4.712	15.6	0.00156	4.187	18.7	0.00187
4.688	15.7	0.00157	4.175	18.8	0.00188
4.655	15.8	0.00158	4.165	18.9	0.00189
4.628	15.9	0.00159	4.155	19	0.0019
4.606	16	0.0016	4.144	19.1	0.00191
4.589	16.1	0.00161	4.134	19.2	0.00192
4.569	16.2	0.00162	4.125	19.3	0.00193
4.546	16.3	0.00163	4.115	19.4	0.00194
4.524	16.4	0.00164	4.107	19.5	0.00195
4.509	16.5	0.00165	4.101	19.6	0.00196
4.489	16.6	0.00166	4.096	19.7	0.00197
4.464	16.7	0.00167	4.09	19.8	0.00198
4.44	16.8	0.00168	4.084	19.9	0.00199
4.424	16.9	0.00169	4.078	20	0.002
4.412	17	0.0017	4.073	20.1	0.00201
4.407	17.1	0.00171	4.068	20.2	0.00202
4.393	17.2	0.00172	4.063	20.3	0.00203
4.38	17.3	0.00173	4.058	20.4	0.00204
4.359	17.4	0.00174	4.054	20.5	0.00205
4.342	17.5	0.00175	4.05	20.6	0.00206
4.325	17.6	0.00176	4.047	20.7	0.00207
4.312	17.7	0.00177	4.044	20.8	0.00208
4.298	17.8	0.00178	4.04	20.9	0.00209
4.284	17.9	0.00179	4.04	21	0.0021
4.272	18	0.0018			

Table A.3 **Raw potentiometric titration data for 2-line ferrihydrite in 0.1 M $NaNO_3$ solution (1 g ferrihydrite/L, 25°C, N_2 glovebox, 1-L reactor, 2-minute equilibration time at each pH point, turbulent hydraulic conditions, $[pH]_o$ = 7.85, 9.9 ml of 0.1-M NaOH used to raise starting pH to 9.951, 0.1 M HNO_3 used to titrate mixture downward to pH ~ 4).**

pH	Acid (ml)	Acid (Equiv.)	pH	Acid (ml)	Acid (Equiv.)
9.951	0.000	0.00E+00	9.584	3.500	3.50E-04
9.947	0.100	1.00E-05	9.562	3.600	3.60E-04
9.941	0.200	2.00E-05	9.547	3.700	3.70E-04
9.936	0.300	3.00E-05	9.535	3.800	3.80E-04
9.931	0.400	4.00E-05	9.521	3.900	3.90E-04
9.926	0.500	5.00E-05	9.508	4.000	4.00E-04
9.920	0.600	6.00E-05	9.490	4.100	4.10E-04
9.913	0.700	7.00E-05	9.471	4.200	4.20E-04
9.904	0.800	8.00E-05	9.464	4.300	4.30E-04
9.895	0.900	9.00E-05	9.440	4.400	4.40E-04
9.885	1.000	1.00E-04	9.421	4.500	4.50E-04
9.876	1.100	1.10E-04	9.409	4.600	4.60E-04
9.865	1.200	1.20E-04	9.395	4.700	4.70E-04
9.852	1.300	1.30E-04	9.375	4.800	4.80E-04
9.842	1.400	1.40E-04	9.355	4.900	4.90E-04
9.831	1.500	1.50E-04	9.332	5.000	5.00E-04
9.819	1.600	1.60E-04	9.311	5.100	5.10E-04
9.808	1.700	1.70E-04	9.293	5.200	5.20E-04
9.797	1.800	1.80E-04	9.273	5.300	5.30E-04
9.785	1.900	1.90E-04	9.255	5.400	5.40E-04
9.771	2.000	2.00E-04	9.234	5.500	5.50E-04
9.759	2.100	2.10E-04	9.208	5.600	5.60E-04
9.739	2.200	2.20E-04	9.189	5.700	5.70E-04
9.732	2.300	2.30E-04	9.175	5.800	5.80E-04
9.719	2.400	2.40E-04	9.154	5.900	5.90E-04
9.706	2.500	2.50E-04	9.129	6.000	6.00E-04
9.693	2.600	2.60E-04	9.112	6.100	6.10E-04
9.681	2.700	2.70E-04	9.106	6.200	6.20E-04
9.663	2.800	2.80E-04	9.088	6.300	6.30E-04
9.645	2.900	2.90E-04	9.072	6.400	6.40E-04
9.636	3.000	3.00E-04	9.037	6.500	6.50E-04
9.626	3.100	3.10E-04	9.010	6.600	6.60E-04
9.617	3.200	3.20E-04	8.985	6.700	6.70E-04
9.608	3.300	3.30E-04	8.955	6.800	6.80E-04
9.598	3.400	3.40E-04	8.923	6.900	6.90E-04

Table A.3 Continued.

pH	Acid (ml)	Acid (Equiv.)	pH	Acid (ml)	Acid (Equiv.)
8.906	7.000	7.00E-04	7.544	11.000	1.10E-03
8.877	7.100	7.10E-04	7.501	11.100	1.11E-03
8.854	7.200	7.20E-04	7.455	11.200	1.12E-03
8.841	7.300	7.30E-04	7.414	11.300	1.13E-03
8.802	7.400	7.40E-04	7.370	11.400	1.14E-03
8.746	7.500	7.50E-04	7.328	11.500	1.15E-03
8.685	7.600	7.60E-04	7.281	11.600	1.16E-03
8.649	7.700	7.70E-04	7.238	11.700	1.17E-03
8.622	7.800	7.80E-04	7.179	11.800	1.18E-03
8.599	7.900	7.90E-04	7.129	11.900	1.19E-03
8.541	8.000	8.00E-04	7.072	12.000	1.20E-03
8.522	8.100	8.10E-04	7.023	12.100	1.21E-03
8.488	8.200	8.20E-04	6.959	12.200	1.22E-03
8.455	8.300	8.30E-04	6.909	12.300	1.23E-03
8.420	8.400	8.40E-04	6.861	12.400	1.24E-03
8.387	8.500	8.50E-04	6.810	12.500	1.25E-03
8.353	8.600	8.60E-04	6.762	12.600	1.26E-03
8.340	8.700	8.70E-04	6.707	12.700	1.27E-03
8.321	8.800	8.80E-04	6.654	12.800	1.28E-03
8.298	8.900	8.90E-04	6.595	12.900	1.29E-03
8.280	9.000	9.00E-04	6.532	13.000	1.30E-03
8.244	9.100	9.10E-04	6.476	13.100	1.31E-03
8.215	9.200	9.20E-04	6.428	13.200	1.32E-03
8.191	9.300	9.30E-04	6.375	13.300	1.33E-03
8.170	9.400	9.40E-04	6.315	13.400	1.34E-03
8.136	9.500	9.50E-04	6.255	13.500	1.35E-03
8.102	9.600	9.60E-04	6.205	13.600	1.36E-03
8.075	9.700	9.70E-04	6.153	13.700	1.37E-03
8.049	9.800	9.80E-04	6.101	13.800	1.38E-03
8.003	9.900	9.90E-04	6.054	13.900	1.39E-03
7.954	10.000	1.00E-03	6.006	14.000	1.40E-03
7.905	10.100	1.01E-03	5.960	14.100	1.41E-03
7.855	10.200	1.02E-03	5.917	14.200	1.42E-03
7.812	10.300	1.03E-03	5.852	14.300	1.43E-03
7.770	10.400	1.04E-03	5.816	14.400	1.44E-03
7.736	10.500	1.05E-03	5.757	14.500	1.45E-03
7.701	10.600	1.06E-03	5.702	14.600	1.46E-03
7.665	10.700	1.07E-03	5.663	14.700	1.47E-03
7.631	10.800	1.08E-03	5.616	14.800	1.48E-03
7.589	10.900	1.09E-03	5.571	14.900	1.49E-03

Table A.3 Continued.

pH	Acid (ml)	Acid (Equiv.)	pH	Acid (ml)	Acid (Equiv.)
5.531	15.000	1.50E-03	4.685	19.000	1.90E-03
5.489	15.100	1.51E-03	4.673	19.100	1.91E-03
5.443	15.200	1.52E-03	4.662	19.200	1.92E-03
5.406	15.300	1.53E-03	4.649	19.300	1.93E-03
5.370	15.400	1.54E-03	4.636	19.400	1.94E-03
5.340	15.500	1.55E-03	4.624	19.500	1.95E-03
5.312	15.600	1.56E-03	4.612	19.600	1.96E-03
5.284	15.700	1.57E-03	4.601	19.700	1.97E-03
5.247	15.800	1.58E-03	4.589	19.800	1.98E-03
5.218	15.900	1.59E-03	4.578	19.900	1.99E-03
5.195	16.000	1.60E-03	4.566	20.000	2.00E-03
5.171	16.100	1.61E-03	4.555	20.100	2.01E-03
5.146	16.200	1.62E-03	4.545	20.200	2.02E-03
5.121	16.300	1.63E-03	4.534	20.300	2.03E-03
5.087	16.400	1.64E-03	4.522	20.400	2.04E-03
5.062	16.500	1.65E-03	4.511	20.500	2.05E-03
5.043	16.600	1.66E-03	4.499	20.600	2.06E-03
5.024	16.700	1.67E-03	4.488	20.700	2.07E-03
5.006	16.800	1.68E-03	4.478	20.800	2.08E-03
4.987	16.900	1.69E-03	4.468	20.900	2.09E-03
4.972	17.000	1.70E-03	4.457	21.000	2.10E-03
4.957	17.100	1.71E-03	4.449	21.100	2.11E-03
4.943	17.200	1.72E-03	4.440	21.200	2.12E-03
4.928	17.300	1.73E-03	4.428	21.300	2.13E-03
4.914	17.400	1.74E-03	4.417	21.400	2.14E-03
4.899	17.500	1.75E-03	4.408	21.500	2.15E-03
4.884	17.600	1.76E-03	4.397	21.600	2.16E-03
4.870	17.700	1.77E-03	4.386	21.700	2.17E-03
4.856	17.800	1.78E-03	4.377	21.800	2.18E-03
4.844	17.900	1.79E-03	4.367	21.900	2.19E-03
4.832	18.000	1.80E-03	4.358	22.000	2.20E-03
4.817	18.100	1.81E-03	4.348	22.100	2.21E-03
4.803	18.200	1.82E-03	4.340	22.200	2.22E-03
4.779	18.300	1.83E-03	4.331	22.300	2.23E-03
4.764	18.400	1.84E-03	4.322	22.400	2.24E-03
4.749	18.500	1.85E-03	4.312	22.500	2.25E-03
4.736	18.600	1.86E-03	4.303	22.600	2.26E-03
4.723	18.700	1.87E-03	4.292	22.700	2.27E-03
4.709	18.800	1.88E-03	4.282	22.800	2.28E-03
4.697	18.900	1.89E-03	4.272	22.900	2.29E-03

Table A.3 Continued.

pH	Acid (ml)	Acid (Equiv.)	pH	Acid (ml)	Acid (Equiv.)
4.263	23.000	2.30E-03	4.200	23.800	2.38E-03
4.254	23.100	2.31E-03	4.194	23.900	2.39E-03
4.245	23.200	2.32E-03	4.188	24.000	2.40E-03
4.237	23.300	2.33E-03	4.183	24.100	2.41E-03
4.228	23.400	2.34E-03	4.178	24.200	2.42E-03
4.220	23.500	2.35E-03	4.174	24.300	2.43E-03
4.214	23.600	2.36E-03	4.171	24.400	2.44E-03
4.207	23.700	2.37E-03	4.167	24.500	2.45E-03

Table A.4 Pb/ferrihydrite sorption isotherm data at pH 4.5 (25°C, N_2 glovebox, 0.01 M $NaNO_3$, 4-hr reaction time under turbulent hydraulic conditions).

$[Pb]_0$ (M)	Ferrihydrite Dose (g/L)	[Pb] 4 hr. (ppm)	[Pb] 4 hr. (M)	Γ (mol Pb/mol Fe)
1.00E-03	0.1	1.965E+02	9.486E-04	4.571E-02
8.00E-04	0.1	1.561E+02	7.534E-04	4.138E-02
6.00E-04	0.1	1.163E+02	5.614E-04	3.426E-02
5.00E-04	0.1	9.716E+01	4.689E-04	2.762E-02
4.00E-04	0.1	7.649E+01	3.692E-04	2.740E-02
2.00E-04	0.1	3.754E+01	1.812E-04	1.672E-02
1.00E-04	0.1	1.825E+01	8.808E-05	1.059E-02
1.00E-03	1	1.250E+02	6.033E-04	3.525E-02
8.00E-04	1	9.640E+01	4.653E-04	2.974E-02
5.00E-04	1	5.213E+01	2.516E-04	2.207E-02
1.00E-04	1	8.560E+00	4.131E-05	5.214E-03
5.00E-05	1	4.333E+00	2.091E-05	2.585E-03
1.00E-05	1	8.250E-01	3.982E-06	5.347E-04
5.00E-06	1	4.150E-01	2.003E-06	2.663E-04
1.00E-06	1	7.850E-02	3.789E-07	5.519E-05
5.00E-07	1	3.470E-02	1.675E-07	2.955E-05
5.00E-07	1	3.580E-02	1.728E-07	2.907E-05

Table A.5 Pb/ferrihydrite sorption isotherm data at pH 5.5 (25°C, N_2 glovebox, 0.01 M $NaNO_3$, 4-hr reaction time under turbulent hydraulic conditions).

$[Pb]_0$ (M)	Ferrihydrite Dose (g/L)	[Pb] 4 hr. (ppm)	[Pb] 4 hr. (M)	Γ (mol Pb/mol Fe)
8.00E-04	0.1	8.750E+01	4.223E-04	3.356E-01
6.00E-04	0.1	5.626E+01	2.715E-04	2.919E-01
5.00E-04	0.1	4.266E+01	2.059E-04	2.613E-01
4.00E-04	0.1	3.032E+01	1.463E-04	2.254E-01
2.00E-04	0.1	1.045E+01	5.043E-05	1.329E-01
1.00E-04	0.1	4.270E+00	2.061E-05	7.054E-02
8.00E-04	1	3.980E+00	1.921E-05	6.937E-02
5.00E-04	1	2.070E+00	9.990E-06	4.354E-02
1.00E-04	1	1.860E-01	8.977E-07	8.805E-03
5.00E-05	1	7.110E-02	3.431E-07	4.412E-03
1.00E-05	1	1.120E-02	5.405E-08	8.837E-04
5.00E-06	1	4.000E-03	1.931E-08	4.425E-04
1.00E-06	1	5.000E-04	2.413E-09	8.864E-05
5.00E-07	1	3.000E-04	1.448E-09	4.430E-05
5.00E-07	1	3.000E-04	1.448E-09	4.430E-05

Table A.6 Pb/ferrihydrite sorption isotherm data at pH 6.5 (25°C, N_2 glovebox, 0.01 M $NaNO_3$, 4-hr reaction time under turbulent hydraulic conditions).

$[Pb]_0$ (M)	Ferrihydrite Dose (g/L)	[Pb] 4 hr. (ppm)	[Pb] 4 hr. (M)	Γ (mol Pb/mol Fe)
8.00E-04	0.1	8.377E+01	4.043E-04	3.516E-01
6.00E-04	0.1	4.950E+01	2.389E-04	3.208E-01
5.00E-04	0.1	3.107E+01	1.500E-04	3.110E-01
4.00E-04	0.1	1.042E+01	5.029E-05	3.107E-01
2.00E-04	0.1	2.670E+00	1.289E-05	1.663E-01
1.00E-04	0.1	6.450E-01	3.113E-06	8.609E-02
8.00E-04	1	6.400E-01	3.089E-06	7.081E-02
5.00E-04	1	2.080E-01	1.004E-06	4.434E-02
1.00E-04	1	8.100E-02	3.909E-07	8.850E-03
5.00E-05	1	2.100E-02	1.014E-07	4.434E-03
1.00E-05	1	3.700E-03	1.786E-08	8.869E-04
5.00E-06	1	2.200E-03	1.062E-08	4.433E-04
1.00E-06	1	3.600E-04	1.737E-09	8.870E-05
5.00E-07	1	2.600E-04	1.255E-09	4.431E-05
5.00E-07	1	2.500E-04	1.207E-09	4.432E-05

Table A.7 Pb/ferrihydrite pH sorption edge data for 50 μM Pb, 1 g ferrihydrite/L, and 0.001 M $NaNO_3$ solution (25°C, N_2 glovebox, 4-hr reaction time under turbulent hydraulic conditions).

pH	[Pb] 4 hr. (ppm)	[Pb] 4 hr. (M)	Γ (mol Pb/mol Fe)	% Pb Sorbed
3.11	7.58	3.66E-05	1.19E-03	26.83
3.497	7.37	3.56E-05	1.28E-03	28.86
4.074	6.81	3.29E-05	1.52E-03	34.27
4.516	3.81	1.84E-05	2.81E-03	63.22
4.996	0.69	3.33E-06	4.15E-03	93.34
5.503	0.08	3.86E-07	4.41E-03	99.23
6.104	0.06	2.90E-07	4.42E-03	99.42
7.062	0.05	2.41E-07	4.42E-03	99.52

Table A.8 Pb/ferrihydrite pH sorption edge data for 50 μM Pb, 1 g ferrihydrite/L, and 0.01 M $NaNO_3$ solution (25°C, N_2 glovebox, 4-hr reaction time under turbulent hydraulic conditions).

pH	[Pb] 4 hr. (ppm)	[Pb] 4 hr. (M)	Γ (mol Pb/mol Fe)	% Pb Sorbed
3.041	8.29	4.00E-05	8.88E-04	19.98
3.521	7.72	3.73E-05	1.13E-03	25.48
4.009	6.75	3.26E-05	1.55E-03	34.85
4.552	4.32	2.08E-05	2.59E-03	58.30
4.76	2.87	1.39E-05	3.21E-03	72.30
5.011	0.82	3.96E-06	4.09E-03	92.08
5.503	0.071	3.43E-07	4.41E-03	99.31
5.528	0.08	3.86E-07	4.41E-03	99.23
6.077	0.05	2.41E-07	4.42E-03	99.52
6.989	0.06	2.90E-07	4.42E-03	99.42

Table A.9 Pb/ferrihydrite pH sorption edge data for 50 μM Pb, 1 g ferrihydrite/L, and 0.1 M $NaNO_3$ solution (25°C, N_2 glovebox, 4-hr reaction time under turbulent hydraulic conditions).

pH	[Pb] 4 hr. (ppm)	[Pb] 4 hr. (M)	Γ (mol Pb/mol Fe)	% Pb Sorbed
3.517	8.205	3.96E-05	9.2411E-04	20.80
4.004	7.351	3.55E-05	1.2903E-03	29.04
4.511	5.248	2.53E-05	2.1921E-03	49.34
4.752	3.069	1.48E-05	3.1265E-03	70.38
5.003	0.805	3.89E-06	4.0974E-03	92.23
5.499	0.05	2.41E-07	4.4212E-03	99.52
6.045	0.04	1.93E-07	4.4254E-03	99.61
7.025	0.03	1.45E-07	4.4297E-03	99.71

Table A.10 Pb/ferrihydrite pH sorption edge data for 0.5 μM Pb, 1 g ferrihydrite/L, and 0.01 M $NaNO_3$ solution (25°C, N_2 glovebox, 4-hr reaction time under turbulent hydraulic conditions).

pH	[Pb] 4 hr. (ppm)	[Pb] 4 hr. (M)	Γ (mol Pb/mol Fe)	% Pb Sorbed
3.523	0.07333	3.54E-07	1.30E-05	29.22
4	0.06835	3.30E-07	1.51E-05	34.03
4.499	0.03995	1.93E-07	2.73E-05	61.44
4.748	0.02684	1.30E-07	3.29E-05	74.09
5.003	0.00735	3.55E-08	4.13E-05	92.91
5.493	0.0005	2.41E-09	4.42E-05	99.52
6.008	0.0004	1.93E-09	4.43E-05	99.61
6.512	0.0002	9.65E-10	4.43E-05	99.81

Table A.11 Pb/ferrihydrite pH sorption edge data for 800 μM Pb, 1 g ferrihydrite/L, and 0.01 M $NaNO_3$ solution (25°C, N_2 glovebox, 4-hr reaction time under turbulent hydraulic conditions).

pH	[Pb] 4 hr. (ppm)	[Pb] 4 hr. (M)	Γ (mol Pb/mol Fe)	% Pb Sorbed
3.516	130.33	6.29E-04	1.52E-02	21.37
4.004	121.75	5.88E-04	1.89E-02	26.55
4.496	95.84	4.63E-04	3.00E-02	42.18
4.71	56.12	2.71E-04	4.70E-02	66.14
5.007	14.5	7.00E-05	6.49E-02	91.25
5.504	4.02	1.94E-05	6.94E-02	97.57
5.995	1.48	7.14E-06	7.04E-02	99.11
6.488	0.61	2.94E-06	7.08E-02	99.63
6.474	0.69	3.33E-06	7.08E-02	99.58

Table A.12 Pb/ferrihydrite pH sorption edge data for 800 μM Pb, 0.1 g ferrihydrite/L, and 0.01 M $NaNO_3$ solution (25°C, N_2 glovebox, 4-hr reaction time under turbulent hydraulic conditions).

pH	[Pb] 4 hr. (ppm)	[Pb] 4 hr. (M)	Γ (mol Pb/mol Fe)	% Pb Sorbed
3.497	161.11	7.78E-04	1.99E-02	2.81
4.074	157.99	7.63E-04	3.33E-02	4.69
4.516	154.96	7.48E-04	4.63E-02	6.52
4.996	120.25	5.80E-04	1.95E-01	27.46
5.503	88.58	4.28E-04	3.31E-01	46.56
5.997	85	4.10E-04	3.46E-01	48.72
6.506	83.12	4.01E-04	3.54E-01	49.86

Appendix B

MULTISTAGE LEAD SORPTION DATA

Table B.1 Pb/ferrihydrite multistage sorption data at pH 5.5 (25°C, N_2 glovebox, 0.01 M $NaNO_3$, 4-hr reaction time under turbulent hydraulic conditions, 0.1 M NaOH or HNO_3 to adjust pH, centrifuged at 12,000 rpm for 20 minutes).

Case	Stage #	g ferrihydrite/L in each stage	Stg. 1 Pb Feed Conc. (ppm)	Pb Effluent Measured
1A	1	1.0	103.6	2.065 ppm 2.153 ppm 2.044 ppm
1B	1	0.5	103.6	9.975 ppm 10.650 ppm 9.314 ppm
	2	0.5		129.000 ppb 132.000 ppb 122.000 ppb
2A	1	4.65	10.36	14.760 ppb 10.900 ppb 15.500 ppb
2B	1	0.253	10.36	340.260 ppb 310.500 ppb 319.250 ppb
	2	0.253		6.300 ppb 4.320 ppb 0.122 ppb
3A	1	0.4	103.6	11.125 ppm 12.075 ppm 11.640 ppm
3B	1	0.2	103.6	22.600 ppm 21.795 ppm 21.750 ppm
	2	0.2		1.605 ppm 1.638 ppm 1.598 ppm

Table B.1 Continued.

Case	Stage #	g ferrihydrite/L in each stage	Stg. 1 Pb Feed Conc. (ppm)	Pb Effluent Measured
3C	1	0.1	103.6	41.280 ppm 40.548 ppm 41.035 ppm
	2	0.1		8.290 ppm 8.000 ppm 8.220 ppm
	3	0.1		402.400 ppb 388.250 ppb 393.750 ppb
	4	0.1		5.770 ppb 6.275 ppb 6.166 ppb

Appendix C

ENGINEERING EVALUATION RESULTS FOR MULTISTAGE LEAD SORPTION ONTO FERRIHYDRITE

Engineering Evaluation for Multistage Lead Sorption Onto Ferrihydrite
Equipment Design Bases and Scopes-of-Work

Design Bases

pH	5.5
Volumetric Flowrate (gpm)	100
Ionic Strength (molal)	0.01
Plant Utility (%)	90

Equalization facilities already provided
1.83 g $FeCl_3$ (100% basis)/g Ferrihydrite

Case	# Stages	Pb Feed Conc. (ppm)	Ferrihyd. Dose/ Stage (g/L)	FeCl3 Dose/ Stage (g/L)
1A	1	103.6	1	1.83
1B	2	103.6	0.5	0.92
2A	1	10.36	4.65	8.51
2B	2	10.36	0.253	0.46
2C	3	10.36	0.08	0.15
3A	1	103.6	0.4	0.73
3B	2	103.6	0.2	0.37
3C	4	103.6	0.1	0.18

1) Wastewater Feed Pumps

Equipment Type:	Centrifugal Feed Pumps	
Design Basis:	100	ft TDH
	63	% Efficiency
	Installed Spare + 20% Overdesign	
MOC	316 S/S	

Case	# Pumps	Flow (gpm)	Total HP	Total KWH/yr
1A	2	120	5	28,300
1B	2	120	5	28,300
2A	2	120	5	28,300
2B	2	120	5	28,300
2C	2	120	5	28,300
3A	2	120	5	28,300
3B	2	120	5	28,300
3C	2	120	5	28,300

Figure C.1 Facility scopes-of-work for multistage Pb sorption case studies.

2) Reactor Clarifier

Equipment Type: Upflow Solids Contact Clarifier
Design Basis: 1000 gal/ft^2 day
2 hour detention time minimum
0.1 hp/1000 gallons agitation
MOC: Epoxy-coated carbon steel or reinforced concrete

Case	# Clarifiers	Area (ft^2)	Diam. (ft)	Depth (ft)	Holdup Time (hr)	Agitator (KWH/yr)	Bare Equipment Cost ($1000)*
1A	1	144	14	12	2.2	7600	85
1B	2	144	14	12	2.2	15199	170
2A	1	144	14	12	2.2	7600	85
2B	2	144	14	12	2.2	15199	170
2C	3	144	14	12	2.2	22799	255
3A	1	144	14	12	2.2	7600	85
3B	2	144	14	12	2.2	15199	170
3C	4	144	14	12	2.2	30398	340

* Gumerman, Burris, and Hansen (1986) Small Water System Treatment Costs. Noyes Data Corporation, Park Ridge, NJ, pg. 397.

3) 30 wt% $FeCl_3$ Storage Tank

Equipment Type: Aboveground Fixed Roof Storage Tank
21 Minimum Days Storage
10 % Freeboard
MOC: FRP

Case	$FeCl_3$ Dose/ Stage (g/L)	30 wt% $FeCl_3$ Soln. (gal/yr)	$FeCl_3$ Use (lb/yr, 100% basis)	21-Day Capacity (gal)	Tank Size (gal)
1A	1.83	26.6	722,400	13,386	15,000
1B	0.92	26.6	722,400	13,386	15,000
2A	8.51	123.5	3,359,300	62,247	70,000
2B	0.46	13.4	365,600	6,774	8,000
2C	0.15	6.4	173,400	3,213	4,000
3A	0.73	10.6	289,000	5,355	6,000
3B	0.37	10.6	289,000	5,355	6,000
3C	0.18	10.6	289,000	5,355	6,000

Figure C.1 Continued.

4) 30 wt% $FeCl_3$ Feed Pumps

Equipment Type: Diaphragm Metering Pumps
Design Basis: 50 psi
40 % Efficiency
Installed Spare + 20% Overdesign
MOC: 304 S/S

Case	# Pumps	Pump Size (gph) @	Total HP	Total KWH/yr
1A	2	32	0.04	229
1B	3	16	0.04	229
2A	2	149	0.18	1065
2B	3	9	0.02	129
2C	4	3	0.01	64
3A	2	13	0.02	93
3B	3	7	0.02	100
3C	5	4	0.02	114

5) NaOH Feed Pumps

$FeCl_3 + 3NaOH = Fe(OH)_3 + 3NaCl$

Equipment Type: Diaphragm Metering Pumps
Design Basis: 50 psi
40 % Efficiency
Installed Spare + 20% Overdesign
MOC: C/S

Case	# Pumps	NaOH Use (lb/yr 100% basis)	50% NaOH (gal/hr)	Pump Size (gph)	Total HP	Total KWH/yr	Filtered Water (Mgal/yr)
1A	2	534,600	10.8	13	0.016	93	192
1B	3	534,600	10.8	7	0.017	100	192
2A	2	2,485,900	50.3	61	0.074	436	893
2B	3	270,500	5.5	4	0.010	57	97
2C	4	128,300	2.6	2	0.007	43	46
3A	2	213,800	4.3	6	0.007	43	77
3B	3	213,800	4.3	3	0.007	43	77
3C	5	213,800	4.3	2	0.010	57	77

Figure C.1 Continued.

6) 50 wt% NaOH Storage Tank

Equipment Type: Aboveground Fixed Roof Storage Tank, Insulated and Heated
30 Minimum Days Storage
10 % Freeboard
MOC: C/S

Case	30-Day Capacity (gal)	Tank Size (gal)
1A	7,796	9,000
1B	7,796	9,000
2A	36,251	41,000
2B	3,945	5,000
2C	1,871	3,000
3A	3,118	4,000
3B	3,118	4,000
3C	3,118	4,000

7) Emulsion Polymer Feed System

Equipment Type: Skid-Mounted Polyblend System
Design Basis: 0.1 wt% polymer solution after dilution
10:1 dilution of stock polymer solution downstream of metering pump
50 psi pump discharge
40 % Pump Efficiency
20% Overdesign
MOC: Polyethylene

Case	lb Polymer/ lb Feed Solids	Avg. Total Solids (includes Pb) Stage (wt%)	mg/L Polymer/ Stage	Total lb/day polymer (100% basis)	Total lb/yr Polymer (100% basis)	lb/hr Conc. Polymer Solution/ Stage	Skid-Mounted Equipment Cost ($1000)
1A	0.005	1.104	6	6.6	2175	28	10
1B	0.006	0.552	3	7.9	2610	17	10
2A	0.004	4.660	19	22.4	7348	93	20
2B	0.007	0.258	2	4.3	1425	9	10
2C	0.008	0.083	1	2.4	790	3	10
3A	0.006	0.504	3	3.6	1191	15	10
3B	0.007	0.252	2	4.2	1390	9	10
3C	0.008	0.126	1	4.8	1588	5	10

Figure C.1 Continued.

Case	# Pumps	Pump Size (gph)	Total HP	Total KWH/yr	Filtered Water (Mgal/yr)
1A	1	4	0.005	28	26
1B	2	2	0.006	34	15
2A	1	13	0.016	96	87
2B	2	1	0.003	19	8
2C	3	0	0.002	10	3
3A	1	2	0.003	16	14
3B	2	1	0.003	18	8
3C	4	1	0.004	21	5

8) pH Control Systems

Design Basis: 1 system per reaction stage
Allow $12,000 capital (uninstalled)/system

Case	# Systems	Cont. Instrumentation Equipment Cost ($1000)
1A	1	12
1B	2	24
2A	1	12
2B	2	24
2C	3	36
3A	1	12
3B	2	24
3C	4	48

Figure C.1 Continued.

9) Clarifier Underflow Pumps

Equipment Type: Progressive Cavity/Centrifugal
Design Basis: 100 ft TDH
30 % Efficiency
Installed Spare + 20% Overdesign
MOC: 316 S/S

Case	# Pumps	Avg. Total Solids (Includes PBV Stage) (g/L)	Underflow Conc. (wt%)	Sludge Flow (gph)	Pump Size (gph)	Total HP	Total KWH/yr
1A	2	1.104	4	161	193	0.3	1638
1B	3	0.552	3	107	129	0.4	2185
2A	2	4.660	6	452	543	0.8	4613
2B	3	0.258	3	50	60	0.2	1022
2C	4	0.083	2	24	29	0.1	743
3A	2	0.504	3	98	117	0.2	997
3B	3	0.252	3	49	59	0.2	997
3C	5	0.126	2	37	44	0.3	1495

10) Clarifier Overflow Pumps

Equipment Type: Centrifugal
Design Basis: 100 ft TDH
63 % Efficiency
Installed Spare + 20% Overdesign
MOC: 316 S/S

Case	# Pumps	Pump Size (gpm)	Total HP	Total KWH/yr
1A	2	120	5	28,300
1B	3	120	10	56,600
2A	2	120	5	28,300
2B	3	120	10	56,600
2C	4	120	14	84,800
3A	2	120	5	28,300
3B	3	120	10	56,600
3C	5	120	19	113,100

Figure C.1 Continued.

11) Sludge Storage Tank

Equipment Type:	Aboveground Fixed Roof Storage Tank, Agitated	
	1	Days Storage
	10	% Freeboard
	0.5	hp/1000 gallons
MOC:	FRP Tank, 304 S/S Agitator	

Case	Capacity (gal)	Tank Size (gal)	Agitator (hp)	Total KWH/yr
1A	3,857	4,300	2	12640
1B	5,143	6,000	3	17637
2A	10,859	13,000	7	38214
2B	2,406	3,000	2	8819
2C	1,750	2,000	1	5879
3A	2,347	3,000	2	8819
3B	2,347	3,000	2	8819
3C	3,520	4,000	2	11758

12) Filter Feed Pump

Equipment Type:	Progressive Cavity/Centrifugal	
Design Basis:	75	psi
	30	% Efficiency
	20% Overdesign	
MOC:	304 S/S	

Case	# Pumps	gpm/ft² filter area	Pump Size (gpm)	Total HP	Total KWH/yr
1A	1	0.36	5	0.76	2965
1B	1	0.47	7	0.99	3884
2A	1	0.26	15	2.20	8642
2B	1	0.35	3	0.46	1817
2C	1	0.47	2	0.33	1298
3A	1	0.34	3	0.45	1772
3B	1	0.34	3	0.45	1772
3C	1	0.51	5	0.67	2611

Figure C.1 Continued.

13) Membrane Pressure Filters

Equipment Type:	Oberlin Filter Press (batch cycle)	
Design Basis:	15	cycle time (min.)
	96	cycle/day
	0.35	lb/Maxflo filter aid/lb dry solids
	40	% solids of dewatered sludge
	81	lb/ft^3 dewatered sludge wet bulk density
	0.75	dewatered sludge thickness (in.)
	20	KWH/yr per ft^2 building for lighting, H&V, etc.
	0.2	KW/ft^2 filter area
	3	# cycles before filter cloth replacement

Case	Total Solids (lb/hr)	Total Solids + Maxflo (lb/hr)	Total Slurry Feed (gph)	Dewatered Sludge (lb/hr)	Dewatered Sludge (lb/yr)	Dewatered Sludge (ft^3/yr)	Filtrate (lb/hr)
1A	55	75	173	187	1,471,000	18,160	1309
1B	55	75	226	187	1,471,000	18,160	1770
2A	233	315	504	788	6,213,000	76,704	3584
2B	26	35	106	87	688,000	8,494	828
2C	13	17	76	42	334,000	4,123	611
3A	25	34	103	85	671,000	8,284	808
3B	25	34	103	85	671,000	8,284	808
3C	25	34	152	85	671,000	8,284	1228

Case	Filtrate (gal/day)	Dewatered Sludge (ft^3/Cycle)	Filter Area/ Cycle (ft^2)	# and Size Filter Presses	Total Filter Area (ft^2)	avg. gpm/ft^2 filter	Building Size (ft^2)
1A	3764	0.58	9	1-12 ft^2	12	0.24	500
1B	5088	0.58	9	1-12 ft^2	12	0.31	500
2A	10302	2.43	39	1-48 ft^2	48	0.17	750
2B	2381	0.27	4	1-7.5 ft^2	7.5	0.24	400
2C	1755	0.13	2	1-4 ft^2	4	0.32	400
3A	2322	0.26	4	1-7.5 ft^2	7.5	0.23	400
3B	2322	0.26	4	1-7.5 ft^2	7.5	0.23	400
3C	3530	0.26	4	1-7.5 ft^2	7.5	0.34	400

Figure C.1 Continued.

Case	Bare Equipment Cost ($1000)	Electricity (KWH/yr)	Pump Time for Slurry (min)	Filter Cloth Usage (ft^2/yr)
1A	135	24,191	10	126,018
1B	135	22,614	10	126,018
2A	300	65,458	10	504,071
2B	115	15,884	10	78,761
2C	100	12,205	10	42,006
3A	115	15,884	10	78,761
3B	115	15,884	10	78,761
3C	115	15,884	10	78,761

14) Maxflo Feed System

Purpose: Filter Aid
Equipment: Hopper & Conveyor, Monorail for Supersacs, Mix Tank w/ Agitator, Dust Collector, Slurry Feed Pump, and Static Mixer
17 % Solids Slurry

Case	Total Solids (lb/hr)	Maxflo (lb/hr)	Maxflo (lb/yr)	Maxflo Slurry (lb/hr)	Maxflo Slurry (gph)	Bare Equipment Cost ($1000)	Electricity (KWH/yr)
1A	55	19	152,600	114	12	30	5,995
1B	55	19	152,600	114	12	30	5,995
2A	233	82	644,300	481	51	40	6,369
2B	26	9	71,400	53	6	25	5,933
2C	13	4	34,600	26	3	25	5,905
3A	25	9	69,600	52	6	25	5,932
3B	25	9	69,600	52	6	25	5,932
3C	25	9	69,600	52	6	25	5,932

Figure C.1 Continued.

15) Filtrate Tank

Equipment Type: Aboveground Fixed Roof Storage Tank
1 Days Storage
10 % Freeboard
MOC: FRP

Case	Capacity (gal)	Tank Size (gal)
1A	3,764	4,200
1B	5,088	5,700
2A	10,302	11,500
2B	2,381	2,700
2C	1,755	2,000
3A	2,322	2,600
3B	2,322	2,600
3C	3,530	4,000

16) Filtrate Pump

Equipment Type: Centrifugal Pump
Design Basis: 100 ft TDH
63 % Efficiency
20% Overdesign
MOC: 316 S/S

Case	# Pumps	Flow (gpm)	Total HP	Total KWH/yr
1A	1	170	7	696
1B	1	230	9	941
2A	1	330	13	1890
2B	1	110	4	450
2C	1	80	3	327
3A	1	100	4	409
3B	1	100	4	409
3C	1	160	6	655

Figure C.1 Continued.

17) Dumpsters

Equipment Type: 4' x 6' x 12' dumpsters (288 ft^3)

Case	Sludge (ft^3/day)	#Dump-sters	Project Level Cost ($1000)
1A	55	2	20
1B	55	2	20
2A	233	6	60
2B	26	1	10
2C	13	1	10
3A	25	1	10
3B	25	1	10
3C	25	1	10

Figure C.1 Continued.

Engineering Evaluation for Multistage Lead Sorption Onto Ferrihydrite
Operating and Maintenance Requirements Summary

Case	$FeCl_3$ (lb/yr)	50% NaOH (lb/yr)	Emulsion Polymer (lb/yr)	Maxflo (lb/yr)	Filter Cloth (ft^2/yr)	Electricity (kWh/yr)	Power (kW)	Sludge Disposal (lb/yr)
1A	722,400	534,600	2175	152,600	126,018	112,675	14	1,471,000
1B	722,400	534,600	2610	152,600	126,018	153,718	19	1,471,000
2A	3,359,300	2,485,900	7348	644,300	504,071	190,981	24	6,213,000
2B	365,600	270,500	1425	71,400	78,761	134,229	17	688,000
2C	173,400	128,300	790	34,600	42,006	162,374	21	334,000
3A	289,000	213,800	1191	69,600	78,761	98,164	12	671,000
3B	289,000	213,800	1390	69,600	78,761	134,073	17	671,000
3C	289,000	213,800	1588	69,600	78,761	210,325	27	671,000

Case	Filtered Water (Mgal/yr)
1A	654
1B	622
2A	2,941
2B	317
2C	147
3A	273
3B	255
3C	244

Material	Cost	Unit for Cost	Basis for Cost
30% $FeCl_3$	0.15	$/lb	100% basis
50% NaOH	0.15	$/lb	100% basis
Emulsion Polymer	1.50	$/lb	100% basis
Maxflo	0.165	$/lb	100% basis
Filter Cloth	0.095	$/$ft^2$	100% basis
Filtered Water	0.15	$/lb	100% basis
Electricity	0.045	$/kWh	100% basis
Hazardous Waste Landfill Disposal	0.085	$/lb	100% basis

Figure C.2 Operating requirements and raw material costs for multistage Pb sorption case studies.

Research Guidance Appraisal

TITLE: Pb Multistage Sorption RGA NAME: Case 1A
CASE NUMBER: Case 1A ACCT NUM:
SCOPE: SITE: Gulf Coast

	Factor %	$M	
ENGINEERED EQUIPMENT		330	EE,TK,COL, HX,PMP,AGIT
RELOCATED/EXISTING EQUIPMENT		0	EX,REL
MISC EQUIPMENT	5	17	
EQUIPMENT SUBTOTAL		347	
FIELD MTL/LABOR/INSUL 3 10 4 17		59	
FIELD ERECTED EQUIPMENT		85	FE
FACTORED FDNS,SUP,PLT	7	24	
IDENTIFIED FDNS,SUP,PLT		0	FSP
EXISTING IN PLACE EQUIPMENT		0	EIP
INSTALLED EQUIPMENT SUBTOTAL		515	
FACTORED PIPING	45	232	
FACTORED INSTRUMENTS	16	82	
FACTORED ELECTRICAL	11	57	
IDENTIFIED PIPING		0	PIPE
IDENTIFIED INSTRUMENTS		12	INSTR
IDENTIFIED ELECTRICAL		0	ELECT
MCC/ICR/ECR EQUIP	6	31	
CONNECTED SUBTOTAL		929	
SPECIAL PROCESS ITEMS		62	SPE
PACKING		0	PACK
OTHER		0	LM
IDENTIFIED BUILDINGS,STRUCTURES		51	BLDG
ISBL SUBTOTAL		1042	
IDENTIFIED PG&S		0	PG&S
FACTORED PG&S	10	104	
IDENTIFIED D&R		0	D&R
FACTORED D&R	2	21	
OSBL INCLUDED SUBTOTAL		1167	
PROJECT CONTINGENCY	15	175	
PROCESS CONTINGENCY	10	117	
DEVELOPED SUBTOTAL		1459	

Figure C.3 Factored investment estimate for multistage Pb sorption Case 1A.

DEVELOPED SUBTOTAL		1459	
LABOR/MATERIAL SPLIT	25		
WORKING CONDITIONS	10	37	
FREIGHT,QA,PROCUREMENT,SALES TAX	11	120	

NET TOTAL		1616	
ABNORMAL PREMIUM TIME	0	0	
MINOR CHANGES	2	32	

DIRECT TOTAL		1648	
ENGG & HOME OFFICE	20	458	
FIELD INDIRECTS	8	183	
SPARES & PORTABLES		20	SPARE,PORT
PROJECT LEVEL ALLOWANCES		0	PROJ
CREDIT FOR EXISTING EQUIPMENT		0	
(INCL CONT,FRT,TAX,QA,PROC)		---	
CURRENT COST		2309	
LOCATION FACTOR	1.00	2309	
ESCALATION TO MPC	1.02	2355	
AUTH 1Q2002 MPC 4Q2002 M/C 2Q2003			
COUNTRY CURRENCY REVALUATION	1.00	2355	
PROJECT COST SAY		2400	

Figure C.3 Continued.

Research Guidance Appraisal

TITLE: Pb Multistage Sorption RGA NAME: Case 1B
CASE NUMBER: Case 1B ACCT NUM:
SCOPE: SITE: Gulf Coast

	Factor %	$M	
ENGINEERED EQUIPMENT		352	EE,TK,COL, HX,PMP,AGIT
RELOCATED/EXISTING EQUIPMENT		0	EX,REL
MISC EQUIPMENT	5	18	
EQUIPMENT SUBTOTAL		370	
FIELD MTL/LABOR/INSUL	3 10 4 17	63	
FIELD ERECTED EQUIPMENT		170	FE
FACTORED FDNS,SUP,PLT	7	26	
IDENTIFIED FDNS,SUP,PLT		0	FSP
EXISTING IN PLACE EQUIPMENT		0	EIP
INSTALLED EQUIPMENT SUBTOTAL		629	
FACTORED PIPING	45	283	
FACTORED INSTRUMENTS	16	101	
FACTORED ELECTRICAL	11	69	
IDENTIFIED PIPING		0	PIPE
IDENTIFIED INSTRUMENTS		24	INSTR
IDENTIFIED ELECTRICAL		0	ELECT
MCC/ICR/ECR EQUIP	6	38	
CONNECTED SUBTOTAL		1144	
SPECIAL PROCESS ITEMS		62	SPE
PACKING		0	PACK
OTHER		0	LM
IDENTIFIED BUILDINGS,STRUCTURES		51	BLDG
ISBL SUBTOTAL		1257	
IDENTIFIED PG&S		0	PG&S
FACTORED PG&S	10	126	
IDENTIFIED D&R		0	D&R
FACTORED D&R	2	25	
OSBL INCLUDED SUBTOTAL		1408	
PROJECT CONTINGENCY	15	211	
PROCESS CONTINGENCY	10	141	
DEVELOPED SUBTOTAL		1760	

Figure C.4 Factored investment estimate for multistage Pb sorption Case 1B.

DEVELOPED SUBTOTAL		1760	
LABOR/MATERIAL SPLIT	25		
WORKING CONDITIONS	10	44	
FREIGHT,QA,PROCUREMENT,SALES TAX	11	145	
NET TOTAL		1949	
ABNORMAL PREMIUM TIME	0	0	
MINOR CHANGES	2	39	
DIRECT TOTAL		1988	
ENGG & HOME OFFICE	20	552	
FIELD INDIRECTS	8	221	
SPARES & PORTABLES		20	SPARE,PORT
PROJECT LEVEL ALLOWANCES		0	PROJ
CREDIT FOR EXISTING EQUIPMENT (INCL CONT,FRT,TAX,QA,PROC)		0	
CURRENT COST		2781	
LOCATION FACTOR	1.00	2781	
ESCALATION TO MPC	1.02	2837	
AUTH 1Q2002 MPC 4Q2002 M/C 2Q2003			
COUNTRY CURRENCY REVALUATION	1.00	2837	
PROJECT COST SAY		2800	

Figure C.4 Continued.

Research Guidance Appraisal

TITLE: Pb Multistage Sorption RGA NAME: Case 2A
CASE NUMBER: Case 2A ACCT NUM:
SCOPE: SITE: Gulf Coast

	Factor %	$M	
ENGINEERED EQUIPMENT		634	EE,TK,COL, HX,PMP,AGIT
RELOCATED/EXISTING EQUIPMENT		0	EX,REL
MISC EQUIPMENT	5	32	
EQUIPMENT SUBTOTAL		666	
FIELD MTL/LABOR/INSUL	3 10 4 17	113	
FIELD ERECTED EQUIPMENT		85	FE
FACTORED FDNS,SUP,PLT	7	47	
IDENTIFIED FDNS,SUP,PLT		0	FSP
EXISTING IN PLACE EQUIPMENT		0	EIP
INSTALLED EQUIPMENT SUBTOTAL		911	
FACTORED PIPING	45	410	
FACTORED INSTRUMENTS	16	146	
FACTORED ELECTRICAL	11	100	
IDENTIFIED PIPING		0	PIPE
IDENTIFIED INSTRUMENTS		12	INSTR
IDENTIFIED ELECTRICAL		0	ELECT
MCC/ICR/ECR EQUIP	6	55	
CONNECTED SUBTOTAL		1634	
SPECIAL PROCESS ITEMS		93	SPE
PACKING		0	PACK
OTHER		0	LM
IDENTIFIED BUILDINGS,STRUCTURES		77	BLDG
ISBL SUBTOTAL		1804	
IDENTIFIED PG&S		0	PG&S
FACTORED PG&S	10	180	
IDENTIFIED D&R		0	D&R
FACTORED D&R	2	36	
OSBL INCLUDED SUBTOTAL		2020	
PROJECT CONTINGENCY	15	303	
PROCESS CONTINGENCY	10	202	
DEVELOPED SUBTOTAL		2525	

Figure C.5 Factored investment estimate for multistage Pb sorption Case 2A.

DEVELOPED SUBTOTAL		2525	
LABOR/MATERIAL SPLIT	25		
WORKING CONDITIONS	10	63	
FREIGHT,QA,PROCUREMENT,SALES TAX	11	208	
NET TOTAL		2796	
ABNORMAL PREMIUM TIME	0	0	
MINOR CHANGES	2	56	
DIRECT TOTAL		2852	
ENGG & HOME OFFICE	20	792	
FIELD INDIRECTS	8	317	
SPARES & PORTABLES		60	SPARE,PORT
PROJECT LEVEL ALLOWANCES		0	PROJ
CREDIT FOR EXISTING EQUIPMENT (INCL CONT,FRT,TAX,QA,PROC)		0	
CURRENT COST		4021	
LOCATION FACTOR	1.00	4021	
ESCALATION TO MPC AUTH 1Q2002 MPC 4Q2002 M/C 2Q2003	1.02	4101	
COUNTRY CURRENCY REVALUATION	1.00	4101	
PROJECT COST SAY		4100	

Figure C.5 Continued.

Research Guidance Appraisal

TITLE: Pb Multistage Sorption RGA NAME: Case 2B
CASE NUMBER: Case 2B ACCT NUM:
SCOPE: SITE: Gulf Coast

	Factor %	$M	
ENGINEERED EQUIPMENT		296	EE,TK,COL, HX,PMP,AGIT
RELOCATED/EXISTING EQUIPMENT		0	EX,REL
MISC EQUIPMENT	5	15	
EQUIPMENT SUBTOTAL		311	
FIELD MTL/LABOR/INSUL 3 10 4 17		53	
FIELD ERECTED EQUIPMENT		170	FE
FACTORED FDNS,SUP,PLT	7	22	
IDENTIFIED FDNS,SUP,PLT		0	FSP
EXISTING IN PLACE EQUIPMENT		0	EIP
INSTALLED EQUIPMENT SUBTOTAL		556	
FACTORED PIPING	45	250	
FACTORED INSTRUMENTS	16	89	
FACTORED ELECTRICAL	11	61	
IDENTIFIED PIPING		0	PIPE
IDENTIFIED INSTRUMENTS		24	INSTR
IDENTIFIED ELECTRICAL		0	ELECT
MCC/ICR/ECR EQUIP	6	33	
CONNECTED SUBTOTAL		1013	
SPECIAL PROCESS ITEMS		54	SPE
PACKING		0	PACK
OTHER		0	LM
IDENTIFIED BUILDINGS,STRUCTURES		41	BLDG
ISBL SUBTOTAL		1108	
IDENTIFIED PG&S		0	PG&S
FACTORED PG&S	10	111	
IDENTIFIED D&R		0	D&R
FACTORED D&R	2	22	
OSBL INCLUDED SUBTOTAL		1241	
PROJECT CONTINGENCY	15	186	
PROCESS CONTINGENCY	10	124	
DEVELOPED SUBTOTAL		1551	

Figure C.6 Factored investment estimate for multistage Pb sorption Case 2B.

DEVELOPED SUBTOTAL		1551	
LABOR/MATERIAL SPLIT	25		
WORKING CONDITIONS	10	39	
FREIGHT,QA,PROCUREMENT,SALES TAX	11	128	
NET TOTAL		1718	
ABNORMAL PREMIUM TIME	0	0	
MINOR CHANGES	2	34	
DIRECT TOTAL		1752	
ENGG & HOME OFFICE	20	487	
FIELD INDIRECTS	8	195	
SPARES & PORTABLES		10	SPARE,PORT
PROJECT LEVEL ALLOWANCES		0	PROJ
CREDIT FOR EXISTING EQUIPMENT (INCL CONT,FRT,TAX,QA,PROC)		0	
CURRENT COST		2444	
LOCATION FACTOR	1.00	2444	
ESCALATION TO MPC	1.02	2493	
AUTH 1Q2002 MPC 4Q2002 M/C 2Q2003			
COUNTRY CURRENCY REVALUATION	1.00	2493	
PROJECT COST SAY		2500	

Figure C.6 Continued.

Research Guidance Appraisal

TITLE: Pb Multistage Sorption RGA NAME: Case 2C
CASE NUMBER: Case 2C ACCT NUM:
SCOPE: SITE: Gulf Coast

	Factor %	$M	
ENGINEERED EQUIPMENT		278	EE,TK,COL, HX,PMP,AGIT
RELOCATED/EXISTING EQUIPMENT		0	EX,REL
MISC EQUIPMENT	5	14	
EQUIPMENT SUBTOTAL		292	
FIELD MTL/LABOR/INSUL	3 10 4 17	50	
FIELD ERECTED EQUIPMENT		255	FE
FACTORED FDNS,SUP,PLT	7	20	
IDENTIFIED FDNS,SUP,PLT		0	FSP
EXISTING IN PLACE EQUIPMENT		0	EIP
INSTALLED EQUIPMENT SUBTOTAL		617	
FACTORED PIPING	45	278	
FACTORED INSTRUMENTS	16	99	
FACTORED ELECTRICAL	11	68	
IDENTIFIED PIPING		0	PIPE
IDENTIFIED INSTRUMENTS		36	INSTR
IDENTIFIED ELECTRICAL		0	ELECT
MCC/ICR/ECR EQUIP	6	37	
CONNECTED SUBTOTAL		1135	
SPECIAL PROCESS ITEMS		54	SPE
PACKING		0	PACK
OTHER		0	LM
IDENTIFIED BUILDINGS,STRUCTURES		41	BLDG
ISBL SUBTOTAL		1230	
IDENTIFIED PG&S		0	PG&S
FACTORED PG&S	10	123	
IDENTIFIED D&R		0	D&R
FACTORED D&R	2	25	
OSBL INCLUDED SUBTOTAL		1378	
PROJECT CONTINGENCY	15	207	
PROCESS CONTINGENCY	10	138	
DEVELOPED SUBTOTAL		1723	

Figure C.7 Factored investment estimate for multistage Pb sorption Case 2C.

DEVELOPED SUBTOTAL		1723	
LABOR/MATERIAL SPLIT	25		
WORKING CONDITIONS	10	43	
FREIGHT,QA,PROCUREMENT,SALES TAX	11	142	
NET TOTAL		1908	
ABNORMAL PREMIUM TIME	0	0	
MINOR CHANGES	2	38	
DIRECT TOTAL		1946	
ENGG & HOME OFFICE	20	541	
FIELD INDIRECTS	8	216	
SPARES & PORTABLES		10	SPARE,PORT
PROJECT LEVEL ALLOWANCES		0	PROJ
CREDIT FOR EXISTING EQUIPMENT (INCL CONT,FRT,TAX,QA,PROC)		0	
CURRENT COST		2713	
LOCATION FACTOR	1.00	2713	
ESCALATION TO MPC	1.02	2767	
AUTH 1Q2002 MPC 4Q2002 M/C 2Q2003			
COUNTRY CURRENCY REVALUATION	1.00	2767	
PROJECT COST SAY		2800	

Figure C.7 Continued.

Research Guidance Appraisal

TITLE: Pb Multistage Sorption RGA NAME: Case 3A
CASE NUMBER: Case 3A ACCT NUM:
SCOPE: SITE: Gulf Coast

	Factor %	$M	
ENGINEERED EQUIPMENT		275	EE,TK,COL, HX,PMP,AGIT
RELOCATED/EXISTING EQUIPMENT		0	EX,REL
MISC EQUIPMENT	5	14	
EQUIPMENT SUBTOTAL		289	
FIELD MTL/LABOR/INSUL	3 10 4 17	49	
FIELD ERECTED EQUIPMENT		85	FE
FACTORED FDNS,SUP,PLT	7	20	
IDENTIFIED FDNS,SUP,PLT		0	FSP
EXISTING IN PLACE EQUIPMENT		0	EIP
INSTALLED EQUIPMENT SUBTOTAL		443	
FACTORED PIPING	45	199	
FACTORED INSTRUMENTS	16	71	
FACTORED ELECTRICAL	11	49	
IDENTIFIED PIPING		0	PIPE
IDENTIFIED INSTRUMENTS		12	INSTR
IDENTIFIED ELECTRICAL		0	ELECT
MCC/ICR/ECR EQUIP	6	27	
CONNECTED SUBTOTAL		801	
SPECIAL PROCESS ITEMS		54	SPE
PACKING		0	PACK
OTHER		0	LM
IDENTIFIED BUILDINGS,STRUCTURES		41	BLDG
ISBL SUBTOTAL		896	
IDENTIFIED PG&S		0	PG&S
FACTORED PG&S	10	90	
IDENTIFIED D&R		0	D&R
FACTORED D&R	2	18	
OSBL INCLUDED SUBTOTAL		1004	
PROJECT CONTINGENCY	15	151	
PROCESS CONTINGENCY	10	100	
DEVELOPED SUBTOTAL		1255	

Figure C.8 Factored investment estimate for multistage Pb sorption Case 3A.

DEVELOPED SUBTOTAL		1255	
LABOR/MATERIAL SPLIT	25		
WORKING CONDITIONS	10	31	
FREIGHT,QA,PROCUREMENT,SALES TAX	11	104	

NET TOTAL		1390	
ABNORMAL PREMIUM TIME	0	0	
MINOR CHANGES	2	28	

DIRECT TOTAL		1418	
ENGG & HOME OFFICE	20	394	
FIELD INDIRECTS	8	158	
SPARES & PORTABLES		10	SPARE,PORT
PROJECT LEVEL ALLOWANCES		0	PROJ
CREDIT FOR EXISTING EQUIPMENT		0	
(INCL CONT,FRT,TAX,QA,PROC)		---	
CURRENT COST		1980	
LOCATION FACTOR	1.00	1980	
ESCALATION TO MPC	1.01	2000	
AUTH 1Q2002 MPC 3Q2002 M/C 1Q2003			
COUNTRY CURRENCY REVALUATION	1.00	2000	
PROJECT COST SAY		2000	

Figure C.8 Continued.

Research Guidance Appraisal

TITLE: Pb Multistage Sorption RGA NAME: Case 3B
CASE NUMBER: Case 3B ACCT NUM:
SCOPE: SITE: Gulf Coast

	Factor %	$M	
ENGINEERED EQUIPMENT		290	EE,TK,COL, HX,PMP,AGIT
RELOCATED/EXISTING EQUIPMENT		0	EX,REL
MISC EQUIPMENT	5	15	
EQUIPMENT SUBTOTAL		305	
FIELD MTL/LABOR/INSUL 3 10 4 17		52	
FIELD ERECTED EQUIPMENT		170	FE
FACTORED FDNS,SUP,PLT	7	21	
IDENTIFIED FDNS,SUP,PLT		0	FSP
EXISTING IN PLACE EQUIPMENT		0	EIP
INSTALLED EQUIPMENT SUBTOTAL		548	
FACTORED PIPING	45	247	
FACTORED INSTRUMENTS	16	88	
FACTORED ELECTRICAL	11	60	
IDENTIFIED PIPING		0	PIPE
IDENTIFIED INSTRUMENTS		24	INSTR
IDENTIFIED ELECTRICAL		0	ELECT
MCC/ICR/ECR EQUIP	6	33	
CONNECTED SUBTOTAL		1000	
SPECIAL PROCESS ITEMS		54	SPE
PACKING		0	PACK
OTHER		0	LM
IDENTIFIED BUILDINGS,STRUCTURES		41	BLDG
ISBL SUBTOTAL		1095	
IDENTIFIED PG&S		0	PG&S
FACTORED PG&S	10	110	
IDENTIFIED D&R		0	D&R
FACTORED D&R	2	22	
OSBL INCLUDED SUBTOTAL		1227	
PROJECT CONTINGENCY	15	184	
PROCESS CONTINGENCY	10	123	
DEVELOPED SUBTOTAL		1534	

Figure C.9 Factored investment estimate for multistage Pb sorption Case 3B.

DEVELOPED SUBTOTAL		1534	
LABOR/MATERIAL SPLIT	25		
WORKING CONDITIONS	10	38	
FREIGHT,QA,PROCUREMENT,SALES TAX	11	127	

NET TOTAL		1699	
ABNORMAL PREMIUM TIME	0	0	
MINOR CHANGES	2	34	

DIRECT TOTAL		1733	
ENGG & HOME OFFICE	20	481	
FIELD INDIRECTS	8	193	
SPARES & PORTABLES		10	SPARE,PORT
PROJECT LEVEL ALLOWANCES		0	PROJ
CREDIT FOR EXISTING EQUIPMENT		0	
(INCL CONT,FRT,TAX,QA,PROC)		---	
CURRENT COST		2417	
LOCATION FACTOR	1.00	2417	
ESCALATION TO MPC	1.02	2465	
AUTH 1Q2002 MPC 4Q2002 M/C 2Q2003			
COUNTRY CURRENCY REVALUATION	1.00	2465	
PROJECT COST SAY		2500	

Figure C.9 Continued.

Research Guidance Appraisal

TITLE: Pb Multistage Sorption RGA NAME: Case 3C
CASE NUMBER: Case 3C ACCT NUM:
SCOPE: SITE: Gulf Coast

	Factor %	$M	
ENGINEERED EQUIPMENT		327	EE,TK,COL, HX,PMP,AGIT
RELOCATED/EXISTING EQUIPMENT		0	EX,REL
MISC EQUIPMENT	5	16	
EQUIPMENT SUBTOTAL		343	
FIELD MTL/LABOR/INSUL	3 10 4 17	58	
FIELD ERECTED EQUIPMENT		340	FE
FACTORED FDNS,SUP,PLT	7	24	
IDENTIFIED FDNS,SUP,PLT		0	FSP
EXISTING IN PLACE EQUIPMENT		0	EIP
INSTALLED EQUIPMENT SUBTOTAL		765	
FACTORED PIPING	45	344	
FACTORED INSTRUMENTS	16	122	
FACTORED ELECTRICAL	11	84	
IDENTIFIED PIPING		0	PIPE
IDENTIFIED INSTRUMENTS		48	INSTR
IDENTIFIED ELECTRICAL		0	ELECT
MCC/ICR/ECR EQUIP	6	46	
CONNECTED SUBTOTAL		1409	
SPECIAL PROCESS ITEMS		54	SPE
PACKING		0	PACK
OTHER		0	LM
IDENTIFIED BUILDINGS,STRUCTURES		41	BLDG
ISBL SUBTOTAL		1504	
IDENTIFIED PG&S		0	PG&S
FACTORED PG&S	10	150	
IDENTIFIED D&R		0	D&R
FACTORED D&R	2	30	
OSBL INCLUDED SUBTOTAL		1684	
PROJECT CONTINGENCY	15	253	
PROCESS CONTINGENCY	10	168	
DEVELOPED SUBTOTAL		2105	

Figure C.10 Factored investment estimate for multistage Pb sorption Case 3C.

DEVELOPED SUBTOTAL		2105	
LABOR/MATERIAL SPLIT	25		
WORKING CONDITIONS	10	53	
FREIGHT,QA,PROCUREMENT,SALES TAX	11	174	

NET TOTAL		2332	
ABNORMAL PREMIUM TIME	0	0	
MINOR CHANGES	2	47	

DIRECT TOTAL		2379	
ENGG & HOME OFFICE	20	661	
FIELD INDIRECTS	8	264	
SPARES & PORTABLES		10	SPARE,PORT
PROJECT LEVEL ALLOWANCES		0	PROJ
CREDIT FOR EXISTING EQUIPMENT		0	
(INCL CONT,FRT,TAX,QA,PROC)		---	
CURRENT COST		3314	
LOCATION FACTOR	1.00	3314	
ESCALATION TO MPC	1.02	3380	
AUTH 1Q2002 MPC 4Q2002 M/C 2Q2003			
COUNTRY CURRENCY REVALUATION	1.00	3380	
PROJECT COST SAY		3400	

Figure C.10 Continued.

Escalation and Cost Factors for Cash Flow Analysis

YEAR END	2002	2003	2004	2005	2006	2007	2008	2009	2010	2011	2012
INVESTMENT, $1000											
4th Quarter CCI	246	252	258	265	272	278	285	292	300	307	315
New Permanent(4Q)	3,400	0	0	0	0	0	0	0	0	0	0
Creep Invest. (% Replace Inv.)	1.5%	51	53	55	57	60	62	65	67	70	73
Total New Book Investment	3400	3451	3504	3559	3617	3676	3738	3803	3870	3940	4012
Replacement Investment	3400	3536	3677	3825	3978	4137	4302	4474	4653	4839	5033
Depreciation 6 year	0.2	0.32	0.19	0.12	0.12	0.05					
OPERATING COSTS, $1000											
Raw Materials	Cost				Escalation Factors						
50% NaOH ($/lb)	0.15	2.5%	2.5%	2.5%	2.5%	2.5%	2.5%	2.5%	2.5%	2.5%	2.5%
30% $FeCl_3$ ($/lb)	0.15	2.5%	2.5%	2.5%	2.5%	2.5%	2.5%	2.5%	2.5%	2.5%	2.5%
Maxflo ($/lb)	0.165	2.5%	2.5%	2.5%	2.5%	2.5%	2.5%	2.5%	2.5%	2.5%	2.5%
Filter Cloth ($/ft^2)	0.095	2.5%	2.5%	2.5%	2.5%	2.5%	2.5%	2.5%	2.5%	2.5%	2.5%
Emulsion Polymer ($/lb)	1.50	2.5%	2.5%	2.5%	2.5%	2.5%	2.5%	2.5%	2.5%	2.5%	2.5%
Utilities											
Electricity ($/kWh)	0.045	2.5%	2.5%	2.5%	2.5%	2.5%	2.5%	2.5%	2.5%	2.5%	2.5%
Filtered Water ($/1000Gal)	0.15	2.5%	2.5%	2.5%	2.5%	2.5%	2.5%	2.5%	2.5%	2.5%	2.5%
General Escalation Factor		2.5%	2.5%	2.5%	2.5%	2.5%	2.5%	2.5%	2.5%	2.5%	2.5%
Waste Disposal											
Hazardous Landfill ($/lb)	0.085	2.5%	2.5%	2.5%	2.5%	2.5%	2.5%	2.5%	2.5%	2.5%	2.5%
Technical Exempt ($1000/yr)	160	2.5%	2.5%	2.5%	2.5%	2.5%	2.5%	2.5%	2.5%	2.5%	2.5%
Operations ($1000/yr)	430	2.5%	2.5%	2.5%	2.5%	2.5%	2.5%	2.5%	2.5%	2.5%	2.5%
Lab Support ($1000/yr)	0	2.5%	2.5%	2.5%	2.5%	2.5%	2.5%	2.5%	2.5%	2.5%	2.5%
Maintenance (60% L, 40% M)	% R. Inv.	4.0%	4.0%	4.0%	4.0%	4.0%	4.0%	4.0%	4.0%	4.0%	4.0%
Taxes & Insurance	% R. Inv.	0.75%	0.75%	0.75%	0.75%	0.75%	0.75%	0.75%	0.75%	0.75%	0.75%
Gen. Inv. Related Plant Ovhd.	% R. Inv.	0.5%	0.5%	0.5%	0.5%	0.5%	0.5%	0.5%	0.5%	0.5%	0.5%
Gen. OL Plant Ovhd. (%(OL+ Supv+ Main Labor))	%	24%	24%	24%	24%	24%	24%	24%	24%	24%	24%
Income Tax Rate	40%	40%	40%	40%	40%	40%	40%	40%	40%	40%	40%
Project Liaison Costs	% of NPI	2.0%									
Startup Costs	% of NPI	10%									
Revenue		2.5%	2.5%	2.5%	2.5%	2.5%	2.5%	2.5%	2.5%	2.5%	2.5%

Figure C.11 Example cash flow analysis for multistage Pb sorption case studies.

Engineering Evaluation for Multistage Lead Sorption Onto Ferrihydrite
2002 Startup Case 3C

CASH FLOW ANALYSIS

YEAR END		2002	2003	2004	2005	2006	2007	2008	2009	2010	2011	2012
INVESTMENT ($1000)												
4th Quarter CCI		246	252	258	265	272	278	285	292	300	307	315
New Permanent(4Q)		3400	51	53	55	57	60	62	65	67	70	73
Working Cap. ($M)		19	157	105	108	112	115	118	122	126	129	133
Total Investment		3419	3608	3609	3667	3728	3791	3857	3925	3996	4069	4146
OPERATING COSTS ($1000)												
									$1000/YEAR			
Raw Materials	Consumption											
50% NaOH (lb/yr)	213800		-33	-34	-35	-35	-36	-37	-38	-39	-40	-41
30% $FeCl_3$ (lb/yr)	289000		-44	-46	-47	-48	-49	-50	-52	-53	-54	-55
Maxflo (lb/yr)	69600		-12	-12	-12	-13	-13	-13	-14	-14	-14	-15
Filter Cloth (ft^2/yr)	78761		-8	-8	-8	-8	-8	-9	-9	-9	-9	-10
Emulsion Polymer (lb/yr)	1588		-2	-3	-3	-3	-3	-3	-3	-3	-3	-3
Utilities												
Electricity (kWh/yr)	210325		-10	-10	-10	-10	-11	-11	-11	-12	-12	-12
Filtered Water (1000Gal/yr)	244		0	0	0	0	0	0	0	0	0	0
Waste Disposal												
Hazardous Landfill (lb/yr)	671000		-58	-60	-61	-63	-65	-66	-68	-69	-71	-73
Lab Support			0	0	0	0	0	0	0	0	0	0
Tech. Exempt (No./yr)	0.35		-57	-59	-60	-62	-63	-65	-67	-68	-70	-72
Operations (No./yr)	0.35		-154	-158	-162	-166	-170	-175	-179	-183	-188	-193
Maintenance			-139	-145	-151	-157	-163	-170	-176	-183	-191	-198
Basic Data Devel. ($1000)	50	-50	0	0	0	0	0	0	0	0	0	0
Project Liaison Costs		-68	0	0	0	0	0	0	0	0	0	0
Startup Costs			-340	-5	-5	-6	-6	-6	-6	-6	-7	-7
Taxes & Insurance			-26	-27	-28	-29	-30	-31	-32	-34	-35	-36
General Plant Overhead			-72	-74	-77	-79	-82	-84	-87	-90	-93	-96
Cash Costs		-118	-956	-639	-659	-678	-699	-720	-742	-764	-787	-811
TOTAL COST, DEPRECIATION, AND CASH FLOW												
Depreciation			-680	-1098	-673	-446	-453	-223	-58	-60	-63	-65
Total Cost		-118	-1636	-1738	-1331	-1124	-1152	-943	-800	-824	-850	-876
Other Revenue ($1000/yr)	0		0	0	0	0	0	0	0	0	0	0
Pretax Earnings		-118	-1636	-1738	-1331	-1124	-1152	-943	-800	-824	-850	-876
Income Taxes		47	654	695	533	450	461	377	320	330	340	351
Operating Earnings		-71	-981	-1043	-799	-674	-691	-566	-480	-495	-510	-526
Net Cash Flow w/o Infinite Life		-3490	-490	55	-184	-289	-301	-408	-490	-505	-521	-537
Fut. Cash Flows (1/2 Infinite Life @12%)												-2238
Fut. Cash Flows (1/2 Infinite Life @25%)												-1074
Net Cash Flow @12% w/ Inf. Life		-3490	-490	55	-184	-289	-301	-408	-490	-505	-521	-2776
Net Cash Flow @25% w/ Inf. Life		-3490	-490	55	-184	-289	-301	-408	-490	-505	-521	-1612
NPC @12% To Start of Yr 1		-3116	-3507	-3468	-3585	-3749	-3902	-4087	-4284	-4467	-4634	-5432
NPC @25% To Start of Yr 1		-2792	-3106	-3078	-3153	-3248	-3327	-3413	-3495	-3563	-3619	-3757

Figure C.11 Continued.

Engineering Evaluation for Multistage Lead Sorption Onto Ferrihydrite
2002 Startup

Data Input

Case	FeCl3 (L/yr)	50% NaOH (L/yr)	Emulsion Polymer (L/yr)	Media (L/yr)	Filter Cloth (ft²/yr)	Electricity (kWh/yr)	Sludge Disposal (L/yr)	Filtered Water (Mgal/yr)	Technical Effort (fte)	Operations (fte)
1A	722,400	534,600	2,175	152,600	126,018	112,675	1,471,000	654	0.25	0.25
1B	722,400	534,600	2,610	152,600	126,018	153,718	1,471,000	622	0.30	0.30
2A	3,359,300	2,485,900	7,348	644,300	504,071	190,981	6,213,000	2,941	0.25	0.40
2B	365,600	270,500	1,425	71,400	78,761	134,229	688,000	317	0.30	0.25
2C	173,400	128,300	790	34,600	42,006	162,374	334,000	147	0.35	0.30
3A	289,000	213,800	1,191	69,600	78,761	98,164	671,000	273	0.25	0.20
3B	289,000	213,800	1,390	69,600	78,761	134,073	671,000	255	0.30	0.25
3C	289,000	213,800	1,588	69,600	78,761	210,325	671,000	244	0.35	0.35

Cash Flow Analysis Output

Case	Investment ($1000)	2002 Cash Operating Cost ($1000/yr)	2002 NPC @12% ($1000)	2002 NPC @25% ($1000)	2002 Annualized Cost ($1000/yr)
1A	2,400	-710	-4,944	-3,185	1,067
1B	2,800	-774	-5,532	-3,601	1,193
2A	4,100	-2,182	-12,559	-7,395	2,745
2B	2,500	-538	-4,289	-2,907	919
2C	2,800	-499	-4,360	-3,042	931
3A	2,000	-445	-3,500	-2,361	750
3B	2,500	-515	-4,192	-2,860	897
3C	3,400	-639	-5,432	-3,757	1,163

Figure C.12 Cash flow analysis results for multistage Pb sorption case studies.

Appendix D

SUPPORTING INFORMATION FOR CHAPTER 5

D.1 Local Extrapolation Model and Error Analysis Model Derivations

Robinson and Hurst (1997) describe a method for statistically quantifying the sources of variance in uncertainty analyses. For a multivariable function

$$y = y\,(x_1, x_2, \ldots, x_n) \qquad [D.1]$$

the sensitivity of y to each input variable, x_i, is given by the partial derivative of y with respect to x_i, normalized to the nominal values of y and x_i to discount the effect of units.

$$\text{Sensitivity} = \left(\frac{\partial y}{\partial x_i}\right)\left(\frac{x_i}{y}\right) \qquad [D.2]$$

Because the multivariable function resides in linear x-y space, Eq. [D.2] gives point values that will likely change significantly, and may even become negative, over the range of possible values for an input variable. In addition, the sensitivity values may depend on the values of other variables (i.e., they are not statistically independent). A Monte Carlo approach is often used to conduct the sensitivity analyses and, ultimately, the uncertainty analyses. Given a distribution of input variables (normal, lognormal, uniform, etc.), the Monte Carlo method will randomly sample the input variable distributions to generate sets of input variables. Each set of input variables is then propagated through the model to generate a distribution of output values. Often, the model will need to be solved > 1000 times to give reliable results. This can be

computationally intensive, particularly for a geochemical fate and transport model with many tens of input variables. A sensitivity analysis, therefore, is often conducted first to identify which input parameters have the largest impact on the output variable(s) of interest. In this way, the number of input variables carried forward to the uncertainty analysis is substantially reduced. Statistical distributions are estimated next for the condensed set of input parameters; then the distributions are randomly sampled using a Monte Carlo method. Finally, the code propagates each set of input variables through the model to obtain the overall cumulative uncertainty in the desired output parameters.

As an alternative to the more rigorous Monte Carlo approach, Robinson and Hurst (1997) advocate that a simple measure of the uncertainty importance of each input variable is to consider both the sensitivity $(\partial y/\partial x_i)$ and the uncertainty (σ_{xi}) in the value of x_i. A first-order (i.e., linearized) approximation of the uncertainty importance of an input variable is given by the equation

$$\text{Uncertainty importance of } x_i = \left(\frac{\partial y}{\partial x_i}\right)\sigma_{x_i} \qquad \text{[D.3]}$$

where σ_{xi} is the sample standard deviation of x_i. First-order or linearized in this case means that only the first-order (i.e., linear) terms from the Taylor series expansion of the multivariable function $y = y\,(x_1, x_2, \ldots, x_n)$ are retained in the general error propagation equation (Coleman and Steele, 1989). When the function $y = y\,(x_1, x_2, \ldots, x_n)$ is <u>also</u> linear, the sample output variance, σ_y^2, will be given by

$$\sigma_y^2 = \left(\frac{\partial y}{\partial x_1}\right)^2 \sigma_{x_1}^2 + \left(\frac{\partial y}{\partial x_2}\right)^2 \sigma_{x_2}^2 + \ldots + \left(\frac{\partial y}{\partial x_n}\right)^2 \sigma_{x_n}^2 \qquad \text{[D.4]}$$

Equation [D.4], therefore, identifies which input variables contribute the most to the output variance, based on the magnitude of $(\partial y/\partial x_i)^2 \sigma_{x_i}^2$. This simplified first-order approach is a local approach, because it assumes that the response surface is a plane over the domain of interest (i.e., $(\partial y/\partial x)$ is constant). This linear response will not occur in many cases, however, such as in chemical equilibrium problems. In linear Cartesian-coordinate space, local will translate to a very narrow range of x_i values, unless a strong linear correlation can be found between the output and input variables. Even then, the values of $\partial y/\partial x_i$ are estimates, only as good as the quality of the linear regression. In summary, if $(\partial y/\partial x_i)$ can be approximated well using linear regression, then Eq. [D.4] is an elegantly simple way to quantify the main sources of uncertainty in a model.

A more robust uncertainty analysis method for situations where the relationship between the output and input variables is nonlinear has been developed and implemented within the OLI Software's ElectroChem solver. While this method is similar in concept to that used by Robinson and Hurst (1997), it does not require that a linear relationship be established between x_i and y in order to estimate $\partial y/\partial x_i$ and, hence, validate the use of Eq. [D.4]. The key differences between the two approaches are:

1. A very good estimate of $\partial y/\partial x_i$ for each input variable is available from the last few iterations of the Newton-Raphson method that is used to solve the set of nonlinear equations in an ElectroChem model. A linear regression of the output vs. input variables, therefore, is not required.

2. The nonlinear relationship between the x_is and y is assumed to be of the form $y = x_1^{a_1} x_2^{a_2} x_3^{a_3} \ldots x_n^{a_n}$, where the exponents are positive or negative constants. This functional form has several advantages. First, it can be linearized in $\log_e$-$\log_e$ space,

meaning that a first-order Taylor series expansion in $\log_e$-$\log_e$ space results in a fairly simple local extrapolation model (i.e., an approximate model) that greatly extends the range of x_i values for which the approximate equation is valid. Experience in the chemical engineering field has shown that the functional form $y = x_1^{a_1} x_2^{a_2} x_3^{a_3} \ldots x_n^{a_n}$, coupled with linearization in $\log_e$-$\log_e$ space, results in a more robust extrapolation tool for the nonlinear equations encountered in chemical equilibrium problems. Second, it avoids the problems in linear x-y space of accurately accounting for very small concentrations of trace constituents and of calculating negative y values when the local model equations are extrapolated too far. For example, rarely does one see negative temperatures and pressures in real systems; however, this is possible when extrapolation happens in linear x-y space. Third, the partial derivative of y with respect to x_i $(\partial y/\partial x_i)$ is equal to $a_i(y/x_i)$, which nicely simplifies the linearized error propagation equation derived below.

In the ElectroChem code, a sensitivity matrix is first prepared from the last few iterations of the Newton-Raphson method that is used to solve the set of nonlinear equations in a chemical equilibrium model. A sensitivity matrix is generated that is comprised of j rows of output variables (OV_j) by i columns of input variables (IV_i), where

$$\left(\frac{\partial y_j}{\partial x_i}\right) \equiv \left(\frac{\partial OV_j}{\partial IV_i}\right) \qquad [D.5]$$

Each parameter in the sensitivity matrix is then normalized as in Eq. [D.2] to give the gain matrix. Given that $(\partial \ln y/\partial \ln x_i) = (\partial y/\partial x_i)(x_i/y) = (\partial \% y/\partial \% x_i)$, the gain matrix parameters are given by:

$$G_{ji} = \left(\frac{IV_i}{OV_j}\right)\left(\frac{\partial OV_j}{\partial IV_i}\right) = \left(\frac{\partial \ln OV_j}{\partial \ln IV_i}\right) = \left(\frac{\partial \% OV_j}{\partial \% IV_i}\right) \qquad [D.6]$$

The numbers in the gain matrix, therefore, represent the percent change in an output variable for a 1% change in the input variable.

For a multivariable function of the form $y = x_1^{a_1} x_2^{a_2} x_3^{a_3} \ldots x_n^{a_n}$, it can be shown that the constants $a_1, a_2, a_3, \ldots, a_n$ are equal in value and sign to the gain matrix values, $G_1, G_2, G_3, \ldots, G_n$. Consider the equation $y = x_1^{a_1} x_2^{a_2}$. Taking the partial derivative of y with respect to x_1 gives

$$\left(\frac{\partial y}{\partial x_1}\right) = a_1 x_1^{a_1 - 1} x_2^{a_2} \qquad [D.7]$$

Multiplying both sides by x_1/y, and substituting $x_1^{a_1} x_2^{a_2}$ for y on the right-hand side of the equation, leads to

$$\frac{x_1}{y}\left(\frac{\partial y}{\partial x_1}\right) = a_1 x_1^{a_1 - 1} x_2^{a_2}\left(\frac{x_1}{x_1^{a_1} x_2^{a_2}}\right) = a_1 \qquad [D.8]$$

However, $G_1 = (x_1/y)(\partial y/\partial x_1)$ as defined in Eq. [D.6]; therefore, Eq. [D.8] simplifies to

$$G_1 = a_1 \qquad [D.9]$$

Similarly, it can be shown that $G_2 = a_2$, and so on. As a result, the gain matrix parameters can be substituted for the a_i exponents in the multivariable function, $y = x_1^{a_1} x_2^{a_2} x_3^{a_3} \ldots x_n^{a_n}$, to give

$$y = x_1^{G_1} x_2^{G_2} x_3^{G_3} \ldots x_n^{G_n} \qquad [D.10]$$

A multivariable function of the form $y = x_1^{G_1} x_2^{G_2} x_3^{G_3} \ldots x_n^{G_n}$ is linearized by taking the natural logarithm of both sides of the equation. This gives

$$\ln y = G_1 \ln x_1 + G_2 \ln x_2 + G_3 \ln x_3 + \ldots + G_n \ln x_n \qquad [D.11]$$

A Taylor series expansion is often used to approximate a nonlinear, multivariable function. The general form of the Taylor series approximation is (Ang and Tang, 1975)

$$y(x_1, x_2, \ldots, x_n) = y(x_{1_o}, x_{2_o}, \ldots, x_{n_o}) + \sum_{i=1}^{n} (x_i - x_{i_o}) \frac{\partial y(x_{1_o}, x_{2_o}, \ldots, x_{n_o})}{\partial x_i} +$$

$$\frac{1}{2} \sum_{i=1}^{n} \sum_{j=1}^{n} (x_i - x_{i_o})(x_j - x_{j_o}) \frac{\partial^2 y(x_{1_o}, x_{2_o}, \ldots, x_{n_o})}{\partial x_i \partial x_j} + \cdots + R_N \qquad [D.12]$$

where the subscript *o* denotes the base case where the value of the function is known, and R_N is the remainder after N terms. This expansion is often truncated at the linear terms, giving a first-order or linearized approximation.

$$y(x_1, x_2, \ldots, x_n) = y(x_{1_o}, x_{2_o}, \ldots, x_{n_o}) + \sum_{i=1}^{n} (x_i - x_{i_o}) \frac{\partial y(x_{1_o}, x_{2_o}, \ldots, x_{n_o})}{\partial x_i} \qquad [D.13]$$

When Eq. [D.13] is applied to Eq. [D.11], the result is

$$\ln y - \ln y_o = G_1(\ln x_1 - \ln x_{1_o}) + G_2(\ln x_2 - \ln x_{2_o}) +$$

$$\ldots + G_n(\ln x_n - \ln x_{n_o}) \qquad [D.14]$$

which simplifies to

$$\ln\left(\frac{y}{y_o}\right) = \sum_{i=1}^{n} G_i \ln\left(\frac{x_i}{x_{i_o}}\right) \qquad [D.15]$$

Rewriting Eq. [D.15] in terms of the OLI gain matrix nomenclature given in Eq. [D.6] leads to

$$\ln\left(\frac{OV_{j_N}}{OV_{j_B}}\right) = \sum_{i=1}^{n} G_{ji} \ln\left(\frac{IV_{i_N}}{IV_{i_B}}\right) \qquad [D.16]$$

where the subscripts N and B refer to the new case and base case, respectively. Finally, converting Eq. [D.16] back to linear x-y space gives the general form of the local extrapolation model equation

$$\left(\frac{OV_{j_N}}{OV_{j_B}}\right)=\prod_i\left(\frac{IV_{i_N}}{IV_{i_B}}\right)^{G_{ji}} \qquad [D.17]$$

In most cases, Eq. [D.17] has been found to be valid for an approximately ten-fold range in values for the input variables (i.e., the values of G_{ji} will eventually change, but they are approximately constant over a wide range). For the case of trace-metal sorption onto ferrihydrite, Eq. [D.17] might take the form

$$\left(\frac{(\%\text{Sorbed})_N}{(\%\text{Sorbed})_B}\right)=\left(\frac{pH_N}{pH_B}\right)^{0.1}\times\left(\frac{Pb_{TOT\,N}}{Pb_{TOT\,B}}\right)^{0.002}\times\ldots\times\left(\frac{(HFO_{IN})_N}{(HFO_{IN})_B}\right)^{0.005} \qquad [D.18]$$

The gain matrix given by Eq. [D.6] provides only half the input needed to assess the uncertainty importance of each input variable; that is, the sensitivity of the model output to the input variable(s). Inspection of the gain matrix alone does not tell which x values contribute most to the uncertainty in the output parameters. Now that a local extrapolation model has been determined, the uncertainty analysis or error propagation equation can be derived. This will provide the other half of the input needed to assess the uncertainty importance of each input variable.

For $y = y\,(x_1, x_2)$, the general form of the linearized error propagation equation is given by (Coleman and Steele, 1989):

$$\sigma_y^2=\left(\frac{\partial y}{\partial x_1}\right)^2\sigma_{x_1}^2+\left(\frac{\partial y}{\partial x_2}\right)^2\sigma_{x_2}^2+2\left(\frac{\partial y}{\partial x_1}\right)\left(\frac{\partial y}{\partial x_2}\right)\sigma_{x_1x_2} \qquad [D.19]$$

where the covariance, $\sigma_{x_1x_2}$, is given by

$$\sigma_{x_1 x_2} = \lim_{N \to \infty} \frac{1}{N} \sum_{i=1}^{N} \varepsilon_{x_{1i}} \varepsilon_{x_{2i}} \qquad [D.20]$$

and $\varepsilon_{x_{1i}}$ and $\varepsilon_{x_{2i}}$ represent the random errors in the variables x_1 and x_2, respectively, and N is the sample size. When x_1 and x_2 are statistically independent, $\sigma_{x_1 x_2}$ goes to zero and Eq. [D.19] simplifies to

$$\sigma_y^2 = \left(\frac{\partial y}{\partial x_1}\right)^2 \sigma_{x_1}^2 + \left(\frac{\partial y}{\partial x_2}\right)^2 \sigma_{x_2}^2 \qquad [D.21]$$

The assumption that $\sigma_{x_1 x_2}$ equals zero will not be a good assumption, of course, if there is significant correlation between the variables. As in Eqs. [D.3] and [D.4], only the first-order (or linear) terms from the Taylor series expansion of the multivariable function $y = y(x_1, x_2)$ have been retained in the linearized error propagation Eqs. [D.19] and [D.21]. Coleman and Steele (1989) emphasize that dividing both sides of the linearized error propagation equation by y often results in an algebraically less complex form. Rewriting Eq. [D.21] in this way and converting to a generalized form gives

$$\left(\frac{\sigma_y}{y}\right)^2 = \left(\frac{\partial y}{\partial x_1}\right)^2 \left(\frac{\sigma_{x_1}}{y}\right)^2 + \left(\frac{\partial y}{\partial x_2}\right)^2 \left(\frac{\sigma_{x_2}}{y}\right)^2 = \sum_{i=1}^{N} \left(\frac{\partial y}{\partial x_i} \frac{\sigma_{x_i}}{y}\right)^2 \qquad [D.22]$$

When the local extrapolation model equation is of the functional form given by Eq. [D.10], the linearized error propagation equation becomes

$$\left(\frac{\sigma_y}{y}\right)^2 = \sum_{i=1}^{N} \left(\frac{G_i \sigma_{x_i}}{x_i}\right)^2 \qquad [D.23]$$

by substituting G_i/x_i for $(\partial y/\partial x_i)(1/y)$ as derived in Eqs. [D.7] through [D.9]. Equation [D.23] assumes that the relationship given by Eqs. [D.10] and [D.17] is continuous and has continuous derivatives in the domain of interest, that the measured

variables x_i are independent of each another, and that the uncertainties in the measured variables σ_{x_i} are also independent of each other. Rewriting Eq. [D.23] in terms of the OLI gain matrix nomenclature given in Eq. [D.6] leads to

$$\left(\frac{\sigma_{OV_j}}{OV_j}\right)^2 = \sum_{i=1}^{N}\left(\frac{G_{ji}\sigma_{IV_i}}{IV_i}\right)^2 \qquad [D.24]$$

where σ_r/r is defined as the coefficient of variation (COV) of variable r. Rewriting Eq. [D.24] in terms of COV variables gives

$$(COV\_OV_j)^2 = \sum_{i=1}^{N}(G_{ji} \times COV\_IV_i)^2 \qquad [D.25]$$

or

$$(COV\_OV_j)^2 = \sum_{i=1}^{N} U_{ji} \qquad [D.26]$$

where $U_{ji} = (G_{ji} \times COV\_IV_i)^2$. It follows, then, that the fraction of the output uncertainty attributable to the uncertainty in a specific input variable can be approximated by

$$\text{Fraction of Total Uncertainty} = FRAC_{U_{ji}} =$$

$$U_{ji} \Big/ \sum_{i=1}^{N} U_{ji} = U_{ji} / (COV\_OV_j)^2 \qquad [D.27]$$

The input variables with the largest values of U_{ji} will contribute the most variance to the overall output variance.

D.2 References

Ang A. H-S. and Tang W. H. (1975) *Probability Concepts in Engineering Planning and Design. Volume I. Basic Principles*. John Wiley & Sons.

Coleman H. W. and Steele W. G. (1989) *Experimentation and Uncertainty Analysis for Engineers*. John Wiley & Sons.

Robinson R. B. and Hurst B. T. (1997) Statistical quantification of the sources of variance in uncertainty analyses. *Risk Anal.* **17,** 447-453.

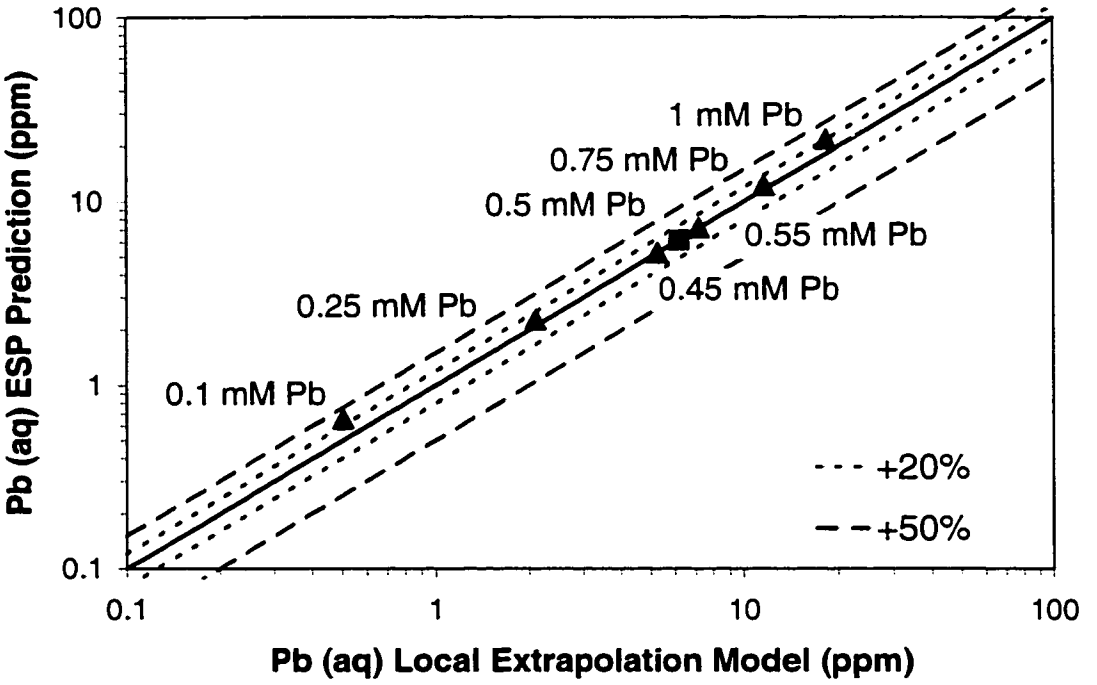

Figure D.1 **Comparison of local extrapolation model estimates to ESP model predictions for Pb_{aq} as a function of Pb feed concentration for one-stage, single-solute sorption of 0.5 mM Pb (base case) onto 0.4 g L^{-1} ferrihydrite at pH 5.5 in 0.01 M $NaNO_3$ solution.**

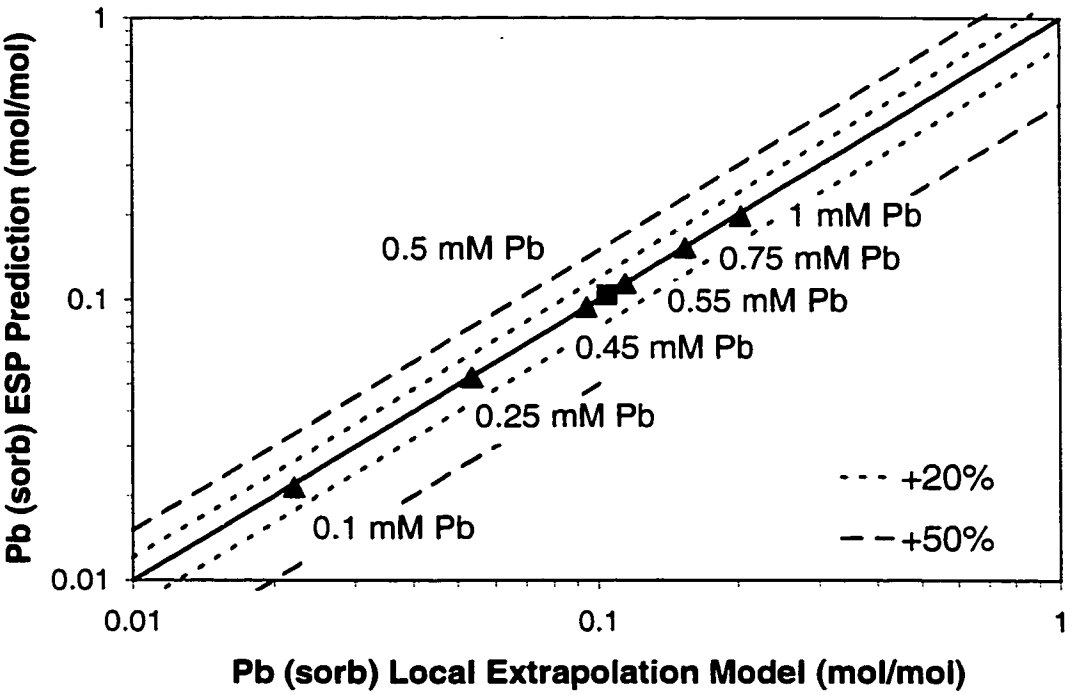

Figure D.2 **Comparison of local extrapolation model estimates to ESP model predictions for Pb_{sorb} as a function of Pb feed concentration for one-stage, single-solute sorption of 0.5 mM Pb (base case) onto 0.4 g L^{-1} ferrihydrite at pH 5.5 in 0.01 M $NaNO_3$ solution.**

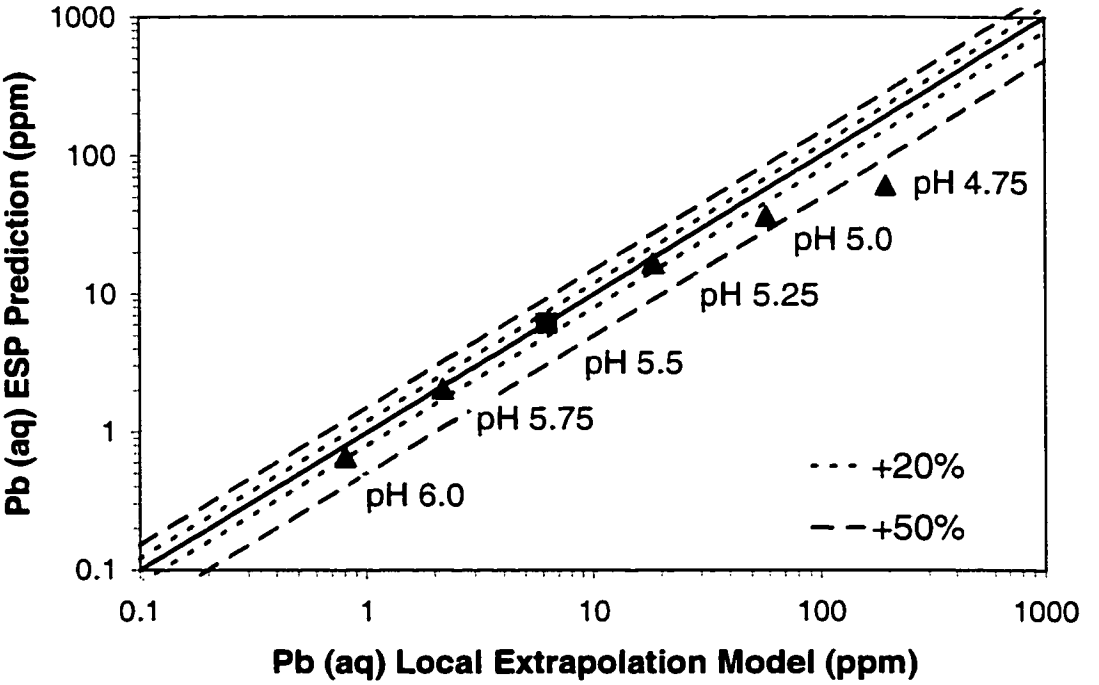

Figure D.3 **Comparison of local extrapolation model estimates to ESP model predictions for Pb_{aq} as a function of pH for one-stage, single-solute sorption of 0.5 mM Pb onto 0.4 g L^{-1} ferrihydrite at pH 5.5 (base case) in 0.01 M $NaNO_3$ solution.**

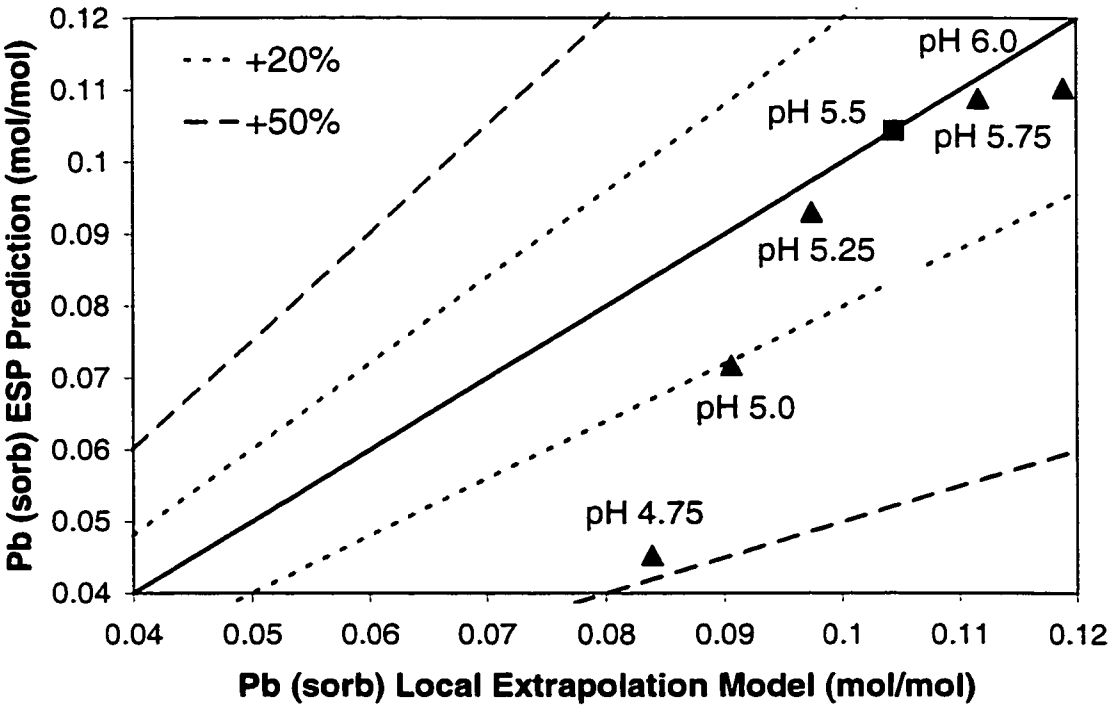

Figure D.4 **Comparison of local extrapolation model estimates to ESP model predictions for Pb_{sorb} as a function of pH for one-stage, single-solute sorption of 0.5 mM Pb onto 0.4 g L^{-1} ferrihydrite at pH 5.5 (base case) in 0.01 M $NaNO_3$ solution.**

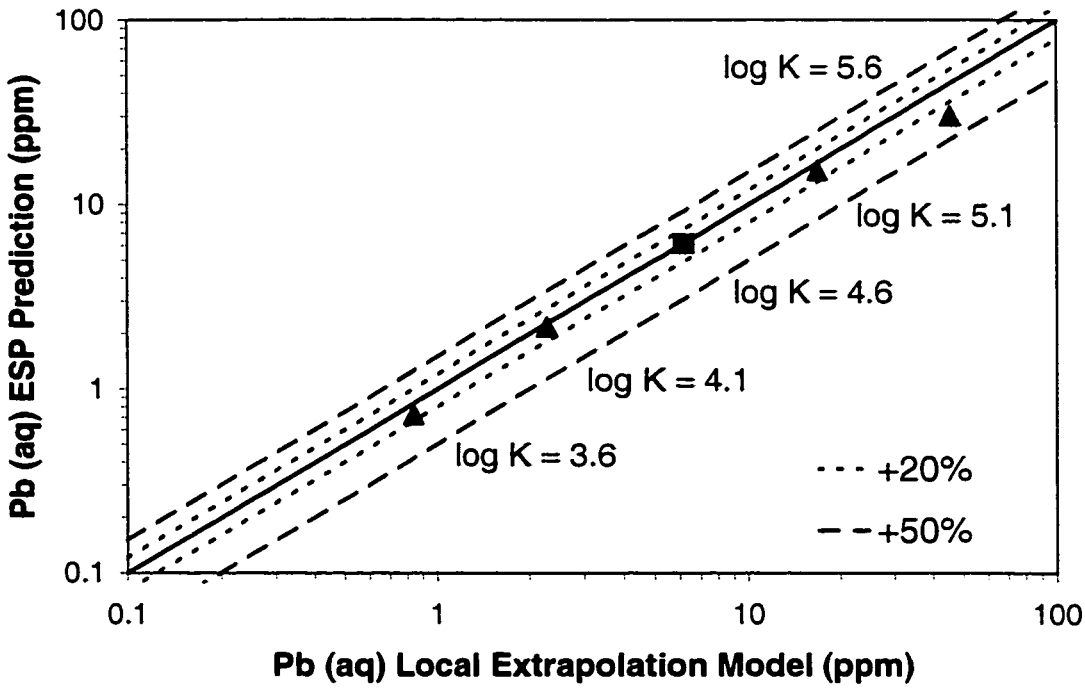

Figure D.5 **Comparison of local extrapolation model estimates to ESP model predictions for Pb_{aq} as a function of log $K^{int}_{(\equiv FeO)_2Pb}$ for one-stage, single-solute sorption of 0.5 mM Pb onto 0.4 g L^{-1} ferrihydrite at pH 5.5 in 0.01 M $NaNO_3$ solution. Base-case log $K^{int}_{(\equiv FeO)_2Pb}$ = 4.6 at 0.4 g L^{-1} ferrihydrite.**

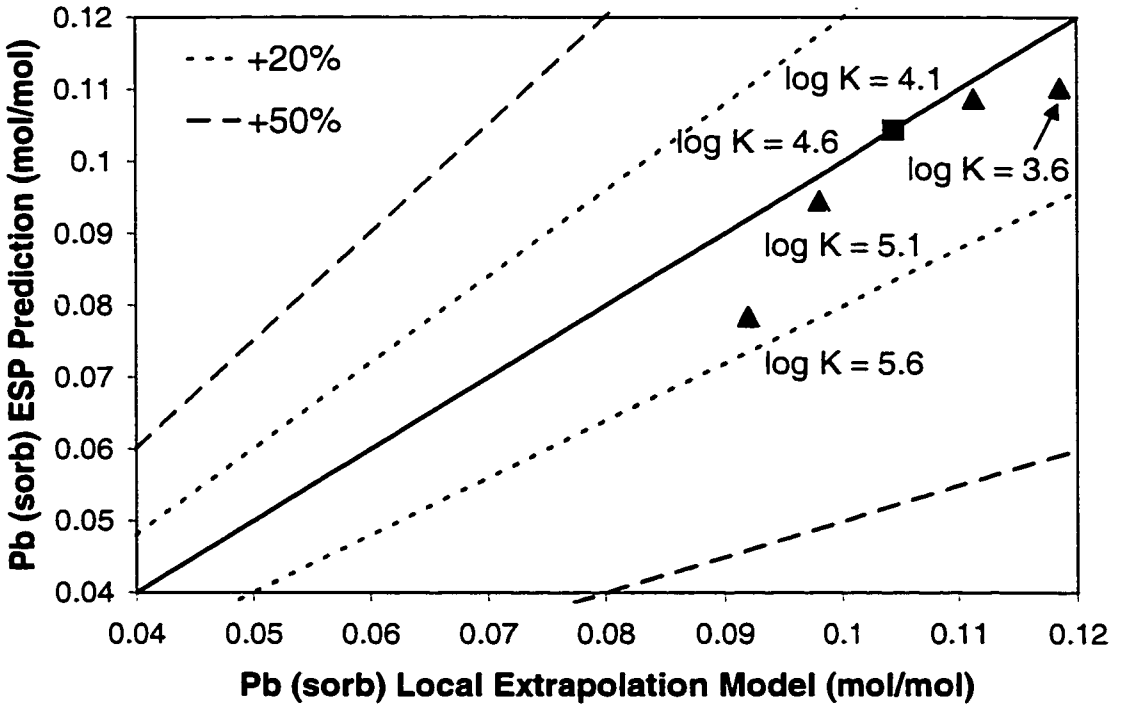

Figure D.6 **Comparison of local extrapolation model estimates to ESP model predictions for Pb_{sorb} as a function of log $K^{int}_{(\equiv FeO)_2Pb}$ for one-stage, single-solute sorption of 0.5 mM Pb onto 0.4 g L^{-1} ferrihydrite at pH 5.5 in 0.01 M $NaNO_3$ solution. Base-case log $K^{int}_{(\equiv FeO)_2Pb}$ = 4.6 at 0.4 g L^{-1} ferrihydrite.**

Appendix E

SINGLE-SOLUTE ZINC SORPTION DATA

Table E.1 Zn/ferrihydrite sorption isotherm data at pH 4.5 (25°C, N_2 glovebox, 0.01 M $NaNO_3$, 4-hr reaction time under turbulent hydraulic conditions).

$[Zn]_0$ (M)	Ferrihydrite Dose (g/L)	[Zn] 4 hr. (ppm)	[Zn] 4 hr. (M)	Γ (mol Zn/mol Fe)
5.00E-07	1	1.89E-02	2.89E-07	1.88E-05
1.00E-06	1	3.90E-02	5.96E-07	3.59E-05
2.00E-06	1	7.35E-02	1.12E-06	7.78E-05
5.00E-06	1	1.91E-01	2.91E-06	1.85E-04
1.00E-05	1	3.88E-01	5.93E-06	3.61E-04
2.00E-05	1	8.02E-01	1.23E-05	6.87E-04
5.00E-05	1	1.98E+00	3.03E-05	1.75E-03
1.00E-04	1	3.85E+00	5.89E-05	3.65E-03
2.00E-04	1	8.33E+00	1.27E-04	6.45E-03
5.00E-04	1	2.20E+01	3.36E-04	1.46E-02
1.00E-03	1	5.13E+01	7.85E-04	1.91E-02
2.00E-03	1	1.09E+02	1.66E-03	2.99E-02
5.00E-03	1	3.02E+02	4.62E-03	3.40E-02
1.00E-02	1	6.25E+02	9.55E-03	3.97E-02
2.00E-02	1	1.28E+03	1.95E-02	4.05E-02

Table E.2 Zn/ferrihydrite sorption isotherm data at pH 5.5 (25°C, N_2 glovebox, 0.01 M $NaNO_3$, 4-hr reaction time under turbulent hydraulic conditions).

$[Zn]_0$ (M)	Ferrihydrite Dose (g/L)	[Zn] 4 hr. (ppm)	[Zn] 4 hr. (M)	Γ (mol Zn/mol Fe)
5.00E-07	1	2.53E-03	3.87E-08	4.10E-05
1.00E-06	1	5.95E-03	9.10E-08	8.08E-05
2.00E-06	1	1.22E-02	1.87E-07	1.61E-04
5.00E-06	1	3.02E-02	4.61E-07	4.03E-04
1.00E-05	1	5.50E-02	8.41E-07	8.14E-04
2.00E-05	1	1.01E-01	1.54E-06	1.64E-03
5.00E-05	1	3.25E-01	4.97E-06	4.00E-03
1.00E-04	1	5.18E-01	7.93E-06	8.18E-03
2.00E-04	1	1.29E+00	1.97E-05	1.60E-02
5.00E-04	1	4.23E+00	6.46E-05	3.87E-02
1.00E-03	1	1.13E+01	1.72E-04	7.36E-02
2.00E-03	1	5.00E+01	7.65E-04	1.10E-01
5.00E-03	1	2.47E+02	3.78E-03	1.09E-01
1.00E-02	1	5.75E+02	8.79E-03	1.08E-01
2.00E-02	1	1.22E+03	1.86E-02	1.26E-01
1.00E-02	0.1	6.44E+02	9.85E-03	1.35E-01
2.00E-02	0.1	1.30E+03	1.99E-02	1.20E-01
3.00E-02	0.1	1.95E+03	2.99E-02	1.32E-01
5.00E-02	0.1	3.26E+03	4.99E-02	1.29E-01

Table E.3 Zn/ferrihydrite sorption isotherm data at pH 6.5 (25°C, N_2 glovebox, 0.01 M $NaNO_3$, 4-hr reaction time under turbulent hydraulic conditions).

$[Zn]_0$ (M)	Ferrihydrite Dose (g/L)	[Zn] 4 hr. (ppm)	[Zn] 4 hr. (M)	Γ (mol Zn/mol Fe)
5.00E-07	1	8.40E-04	1.28E-08	4.33E-05
1.00E-06	1	2.20E-03	3.36E-08	8.59E-05
2.00E-06	1	3.90E-03	5.96E-08	1.72E-04
5.00E-06	1	1.04E-02	1.59E-07	4.30E-04
1.00E-05	1	2.11E-02	3.22E-07	8.60E-04
2.00E-05	1	4.50E-02	6.87E-07	1.72E-03
5.00E-05	1	9.48E-02	1.45E-06	4.31E-03
1.00E-04	1	1.57E-01	2.39E-06	8.67E-03
2.00E-04	1	3.82E-01	5.83E-06	1.73E-02
5.00E-04	1	9.75E-01	1.49E-05	4.31E-02
1.00E-03	1	2.82E+00	4.31E-05	8.50E-02
2.00E-03	1	9.75E+00	1.49E-04	1.64E-01
5.00E-03	1	1.27E+02	1.94E-03	2.72E-01
1.00E-02	1	4.05E+02	6.19E-03	3.38E-01
2.00E-02	1	1.12E+03	1.71E-02	2.62E-01
1.00E-02	0.1	6.31E+02	9.64E-03	3.18E-01
2.00E-02	0.1	1.29E+03	1.97E-02	2.83E-01
3.00E-02	0.1	1.94E+03	2.97E-02	2.95E-01
5.00E-02	0.1	3.25E+03	4.97E-02	3.06E-01

Table E.4 Zn/ferrihydrite sorption isotherm data at pH 7.5 (25°C, N_2 glovebox, 0.01 M $NaNO_3$, 4-hr reaction time under turbulent hydraulic conditions).

$[Zn]_0$ (M)	Ferrihydrite Dose (g/L)	[Zn] 4 hr. (ppm)	[Zn] 4 hr. (M)	Γ (mol Zn/mol Fe)
5.00E-07	1	7.50E-04	1.15E-08	4.34E-05
1.00E-06	1	1.45E-03	2.22E-08	8.69E-05
2.00E-06	1	2.65E-03	4.05E-08	1.74E-04
5.00E-06	1	7.35E-03	1.12E-07	4.34E-04
1.00E-05	1	1.47E-02	2.25E-07	8.69E-04
2.00E-05	1	2.39E-02	3.65E-07	1.74E-03
5.00E-05	1	6.07E-02	9.28E-07	4.36E-03
1.00E-04	1	1.44E-01	2.20E-06	8.69E-03
2.00E-04	1	3.03E-01	4.64E-06	1.74E-02
5.00E-04	1	5.67E-01	8.67E-06	4.37E-02
1.00E-03	1	1.42E+00	2.17E-05	8.69E-02
2.00E-03	1	4.09E+00	6.25E-05	1.72E-01
2.50E-03	1	6.80E+00	1.04E-04	2.13E-01
1.00E-03	0.1	3.55E+01	5.43E-04	4.06E-01
1.50E-03	0.1	6.66E+01	1.02E-03	4.28E-01
2.00E-03	0.1	9.72E+01	1.49E-03	4.56E-01
2.50E-03	0.1	1.30E+02	1.98E-03	4.62E-01

Table E.5 **Zn/ferrihydrite pH sorption edge data for 50 μM Zn, 1 g ferrihydrite/L, and 0.001 M $NaNO_3$ solution (25°C, N_2 glovebox, 4-hr reaction time under turbulent hydraulic conditions).**

pH	[Zn] 4 hr. (ppm)	[Zn] 4 hr. (M)	Γ (mol Zn/mol Fe)	% Zn Sorbed
4.016	2.39	3.65E-05	1.20E-03	26.90
4.493	1.945	2.97E-05	1.80E-03	40.51
4.999	1.156	1.77E-05	2.87E-03	64.64
5.502	0.413	6.32E-06	3.88E-03	87.37
6.010	0.167	2.55E-06	4.22E-03	94.89
6.511	0.0825	1.26E-06	4.33E-03	97.48
7.020	0.0695	1.06E-06	4.35E-03	97.87
7.497	0.048	7.34E-07	4.38E-03	98.53
8.035	0.0432	6.607E-07	4.38E-03	98.68

Table E.6 **Zn/ferrihydrite pH sorption edge data for 50 μM Zn, 1 g ferrihydrite/L, and 0.01 M $NaNO_3$ solution (25°C, N_2 glovebox, 4-hr reaction time under turbulent hydraulic conditions).**

pH	[Zn] 4 hr. (ppm)	[Zn] 4 hr. (M)	Γ (mol Zn/mol Fe)	% Zn Sorbed
4.005	2.417	3.70E-05	1.16E-03	26.07
4.508	2.013	3.08E-05	1.71E-03	38.43
5.017	1.205	1.84E-05	2.81E-03	63.14
5.494	0.4578	7.00E-06	3.82E-03	86.00
6.030	0.1455	2.23E-06	4.24E-03	95.55
6.510	0.0809	1.24E-06	4.33E-03	97.53
7.040	0.0534	8.17E-07	4.37E-03	98.37
7.505	0.0492	7.52E-07	4.38E-03	98.50
8.014	0.0417	6.377E-07	4.39E-03	98.72

Table E.7 Zn/ferrihydrite pH sorption edge data for 50 μM Zn, 1 g ferrihydrite/L, and 0.1 M $NaNO_3$ solution (25°C, N_2 glovebox, 4-hr reaction time under turbulent hydraulic conditions).

pH	[Zn] 4 hr. (ppm)	[Zn] 4 hr. (M)	Γ (mol Zn/mol Fe)	% Zn Sorbed
4.013	2.50095	3.82E-05	1.04E-03	23.51
4.505	2.05721	3.15E-05	1.65E-03	37.08
5.033	1.23333	1.89E-05	2.77E-03	62.28
5.496	0.45274	6.92E-06	3.83E-03	86.15
6.008	0.19225	2.94E-06	4.18E-03	94.12
6.505	0.09505	1.45E-06	4.31E-03	97.09
6.989	0.07577	1.16E-06	4.34E-03	97.68
7.497	0.06833	1.04E-06	4.35E-03	97.91
7.988	0.06075	9.29E-07	4.36E-03	98.14

Table E.8 Zn/ferrihydrite pH sorption edge data for 5 μM Zn, 1 g ferrihydrite/L, and 0.01 M $NaNO_3$ solution (25°C, N_2 glovebox, 4-hr reaction time under turbulent hydraulic conditions).

pH	[Zn] 4 hr. (ppm)	[Zn] 4 hr. (M)	Γ (mol Zn/mol Fe)	% Zn Sorbed
4.022	0.22999	3.52E-06	1.32E-04	29.66
4.511	0.19217	2.94E-06	1.83E-04	41.22
5.017	0.09785	1.50E-06	3.11E-04	70.07
5.510	0.03102	4.74E-07	4.02E-04	90.51
6.011	0.01414	2.16E-07	4.25E-04	95.68
6.494	0.01	1.53E-07	4.31E-04	96.94
7.000	0.00755	1.15E-07	4.34E-04	97.69
7.506	0.00708	1.08E-07	4.35E-04	97.83
7.965	0.0047	7.19E-08	4.38E-04	98.56

Table E.9 Zn/ferrihydrite pH sorption edge data for 500 μM Zn, 1 g ferrihydrite/L, and 0.01 M $NaNO_3$ solution (25°C, N_2 glovebox, 4-hr reaction time under turbulent hydraulic conditions).

pH	[Zn] 4 hr. (ppm)	[Zn] 4 hr. (M)	Γ (mol Zn/mol Fe)	% Zn Sorbed
4.012	24.3708	3.73E-04	1.13E-02	25.46
4.492	22.0305	3.37E-04	1.45E-02	32.62
5.014	10.8656	1.66E-04	2.97E-02	66.77
5.505	4.1986	6.42E-05	3.87E-02	87.16
6.006	1.66666	2.55E-05	4.22E-02	94.90
6.500	1.00099	1.53E-05	4.31E-02	96.94
7.003	0.7315	1.12E-05	4.34E-02	97.76
7.509	0.58721	8.98E-06	4.36E-02	98.20
7.899	0.5432	8.31E-06	4.37E-02	98.34

Table E.10 Zn/ferrihydrite pH sorption edge data for 1000 μM Zn, 1 g ferrihydrite/L, and 0.01 M $NaNO_3$ solution (25°C, N_2 glovebox, 4-hr reaction time under turbulent hydraulic conditions).

pH	[Zn] 4 hr. (ppm)	[Zn] 4 hr. (M)	Γ (mol Zn/mol Fe)	% Zn Sorbed
4.007	56.0874	8.58E-04	1.26E-02	14.23
4.497	52.566	8.04E-04	1.74E-02	19.61
5.003	26.84511	4.11E-04	5.24E-02	58.95
5.499	11.289	1.73E-04	7.35E-02	82.74
6.015	5.83333	8.92E-05	8.09E-02	91.08
6.502	2.8773	4.40E-05	8.49E-02	95.60
6.993	2.0355	3.11E-05	8.61E-02	96.89
7.498	1.4925	2.28E-05	8.68E-02	97.72
8.000	1.3296	2.03E-05	8.70E-02	97.97

Appendix F

MULTISTAGE ZINC SORPTION DATA

Table F.1 Zn/ferrihydrite multistage sorption data at pH 6.5 (25°C, N_2 glovebox, 0.01 M $NaNO_3$, 4-hr reaction time under turbulent hydraulic conditions, 0.1 M NaOH or HNO_3 to adjust pH, centrifuged at 12,000 rpm for 20 minutes).

Case	Stage #	g ferrihydrite/L in each stage	Stg. 1 Zn Feed Conc. (ppm)	Zn Effluent Measured
1A	1	1.0	39.23	1.090 ppm 1.170 ppm 1.253 ppm
1B	1	0.5	39.23	3.178 ppm 3.502 ppm 3.381 ppm
	2	0.5		106.500 ppb 117.000 ppb 102.250 ppb
2A	1	5.12	1.63	7.889 ppb 9.048 ppb 7.846 ppb
2B	1	0.34	1.63	105.635 ppb 113.750 ppb 112.656 ppb
	2	0.34		6.886 ppb 6.931 ppb 7.394 ppb
2C	1	0.15	1.63	308.740 ppb 293.060 ppb 302.280 ppb
	2	0.15		50.944 ppb 49.361 ppb 50.611 ppb
	3	0.15		7.021 ppb 7.389 ppb 7.404 ppb

Table F.1 Continued.

Case	Stage #	g ferrihydrite/L in each stage	Stg. 1 Zn Feed Conc. (ppm)	Zn Effluent Measured
3A	1	0.4	16.35	1.117 ppm 1.202 ppm 1.184 ppm
3B	1	0.2	16.35	3.396 ppm 3.412 ppm 3.404 ppm
	2	0.2		418.050 ppb 413.650 ppb 407.550 ppb
3C	1	0.1	16.35	6.175 ppm 6.244 ppm 6.102 ppm
	2	0.1		1.774 ppm 1.694 ppm 1.791 ppm
	3	0.1		423.605 ppb 422.445 ppb 430.115 ppb
	4	0.1		81.957 ppb 83.405 ppb 681.675 ppb

Appendix G

ENGINEERING EVALUATION RESULTS FOR MULTISTAGE ZINC SORPTION ONTO FERRIHYDRITE

Engineering Evaluation for Multistage Zinc Sorption Onto Ferrihydrite
Equipment Design Bases and Scopes-of-Work

Design Bases

pH	6.5
Volumetric Flowrate (gpm)	100
Ionic Strength (molal)	0.01
Plant Utility (%)	90

Equalization facilities already provided
1.83 g $FeCl_3$ (100% basis)/g Ferrihydrite

Case	# Stages	Zn Feed Conc. (ppm)	Ferrihyd. Dose/ Stage (g/L)	$FeCl_3$ Dose/ Stage (g/L)
1A	1	39.23	1	1.83
1B	2	39.23	0.5	0.92
2A	1	1.63	5.12	9.37
2B	2	1.63	0.34	0.62
2C	3	1.63	0.15	0.27
3A	1	16.35	0.4	0.73
3B	2	16.35	0.2	0.37
3C	4	16.35	0.1	0.18

1) Wastewater Feed Pumps

Equipment Type:	Centrifugal Feed Pumps	
Design Basis:	100	ft TDH
	63	% Efficiency
	Installed Spare + 20% Overdesign	
MOC	316 S/S	

Case	# Pumps	Flow (gpm)	Total HP	Total KWH/yr
1A	2	120	5	28,300
1B	2	120	5	28,300
2A	2	120	5	28,300
2B	2	120	5	28,300
2C	2	120	5	28,300
3A	2	120	5	28,300
3B	2	120	5	28,300
3C	2	120	5	28,300

Figure G.1 Facility scopes-of-work for multistage Zn sorption case studies.

2) Reactor Clarifier

Equipment Type:	Upflow Solids Contact Clarifier	
Design Basis:	1000	gal/ft^2 day
	2	hour detention time minimum
	0.1	hp/1000 gallons agitation
MOC:	Epoxy-coated carbon steel or reinforced concrete	

Case	# Clarifiers	Area (ft^2)	Diam. (ft)	Depth (ft)	Holdup Time (hr)	Agitator (KWH/yr)	Bare Equipment Cost ($1000)*
1A	1	144	14	12	2.2	7600	85
1B	2	144	14	12	2.2	15199	170
2A	1	144	14	12	2.2	7600	85
2B	2	144	14	12	2.2	15199	170
2C	3	144	14	12	2.2	22799	255
3A	1	144	14	12	2.2	7600	85
3B	2	144	14	12	2.2	15199	170
3C	4	144	14	12	2.2	30398	340

* Gumerman, Burris, and Hansen (1986) Small Water System Treatment Costs. Noyes Data Corporation, Park Ridge, NJ, pg. 397.

3) 30 wt% $FeCl_3$ Storage Tank

Equipment Type:	Aboveground Fixed Roof Storage Tank	
	21	Minimum Days Storage
	10	% Freeboard
MOC:	FRP	

Case	$FeCl_3$ Dose/ Stage (g/L)	30 wt% $FeCl_3$ Soln. (gal/hr)	$FeCl_3$ Use (lb/yr 100% basis)	21-Day Capacity (gal)	Tank Size (gal)
1A	1.83	26.6	722,400	13,386	15,000
1B	0.92	26.6	722,400	13,386	15,000
2A	9.37	136.0	3,698,900	68,538	77,000
2B	0.62	18.1	491,300	9,103	11,000
2C	0.27	12.0	325,100	6,024	7,000
3A	0.73	10.6	289,000	5,355	6,000
3B	0.37	10.6	289,000	5,355	6,000
3C	0.18	10.6	289,000	5,355	6,000

Figure G.1 Continued.

4) 30 wt% $FeCl_3$ Feed Pumps

Equipment Type: Diaphragm Metering Pumps
Design Basis: 50 psi
40 % Efficiency
Installed Spare + 20% Overdesign
MOC: 304 S/S

Case	# Pumps	Pump Size (gph)	Total HP	Total KWH/yr
1A	2	32	0.04	229
1B	3	16	0.04	229
2A	2	164	0.20	1172
2B	3	11	0.03	157
2C	4	5	0.02	107
3A	2	13	0.02	93
3B	3	7	0.02	100
3C	5	4	0.02	114

5) NaOH Feed Pumps

$FeCl_3 + 3NaOH = Fe(OH)_3 + 3NaCl$

Equipment Type: Diaphragm Metering Pumps
Design Basis: 50 psi
40 % Efficiency
Installed Spare + 20% Overdesign
MOC: C/S

Case	# Pumps	NaOH Use (lb/yr 100% basis)	50% NaOH (gal/hr)	Pump Size (gph)	Total HP	Total KWH/yr	Filtered Water (Mgal/yr)
1A	2	534,600	10.8	13	0.016	93	192
1B	3	534,600	10.8	7	0.017	100	192
2A	2	2,737,200	55.4	67	0.081	479	983
2B	3	363,500	7.4	5	0.012	71	131
2C	4	240,600	4.9	2	0.007	43	86
3A	2	213,800	4.3	6	0.007	43	77
3B	3	213,800	4.3	3	0.007	43	77
3C	5	213,800	4.3	2	0.010	57	77

Figure G.1 Continued.

6) 50 wt% NaOH Storage Tank

Equipment Type: Aboveground Fixed Roof Storage Tank, Insulated and Heated
30 Minimum Days Storage
10 % Freeboard
MOC: C/S

Case	30-Day Capacity (gal)	Tank Size (gal)
1A	7,796	9,000
1B	7,796	9,000
2A	39,916	45,000
2B	5,301	6,000
2C	3,509	4,000
3A	3,118	4,000
3B	3,118	4,000
3C	3,118	4,000

7) Emulsion Polymer Feed System

Equipment Type: Skid-Mounted Polyblend System
Design Basis: 0.1 wt% polymer solution after dilution
10:1 dilution of stock polymer solution downstream of metering pump
50 psi pump discharge
40 % Pump Efficiency
20% Overdesign
MOC: Polyethylene

Case	lb Polymer/ lb Emlsyd. Solids	Avg. Total Solids (Includes Zn)* Stage (g/L)	mg/L Polymer/ Stage	Total lb/day polymer (100% basis)	Total lb/yr Polymer (100% basis)	lb/hr Conc. Polymer Solution/ Stage	Skid-Mounted Equipment Cost ($1000)
1A	0.005	1.039	5	6.2	2048	26	10
1B	0.006	0.520	3	7.5	2458	16	10
2A	0.004	5.122	20	24.6	8076	102	20
2B	0.007	0.341	2	5.7	1881	12	10
2C	0.008	0.151	1	4.3	1424	6	10
3A	0.006	0.416	2	3.0	985	12	10
3B	0.007	0.208	1	3.5	1149	7	10
3C	0.008	0.104	1	4.0	1313	4	10

Figure G.1 Continued.

Case	# Pumps	Pump Size (gph)	Total HP	Total KWH/yr	Filtered Water (Mgal/yr)
1A	1	4	0.005	27	24
1B	2	2	0.005	32	14
2A	1	15	0.018	105	96
2B	2	2	0.004	25	11
2C	3	1	0.003	19	6
3A	1	2	0.002	13	12
3B	2	1	0.003	15	7
3C	4	1	0.003	17	4

8) pH Control Systems

Design Basis: 1 system per reaction stage
Allow $12,000 capital (uninstalled)/system

Case	# Systems	Contr. Instru-ments Equip-ment Cost ($1000)
1A	1	12
1B	2	24
2A	1	12
2B	2	24
2C	3	36
3A	1	12
3B	2	24
3C	4	48

Figure G.1 Continued.

9) Clarifier Underflow Pumps

Equipment Type: Progressive Cavity/Centrifugal
Design Basis: 100 ft TDH
30 % Efficiency
Installed Spare + 20% Overdesign
MOC: 316 S/S

Case	# Pumps	Avg. Total Solids (includes Zn)/ Stage (g/L)	Under-flow Conc. (wt%)	Sludge Flow (gph)	Pump Size (gph)	Total HP	Total KWH/yr
1A	2	1.039	4	151	182	0.3	1543
1B	3	0.520	3	101	121	0.3	2057
2A	2	5.122	6	497	597	0.9	5069
2B	3	0.341	3	66	79	0.2	1349
2C	4	0.151	2	44	53	0.2	1341
3A	2	0.416	3	81	97	0.1	824
3B	3	0.208	3	40	49	0.1	824
3C	5	0.104	2	30	36	0.2	1236

10) Clarifier Overflow Pumps

Equipment Type: Centrifugal
Design Basis: 100 ft TDH
63 % Efficiency
Installed Spare + 20% Overdesign
MOC: 316 S/S

Case	# Pumps	Pump Size (gpm)	Total HP	Total KWH/yr
1A	2	120	5	28,300
1B	3	120	10	56,600
2A	2	120	5	28,300
2B	3	120	10	56,600
2C	4	120	14	84,800
3A	2	120	5	28,300
3B	3	120	10	56,600
3C	5	120	19	113,100

Figure G.1 Continued.

11) Sludge Storage Tank

Equipment Type:	Aboveground Fixed Roof Storage Tank, Agitated	
	1	Days Storage
	10	% Freeboard
	0.5	hp/1000 gallons
MOC:	FRP Tank, 304 S/S Agitator	

Case	Capacity (gal)	Tank Size (gal)	Agitator (hp)	Total KWH/yr
1A	3,632	4,100	2	12052
1B	4,843	6,000	3	17637
2A	11,934	14,000	7	41154
2B	3,177	4,000	2	11758
2C	3,157	4,000	2	11758
3A	1,940	3,000	2	8819
3B	1,940	3,000	2	8819
3C	2,910	4,000	2	11758

12) Filter Feed Pump

Equipment Type:	Progressive Cavity/Centrifugal	
Design Basis:	75	psi
	30	% Efficiency
	20% Overdesign	
MOC:	304 S/S	

Case	# Pumps	gpm/ft² filter area	Pump Size (gpm)	Total HP	Total KWH/yr
1A	1	0.34	5	0.71	2792
1B	1	0.44	6	0.93	3657
2A	1	0.29	17	2.42	9497
2B	1	0.47	4	0.61	2399
2C	1	0.46	4	0.60	2341
3A	1	0.53	3	0.37	1465
3B	1	0.53	3	0.37	1465
3C	1	0.79	4	0.55	2159

Figure G.1 Continued.

13) Membrane Pressure Filters

Equipment Type:	Oberlin Filter Press (batch cycle)	
Design Basis:	15	cycle time (min.)
	96	cycle/day
	0.35	lb/Maxflo filter aid/lb dry solids
	40	% solids of dewatered sludge
	81	lb/ft^3 dewatered sludge wet bulk density
	0.75	dewatered sludge thickness (in.)
	20	KWH/yr per ft^2 building for lighting, H&V, etc.
	0.2	KW/ft^2 filter area
	3	# cycles before filter cloth replacement

Case	Total Solids (lb/hr)	Total Solids + Maxflo (lb/hr)	Total Slurry Feed (gph)	Dewatered Sludge (lb/hr)	Dewatered Sludge (lb/yr)	Dewatered Sludge (ft^3/yr)	Filtrate (lb/hr)
1A	52	70	163	176	1,385,000	17,099	1233
1B	52	70	213	176	1,385,000	17,099	1667
2A	257	346	554	866	6,828,000	84,296	3939
2B	34	46	140	115	909,000	11,222	1093
2C	23	31	137	76	602,000	7,432	1102
3A	21	28	85	70	555,000	6,852	668
3B	21	28	85	70	555,000	6,852	668
3C	21	28	126	70	555,000	6,852	1016

Case	Filtrate (gal/day)	Dewatered Sludge (ft^3/cycle)	Filter Area/ Cycle (ft^2)	# and Size Filter Presses	Total Filter Area (ft^2)	avg. gpm/ft^2 filter	Building Size (ft^2)
1A	3544	0.54	9	1-12 ft^2	12	0.23	500
1B	4791	0.54	9	1-12 ft^2	12	0.30	500
2A	11321	2.67	43	1-48 ft^2	48	0.19	750
2B	3143	0.36	6	1-7.5 ft^2	7.5	0.31	400
2C	3166	0.24	4	1-7.5 ft^2	7.5	0.30	400
3A	1920	0.22	3	1-4 ft^2	4	0.36	400
3B	1920	0.22	3	1-4 ft^2	4	0.36	400
3C	2919	0.22	3	1-4 ft^2	4	0.52	400

Figure G.1 Continued.

Case	Bare Equipment Cost ($1000)	Electricity (KWH/yr)	Pump Time for Slurry (min)	Filter Cloth Usage (ft²/yr)
1A	135	24,191	10	126,018
1B	135	22,614	10	126,018
2A	300	65,458	10	504,071
2B	115	15,884	10	78,761
2C	115	15,884	10	78,761
3A	100	12,205	10	42,006
3B	100	12,205	10	42,006
3C	100	12,205	10	42,006

14) Maxflo Feed System

Purpose: Filter Aid
Equipment: Hopper & Conveyor, Monorail for Supersacs, Mix Tank w/ Agitator, Dust Collector, Slurry Feed Pump, and Static Mixer
17 % Solids Slurry

Case	Total Solids (lb/hr)	Maxflo (lb/hr)	Maxflo (lb/yr)	Maxflo Slurry (lb/hr)	Maxflo Slurry (gph)	Bare Equipment Cost ($1000)	Electricity (KWH/yr)
1A	52	18	143,700	107	11	30	5,988
1B	52	18	143,700	107	11	30	5,988
2A	257	90	708,000	528	57	40	6,418
2B	34	12	94,200	70	8	25	5,951
2C	23	8	62,400	47	5	25	5,927
3A	21	7	57,600	43	5	25	5,923
3B	21	7	57,600	43	5	25	5,923
3C	21	7	57,600	43	5	25	5,923

Figure G.1 Continued.

15) Filtrate Tank

Equipment Type: Aboveground Fixed Roof Storage Tank
1 Days Storage
10 % Freeboard
MOC: FRP

Case	Capacity (gal)	Tank Size (gal)
1A	3,544	4,000
1B	4,791	5,400
2A	11,321	12,600
2B	3,143	3,500
2C	3,166	3,600
3A	1,920	2,200
3B	1,920	2,200
3C	2,919	3,300

16) Filtrate Pump

Equipment Type: Centrifugal Pump
Design Basis: 100 ft TDH
63 % Efficiency
20% Overdesign
MOC: 316 S/S

Case	# Pumps	Flow (gpm)	Total HP	Total KWH/yr
1A	1	160	6	655
1B	1	220	9	900
2A	1	360	14	2062
2B	1	140	6	573
2C	1	140	6	573
3A	1	90	4	368
3B	1	90	4	368
3C	1	130	5	532

Figure G.1 Continued.

17) Dumpsters

Equipment Type: 4' x 6' x 12' dumpsters (288 ft^3)

Case	Sludge (ft^3/day)	# Dumpsters	Project Level Cost ($1000)
1A	52	2	20
1B	52	2	20
2A	257	6	60
2B	34	1	10
2C	23	1	10
3A	21	1	10
3B	21	1	10
3C	21	1	10

Figure G.1 Continued.

Engineering Evaluation for Multistage Zinc Sorption Onto Ferrihydrite
Operating and Maintenance Requirements Summary

Case	FeCl3 (lb/yr)	50% NaOH (lb/yr)	Emulsion Polymer (lb/yr)	Maxflo (lb/yr)	Filter Cloth (ft^2/yr)	Electricity (KWh/yr)	Power (KW)	Sludge Disposal (lb/yr)
1A	722,400	534,600	2048	143,700	126,018	111,769	14	1,385,000
1B	722,400	534,600	2458	143,700	126,018	153,314	19	1,385,000
2A	3,698,900	2,737,200	8076	708,000	504,071	195,613	25	6,826,000
2B	491,300	363,500	1881	94,200	78,761	138,266	18	909,000
2C	325,100	240,600	1424	62,400	78,761	173,891	22	602,000
3A	289,000	213,800	985	57,600	42,006	93,952	12	555,000
3B	289,000	213,800	1149	57,600	42,006	129,861	16	555,000
3C	289,000	213,800	1313	57,600	42,006	205,799	26	555,000

Case	Filtered Water (Mgal/yr)
1A	649
1B	619
2A	3,238
2B	425
2C	276
3A	265
3B	251
3C	242

Material	Cost	Units for Cost	Basis for Cost
30% $FeCl_3$	0.15	$/lb	100% basis
50% NaOH	0.15	$/lb	100% basis
Emulsion Polymer	1.50	$/lb	100% basis
Maxflo	0.165	$/lb	100% basis
Filter Cloth	0.095	$/$ft^2$	100% basis
Filtered Water	0.15	$/lb	100% basis
Electricity	0.045	$/kWh	100% basis
Hazardous Waste Landfill Disposal	0.085	$/lb	100% basis

Figure G.2 Operating requirements and raw material costs for multistage Zn sorption case studies.

Research Guidance Appraisal

TITLE: Zinc Multistage Sorption RGA NAME: Case 1A
CASE NUMBER: Case 1A ACCT NUM:
SCOPE: SITE: Gulf Coast

	Factor %	$M	
ENGINEERED EQUIPMENT		329	EE,TK,COL, HX,PMP,AGIT
RELOCATED/EXISTING EQUIPMENT		0	EX,REL
MISC EQUIPMENT	5	16	
EQUIPMENT SUBTOTAL		345	
FIELD MTL/LABOR/INSUL 3 10 4 17		59	
FIELD ERECTED EQUIPMENT		85	FE
FACTORED FDNS,SUP,PLT	7	24	
IDENTIFIED FDNS,SUP,PLT		0	FSP
EXISTING IN PLACE EQUIPMENT		0	EIP
INSTALLED EQUIPMENT SUBTOTAL		513	
FACTORED PIPING	45	231	
FACTORED INSTRUMENTS	16	82	
FACTORED ELECTRICAL	11	56	
IDENTIFIED PIPING		0	PIPE
IDENTIFIED INSTRUMENTS		12	INSTR
IDENTIFIED ELECTRICAL		0	ELECT
MCC/ICR/ECR EQUIP	6	31	
CONNECTED SUBTOTAL		925	
SPECIAL PROCESS ITEMS		62	SPE
PACKING		0	PACK
OTHER		0	LM
IDENTIFIED BUILDINGS,STRUCTURES		52	BLDG
ISBL SUBTOTAL		1039	
IDENTIFIED PG&S		0	PG&S
FACTORED PG&S	10	104	
IDENTIFIED D&R		0	D&R
FACTORED D&R	2	21	
OSBL INCLUDED SUBTOTAL		1164	
PROJECT CONTINGENCY	15	175	
PROCESS CONTINGENCY	10	116	
DEVELOPED SUBTOTAL		1455	

Figure G.3 Factored investment estimate for multistage Zn sorption Case 1A.

DEVELOPED SUBTOTAL		1455	
LABOR/MATERIAL SPLIT	25		
WORKING CONDITIONS	10	36	
FREIGHT,QA,PROCUREMENT,SALES TAX	11	120	

NET TOTAL		1611	
ABNORMAL PREMIUM TIME	0	0	
MINOR CHANGES	2	32	

DIRECT TOTAL		1643	
ENGG & HOME OFFICE	20	456	
FIELD INDIRECTS	8	183	
SPARES & PORTABLES		20	SPARE,PORT
PROJECT LEVEL ALLOWANCES		0	PROJ
CREDIT FOR EXISTING EQUIPMENT		0	
(INCL CONT,FRT,TAX,QA,PROC)		---	
CURRENT COST		2302	
LOCATION FACTOR	1.00	2302	
ESCALATION TO MPC	1.02	2348	
AUTH 1Q2002 MPC 4Q2002 M/C 2Q2003			
COUNTRY CURRENCY REVALUATION	1.00	2348	
PROJECT COST SAY		2300	

Figure G.3 Continued.

Research Guidance Appraisal

TITLE: Zinc Multistage Sorption RGA NAME: Case 1B
CASE NUMBER: Case 1B ACCT NUM:
SCOPE: SITE: Gulf Coast

	Factor %	$M	
ENGINEERED EQUIPMENT		351	EE,TK,COL, HX,PMP,AGIT
RELOCATED/EXISTING EQUIPMENT		0	EX,REL
MISC EQUIPMENT	5	18	
EQUIPMENT SUBTOTAL		369	
FIELD MTL/LABOR/INSUL	3 10 4 17	63	
FIELD ERECTED EQUIPMENT		170	FE
FACTORED FDNS,SUP,PLT	7	26	
IDENTIFIED FDNS,SUP,PLT		0	FSP
EXISTING IN PLACE EQUIPMENT		0	EIP
INSTALLED EQUIPMENT SUBTOTAL		628	
FACTORED PIPING	45	283	
FACTORED INSTRUMENTS	16	100	
FACTORED ELECTRICAL	11	69	
IDENTIFIED PIPING		0	PIPE
IDENTIFIED INSTRUMENTS		24	INSTR
IDENTIFIED ELECTRICAL		0	ELECT
MCC/ICR/ECR EQUIP	6	38	
CONNECTED SUBTOTAL		1142	
SPECIAL PROCESS ITEMS		62	SPE
PACKING		0	PACK
OTHER		0	LM
IDENTIFIED BUILDINGS,STRUCTURES		52	BLDG
ISBL SUBTOTAL		1256	
IDENTIFIED PG&S		0	PG&S
FACTORED PG&S	10	126	
IDENTIFIED D&R		0	D&R
FACTORED D&R	2	25	
OSBL INCLUDED SUBTOTAL		1407	
PROJECT CONTINGENCY	15	211	
PROCESS CONTINGENCY	10	141	
DEVELOPED SUBTOTAL		1759	

Figure G.4 Factored investment estimate for multistage Zn sorption Case 1B.

DEVELOPED SUBTOTAL		1759	
LABOR/MATERIAL SPLIT	25		
WORKING CONDITIONS	10	44	
FREIGHT,QA,PROCUREMENT,SALES TAX	11	145	
NET TOTAL		1948	
ABNORMAL PREMIUM TIME	0	0	
MINOR CHANGES	2	39	
DIRECT TOTAL		1987	
ENGG & HOME OFFICE	20	552	
FIELD INDIRECTS	8	221	
SPARES & PORTABLES		20	SPARE,PORT
PROJECT LEVEL ALLOWANCES		0	PROJ
CREDIT FOR EXISTING EQUIPMENT (INCL CONT,FRT,TAX,QA,PROC)		0	
CURRENT COST		2780	
LOCATION FACTOR	1.00	2780	
ESCALATION TO MPC	1.02	2836	
AUTH 1Q2002 MPC 4Q2002 M/C 2Q2003			
COUNTRY CURRENCY REVALUATION	1.00	2836	
PROJECT COST SAY		2800	

Figure G.4 Continued.

Research Guidance Appraisal

TITLE: Zinc Multistage Sorption RGA NAME: Case 2A
CASE NUMBER: Case 2A ACCT NUM:
SCOPE: SITE: Gulf Coast

	Factor %	$M	
ENGINEERED EQUIPMENT		665	EE,TK,COL, HX,PMP,AGIT
RELOCATED/EXISTING EQUIPMENT		0	EX,REL
MISC EQUIPMENT	5	33	
EQUIPMENT SUBTOTAL		698	
FIELD MTL/LABOR/INSUL	3 10 4 17	119	
FIELD ERECTED EQUIPMENT		85	FE
FACTORED FDNS,SUP,PLT	7	49	
IDENTIFIED FDNS,SUP,PLT		0	FSP
EXISTING IN PLACE EQUIPMENT		0	EIP
INSTALLED EQUIPMENT SUBTOTAL		951	
FACTORED PIPING	45	428	
FACTORED INSTRUMENTS	16	152	
FACTORED ELECTRICAL	11	105	
IDENTIFIED PIPING		0	PIPE
IDENTIFIED INSTRUMENTS		12	INSTR
IDENTIFIED ELECTRICAL		0	ELECT
MCC/ICR/ECR EQUIP	6	57	
CONNECTED SUBTOTAL		1705	
SPECIAL PROCESS ITEMS		93	SPE
PACKING		0	PACK
OTHER		0	LM
IDENTIFIED BUILDINGS,STRUCTURES		78	BLDG
ISBL SUBTOTAL		1876	
IDENTIFIED PG&S		0	PG&S
FACTORED PG&S	10	188	
IDENTIFIED D&R		0	D&R
FACTORED D&R	2	38	
OSBL INCLUDED SUBTOTAL		2102	
PROJECT CONTINGENCY	15	315	
PROCESS CONTINGENCY	10	210	
DEVELOPED SUBTOTAL		2627	

Figure G.5 Factored investment estimate for multistage Zn sorption Case 2A.

DEVELOPED SUBTOTAL		2627	
LABOR/MATERIAL SPLIT	25		
WORKING CONDITIONS	10	66	
FREIGHT,QA,PROCUREMENT,SALES TAX	11	217	

NET TOTAL		2910	
ABNORMAL PREMIUM TIME	0	0	
MINOR CHANGES	2	58	

DIRECT TOTAL		2968	
ENGG & HOME OFFICE	20	824	
FIELD INDIRECTS	8	330	
SPARES & PORTABLES		60	SPARE,PORT
PROJECT LEVEL ALLOWANCES		0	PROJ
CREDIT FOR EXISTING EQUIPMENT		0	
(INCL CONT,FRT,TAX,QA,PROC)		----------	
CURRENT COST		4182	
LOCATION FACTOR	1.00	4182	
ESCALATION TO MPC	1.02	4266	
AUTH 1Q2002 MPC 4Q2002 M/C 2Q2003			
COUNTRY CURRENCY REVALUATION	1.00	4266	
PROJECT COST SAY		4300	

Figure G.5 Continued.

Research Guidance Appraisal

TITLE: Zinc Multistage Sorption RGA NAME: Case 2B
CASE NUMBER: Case 2B ACCT NUM:
SCOPE: SITE: Gulf Coast

	Factor %	$M	
ENGINEERED EQUIPMENT		307	EE,TK,COL, HX,PMP,AGIT
RELOCATED/EXISTING EQUIPMENT		0	EX,REL
MISC EQUIPMENT	5	15	
EQUIPMENT SUBTOTAL		322	
FIELD MTL/LABOR/INSUL 3 10 4 17		55	
FIELD ERECTED EQUIPMENT		170	FE
FACTORED FDNS,SUP,PLT	7	23	
IDENTIFIED FDNS,SUP,PLT		0	FSP
EXISTING IN PLACE EQUIPMENT		0	EIP
INSTALLED EQUIPMENT SUBTOTAL		570	
FACTORED PIPING	45	257	
FACTORED INSTRUMENTS	16	91	
FACTORED ELECTRICAL	11	63	
IDENTIFIED PIPING		0	PIPE
IDENTIFIED INSTRUMENTS		24	INSTR
IDENTIFIED ELECTRICAL		0	ELECT
MCC/ICR/ECR EQUIP	6	34	
CONNECTED SUBTOTAL		1039	
SPECIAL PROCESS ITEMS		54	SPE
PACKING		0	PACK
OTHER		0	LM
IDENTIFIED BUILDINGS,STRUCTURES		41	BLDG
ISBL SUBTOTAL		1134	
IDENTIFIED PG&S		0	PG&S
FACTORED PG&S	10	113	
IDENTIFIED D&R		0	D&R
FACTORED D&R	2	23	
OSBL INCLUDED SUBTOTAL		1270	
PROJECT CONTINGENCY	15	191	
PROCESS CONTINGENCY	10	127	
DEVELOPED SUBTOTAL		1588	

Figure G.6 Factored investment estimate for multistage Zn sorption Case 2B.

DEVELOPED SUBTOTAL		1588	
LABOR/MATERIAL SPLIT	25		
WORKING CONDITIONS	10	40	
FREIGHT,QA,PROCUREMENT,SALES TAX	11	131	

NET TOTAL		1759	
ABNORMAL PREMIUM TIME	0	0	
MINOR CHANGES	2	35	

DIRECT TOTAL		1794	
ENGG & HOME OFFICE	20	498	
FIELD INDIRECTS	8	199	
SPARES & PORTABLES		10	SPARE,PORT
PROJECT LEVEL ALLOWANCES		0	PROJ
CREDIT FOR EXISTING EQUIPMENT		0	
(INCL CONT,FRT,TAX,QA,PROC)		---	
CURRENT COST		2501	
LOCATION FACTOR	1.00	2501	
ESCALATION TO MPC	1.02	2551	
AUTH 1Q2002 MPC 4Q2002 M/C 2Q2003			
COUNTRY CURRENCY REVALUATION	1.00	2551	
PROJECT COST SAY		2600	

Figure G.6 Continued.

Research Guidance Appraisal

TITLE: Zinc Multistage Sorption RGA NAME: Case 2C
CASE NUMBER: Case 2C ACCT NUM:
SCOPE: SITE: Gulf Coast

	Factor %	$M	
ENGINEERED EQUIPMENT		308	EE,TK,COL, HX,PMP,AGIT
RELOCATED/EXISTING EQUIPMENT		0	EX,REL
MISC EQUIPMENT	5	15	
EQUIPMENT SUBTOTAL		323	
FIELD MTL/LABOR/INSUL	3 10 4 17	55	
FIELD ERECTED EQUIPMENT		255	FE
FACTORED FDNS,SUP,PLT	7	23	
IDENTIFIED FDNS,SUP,PLT		0	FSP
EXISTING IN PLACE EQUIPMENT		0	EIP
INSTALLED EQUIPMENT SUBTOTAL		656	
FACTORED PIPING	45	295	
FACTORED INSTRUMENTS	16	105	
FACTORED ELECTRICAL	11	72	
IDENTIFIED PIPING		0	PIPE
IDENTIFIED INSTRUMENTS		36	INSTR
IDENTIFIED ELECTRICAL		0	ELECT
MCC/ICR/ECR EQUIP	6	39	
CONNECTED SUBTOTAL		1203	
SPECIAL PROCESS ITEMS		54	SPE
PACKING		0	PACK
OTHER		0	LM
IDENTIFIED BUILDINGS,STRUCTURES		41	BLDG
ISBL SUBTOTAL		1298	
IDENTIFIED PG&S		0	PG&S
FACTORED PG&S	10	130	
IDENTIFIED D&R		0	D&R
FACTORED D&R	2	26	
OSBL INCLUDED SUBTOTAL		1454	
PROJECT CONTINGENCY	15	218	
PROCESS CONTINGENCY	10	145	
DEVELOPED SUBTOTAL		1817	

Figure G.7 Factored investment estimate for multistage Zn sorption Case 2C.

DEVELOPED SUBTOTAL		1817	
LABOR/MATERIAL SPLIT	25		
WORKING CONDITIONS	10	45	
FREIGHT,QA,PROCUREMENT,SALES TAX	11	150	

NET TOTAL		2012	
ABNORMAL PREMIUM TIME	0	0	
MINOR CHANGES	2	40	

DIRECT TOTAL		2052	
ENGG & HOME OFFICE	20	570	
FIELD INDIRECTS	8	228	
SPARES & PORTABLES		10	SPARE,PORT
PROJECT LEVEL ALLOWANCES		0	PROJ
CREDIT FOR EXISTING EQUIPMENT		0	
(INCL CONT,FRT,TAX,QA,PROC)		---	
CURRENT COST		2860	
LOCATION FACTOR	1.00	2860	
ESCALATION TO MPC	1.02	2917	
AUTH 1Q2002 MPC 4Q2002 M/C 2Q2003			
COUNTRY CURRENCY REVALUATION	1.00	2917	
PROJECT COST SAY		2900	

Figure G.7 Continued.

Research Guidance Appraisal

TITLE: Zinc Multistage Sorption RGA NAME: Case 3A
CASE NUMBER: Case 3A ACCT NUM:
SCOPE: SITE: Gulf Coast

	Factor %	$M	
ENGINEERED EQUIPMENT		259	EE,TK,COL, HX,PMP,AGIT
RELOCATED/EXISTING EQUIPMENT		0	EX,REL
MISC EQUIPMENT	5	13	
EQUIPMENT SUBTOTAL		272	
FIELD MTL/LABOR/INSUL 3 10 4 17		46	
FIELD ERECTED EQUIPMENT		85	FE
FACTORED FDNS,SUP,PLT	7	19	
IDENTIFIED FDNS,SUP,PLT		0	FSP
EXISTING IN PLACE EQUIPMENT		0	EIP
INSTALLED EQUIPMENT SUBTOTAL		422	
FACTORED PIPING	45	190	
FACTORED INSTRUMENTS	16	68	
FACTORED ELECTRICAL	11	46	
IDENTIFIED PIPING		0	PIPE
IDENTIFIED INSTRUMENTS		12	INSTR
IDENTIFIED ELECTRICAL		0	ELECT
MCC/ICR/ECR EQUIP	6	25	
CONNECTED SUBTOTAL		763	
SPECIAL PROCESS ITEMS		54	SPE
PACKING		0	PACK
OTHER		0	LM
IDENTIFIED BUILDINGS,STRUCTURES		41	BLDG
ISBL SUBTOTAL		858	
IDENTIFIED PG&S		0	PG&S
FACTORED PG&S	10	86	
IDENTIFIED D&R		0	D&R
FACTORED D&R	2	17	
OSBL INCLUDED SUBTOTAL		961	
PROJECT CONTINGENCY	15	144	
PROCESS CONTINGENCY	10	96	
DEVELOPED SUBTOTAL		1201	

Figure G.8 Factored investment estimate for multistage Zn sorption Case 3A.

DEVELOPED SUBTOTAL		1201	
LABOR/MATERIAL SPLIT	25		
WORKING CONDITIONS	10	30	
FREIGHT,QA,PROCUREMENT,SALES TAX	11	99	
NET TOTAL		1330	
ABNORMAL PREMIUM TIME	0	0	
MINOR CHANGES	2	27	
DIRECT TOTAL		1357	
ENGG & HOME OFFICE	20	377	
FIELD INDIRECTS	8	151	
SPARES & PORTABLES		10	SPARE,PORT
PROJECT LEVEL ALLOWANCES		0	PROJ
CREDIT FOR EXISTING EQUIPMENT (INCL CONT,FRT,TAX,QA,PROC)		0	
CURRENT COST		1895	
LOCATION FACTOR	1.00	1895	
ESCALATION TO MPC	1.01	1914	
AUTH 1Q2002 MPC 3Q2002 M/C 1Q2003			
COUNTRY CURRENCY REVALUATION	1.00	1914	
PROJECT COST SAY		1900	

Figure G.8 Continued.

Research Guidance Appraisal

TITLE: Zinc Multistage Sorption RGA NAME: Case 3B
CASE NUMBER: Case 3B ACCT NUM:
SCOPE: SITE: Gulf Coast

	Factor %	$M	
ENGINEERED EQUIPMENT		274	EE,TK,COL, HX,PMP,AGIT
RELOCATED/EXISTING EQUIPMENT		0	EX,REL
MISC EQUIPMENT	5	14	
EQUIPMENT SUBTOTAL		288	
FIELD MTL/LABOR/INSUL	3 10 4 17	49	
FIELD ERECTED EQUIPMENT		170	FE
FACTORED FDNS,SUP,PLT	7	20	
IDENTIFIED FDNS,SUP,PLT		0	FSP
EXISTING IN PLACE EQUIPMENT		0	EIP
INSTALLED EQUIPMENT SUBTOTAL		527	
FACTORED PIPING	45	237	
FACTORED INSTRUMENTS	16	84	
FACTORED ELECTRICAL	11	58	
IDENTIFIED PIPING		0	PIPE
IDENTIFIED INSTRUMENTS		24	INSTR
IDENTIFIED ELECTRICAL		0	ELECT
MCC/ICR/ECR EQUIP	6	32	
CONNECTED SUBTOTAL		962	
SPECIAL PROCESS ITEMS		54	SPE
PACKING		0	PACK
OTHER		0	LM
IDENTIFIED BUILDINGS,STRUCTURES		41	BLDG
ISBL SUBTOTAL		1057	
IDENTIFIED PG&S		0	PG&S
FACTORED PG&S	10	106	
IDENTIFIED D&R		0	D&R
FACTORED D&R	2	21	
OSBL INCLUDED SUBTOTAL		1184	
PROJECT CONTINGENCY	15	178	
PROCESS CONTINGENCY	10	118	
DEVELOPED SUBTOTAL		1480	

Figure G.9 Factored investment estimate for multistage Zn sorption Case 3B.

DEVELOPED SUBTOTAL		1480	
LABOR/MATERIAL SPLIT	25		
WORKING CONDITIONS	10	37	
FREIGHT,QA,PROCUREMENT,SALES TAX	11	122	
NET TOTAL		1639	
ABNORMAL PREMIUM TIME	0	0	
MINOR CHANGES	2	33	
DIRECT TOTAL		1672	
ENGG & HOME OFFICE	20	464	
FIELD INDIRECTS	8	186	
SPARES & PORTABLES		10	SPARE,PORT
PROJECT LEVEL ALLOWANCES		0	PROJ
CREDIT FOR EXISTING EQUIPMENT (INCL CONT,FRT,TAX,QA,PROC)		0	
CURRENT COST		2332	
LOCATION FACTOR	1.00	2332	
ESCALATION TO MPC AUTH 1Q2002 MPC 4Q2002 M/C 2Q2003	1.02	2379	
COUNTRY CURRENCY REVALUATION	1.00	2379	
PROJECT COST SAY		2400	

Figure G.9 Continued.

Research Guidance Appraisal

TITLE: Zinc Multistage Sorption RGA NAME: Case 3C
CASE NUMBER: Case 3C ACCT NUM:
SCOPE: SITE: Gulf Coast

	Factor %	$M	
ENGINEERED EQUIPMENT		311	EE,TK,COL, HX,PMP,AGIT
RELOCATED/EXISTING EQUIPMENT		0	EX,REL
MISC EQUIPMENT	5	16	
EQUIPMENT SUBTOTAL		327	
FIELD MTL/LABOR/INSUL	3 10 4 17	56	
FIELD ERECTED EQUIPMENT		340	FE
FACTORED FDNS,SUP,PLT	7	23	
IDENTIFIED FDNS,SUP,PLT		0	FSP
EXISTING IN PLACE EQUIPMENT		0	EIP
INSTALLED EQUIPMENT SUBTOTAL		746	
FACTORED PIPING	45	336	
FACTORED INSTRUMENTS	16	119	
FACTORED ELECTRICAL	11	82	
IDENTIFIED PIPING		0	PIPE
IDENTIFIED INSTRUMENTS		48	INSTR
IDENTIFIED ELECTRICAL		0	ELECT
MCC/ICR/ECR EQUIP	6	45	
CONNECTED SUBTOTAL		1376	
SPECIAL PROCESS ITEMS		54	SPE
PACKING		0	PACK
OTHER		0	LM
IDENTIFIED BUILDINGS,STRUCTURES		41	BLDG
ISBL SUBTOTAL		1471	
IDENTIFIED PG&S		0	PG&S
FACTORED PG&S	10	147	
IDENTIFIED D&R		0	D&R
FACTORED D&R	2	29	
OSBL INCLUDED SUBTOTAL		1647	
PROJECT CONTINGENCY	15	247	
PROCESS CONTINGENCY	10	165	
DEVELOPED SUBTOTAL		2059	

Figure G.10 Factored investment estimate for multistage Zn sorption Case 3C.

DEVELOPED SUBTOTAL		2059	
LABOR/MATERIAL SPLIT	25		
WORKING CONDITIONS	10	52	
FREIGHT,QA,PROCUREMENT,SALES TAX	11	170	

NET TOTAL		2281	
ABNORMAL PREMIUM TIME	0	0	
MINOR CHANGES	2	46	

DIRECT TOTAL		2327	
ENGG & HOME OFFICE	20	646	
FIELD INDIRECTS	8	259	
SPARES & PORTABLES		10	SPARE,PORT
PROJECT LEVEL ALLOWANCES		0	PROJ
CREDIT FOR EXISTING EQUIPMENT		0	
(INCL CONT,FRT,TAX,QA,PROC)		---	
CURRENT COST		3242	
LOCATION FACTOR	1.00	3242	
ESCALATION TO MPC	1.02	3307	
AUTH 1Q2002 MPC 4Q2002 M/C 2Q2003			
COUNTRY CURRENCY REVALUATION	1.00	3307	
PROJECT COST SAY		3300	

Figure G.10 Continued.

Escalation and Cost Factors for Cash Flow Analysis

YEAR END	2002	2003	2004	2005	2006	2007	2008	2009	2010	2011	2012
INVESTMENT, $1000											
4th Quarter CCI	246	252	258	265	272	278	285	292	300	307	315
New Permanent(4Q)	3,300	0	0	0	0	0	0	0	0	0	0
Creep Invest. (% Replace Inv.)	1.5%	50	51	54	56	58	60	63	65	68	70
Total New Book Investment	3300	3350	3401	3455	3510	3568	3628	3691	3756	3824	3894
Replacement Investment	3300	3432	3569	3712	3861	4015	4176	4343	4516	4697	4885
Depreciation 6 year	0.2	0.32	0.19	0.12	0.12	0.05					
OPERATING COSTS, $1000											
Raw Materials	Cost				Escalation Factors						
50% NaOH ($/lb)	0.15	2.5%	2.5%	2.5%	2.5%	2.5%	2.5%	2.5%	2.5%	2.5%	2.5%
30% $FeCl_3$ ($/lb)	0.15	2.5%	2.5%	2.5%	2.5%	2.5%	2.5%	2.5%	2.5%	2.5%	2.5%
Maxflo ($/lb)	0.165	2.5%	2.5%	2.5%	2.5%	2.5%	2.5%	2.5%	2.5%	2.5%	2.5%
Filter Cloth ($/ft^2)	0.095	2.5%	2.5%	2.5%	2.5%	2.5%	2.5%	2.5%	2.5%	2.5%	2.5%
Emulsion Polymer ($/lb)	1.50	2.5%	2.5%	2.5%	2.5%	2.5%	2.5%	2.5%	2.5%	2.5%	2.5%
Utilities											
Electricity ($/kWh)	0.045	2.5%	2.5%	2.5%	2.5%	2.5%	2.5%	2.5%	2.5%	2.5%	2.5%
Filtered Water ($/1000Gal)	0.15	2.5%	2.5%	2.5%	2.5%	2.5%	2.5%	2.5%	2.5%	2.5%	2.5%
General Escalation Factor		2.5%	2.5%	2.5%	2.5%	2.5%	2.5%	2.5%	2.5%	2.5%	2.5%
Waste Disposal											
Hazardous Landfill ($/lb)	0.085	2.5%	2.5%	2.5%	2.5%	2.5%	2.5%	2.5%	2.5%	2.5%	2.5%
Technical Exempt ($1000/yr)	160	2.5%	2.5%	2.5%	2.5%	2.5%	2.5%	2.5%	2.5%	2.5%	2.5%
Operations ($1000/yr)	430	2.5%	2.5%	2.5%	2.5%	2.5%	2.5%	2.5%	2.5%	2.5%	2.5%
Lab Support ($1000/yr)	0	2.5%	2.5%	2.5%	2.5%	2.5%	2.5%	2.5%	2.5%	2.5%	2.5%
Maintenance (60% L, 40% M)	% R. Inv.	4.0%	4.0%	4.0%	4.0%	4.0%	4.0%	4.0%	4.0%	4.0%	4.0%
Taxes & Insurance	% R. Inv.	0.75%	0.75%	0.75%	0.75%	0.75%	0.75%	0.75%	0.75%	0.75%	0.75%
Gen. Inv. Related Plant Ovhd.	% R. Inv.	0.5%	0.5%	0.5%	0.5%	0.5%	0.5%	0.5%	0.5%	0.5%	0.5%
Gen. OL Plant Ovhd. (%(OL+ Supv+ Main Labor))	%	24%	24%	24%	24%	24%	24%	24%	24%	24%	24%
Income Tax Rate	40%	40%	40%	40%	40%	40%	40%	40%	40%	40%	40%
Project Liaison Costs	% of NPI	2.0%									
Startup Costs	% of NPI	10%									
Revenue		2.5%	2.5%	2.5%	2.5%	2.5%	2.5%	2.5%	2.5%	2.5%	2.5%

Figure G.11 Example cash flow analysis for multistage Zn sorption case studies.

Engineering Evaluation for Multistage Zinc Sorption Onto Ferrihydrite
2002 Startup Case: 3C

CASH FLOW ANALYSIS

YEAR END		2002	2003	2004	2005	2006	2007	2008	2009	2010	2011	2012
INVESTMENT ($1000)												
4th Quarter CCI		246	252	258	265	272	278	285	292	300	307	315
New Permanent(4Q)		3300	50	51	54	56	58	60	63	65	68	70
Working Cap. ($M)		19	152	101	104	107	111	114	118	121	125	129
Total Investment		3319	3501	3502	3559	3618	3679	3742	3809	3877	3949	4023
OPERATING COSTS ($1000)											**$1000/YEAR**	
Raw Materials	Consumption											
50% NaOH (lb/yr)	213800		-33	-34	-35	-35	-36	-37	-38	-39	-40	-41
30% $FeCl_3$ (lb/yr)	289000		-44	-46	-47	-48	-49	-50	-52	-53	-54	-55
Maxflo (lb/yr)	57600		-10	-10	-10	-10	-11	-11	-11	-12	-12	-12
Filter Cloth (ft^2/yr)	42006		-4	-4	-4	-4	-5	-5	-5	-5	-5	-5
Emulsion Polymer (lb/yr)	1313		-2	-2	-2	-2	-2	-2	-2	-2	-2	-3
Utilities												
Electricity (kWh/yr)	205799		-9	-10	-10	-10	-10	-11	-11	-11	-12	-12
Filtered Water (1000Gal/yr)	242		0	0	0	0	0	0	0	0	0	0
Waste Disposal												
Hazardous Landfill (lb/yr)	555000		-48	-50	-51	-52	-53	-55	-56	-57	-59	-60
Lab Support			0	0	0	0	0	0	0	0	0	0
Tech. Exempt (No./yr)	0.35		-57	-59	-60	-62	-63	-65	-67	-68	-70	-72
Operations (No./yr)	0.35		-154	-158	-162	-166	-170	-175	-179	-183	-188	-193
Maintenance			-135	-141	-146	-152	-158	-165	-171	-178	-185	-193
Basic Data Devel. ($1000)	50	-50	0	0	0	0	0	0	0	0	0	0
Project Liaison Costs		-66	0	0	0	0	0	0	0	0	0	0
Startup Costs			-330	-5	-5	-5	-6	-6	-6	-6	-7	-7
Taxes & Insurance			-25	-26	-27	-28	-29	-30	-31	-33	-34	-35
General Plant Overhead			-71	-73	-75	-78	-81	-83	-86	-89	-92	-95
Cash Costs		-116	-924	-616	-635	-654	-674	-694	-715	-737	-759	-782
TOTAL COST, DEPRECIATION, AND CASH FLOW												
Depreciation			-660	-1066	-653	-433	-440	-217	-56	-58	-61	-63
Total Cost		-116	-1584	-1682	-1288	-1087	-1114	-911	-771	-795	-820	-845
Other Revenue ($1000/yr)	0		0	0	0	0	0	0	0	0	0	0
Pretax Earnings		-116	-1584	-1682	-1288	-1087	-1114	-911	-771	-795	-820	-845
Income Taxes		46	633	673	515	435	445	364	309	318	328	338
Operating Earnings		-70	-950	-1009	-773	-652	-668	-546	-463	-477	-492	-507
Net Cash Flow w/o Infinite Life		-3389	-472	56	-176	-278	-289	-393	-473	-487	-503	-518
Fut. Cash Flows (1/2 Infinite Life @12%)												-2160
Fut. Cash Flows (1/2 Infinite Life @25%)												-1037
Net Cash Flow @12% w/ Inf. Life		-3389	-472	56	-176	-278	-289	-393	-473	-487	-503	-2678
Net Cash Flow @25% w/ Inf. Life		-3389	-472	56	-176	-278	-289	-393	-473	-487	-503	-1555
NPC @12% To Start of Yr 1		-3026	-3402	-3363	-3475	-3632	-3779	-3957	-4148	-4324	-4485	-5255
NPC @25% To Start of Yr 1		-2711	-3013	-2985	-3057	-3148	-3224	-3306	-3386	-3451	-3505	-3639

Figure G.11 Continued.

Engineering Evaluation for Multistage Zinc Sorption Onto Ferrihydrite
2002 Startup

Data Input

Case	FeCl3 (L/yr)	50% NaOH (L/yr)	Emulsion Polymer (L/yr)	Waste (L/yr)	Filter Cloth (ft²/yr)	Electricity (kWh/yr)	Sludge Disposal ($/yr)	Filtered Water (kg/yr)	Technical Exempt (No.)	Operations (No.)
1A	722,400	534,600	2,048	143,700	126,018	111,769	1,385,000	649	0.25	0.25
1B	722,400	534,600	2,458	143,700	126,018	153,314	1,385,000	619	0.30	0.30
2A	3,698,900	2,737,200	8,076	708,000	504,071	195,613	6,828,000	3,238	0.25	0.40
2B	491,300	363,500	1,881	94,200	78,761	138,266	909,000	425	0.30	0.25
2C	325,100	240,600	1,424	62,400	78,761	173,891	602,000	276	0.35	0.30
3A	289,000	213,800	985	57,600	42,006	93,952	555,000	265	0.25	0.20
3B	289,000	213,800	1,149	57,600	42,006	129,861	555,000	251	0.30	0.25
3C	289,000	213,800	1,313	57,600	42,006	205,799	555,000	242	0.35	0.35

Cash Flow Analysis Output

Case	Investment ($1000)	2004 Cash Operating Cost ($1000/yr)	2002 NPC @12% ($1000)	2002 NPC @25% ($1000)	2002 Annualized Cost ($1000/yr)
1A	2,300	-694	-4,798	-3,081	1,035
1B	2,800	-764	-5,492	-3,582	1,184
2A	4,300	-2,355	-13,454	-7,890	2,943
2B	2,600	-603	-4,647	-3,111	998
2C	2,900	-581	-4,788	-3,280	1,025
3A	1,900	-422	-3,324	-2,242	711
3B	2,400	-492	-4,015	-2,742	859
3C	3,300	-616	-5,255	-3,639	1,124

Figure G.12 Cash flow analysis results for multistage Zn sorption case studies.